BULLETIN OF RUSSIAN STATE MEDICAL UNIVERSITY

BIOMEDICAL JOURNAL OF PIROGOV RUSSIAN NATIONAL RESEARCH MEDICAL UNIVERSITY

SUBMISSION

SUBMISSION http://vestnik.rsmu.press/login?lang=en
CORRESPONDENCE editor@rsmu.press
COLLABORATION manager@rsmu.press
ADDRESS ul. Ostrovityanova, d. 1, Moscow, Russia, 117997

Indexed in Scopus. CiteScore 2024: 0.7

Indexed in WoS. JIF 2024: 0.4

Five-year h-index is 11

SCImago Journal & Country Rank 2024: 0.166

Indexed in DOAJ

Open access to archive

Issue DOI: 10.24075/brsmu.2026-02
Mass media registration certificate No. 012769, issued on July 29, 1994.
ISSN (Print): 2500-1094, ISSN (Online): 2542-1204.
Founder and publisher: Pirogov Russian National Research Medical University (Moscow, Russia).
The journal is indexed in the following scientific databases: Scopus, Web of Science, Google Scholar, SJR, DOAJ, Scilit, CyberLeninka, Embase, EZB, Lens.org, MIT Libraries, OpenAlex, Research4Life, Scholia, Wikidata, and ZDB.

Approved for print 30.04.2026
Circulation: 100 copies. Printed by Print.Formula
www.print-formula.ru

ВЕСТНИК РОССИЙСКОГО ГОСУДАРСТВЕННОГО МЕДИЦИНСКОГО УНИВЕРСИТЕТА

НАУЧНЫЙ МЕДИЦИНСКИЙ ЖУРНАЛ РНИМУ ИМ. Н. И. ПИРОГОВА

ПОДАЧА РУКОПИСЕЙ

ПОДАЧА РУКОПИСЕЙ https://vestnik.rsmu.press/login?lang=ru
ПЕРЕПИСКА С РЕДАКЦИЕЙ editor@rsmu.press
СОТРУДНИЧЕСТВО manager@rsmu.press
АДРЕС РЕДАКЦИИ ул. Островитянова, д. 1, г. Москва, 117997

Журнал включен в Scopus. CiteScore 2024: 0,7 — Журнал включен в WoS. JIF 2024: 0,4 — Индекс Хирша (h⁵) журнала по оценке Google Scholar: 11

SJR SCImago Journal & Country Rank 2024: 0,166 — Журнал включен в DOAJ — Здесь находится открытый архив журнала

DOI выпуска: 10.24075/vrgmu.2026-02
Свидетельство о регистрации средства массовой информации № 012769 от 29 июля 1994 г.
ISSN (Print): 2500-1094, ISSN (Online): 2542-1204.
Учредитель и издатель — Российский национальный исследовательский медицинский университет имени Н. И. Пирогова (Москва, Россия).
Журнал индексируется в научных базах Scopus, Web of Science, Google Scholar, SJR, DOAJ, Scilit, CyberLeninka, Embase, EZB, Lens.org, MITLibaries, OpenAlex, Research4Life, Scholia, Wikidata, ZDB.

Подписано в печать 30.04.2026
Тираж 100 экз. Отпечатано в типографии Print.Formula
www.print-formula.ru

BULLETIN OF RSMU **2, 2026**
ВЕСТНИК РГМУ

Contents
Содержание

POSTMENOPAUSAL CHANGE IN MSCs SENSITIVITY TO TESTOSTERONE, 17β-ESTRADIOL, AND PTH ARE ASSOCIATED WITH IMPAIRED ADIPOGENESIS

Zinoveva AA, Bakhchinian E, Kamenkov SS, Shcherbakova LN, Bugerenko AE, Ogay DS, Voloshin NS, Chechekhina ES ✉, Kulebyakin KYu

Lomonosov Moscow State University, Moscow, Russia

The menopausal transition is accompanied by the decrease in estrogen levels and changes in the estrogen to androgen ratio, resulting in dysregulation of multipotent mesenchymal stem cell (MSCs) differentiation in the subcutaneous adipose tissue, reduction of their adipogenic potential, adipocyte hypertrophy, and metabolic disorder progression. Menopausal hormone therapy (MHT) is used to manage menopausal symptoms. However, the effects of exogenous hormones on MSCs are still poorly understood. The study aimed to assess adipogenic differentiation of the subcutaneous adipose tissue MSCs and their sensitivity to testosterone, 17β-estradiol, and parathyroid hormone (PTH) in postmenopause. A total of six patients with benign gynecological disorders were included in the study, among them two were of reproductive age, one was perimenopausal, and three were postmenopausal. The MSCs adipogenic differentiation was performed throughout 14 days with the addition of testosterone, 17β-estradiol, or PTH, 10 nM each, then the proportion of cells containing lipid droplets was assessed. The adipogenesis level in control samples was 26–30% in patients of childbearing age and 12–42% in postmenopausal ones, with the pronounced interindividual variability. Hormonal stimulation considerably suppressed MSCs adipogenesis in postmenopause: testosterone reduced adipogenesis to 46–56% of control levels, estradiol to 51–84%, PTH to 53–66%, while patients of childbearing age showed a less pronounced effect (65–85%). The obtained data demonstrate a shift in hormonal sensitivity of MSCs from subcutaneous adipose tissue in postmenopause and suggest that MHT may exert an additional inhibiting effect on adipogenesis through suppression of MSCs differentiation.

Keywords: mesenchymal stem cells, testosterone, 17β-estradiol, PTH, adipogenic potential, menopause, menopausal hormone therapy

Funding: the study was supported by the RSF grant 25-75-30005 “Regulation of Body’s Cell Renewal Processes, the Fundamentals for Long-term Maintenance of Functional Activity of Organs and Tissues, Human Health and Active Longevity”.

Author contribution: Zinoveva AA, Bakhchinian E — experiments on MSC differentiation, processing of the results; Kamenkov SS — MSC isolation and culturing, statistical data processing, manuscript writing; Shcherbakova LN — clinical phase management, biomaterial acquisition, interpretation of the results, manuscript editing; Bugerenko AE, Ogay DS — clinical phase management, biomaterial acquisition; Voloshin NS — adipogenic differentiation quantification; Chechekhina ES — study concept and design, MSC isolation and culturing, interpretation of the results, manuscript writing; Kulebyakin KYu — study concept and design, interpretation of the results, manuscript editing.

Compliance with ethical standards: the study was approved by the Ethics Committee of the Lomonosov Moscow State University (IRB00010587, protocol No. 4 dated 4 June 2018, protocol No. 9 dated 29 October 2018) was conducted in accordance with the principles of the Declaration of Helsinki. All the patients provided informed consent before biomaterial collection.

✉ **Correspondence should be addressed:** Elizaveta S. Chechekhina
Lomonosovsky Prospect 27/1, Moscow, 119192, Russia; voynovaes@my.msu.ru

Received: 09.03.2026 **Accepted:** 05.04.2026 **Published online:** 16.04.2026

DOI: 10.24075/brsmu.2026.013

ПОСТМЕНОПАУЗАЛЬНОЕ ИЗМЕНЕНИЕ ЧУВСТВИТЕЛЬНОСТИ МСК К ТЕСТОСТЕРОНУ, 17β-ЭСТРАДИОЛУ И ПТГ АССОЦИИРОВАНО С НАРУШЕНИЕМ АДИПОГЕНЕЗА

А. А. Зиновьева, Е. Бахчинян, С. С. Каменков, Л. Н. Щербакова, А. Е. Бугеренко, Д. С. Огай, Н. С. Волошин, Е. С. Чечехина ✉, К. Ю. Кулебякин

Московский государственный университет имени М. В. Ломоносова, Москва, Россия

Менопаузальный переход сопровождается снижением уровня эстрогенов и изменением соотношения эстрогенов и андрогенов, что приводит к дисрегуляции дифференцировки мультипотентных мезенхимных стромальных клеток (МСК) подкожной жировой ткани, снижению их адипогенного потенциала, гипертрофии адипоцитов и прогрессированию метаболических нарушений. Для коррекции менопаузальных расстройств назначается менопаузальная гормональная терапия (МГТ), однако влияние экзогенных гормонов на МСК остается малоизученным. Целью исследования было изучить адипогенную дифференцировку МСК подкожной жировой ткани и их чувствительность к тестостерону, 17β-эстрадиолу и паратиреоидному гормону (ПТГ) в постменопаузе. В исследование включено шесть пациенток с доброкачественной гинекологической патологией, из них две в репродуктивном периоде, одна в перименопаузе и три в постменопаузе. Адипогенную дифференцировку МСК проводили в течение 14 дней с добавлением тестостерона, 17β-эстрадиола или ПТГ по 10 нМ, после чего оценили долю клеток с жировыми каплями. Базовый уровень адипогенеза в контроле составил 26–30% у пациенток репродуктивного возраста и 12–42% в постменопаузе с выраженной межиндивидуальной вариабельностью. Гормональная стимуляция значительно подавляла адипогенез МСК в постменопаузе: тестостерон снизил эффективность до 46–56% от контроля, эстрадиол — до 51–84%, ПТГ — до 53–66%, тогда как в репродуктивном возрасте эффект был умеренным (65–85%). Полученные данные демонстрируют сдвиг гормональной чувствительности МСК подкожной жировой ткани в постменопаузе и свидетельствуют о том, что МГТ может оказывать дополнительное ингибирующее действие на адипогенез через подавление дифференцировки МСК.

Ключевые слова: мультипотентные мезенхимные стромальные клетки, тестостерон, 17β-эстрадиол, ПТГ, адипогенный потенциал, менопауза, менопаузальная гормональная терапия

Финансирование: работа выполнена при поддержке гранта РНФ 25-75-30005 «Регуляция процессов обновления клеток в организме, фундаментальной основы длительного сохранения функциональной активности органов и тканей, здоровья и активного долголетия человека».

Вклад авторов: А. А. Зиновьева, Е. Бахчинян — эксперименты по дифференцировке МСК, обработка результатов; С. С. Каменков — выделение и культивирование МСК, статистическая обработка данных, написание рукописи; Л. Н. Щербакова — организация клинического этапа, получение биологического материала, интерпретация результатов, редактирование рукописи; А. Е. Бугеренко, Д. С. Огай — организация клинического этапа, получение биологического материала; Н. С. Волошин — количественная оценка адипогенной дифференцировки; Е. С. Чечехина — концепция и дизайн исследования, выделение и культивирование МСК, интерпретация результатов, написание рукописи; К. Ю. Кулебякин — концепция и дизайн исследования, интерпретация результатов, редактирование рукописи.

Соблюдение этических стандартов: исследование одобрено этическим комитетом МГУ имени М. В. Ломоносова (IRB00010587, протокол № 4 от 4 июня 2018 г., протокол № 9 от 29 октября 2018 г.), проведено в соответствии с принципами Хельсинкской декларации. Все пациенты подписали информированное согласие перед сбором материала.

✉ **Для корреспонденции:** Елизавета Сергеевна Чечехина
Ломоносовский проспект, д. 27, корпус 1, г. Москва, 119192, Россия; voynovaes@my.msu.ru

Статья получена: 09.03.2026 **Статья принята к печати:** 05.04.2026 **Опубликована онлайн:** 16.04.2026

DOI: 10.24075/vrgmu.2026.013

The menopausal transition represents a unique stage of a woman's life, when sudden rearrangement of neuroendocrine regulation leads to the profound change of both the function of classic hormone-dependent target organs and the behavior of multipotent mesenchymal stem cells (MSCs) of adipose and bone tissues [1, 2]. MSCs represent a key element of mesodermal tissue regeneration and have a unique ability to differentiate in different directions (adipogenic, osteogenic, and chondrogenic) [3]. The MSCs activity is under strict neuroendocrine control to ensure timely adjustment to the body's current demands [4]. In particular, in the female body, 17β-estradiol signaling is involved in the stromal tissue morphology and energy balance regulation during the menstrual cycle [5]. After menopause, the decrease in 17β-estradiol levels and changes in the estrogen to androgen ratio lead to the dysregulation of MSCs differentiation, as well as to changes in sensitivity to homeostatic hormones, such as parathyroid hormone (PTH) [6, 7]. Simultaneously, the MSCs senescent phenotype is formed, which results in the reduced MSC functional activity and worse tissue regeneration capacity [8–11]. An interplay between these processes leads to gender-specific manifestations of aging, including changes in the adipose tissue distribution, osteoporosis, and increased cardiometabolic risk [12, 13].

Traditionally, symptoms are alleviated by prescribing the menopausal hormone therapy (MHT) aimed mainly at replenishing estrogen (primarily 17β-estradiol) deficiency. MHT has a complex effect on adipose and bone tissues. It is well known that transdermal 17β-estradiol administration enhances the adipogenic potential of MSCs in the adipose tissue of the femoral depot without any considerable effect on abdominal cells [14]. As for the bone tissue, MHT slows down weight loss, stimulates MSCs osteogenic differentiation, suppresses osteoclast activity, and reduces bone resorption, thereby contributing to lower risk of osteoporosis [15]. Despite all the benefits, MHT prescription has several contraindications and is associated with some risk factors (thrombosis, cancer). Furthermore, it is not recommended to use MHT for adjustment of age-associated metabolic disorders and prevention of cardiovascular disorders [16]. In a number of countries, androgen-based drugs are prescribed to adjust vulvovaginal atrophy and increase libido, along with conventional MHT [17]. No testosterone-based drugs for treatment of menopausal symptoms have been registered in the Russian Federation. Furthemore, it is not recommended to prescribe testosterone-based drugs to women with cognitive impairment, cardiovascular and metabolic disorders [16, 18]. With respect to the existing limitations of systemic hormone therapy, the development of targeted methods based on the use of MSCs itself or their secretome (bioactive factors capable of locally modulating the MSCs differentiation processes without any systemic hormonal load) is becoming a promising area [19, 20]. In-depth knowledge of the mechanisms underlying the hormone-dependent MSCs differentiation in both young and elderly women will open new areas for personalized therapeutic approaches to adjustment of metabolic disorders in postmenopausal women in the future.

We assumed that there is a shift in the MSCs sensitivity to hormones in peri- and postmenopause, due to which testosterone, 17β-estradiol, and PTH have a more pronounced anti-adipogenic effect, than in women of childbearing age.

The study aimed to assess the features of adipogenic differentiation of the subcutaneous adipose tissue MSCs in women of childbearing age, peri- and postmenopausal women, as well as to assess changes in the MSCs sensitivity to testosterone, 17β-estradiol, and PTH in postmenopause.

METHODS

Patient characteristics

A total of six patients, who underwent elective surgery due to benign gynecological disorders, were included in the study. Two patients of childbearing age underwent diagnostic laparoscopy aimed to rule out tubal factor infertility; one patient, who were through perimenopausal transition, underwent hysterectomy due to multiple fibroids; three patients, who were in their late postmenopause (postmenopausal for more than 20 years), underwent surgery due to pelvic organ prolapse.

Inclusion criteria: elective laparoscopic surgery due to benign gynecological disorders. Patients of childbearing age (under 45), perimenopausal and postmenopausal patients were included. Exclusion criteria: malignant neoplasms, acute inflammatory disorders at the time of surgery, diabetes mellitus. Clinical characteristics of the patients included in the study are provided in Table 1.

MSCs isolation from the subcutaneous adipose tissue

The subcutaneous adipose tissue samples were obtained during laparoscopic gynecological surgery. Samples were collected from the umbilical area (first trocar insertion site); the sample volume was about 1 cm^3. Samples were transported in sterile containers with the Hanks' Balanced Salt Solution (PanEco, Russia) supplemented with 5% penicillin/streptomycin (Gibco, USA) at a temperature of 4 °C and processed within 2 hours after collection.

The subcutaneous adipose tissue samples were placed in a Petri dish and washed three times with the cooled sterile

Table 1. Clinical characteristics of patients

ID	Age, years	BMI, kg/m^2	Reproductive aging stage (Straw classification)	Extent of surgery	Somatic diseases
1	35	25.5	-4	Diagnostic laparoscopy, chromopertubation	Migraine
2	25	22.3	-4	Diagnostic laparoscopy, chromopertubation	Not detected
3	45	20.1	-1	Laparoscopic hysterectomy due to multiple fibroids	Hashimoto's thyroiditis
4*	71	25.3	2	Laparoscopic sacral colpopexy	Grade 3 hypertension, Cardiovascular risk class 3
5	69	24.3	2	Laparoscopic sacral colpopexy	Not detected
6	71	40.6	2	Laparoscopic sacral colpopexy	Grade 3 hypertension, Cardiovascular risk class 4. CAD: angina pectoris

Note: * — the patient had a history of using topical estrogens.

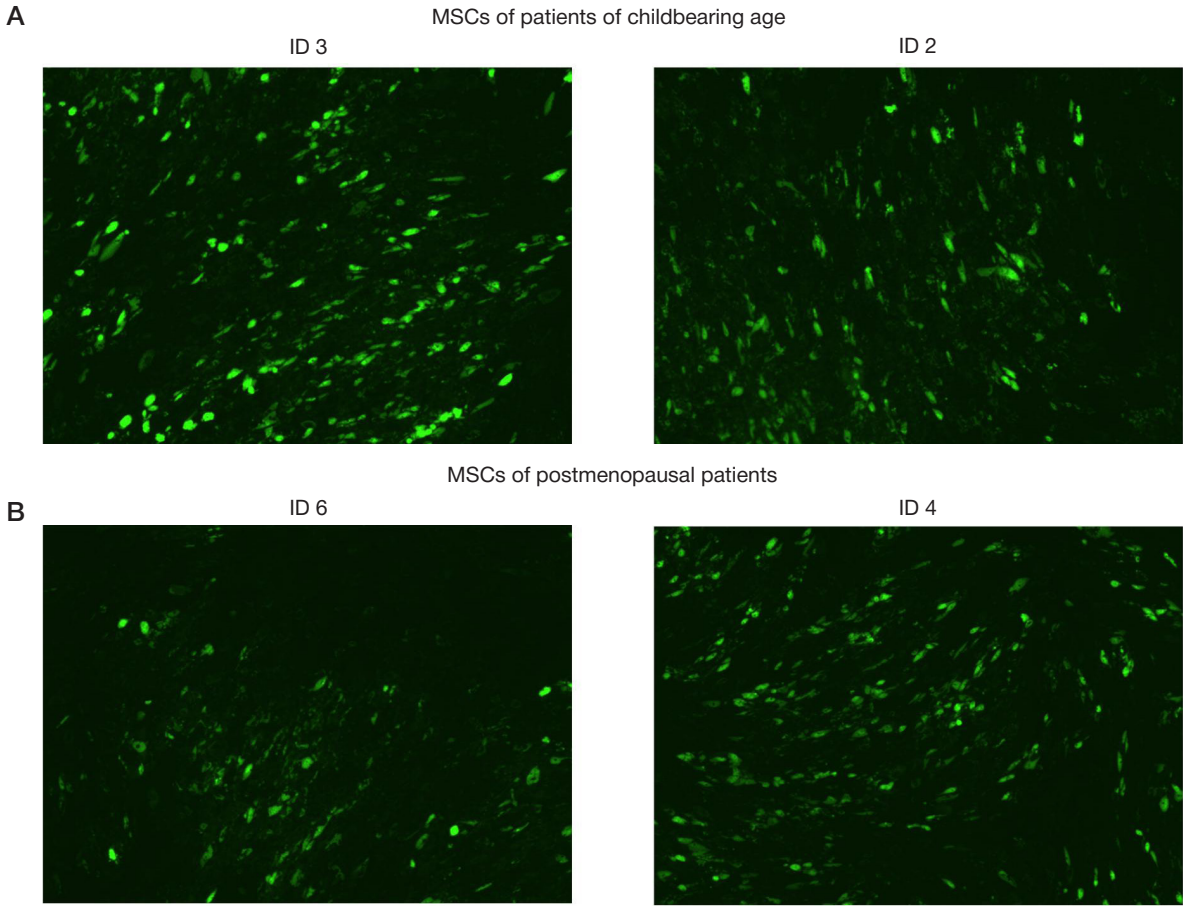

Fig. 1. Adipogenic differentiation of the MSCs obtained from patients of childbearing age and postmenopausal patients in the control differentiation medium. **A**. Images of the MSCs obtained from patients of childbearing age at the differentiation endpoint (day 14) with the Nile Red stained lipid droplets. **B**. Images of the MSCs obtained from postmenopausal patients at the differentiation endpoint (day 14) with the Nile Red stained lipid droplets

phosphate-buffered saline (PanEco, Russia) to eliminate remnants of blood and tissue fluid. Then the tissue washed was thoroughly minced using a sterile scalpel for 5–10 min until a homogeneous suspension was obtained. The processed material was transferred to the sterile 50 mL test tube and mixed with type I collagenase (Worthington, USA) in a concentration of 1.5 mg/mL dissolved in the Hanks' Balanced Salt Solution. The collagenase volume was calculated based on the ratio 1 : 2 by weight of tissue. Incubation was done at 37 °C in the 5% CO_2 atmosphere for 50–60 min, with regular stirring (every 10 min).

The resulting suspension was centrifuged at 180 g for 10 min at 4 °C. Centrifugation yielded three layers: the upper layer comprising the floating mature adipocytes and lipids, intermediate layer, and the lower layer comprising the stromal vascular fraction (SVF) in the form of the dark red sediment. The upper two layers were carefully removed using a pipette. The lower layer comprising SVF was resuspended in the Hanks' Balanced Salt Solution. The resulting suspension was filtered through a 100 μm nylon mesh in order to remove the intact tissue fragments trapped in the sediment. The filtrate was transferred into clean test tubes. The filtered suspension was centrifuged at 180 g for 10 min. Then the resulting sediment was resuspended in 3–5 mL of the complete culture medium, mixed thoroughly, and transferred to Petri dishes.

MSCs culturing

The cells were passaged in the DMEM medium with the low glucose content (PanEco, Russia) supplemented with the 10% fetal bovine serum (Gibco, USA) and 1% penicillin/streptomycin (Gibco, USA). The cells were passaged, when the 100% confluency was reached. The medium was collected from the culture dish, washed three times with the Versene solution (PanEco, Russia), then added a small amount of the 0.25% trypsin solution (PanEco, Russia), distributed evenly across the bottom of the dish, and incubated at 37 °C for 3–5 min. After the rounded detached cells appeared (this was controlled using the inverted microscope), the suspension was added the complete culture medium to the working volume, pipetted carefully to obtain a homogenous suspension, and transferred into the new Petri dish.

Adipogenic differentiation

MSCs were seeded onto 6-well plates (at 90–100% confluence) and incubated for 14 days in the complete culture medium supplemented with the reduced adipogenic cocktail (10 μg/mL insulin (Merck Millipore, Germany), 1 μM dexamethasone (Abcam, UK), 0.5 mM IBMX (Abcam, UK)). One hormone was added to certain wells: 10 nM 17β-estradiol (Tocris Bioscience, UK), 10 nM testosterone (Cloud-Clone Corp., USA), or 10 nM PTH (Tocris Bioscience, UK), other conditions remained the same.

To visualize lipid droplets in the differentiated adipocytes, the cells were stained with Nile Red (Merck, Germany), the lipophilic fluorescent dye showing high specificity and luminescence intensity when bound to neutral lipids, on day 14 of differentiation. Then the cells were imaged using the Nikon Eclipse Ti2 microscope (Nikon; Japan) with the Nikon Plan Fluor 10x/0.3 lens and Kinetix camera (Teledyne Photometrics, USA). The quantitative analysis was performed

Table 2. Absolute adipogenic differentiation efficiency values (proportion of cells with lipid droplets) in patients of various age groups

ID	Age, years	Reproductive aging stage (Straw classification)	Adipogenic differentiation, control	Adipogenic differentiation + testosterone	Adipogenic differentiation + 17β-estradiol	Adipogenic differentiation + PTH
1	35	–4	26.23%	18.77%	21.84%	19.68%
2	25	–4	29.85%	22.22%	25.25%	19.49%
3	45	–1	19.78%	11.35%	11.15%	10.66%
4	71	2	41.90%	23.56%	35.09%	27.80%
5	69	2	21.48%	11.24%	10.97%	11.28%
6	71	2	12.30%	5.63%	8.06%	6.55%

using the AI module for automated image assessment being part of the NIS-Elements 5.42.02 software (Nikon, Japan). All the cells in each image were segmented using the Segment Objects.ai model. Then each cell was tested for the presence of lipid droplets in it. The overall adipogenic differentiation efficiency was estimated as a percentage of cells with lipid droplets relative to the total number of cells. The analysis was performed on a number of randomly selected fields of view from different wells of the plate, which ensured the sample representativeness.

Statistical analysis

Statistical analysis of the results was performed using the SigmaPlot 11.0 software package (Systat Software Inc., San Jose, California, USA). The data distribution was tested for normality using the Shapiro–Wilk test. Independent groups were compared using the Student's t-test (for the normally distributed data) and Mann–Whitney *U*-test (for the non-normally distributed data). The differences were considered significant at $p < 0.05$. The values are presented as the mean ± standard error of the mean (mean ± SEM).

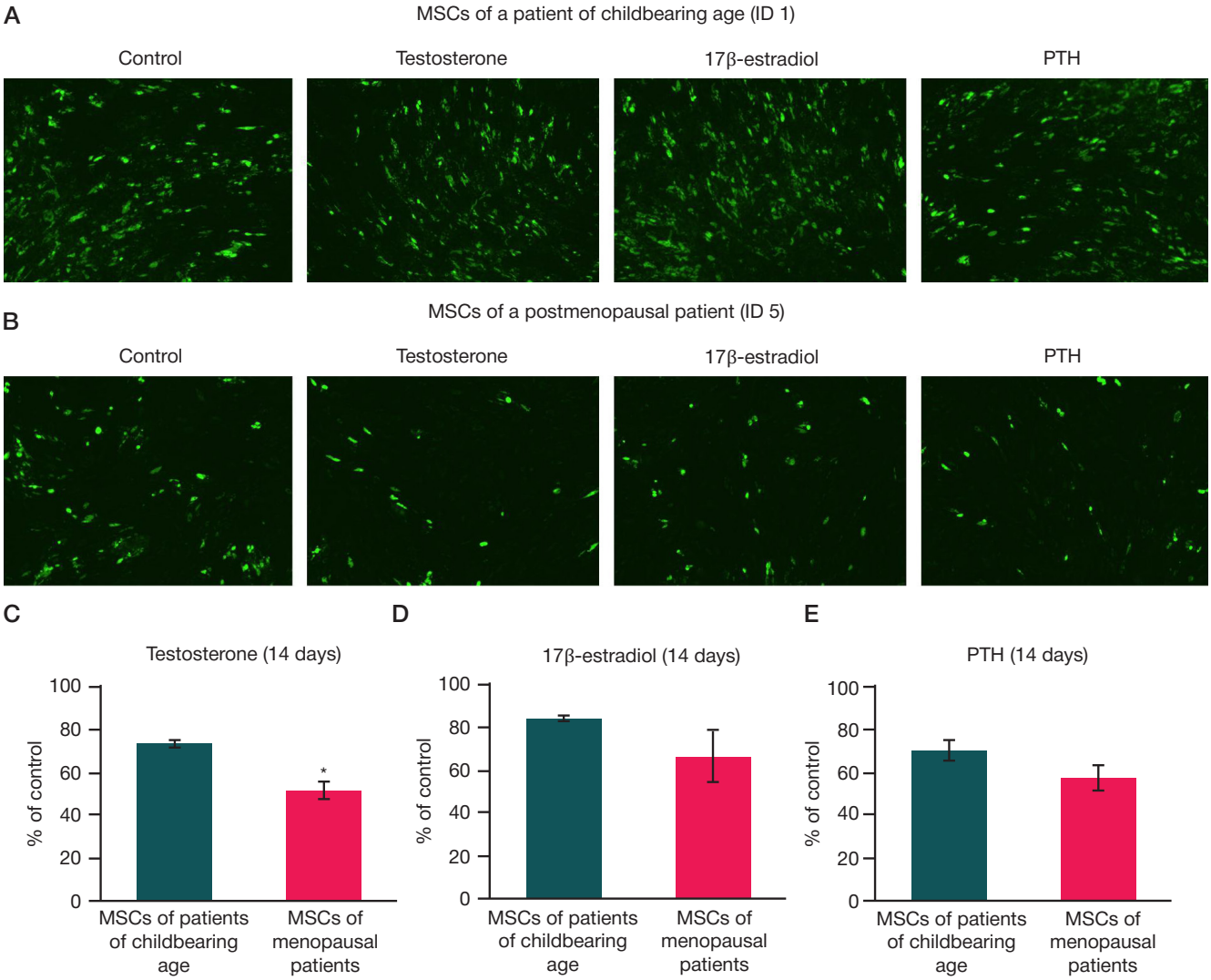

Fig. 2. Adipogenic differentiation of the MSCs obtained from patients of childbearing age and postmenopausal patients in the control differentiation medium, as well as in the differentiation medium supplemented with testosterone, 17β-estradiol, and PTH. **A**. Images of the MSCs obtained from patients of childbearing age at the differentiation endpoint (day 14) with the Nile Red stained lipid droplets. B. Images of the MSCs obtained from postmenopausal patients at the differentiation endpoint (day 14) with the Nile Red stained lipid droplets. **C**–**E**. Results of quantification of adipogenic differentiation in the presene of testosterone (**C**), 17β-estradiol (**D**), and PTH (**E**) normalized to the control differentiation conditions (n = 2,3; * — $p < 0.05$; t-test).

Table 3. Changes in adipogenic differentiation efficiency depending on testosterone, 17β-estradiol, and PTH supplementation in patients of various age groups

ID	Age, years	Reproductive aging stage (Straw classification)	Adipogenic differentiation + testosterone, % of control differentiation	Adipogenic differentiation + 17β-estradiol, % of control differentiation	Adipogenic differentiation + PTH, % of control differentiation
1	35	–4	72%	83%	75%
2	25	–4	74%	85%	65%
3	45	–1	57%	56%	54%
4	71	2	56%	84%	66%
5	69	2	52%	51%	53%
6	71	2	46%	66%	53%

RESULTS

Adipogenesis visual and quantitative characteristics in control conditions

Images of the fluorescence stained MSCs cultures obtained from patients of childbearing age (25–35 years, STRAW –4) showed high differentiation efficiency: lipid droplets occupying a large part of the cytoplasm were found in a large proportion of cells, which suggested active terminal phase of adipogenesis (Fig. 1A). In contrast, there were a considerably lower number of such cells in the MSCs cultures obtained from postmenopausal patients (69–71 years, STRAW +2) (Fig. 1B). The baseline proportion of Nile Red+ cells in the control was 26–30% in patients of childbearing age and 12–42% in postmenopausal patients, with the marked interindividual variability in the latter (Fig. 1B, Table 2).

We should also mention the detected discrepancy between age and the control values of adipogenic MSCs differentiation in two patients. Thus, patient 4 (71 years, postmenopause for more than 20 years) showed a relatively high adipogenesis level in the control (41.9%) (Fig. 1B; Table 2), which was much higher compared to the values of other patients of the same age. One possible explanation of this phenomenon can be personal clinical features of the patient: she received topical estriol for 1 month during the postoperative period, which could positively affect MSCs and their differentiation capacity. In contrast, patient 3 (45 years, late menopausal transition) showed a low level of adipogenic differentiation in the control (about 20%) (Table 2), which suggests the decrease in the cells' functional sensitivity already during the menopausal transition, which is characterized by unstable hormone levels with the preserved menstrual cycle. The data obtained emphasize considerable heterogeneity of the age-related MSCs alterations resulting from both baseline hormone levels and clinical factors, which should be taken into account when interpreting the MSCs differentiation results and developing the drugs for adjustment of metabolic disorders based on MSCs and their secretome.

Hormone-dependent effects on adipogenic differentiation

Testosterone supplementation caused the most pronounced adipogenesis suppression in the MSCs obtained from postmenopausal patients. Relative adipogenesis efficiency decreased to 46–56% compared to the control values (ID 4–6), while patients of childbearing age showed a moderate effect (72–74%) (Fig. 2A–C; Table 3). 17β-estradiol and PTH also inhibited differentiation in the late postmenopausal women (51–84% and 53–66% of the control, respectively) (Fig. 2 A–B, D–E; Table 3).

On the group of postmenopausal patients, patient 4 with the history of topical estradiol therapy having an abnomally high basal adipogenesis value turned out to be especially insensitive to the effects of 17β-estradiol and PTH (Fig. 1B; Table 3). In patient 3, all the hormones reduced relative differentiation efficiency to postmenopausal levels (54–57%), which confirms the data on the premature shift in MSC sensitivity to hormonal stimuli (Table 3).

Based on the data obtained we can conclude that the MSCs adipogenic differentiation depends on both women's age and hormone levels. High adipogenic differentiation efficiency is observed in the childbearing age, while in postmenopause (without systemic or topical hormone therapy) it is significantly decreased. High adipogenic activity in the 71-year-old postmenopausal patient, who received topical estriol therapy and, conversely, low differentiation level in a younger patient (ID 3; 45 years), being through her menopausal transition, suggest that the hormonal status can have a more pronounced effect on the MSCs functional state, than chronological age, and should be taken into account when interpreting experimental data and developing targeted therapeutic approaches.

Hormonal stimulation has fundamentally different effects on the MSCs obtained from patients of childbearing age and postmenopausal patients. It is clear that MSCs from postmenopausal patients demonstrate a pronounced decrease in adipogenesis efficiency in response to testosterone, estrogen, and PTH exposure. However, no similar anti-adipogenic effect is observed in the MSCs of younger patients. Thus, our findings suggest that there is a shift in the MSCs sensitivity to hormones in peri- and postmenopause.

DISCUSSION

The menopause represents a critical phase of a woman's life, associated with significant changes in the levels of circulating hormones. It is characterized by the decrease in estrogen levels and the increase in the androgen to estrogen ratio. In postmenopause, estrogens are predominantly synthesized in the adipose tissue from androgen precursors generated in the adrenal glands and ovaries. Androgen and estrogen concentrations in the adipose tissue are higher compared to circulating levels, reflecting the role of the adipose tissue as a critical reservoir and a site for the sex steroid metabolism [21]. The changes that occur during menopause are exacerbated by the overall aging of the body. The age-related and menopausal processes directly affect both terminally differentiated cells and stem cells, reducing their proliferation and differentiation potential.

In our study we have shown that the menopausal transition has a pronounced effect on the adipose tissue MSCs functions. MSCs of postmenopausal women demonstrate the decrease in adipogenic potential compared to MSCs of women of childbearing age [14, 22, 23]. The MSCs differentiation potential decrease in postmenopause can have a direct effect on the adipose tissue structure and functions. Since MSCs

represent the source of new adipocytes, disturbances of their differentiation lead to reduction of the pool of young functional adipocytes, hypertrophy of the existing cells, and accumulation of excess lipid droplets in the cells.

Earlier it has been shown that in premenopause the adipose tissue is characterized by high estrogen metabolism enzyme activity and estrogen concentrations significantly exceeding the serum levels. Following the onset of menopause, there is a significant decrease in both estrogen levels and the activity of appropriate enzymes. Furthermore, comparative analysis of the estrogen metabolism enzyme mRNA expression in the adipose tissue revealed similar patterns, regardless of the menopausal status, which suggests the key role of post-transcription mechanisms in reducing the tissue enzyme activity [24].

The results of our study provide a possible explanation of the mechanisms underlying such post-transcriptional alterations. Reduction of the subcutaneous MSCs adipogenic potential in postmenopausal women can be the first event initiating the cascade of changes in the adipose tissue. The lack of young functional adipocytes resulting from the decreased MSCs differentiation disturbs the adipose tissue normal architecture and cellular composition. This leads to accumulation of hypertrophic adipocytes showing the significantly decreased synthetic activity in the adipose tissue, which, in turn, decreases its overall enzyme activity.

We have shown that adding 17β-estradiol, PTH and especially testosterone significantly inhibits adipogenic differentiation of MSCs in postmenopausal patients, reducing the efficiency to 46–84% of the control, while young women show only a moderate effect. This change in sensitivity is of particular importance when prescribing MHT. It is well known that the adipose tissue of patients receiving MHT maintains high local estrogen concentrations and remains capable of active sex steroid metabolism, which prevents the development of visceral obesity typical for postmenopausal women [25]. Despite the fact that the mechanisms of the adipose tissue distribution hormonal regulation are complex and involve effects on the lipolysis, lipogenesis, and insulin sensitivity, our data suggest one more previously undescribed mechanism: the MHT-associated adipose tissue redistribution slowdown occurs not only due to the direct metabolic effects of estrogens, but also indirectly through the inhibition of the MSCs adipogenic differentiation by sex steroids.

Our study has shown the pronounced individual variability of the MSCs adipogenic potential in postmenopause. Such variability is determined not only by age and the time of onset of menopause, but also by the individual history of hormone therapy. The best example is patient 4, in whom, despite short-term use of topical estriol, relatively high basal adipogenesis was maintained, comparable with the values of younger patients. Such individual variability emphasizes the need to consider medical history data, including the history of using hormonal drugs, when interpreting the MSCs functional properties and developing personalized approaches to adjustment of postmenopausal disorders.

Our study fits well into modern concepts of the clinical and molecular mechanisms underlying the female body aging and changing balance of estrogens and androgens with the ovarian function loss [12, 26]. The data obtained are well correlated with the available data on the impact of estrogen deficiency on metabolic processes, tissue regeneration, and pathogenesis of postmenopausal disorders [27–30]. The approach involving the use of MSCs or their secretome for targeted therapy can open new promising methods for adjustment of postmenopausal disorders without systemic hormonal load [19, 20].

At the same time, the detected considerable interindividual variability of the MSCs functional properties requires further investigation of the mechanisms underlying regulation of MSCs differentiation and senescence considering the hormonal status, genetic and epigenetic context of each patient. This emphasizes the need for a comprehensive personalized approach to both selection of conventional menopausal hormone therapy and development of new MSC-based biotechnological methods for treatment of postmenopausal women.

Study limitations and the direction of future research

Small sample size (n = 2–3) significantly limits the study statistical power and reduces the possibility of extrapolating the results to a wider population of menopausal women. The perimenopause group is represented by only one patient (ID 3), which makes it impossible to assess the dynamic changes during the transition period. The data obtained suggest the potentially premature adipogenesis decrease. However, this conclusion needs to be confirmed in the larger cohort.

In the future it is planned to expand the sample of patients to increase the statistical power, reduce the effect of interindividual variability, and validate the results. Considerable basal adipogenesis variability (12–42% in postmenopausal patients) can be associated with individual differences in the hormonal status, concomitant disorders (hypertension, CAD), and therapy features (such as the use of topical estriol in patient 4). These factors make it difficult to distinguish between the effects directly related to menopause and the influence of individual patient characteristics.

Moreover, the study is based solely on the abdominal subcutaneous adipose tissue samples, which makes it impossible to assess the impact of hormonal factors on the visceral adipose tissue. In the future it is planned to include various adipose tissue types in the studies for more comprehensive assessment of the impact of menopause on the adipogenic potential.

CONCLUSIONS

It has been shown that the menopausal transition reduces the subcutaneous adipose tissue multipotent mesenchymal stem cell (MSCs) adipogenic differentiation capability. This triggers the cascade of changes in the adipose tissue: reduction of the proportion of young adipocytes, hypertrophy of mature cells, and the decrease in the local estrogen metabolism activity. Sex steroids (17β-estradiol, testosterone) and PTH enhance adipogenesis inhibition in postmenopausal women compared to women of childbearing age, which suggests the shift in the MSCs sensitivity to hormones following the ovarian failure. This mechanism can explain the adipose tissue redistribution slowdown associated with MHT not only by the direct metabolic effects of estrogens, but also through the MSCs differentiation modulation. To gain a deeper understanding of the mechanisms that determine the shift in hormonal sensitivity of MSCs in postmenopause, further study of the post-transcriptional regulation and senescence of these cells, considering genetic and epigenetic factors, is recommended. The results of such analysis can be used when developing the MSCs secretome-based cell preparations for adjustment of postmenopausal metabolic disorders.

References

1. Jin W-J, et al. Differential responsiveness to 17β-estradiol of mesenchymal stem cells from postmenopausal women between osteoporosis and osteoarthritis. Osteoporos. Int. 2012; 23 (10): 2469–78.
2. Niada S, et al. 17β-estradiol differently affects osteogenic differentiation of mesenchymal stem/stromal cells from adipose tissue and bone marrow. Differentiation. 2016; 92 (5): 291–7.
3. Naji A, et al. Biological functions of mesenchymal stem cells and clinical implications. Cell Mol Life Sci. 2019; 76 (17): 3323–48.
4. Isern J, Méndez-Ferrer S. Stem Cell Interactions in a Bone Marrow Niche. Curr. Osteoporos. Rep. 2011; 9 (4): 210–8.
5. Tucker JAL, et al. The Effect of the Menstrual Cycle on Energy Intake: A Systematic Review and Meta-analysis. Nutr Rev. 2025; 83 (3): e866–e876.
6. Nordin BEC, et al. A longitudinal study of bone-related biochemical changes at the menopause. Clin Endocrinol (Oxf). 2004; 61 (1): 123–30.
7. Ogita M, et al. Differentiation and Proliferation of Periosteal Osteoblast Progenitors Are Differentially Regulated by Estrogens and Intermittent Parathyroid Hormone Administration. Endocrinology. 2008; 149 (11): 5713–23.
8. Chechekhina E, et al. Extracellular Vesicles of Adipose Multipotent Mesenchymal Stromal Cells Propagate Senescent Phenotype by Affecting PTEN Nuclear Import. Int J Mol Sci. 2025; 26 (15): 7164.
9. Chechekhina ES, et al. Changes in Noradrenaline- and Serotonin-Dependent Intracellular Signaling in Senescent Multipotent Mesenchymal Stromal Cells. Cell Tiss Biol. 2026; 20: 200–11.
10. Voynova E, et al. Declined adipogenic potential of senescent MSCs due to shift in insulin signaling and altered exosome cargo. Front Cell Dev Biol. 2022; 10: 1050489.
11. Weng Z, et al. Mesenchymal Stem/Stromal Cell Senescence: Hallmarks, Mechanisms, and Combating Strategies. Stem Cells Transl Med. 2022; 11 (4): 356–71.
12. Chazenbalk G, et al. Androgens inhibit adipogenesis during human adipose stem cell commitment to predipocyte formation. Steroids. 2013; 78 (9): 920–6.
13. Li J, et al. The relationship between bone marrow adipose tissue and bone metabolism in postmenopausal osteoporosis. Cytokine Growth Factor Rev. 2020; 52: 88–98.
14. Cox-York KA, et al. Region-specific effects of oestradiol on adipose-derived stem cell differentiation in post-menopausal women. J Cell Mol Med. 2017; 21 (4): 677–84.
15. Syed FA, et al. Effects of estrogen therapy on bone marrow adipocytes in postmenopausal osteoporotic women. Osteoporos Int. 2008; 19 (9): 1323–30.
16. Klinicheskie rekomendatsii Ministerstva zdravookhraneniya Rossiyskoy Federatsii «Menopauza i klimaktericheskoe sostoyanie u zhenshchiny». Available from: https://cr.minzdrav.gov.ru/view-cr/117_3 (data obrashcheniya: 25.02.2026).
17. Andreeva EN, Sheremetyeva EV. The role of estriol in the treatment of atrophy of the mucous membrane of the lower genitourinary tract in postmenopausal women. Probl Endokrinol. 2022; 68 (6): 157–63.
18. Islam RM, et al. Safety and efficacy of testosterone for women: a systematic review and meta-analysis of randomised controlled trial data. Lancet Diabetes Endocrinol. 2019; 7 (10): 754–66.
19. Chen Y, et al. Enhancing osteoporosis treatment with engineered mesenchymal stem cell-derived extracellular vesicles: mechanisms and advances. Cell Death Dis. 2024; 15 (2): 119.
20. Guo C, et al. Mesenchymal stem cells therapy improves ovarian function in premature ovarian failure: a systematic review and meta-analysis based on preclinical studies. Front Endocrinol. 2023; 14.
21. Hetemäki N, et al. Estrogen Metabolism in Abdominal Subcutaneous and Visceral Adipose Tissue in Postmenopausal Women. J Clin Endocrinol Metab. 2017; 102 (12): 4588–95.
22. Anderson LA, et al. The effects of androgens and estrogens on preadipocyte proliferation in human adipose tissue: influence of gender and site. J Clin Endocrinol Metab. 2001; 86 (10): 5045–51.
23. Blouin K, et al. Effects of androgens on adipocyte differentiation and adipose tissue explant metabolism in men and women. Clin Endocrinol (Oxf). 2010; 72 (2): 176–88.
24. Hetemäki N, et al. Adipose tissue estrogen production and metabolism in premenopausal women. J Steroid Biochem Mol Biol. 2021; 209: 105849.
25. Hetemäki N, et al. Adipose Tissue Sex Steroids in Postmenopausal Women With and Without Menopausal Hormone Therapy. J Clin Endocrinol Metab. 2025; 110 (2): 511–22.
26. Kim C, et al. Changes in androstenedione, dehydroepiandrosterone, testosterone, estradiol, and estrone over the menopausal transition. Womens Midlife Health. 2017; 3 (1): 9.
27. Greendale GA, et al. Changes in Regional Fat Distribution and Anthropometric Measures Across the Menopause Transition. J Clin Endocrinol Metab. 2021; 106 (9): 2520–34.
28. Kodoth V, Scaccia S, Aggarwal B. Adverse Changes in Body Composition During the Menopausal Transition and Relation to Cardiovascular Risk: A Contemporary Review. Womens Health Rep (New Rochelle). 2022; 3 (1): 573–81.
29. Fenton A. Weight, Shape, and Body Composition Changes at Menopause. J Life Health. 2021; 12 (3): 187–92.
30. Piché M-E, et al. Regional body fat distribution and metabolic profile in postmenopausal women. Metabolism. 2008; 57 (8): 1101–7.

Литература

1. Jin W-J, et al. Differential responsiveness to 17β-estradiol of mesenchymal stem cells from postmenopausal women between osteoporosis and osteoarthritis. Osteoporos. Int. 2012; 23 (10): 2469–78.
2. Niada S, et al. 17β-estradiol differently affects osteogenic differentiation of mesenchymal stem/stromal cells from adipose tissue and bone marrow. Differentiation. 2016; 92 (5): 291–7.
3. Naji A, et al. Biological functions of mesenchymal stem cells and clinical implications. Cell Mol Life Sci. 2019; 76 (17): 3323–48.
4. Isern J, Méndez-Ferrer S. Stem Cell Interactions in a Bone Marrow Niche. Curr. Osteoporos. Rep. 2011; 9 (4): 210–8.
5. Tucker JAL, et al. The Effect of the Menstrual Cycle on Energy Intake: A Systematic Review and Meta-analysis. Nutr Rev. 2025; 83 (3): e866–e876.
6. Nordin BEC, et al. A longitudinal study of bone-related biochemical changes at the menopause. Clin Endocrinol (Oxf). 2004; 61 (1): 123–30.
7. Ogita M, et al. Differentiation and Proliferation of Periosteal Osteoblast Progenitors Are Differentially Regulated by Estrogens and Intermittent Parathyroid Hormone Administration. Endocrinology. 2008; 149 (11): 5713–23.
8. Chechekhina E, et al. Extracellular Vesicles of Adipose Multipotent Mesenchymal Stromal Cells Propagate Senescent Phenotype by Affecting PTEN Nuclear Import. Int J Mol Sci. 2025; 26 (15): 7164.
9. Chechekhina ES, et al. Changes in Noradrenaline- and Serotonin-Dependent Intracellular Signaling in Senescent Multipotent Mesenchymal Stromal Cells. Cell Tiss Biol. 2026; 20: 200–11.
10. Voynova E, et al. Declined adipogenic potential of senescent MSCs due to shift in insulin signaling and altered exosome cargo. Front Cell Dev Biol. 2022; 10: 1050489.
11. Weng Z, et al. Mesenchymal Stem/Stromal Cell Senescence: Hallmarks, Mechanisms, and Combating Strategies. Stem Cells Transl Med. 2022; 11 (4): 356–71.
12. Chazenbalk G, et al. Androgens inhibit adipogenesis during human adipose stem cell commitment to predipocyte formation. Steroids. 2013; 78 (9): 920–6.
13. Li J, et al. The relationship between bone marrow adipose tissue and bone metabolism in postmenopausal osteoporosis. Cytokine Growth Factor Rev. 2020; 52: 88–98.
14. Cox-York KA, et al. Region-specific effects of oestradiol on adipose-derived stem cell differentiation in post-menopausal women. J Cell Mol Med. 2017; 21 (4): 677–84.
15. Syed FA, et al. Effects of estrogen therapy on bone marrow adipocytes in postmenopausal osteoporotic women. Osteoporos

Int. 2008; 19 (9): 1323–30.
16. Клинические рекомендации Министерства здравоохранения Российской Федерации «Менопауза и климактерическое состояние у женщины». Доступно по ссылке: https://cr.minzdrav.gov.ru/view-cr/117_3 (дата обращения: 25.02.2026).
17. Andreeva EN, Sheremetyeva EV. The role of estriol in the treatment of atrophy of the mucous membrane of the lower genitourinary tract in postmenopausal women. Probl Endokrinol. 2022; 68 (6): 157–63.
18. Islam RM, et al. Safety and efficacy of testosterone for women: a systematic review and meta-analysis of randomised controlled trial data. Lancet Diabetes Endocrinol. 2019; 7 (10): 754–66.
19. Chen Y, et al. Enhancing osteoporosis treatment with engineered mesenchymal stem cell-derived extracellular vesicles: mechanisms and advances. Cell Death Dis. 2024; 15 (2): 119.
20. Guo C, et al. Mesenchymal stem cells therapy improves ovarian function in premature ovarian failure: a systematic review and meta-analysis based on preclinical studies. Front Endocrinol. 2023; 14.
21. Hetemäki N, et al. Estrogen Metabolism in Abdominal Subcutaneous and Visceral Adipose Tissue in Postmenopausal Women. J Clin Endocrinol Metab. 2017; 102 (12): 4588–95.
22. Anderson LA, et al. The effects of androgens and estrogens on preadipocyte proliferation in human adipose tissue: influence of gender and site. J Clin Endocrinol Metab. 2001; 86 (10): 5045–51.
23. Blouin K, et al. Effects of androgens on adipocyte differentiation and adipose tissue explant metabolism in men and women. Clin Endocrinol (Oxf). 2010; 72 (2): 176–88.
24. Hetemäki N, et al. Adipose tissue estrogen production and metabolism in premenopausal women. J Steroid Biochem Mol Biol. 2021; 209: 105849.
25. Hetemäki N, et al. Adipose Tissue Sex Steroids in Postmenopausal Women With and Without Menopausal Hormone Therapy. J Clin Endocrinol Metab. 2025; 110 (2): 511–22.
26. Kim C, et al. Changes in androstenedione, dehydroepiandrosterone, testosterone, estradiol, and estrone over the menopausal transition. Womens Midlife Health. 2017; 3 (1): 9.
27. Greendale GA, et al. Changes in Regional Fat Distribution and Anthropometric Measures Across the Menopause Transition. J Clin Endocrinol Metab. 2021; 106 (9): 2520–34.
28. Kodoth V, Scaccia S, Aggarwal B. Adverse Changes in Body Composition During the Menopausal Transition and Relation to Cardiovascular Risk: A Contemporary Review. Womens Health Rep (New Rochelle). 2022; 3 (1): 573–81.
29. Fenton A. Weight, Shape, and Body Composition Changes at Menopause. J Life Health. 2021; 12 (3): 187–92.
30. Piché M-E, et al. Regional body fat distribution and metabolic profile in postmenopausal women. Metabolism. 2008; 57 (8): 1101–7.

NGS TECHNOLOGY AS A TOOL FOR THE WILSON'S DISEASE DIAGNOSIS AND SEVERITY ASSESSMENT

Balashova MS[1,2], Zhuchenko NA[1], Tuluzanovskaya IG[1] ✉, Glotov OS[3,4,5], Senina OS[1], Ignatova TM[6], Asanov AYu[1]

[1] Sechenov First Moscow State Medical University (Sechenov University), Moscow, Russia
[2] Petrovsky National Research Centre of Surgery, Moscow, Russia
[3] Moscow Scientific and Practical Center for Laboratory Research, Moscow, Russia
[4] Ott Research Institute of Obstetrcis, Gynecology and Reproductive Medicine, St. Petersburg, Russia
[5] Federal Scientific and Clinical Center for Infectious Diseases of the Federal Medical Biological Agency, St. Petersburg, Russia
[6] State Scientific Center of the Russian Federation — Federal Medical Biophysical Center named after A. I. Burnazyan, Moscow, Russia

For several decades, Wilson's disease (WD) has remained the focus of attention for a wide range of specialists, including hepatologists, general practitioners, neurologists, geneticists, etc. However, despite significant advances in understanding its molecular basis, establishing clear correlations between the genotype and clinical phenotype of the disease remains a key unresolved issue. The study aimed to identify patterns between genetic variants in the *ATP7B* gene and the WD clinical manifestations using next-generation sequencing. The data from 81 WD patients, who were followed up between 2015 and 2019, were used in the study. Molecular genetic testing of biomaterial (blood) samples was performed by NGS. The analysis of the molecular genetic testing results using targeted NGS revealed 31 pathogenic variants. The following variants were the most frequent: c.3207C>A (p.His1069Gln) — 51.85% alleles, c.3190G>A (p.Glu1064Lys) — 8.64% alleles, and c.3402delC (p.Ala1135fs) — 6.17% alleles. A moderate correlation between genotype and phenotype was established: pathogenic variants (nonsense, frameshift, splicing) in the homo- or compound heterozygous state are associated with severe liver damage, severe degree of cirrhosis, and lower cholinesterase levels. The data obtained emphasize the importance of molecular genetic diagnosis for clarifying the diagnosis of WD and predicting the disease severity.

Keywords: Wilson's disease, *ATP7B* gene, genotype-phenotype correlation, next-generation sequencing

Author contribution: Balashova MS — follow-up of patients, NGS data analysis, manuscript writing; Zhuchenko NA — literature review and analysis, manuscript writing; Tuluzanovskaya IG — follow-up of patients, literature analysis and processing, manuscript writing; Glotov OS — molecular genetic testing data preparation, manuscript editing; Senina OS — data entry, manuscript writing; Ignatova TM — literature analysis, manuscript editing; Asanov AYu — literature analysis, manuscript writing and editing.

Compliance with ethical standards: the study was approved by the Ethics Committee of the Sechenov University (protocol No. 07-23 dated 27 April 2023). All subjects or their legall representatives submitted the informed consent for participation in the study.

✉ **Correspondence should be addressed:** Inna G. Tuluzanovskaya
Yelansky, 2, bld. 2, 119435, Moscow, Russia; inna_t77@mail.ru

Received: 24.02.2026 **Accepted:** 11.03.2026 **Published online:** 01.04.2026

DOI: 10.24075/brsmu.2026.012

NGS-ТЕХНОЛОГИИ КАК ИНСТРУМЕНТ ДИАГНОСТИКИ И ОЦЕНКИ ТЯЖЕСТИ ПАТОЛОГИЧЕСКОГО ПРОЦЕССА ПРИ БОЛЕЗНИ ВИЛЬСОНА–КОНОВАЛОВА

М. С. Балашова[1,2], Н. А. Жученко[1], И. Г. Тулузановская[1] ✉, О. С. Глотов[3,4,5], О. С. Сенина[1], Т. М. Игнатова[6], А. Ю. Асанов[1]

[1] Первый Московский государственный медицинский университет имени И. М. Сеченова (Сеченовский Университет), Москва, Россия
[2] Российский научный центр хирургии имени Б. В. Петровского, Москва, Россия
[3] Московский научно-практический центр лабораторных исследований, Москва, Россия
[4] Научно-исследовательский институт акушерства, гинекологии и репродуктологии имени Д. О. Отта, Санкт-Петербург, Россия
[5] Федеральный научно-клинический центр инфекционных болезней Федерального медико-биологического агентства России, Санкт-Петербург, Россия
[6] Государственный научный центр Российской Федерации — Федеральный медицинский биофизический центр имени А. И. Бурназяна, Москва, Россия

На протяжении нескольких десятилетий болезнь Вильсона–Коновалова (БВК) остается в фокусе внимания широкого круга специалистов: гепатологов, терапевтов, неврологов, генетиков и др. Однако несмотря на значительный прогресс в понимании ее молекулярных основ, одной из ключевых нерешенных проблем остается установление четких корреляций между генотипом и клиническим фенотипом заболевания. Целью работы было выявить закономерности между генетическими вариантами в гене *ATP7B* и клиническими проявлениями БВК на основе метода секвенирования нового поколения. В работе использовали данные 81 пациента с БВК, которых наблюдали в период с 2015 по 2019 гг. Молекулярно-генетическое исследование образцов биоматериала (кровь) проводили методом NGS. При анализе результатов молекулярно-генетического исследования методом таргетного NGS выявлен 31 патогенный вариант. Наибольшую частоту имели варианты: c.3207C>A (p.His1069Gln) — 51,85% аллелей, c.3190G>A (p.Glu1064Lys) — 8,64% аллелей и c.3402delC (p.Ala1135fs) — 6,17% аллелей. Установлена умеренная корреляция генотипа и фенотипа: патогенные варианты (нонсенс, фреймшифт, сплайсинг) в гомо- или компаунд-гетерозиготном состоянии ассоциированы с тяжелым поражением печени, выраженной степенью цирроза и более низким уровнем холинэстеразы. Полученные данные подчеркивают важность молекулярно-генетической диагностики для уточнения диагноза БВК и прогнозирования тяжести течения заболевания.

Ключевые слова: болезнь Вильсона–Коновалова, ген *ATP7B*, корреляция генотип-фенотип, секвенирование нового поколения

Вклад авторов: М. С. Балашова — курация пациентов, анализ данных NGS, написание статьи; Н. А. Жученко — обзор и анализ литературы, написание статьи; И. Г. Тулузановская — курация пациентов, анализ литературы, обработка и написание статьи; О. С. Глотов — подготовка данных молекулярно-генетического исследования, редактирование статьи; О. С. Сенина — работа с данными, редактирование статьи; Т. М. Игнатова — анализ литературы, редактирование статьи; А. Ю. Асанов — анализ литературы, написание и редактирование статьи.

Соблюдение этических стандартов: исследование одобрено этическим комитетом Сеченовского университета (протокол № 07-23, от 27 апреля 2023 г.). Все участники исследования либо их законные представители подписали добровольное информированное согласие на участие в научном исследовании.

✉ **Для корреспонденции:** Инна Геннадьевна Тулузановская
ул. Еланского, д. 2, строение 2, г. Москва, 119435, Россия; inna_t77@mail.ru

Статья получена: 24.02.2026 **Статья принята к печати:** 11.03.2026 **Опубликована онлайн:** 01.04.2026

DOI: 10.24075/vrgmu.2026.012

Wilson's disease (WD, OMIM #277900) is an autosomal recessive copper metabolism disorder caused by pathogenic and likely pathogenic variants in the gene *ATP7B* encoding the hepatocyte copper-transporting ATPase [1]. The disease is characterized by excessive accumulation of copper in the liver, brain, cornea, and other organs, resulting in the broad spectrum of clinical manifestations: from acute liver failure to neurological and psychiatric symptoms. Despite its monogenic nature, the WD phenotypic heterogeneity is extremely high: the age of onset can vary between 2 and 72 years, and clinical features can include isolated liver damage, as well as neurological symptoms without liver failure, the combination of those, and various extrahepatic manifestations [1].

The genotype-phenotype correlation is one of the key factors of such variability. To date, more than 1000 variants in *ATP7B* associated with WB have been reported; a number of studies demonstrate the association of certain variants with the earlier onset and more severe disease course, or with the late onset and predominantly hepatic form [2, 3].

In various populations, the genotype-phenotype differences manifest themselves in view of the most common/major variant. Thus, p.His1069Gln (H1069Q) is most common in Europe; homozygosity for the variant is associated with the late disease onset and predominance of neurological symptoms [3, 4]. The p.Arg778Leu (R778L) variant, which is associated with the earlier onset (often in childhood) and predominantly hepatic form, prevails in East Asian populations [2, 5].

The unique/specific frequent nucleotide sequences also showing characteristic clinical features are found in some regions (for example, c.-436_-422del in India and p.Val1146Met in Sardinia) [6].

Meta-analyses confirm that nonsense and frameshift variants leading to complete absence of functional protein are correlated to the more severe and earlier disease, while the missense variants preserving ATP7B residual activity are more often associated with the milder phenotype and late onset [2, 7].

Thus, understanding of genotype-phenotype correlations in Wilson's disease are of not only theoretical, but also practical significance: it allows one to predict the disease course, determine screening priority in specific ethnic groups, and, perhaps, develop personalized approaches to therapy in the future.

The study aimed to identify correlations between genetic variants in the *ATP7B* gene and the WD clinical manifestations using next-generation sequencing.

METHODS

The study was based on the analysis of data of 81 patients with the diagnosis of Wilson's disease verified by next generation sequencing (NGS). Information was obtained from the clinical genetic database containing the data on 296 WD patients. The patients were followed up at the Clinical Center (Tareyev Rheumatology, Nephrology, and Occupational Pathology Clinic) of the Sechenov First Moscow State Medical University (Sechenov University) between 2015 and 2019.

The diagnosis of WD was established in accordance with the Russian and European guidelines using the Leipzig Score (Leipzig, 2001). The main criteria for establishing the diagnosis were as follows: results of the gene *ATP7B* molecular genetic testing; typical clinical manifestations (hepatic and neurological symptoms, Kayser–Fleischer ring); copper metabolism indicators.

The laboratory diagnosis included complete blood counts and clinical urine test; blood biochemistry panel (including assessment of the levels of liver transaminase activity, lipid profile, iron metabolism indicators); copper metabolism indicator testing (plasma ceruloplasmin, 24-hour urine copper tests). Instrumental methods included abdominal ultrasound, ophtalmological slit lamp examination.

Molecular genetic testing of biomaterial (blood) samples by NGS was performed at the Ott Research Institute of Obstetrcis, Gynecology and Reproductive Medicine. The target NGS panel was used that included the *ATP7B* gene and a number of potential genetic modifiers: *HFE*, *COMMD1*, *XIAP, CFTR*, *APOE*, *PRNP*.

The panel was implemented on the NimbleGen SeqCap EZ Choice platform (151012_HG38_CysFib_EZ_HX3, ROCHE, Switzerland). Sequencing was performed using the MiSeq Sequencing System (Illumina, USA) ensuring high-throughput whole genome sequencing.

The variants identified were confirmed by Sanger sequencing.

Bioinformatics analysis

Bioinformatics analysis of the DNA sample sequencing results was conducted using the following software tools: GeneTalk (https://www.gene-talk.de/), UGENE (http://ugene.unipro.ru/), IonReporter (https://ionreporter.lifetechnologies.com/ir/), PolyPhen-2 (genetics.bwh.harvard.edu/pph2/), and PAPI ((http://papi.unipv.it/).

The data obtained were interpreted in accordance with the recommendations of the data interpretation Guidelines [8, 9].

Pathogenicity prediction software tools were used to predict the effect of variants: SIFT (http://sift.jcvi.org/), PolyPhen-2 (genetics.bwh.harvard.edu/pph2/), ClinVar, PROVEAN, fathmm-MKL, WilsonGen, etc.

Statistical analysis

Standard statistical analysis methods were used in the study. Statistical data processing was performed using the IBM SPSS Statistics software package (USA), as well as Microsoft Excel.

RESULTS

Biomaterials of patients, which were through *ATP7B* testing by NGS, were selected in the clinical genetic database of WD patients formed [10]. The total number of patients was 81 (among them 23 males and 58 females), the patients' average age at the time of examination was 29.21 ± 6.5 (8–68 years).

Clinical characteristics

Signs of liver damage prevailed in the vast majority of patients (60%). A total of 65.72% of these patients had hepatic manifestations only, and 34.28% of patients showed minimal neurological manifestations.

The combination of hepatic and cerebral manifestations (neurological and psychiatric) was found in 31%. A total of 9% were asymptomatic (the disease was detected during family screening, and treatment was started before the disease onset). The average age of the patients identified during family screening was 15.85 (7–27 years)

The WD onset variants were segregated by severity: severe course (decompensated cirrhosis, fulminant hepatitis, liver failure) — 25.8%; relatively mild course (chronic hepatitis, cirrhosis without failure, extrahepatic manifestations) — 38.5%; extrahepatic pathology — 35.7% of cases.

The average age of WD onset was 18.21 ± 8.55 (5–45 years) (Fig.).

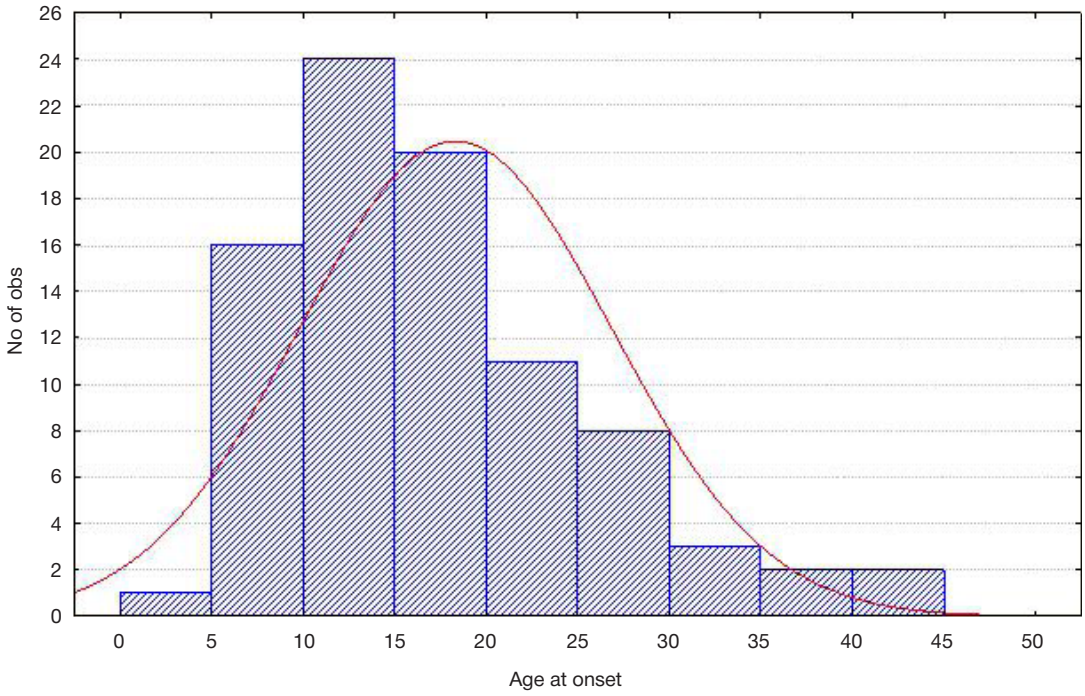

Fig. Patients' age of disease onset

Assessment of biochemical markers also showed that the patients' average ceruloplasmin level reached 0.113 g/L. The distribution of values across groups was as follows: 38.7% had the levels below 0.1 g/L, a half of surveyed individuals (50%) had the levels between 0.1 and 0.2 g/L, and 11.3% had normal values (over 0.2 g/L).

The analysis of 24-h urinary copper excretion showed that the average value was 466.75 μg/day, with the considerable variation (standard deviation 635.82). The levels did not exceed the normal value of 50 μg/day only in a small number of patients (4.6%).

The diagnosis timing analysis revealed a significant delay in the majority of cases. Wilson's disease was detected within three months after the emergence of symptoms only in a third of patients (33%). In 29% of patients the diagnosis took from three months to a year, in 30% — from one year to 10 years, and in 8% of patients the diagnosis was established more than 10 years after the disease onset.

During therapy 48.8% of patients received combination treatment with D-PAm and zinc sulfate. A total of 40.2% received D-Pam monotherapy, and 8.5% took zinc sulfate only. The average duration of anti-copper therapy before clinical stabilization was achieved was 10.25 ± 4.7 months, and individual ranges varied between 2 and 36 months.

The WD development dynamics was assessed no earlier than two years after the diagnosis and start of treatment (Table 1). In the Tareyev Clinic, patients were followed up for on average of 5.8 years; the longest follow-up period was 46 years.

Range and frequency of pathogenic and likely pathogenic variants in the gene ATP7B

The study involved *ATP7B* gene sequencing in 81 patients with confirmed WD. The core group of patients was represented by Russians. A total of 31 pathogenic variants were identified. The list, characteristics, and abundance of those are provided in Table 2.

NGS allowed us to identify nucleotide sequences on both chromosomes in 96% and 98% of alleles. In 4% of patients (2% of alleles), no candidate variants were found, despite elaborative clinical features of WD.

Three variants predominated among the nucleotide sequences identified: c.3207C>A (p.His1069Gln) — the most common, found in 51.85% of alleles; c.3190G>A (p.Glu1064Lys) — found in 8.64% of alleles; c.3402delC (p.Ala1135fs) — reported in 6.17% of alleles. The majority of patients (72.5%) turned out to be compound heterozygotes; in 16.15% of cases, sporadic rare *ATP7B* gene variants were identified. The previously undescribed variants potentially associated with the WD development were detected: c.1870-8A>G; c.3655A>T (p.Ile1219Phe); c.3036dupC (p.Lys1013fs).

The distribution of variants by effects was as follows: 73.33% — missense, 14% of alleles — frameshift, 4.67% — splice site variants, 4% — nonsense, 4% — indel. Variants were found in all the *ATP7B* gene exons, except 1, 3, 5, 9, 10, 12, and 21.

Table 1. Dynamic changes in the disease course

Indicators	Initial examination	Follow-up examination
Liver cirrhosis (decompensated)	23.90%	0
Neurological symptoms (including sleep disorder, headache)	29.10%	20.90%
Kidney disease	15.10%	10.50%
Kayser–Fleischer ring	72.10%	19.80%
Hepatomegaly (ultrasonography)	64%	42.80%
Complaints (no complaints)	30.60%	40.70%

Table 2. *ATP7B* gene variants identified

Domain	Exon	Variant	Effect	Abundance, %
Metal-binding	2	c.331C>T (p.Gln111*)	stop	1.85
	2	c.403_404delTC(p.Ser135fs)	frameshift	0.62
	2	c.414_415insAG (p.Pro139fs)	frameshift	1.24
	4	c.1630C>T (p.Gln544*)	stop	0.62
Transmembrane	6	c.1870-8A>G	splising	0.62
	7	c.1969A>C (p.Ser657Arg)	missens	0.62
		c.1971dupC (p.Met658fs)	frameshift	0.62
		c.2121+3A>G	splising	0.62
	8	c.2128G>A (p.Gly710Ser)	missens	0.62
		c.2293G>A (p.Asp765Asn)	missens	0.62
		c.2304dupC (p.Met769fs)	frameshift	4.94
		c.2332C>G (p.Arg778Gly)	missens	2.47
		c.2336G>A (p.Trp779*)	stop	0.62
Phosphatase	11	c.2605G>T (p.Gly869*)	stop	0.62
Transmembrane	13	c.2998G>A (p.Gly1000Arg)	missens	0.62
		c.3036dupC (p.Lys1013fs)	frameshift	1.23
Phosphorylating	14	c.3190G>A (p.Glu1064Lys)	missens	8.64
		c.3207C>A (p.His1069Gln)	missens	51.85
Transmembrane	15	c.3402delC (p.Ala1135fs)	frameshift	6.17
	16	c.3556+1G>T	splising	0.62
ATP-binding	17	c.3098C>T(p.Thr1033Ile)	missens	0.62
		c.3646G>A (p.Val1216Met)	missens	0.62
		c.3649_3654delGTTCTG	indel	4.32
		c.3655A>T (p.Ile1219Phe)	missens	0.62
		c.3659C>T (p.Thr1220Met)	missens	0.62
Phosphorylating	18	c.3809A>G (p.Asn1270Ser)	missens	0.62
Transmembrane	19	c.3948delG (p.Thr1317fs)	frameshift	0.62
		c.3955C>T (p.Arg1319*)	stop	0.62
		c.3965G>C (p.Arg1322Pro)	missens	0.62
C-terminus (stabilizing function)	20	c.4022G>A (p.Gly1341Asp)	missens	0.62
		c.4125-2A>G	splising	2.47

Note: adapted from [11].

Assessment of the relationship between nucleotide variants and WD severity

In the study, we analyzed the association of the effect of nucleotide sequences in the gene *ATP7B* and the WD severity. The following were considered as the disease severity criteria: age of onset (three categories: under the age of 15 years; 15–31 years; over the age of 31 years); the degree of liver damage at the time of disease onset (decompensated cirrhosis — 33%, compensated cirrhosis — 49.4%, no cirrhosis — 17.3%).

Nucleotide sequences were grouped based on their potential effects on the protein product (Table 3):

1. Severe abnormalities in both gene copies — nonsense variants, frameshift variants, splice site variants.

2. Mixed effect — severe abnormalities in one gene copy (nonsense, frameshift, splicing) and relatively mild in another one (missense variants, indels).

3. Mild abnormalities in both gene copies — missense variants, indels.

Age of onset: no significant correlation between the genotype (based on the nucleotide sequence effect on protein synthesis) and the age of disease onset was revealed; the cases of late onset (≥ 31 years) were reported only in patients, who were homozygous or compound heterozygous for the major variant.

Liver damage: the lack of cirrhosis was more often reported in homozygous or compound heterozygous carriers of the c.3207C>A (p.His1069Gln) variants (15% vs. 2.3%); patients with nonsense, frameshift or splicing variants in both ATP7B gene copies more often showed decompensated liver cirrhosis at onset, and the age of onset was below 15 years.

Thus, the following correlations were reported:

– moderate correlation between the WD manifestation type and the genotype (based on the nucleotide sequence effect on protein synthesis): correlation coefficient $r = -0.305$ ($p = 0.009$);

– moderate correlation between the liver cirrhosis class (Child-Pugh score) and the potential effect of nucleotide variants: $r = -0.374$ ($p = 0.004$);

– moderate correlation between blood cholinesterase (CE) levels and the effect of nucleotide sequences: moderate correlation $r = 0.5368$ ($p = 0.004$).

DISCUSSION

The paper reports the data of patients diagnosed with Wilson's disease verified by NGS, as well as the results of assessing the

Table 3. Distribution of patients when divided into groups based on the nucleotide sequence potential effect

Genotype	Percentage of distinct genotypes	Mutation severity group	Percentage of groups based on the effect
frameshift/ frameshift	3%	1	8%
frameshift /nonsence	2%		
frameshift/splising	3%		
frameshift /indel	3%	2	34%
frameshift /missense	19%		
missense / nonsence	8%		
missense / splising	4%		
missense / missense	56%	3	58%
missense / indel	2%		

relationship between the disease severity and types of variants in the gene *TP7B*.

The analysis has shown that the data obtained are consistent with the up-to-date understanding of the WD clinical manifestations and genetic diversity. In particular, it has been proven that variants with complete loss of protein function are correlated to the more severe disease form. At the same time, we have identified some features specific for the studied cohort.

Clinical polymorphism of the disease and predominance of the abdominal form have been confirmed [12–14]. The age of onset and diagnosis timing are consistent with global trends [12, 15]. However, some differences have been noted. Thus, the share of asymptomatic cases in our cohort (30.6%) was higher, than in most published studies (10–20%) [16].

Today, the NGS method is extensively used to study WD genetic features all over the world. In our study, the c.3207C>A (p.His1069Gln) variant turned out to be the most common (51.85% of alleles), which is in line with the data reported for Russia and Eastern Europe [17, 18]. The c.3190G>A (p.Glu1064Lys) variant ranked second in frequency (8.63% of alleles), c.3402delC (p.Ala1135fs) ranked third (6.17% of alleles). Rare mutations were identified in 16.15% of alleles. Three nucleotide variants (c.1870–8A>G, c.3655A>T, c.3036dupC) were first described as pathogenic in terms of WD.

In a study by scientists from the Far East, a cohort of 100 people from Eastern Eurasia was analyzed. The major nucleotide sequence p.His1069Gln (c.3207C>A) was found in 48% of patients (homozygous form — in 30%); the p.Glu1064Lys (c.3190G>A) variant was found in 20%; the p.Met769HisfsTer26 (c.2304insC) was found in 8%; other variants accounted for 23.9% [17].

According to the Human Gene Mutation Database, the distribution of nucleotide sequence types in the gene *ATP7B* (60% — missense and nonsense variants; 26% — indels, 9% — splice site variants) was similar, but there was a larger share of missense variants (73.33%) [19].

In addition, we compared the range of nucleotide sequences identified in the gene *ATP7B* in this study with the diagnostic panel for Wilson's disease most commonly used in the RF (Table 4). Of 12 variants included in the routine diagnostic panel, four variants were detected: c.2304insC; c.3207C>A; c.3402delC; c.3649_3654del6. We identified three variants, which were regularly reported in patients we examined, but were not included in the standard panel: c.2332C>G (p.Arg778Gly); c.4125–2A>G; c.3190G>A (p.Glu1064Lys).

Molecular genetic testing by next-generation sequencing (NGS) showed high informational value when used to identify pathogenic variants associated with WD. The standard diagnostic panel used in the RF covers only part of the range of variants typical for the Russian population of patients with WD. The NGS method allows one to detect both common and rare variants, not included in standard panels. The data obtained substantiate the need to expand the existing diagnostic panels considering the regional specifics of the patients' genetic profile.

In the study, we assessed the relationship between genetic features (variant type, its pathogenetic effect) and WD clinical manifestations, specifically the disease course. We also revealed no significant correlation between the fact of being a homozygous major variant carrier and the disease severity or other clinical characteristics tested, as well as age and gender, like in the study conducted by Ferenci [14].

We revealed a significant correlation between the nucleotide sequences severely impairing the protein product function (nonsense, frameshift, splice site variants) and the following clinical signs: WD manifestation with severe liver damage; more severe liver cirrhosis at the time of diagnosis; decreased cholinesterase (CE) levels.

The findings are consistent with some studies. Thus, in one study a significant correlation was reported for nonsense mutations only, while the correlation for missense mutations was weak or lacking [4]. The correlation of nonsense and

Table 4. Informational value depending on the scope of genetic testing

Scope of the study	Informational value, %	
	By patients	By alleles
Only c.3207C>A	72.90%	51.85%
12 frequent variants: c.1340_1343del4, c.1770incT, c.2304insC, c.2532delCA, c.3026_3028delTCA, c.3029insT, c.3031insC, c.3207C>A, c.3402delC, c.3627_3630del4, c.3649_3654del6, c.3942deLAT, 3947deL	88.30%	62.80%
NGS of the gene *ATP7B*	96%	98%

frameshift variants with the earlier disease onset and more severe WD course was shown [20].

A number of large-scale studies showed only weak or lacking genotype-phenotype correlation. According to the study conducted by Chinese researchers, only 38% of age of onset variability can be explained by genotype [7].

According to the EuroWilson registry, genotype explains about 27% of age of onset variability and less than 20% of disease form variability (hepatic or neurological form) [21]. With the p.His1069Gln and p.Glu1064Lys missense variants, motor impairment was reported in в 53–58% of cases, brain MRI alterations in 59–69%, Kayser–Fleischer rings in 29–31%, cognitive impairment in 24–27% of cases. With the LOF variant p.Met769HisfsTer26, ultrasonography revealed changes in the liver in 60% of patients. No gender dependence was found [17].

Despite moderate correlation between the pattern of nucleotide sequences in the *ATP7B* gene and the Wilson's disease course severity identified in our study, it is still difficult to clearly determine genotype-phenotype relationships. This is due to a complex of interrelated factors that can be systematized in several key directions.

Genetic factors

Variable expression and clinical polymorphism. Thus, a broad spectrum of clinical manifestations, from asymptomatic course to severe multiple organ failure, was found within the same family having the same genotype [14, 22]. This suggests the impact of additional genetic and environmental modifiers.

High genetic heterogeneity. More than 60% of patients turned out to be compound heterozygotes for two different pathogenic variants. However, functional sequelae of the majority of rare nucleotide sequences are still poorly understood, which makes it difficult to predict the phenotype [23].

Lack of phenotype homogeneity in homozygotes for the major variant. Patients with the same genotype (for example, homozygotes for p.H1069Q) demonstrate significant differences in the age of onset, liver damage severity, and neurological symptoms [4, 7].

Influence of genetic modifiers. Along with the main gene *ATP7B*, the phenotype is influenced by variants in other genes: MTHFR (homocysteine metabolism); *COMD1*, *ATOX1*, *XIAP* (copper homeostasis); *APOE* (lipid metabolism); *PRNP*, *HFE* (common metabolic pathways), etc. These polymorphic variants have a significant impact on the age of onset (before 5–12 years) [24, 25].

Clinical and demographic factors

Gender differences. In females, the WD onset occurs on average 3–6 years later, than in males, which is associated with protective effects of estrogens on copper metabolism. Hormone levels, puberty, and menopause can provoke aggravation of symptoms or alter their severity [26].

Environmental and epigenetic factors

Features of the diet, increased copper consumption (for example, with drinking water or food products) can accelerate the disease onset.

Comorbidities. Viral hepatitis infection, alcohol abuse, or the use of hepatotoxic drugs worsens liver damage.

Epigenetic states. DNA methylation, histone modifications, and the action of non-coding RNAs can modulate the expression of ATP7B and modifier genes, affecting the phenotype [27].

Methodological study limitations

Heterogeneity of phenotyping criteria. Various scores for assessing the severity of liver damage, neurological symptoms, and biochemical markers are used in different studies. Insufficient family screening coverage. The lack of information about the relatives hampers segregation of genotypes and phenotypes in families.

Late diagnosis. Many patients seek care as late as in the phase of cirrhosis decompensation or neurological complications, which results in misrepresentation of the natural disease history.

Selective data loss. Patients with severe genotypes are more likely to undergo liver transplantation or die before inclusion in the study, which results in survivorship bias.

Small sample size. Small cohort size reduces statistical power to detect correlations, especially for rare mutations [13, 28].

The ED pathogenesis multifactorial nature explains difficulties in determining clear genotype-phenotype associations. The following is necessary to overcome these limitations: large multicenter studies involving the standardized phenotyping criteria; comprehensive analysis of not only *ATP7B*, but also genetic modifiers; consideration of environmental and epigenetic factors in prediction models; prospective follow-up of families with the identified genotype.

It is only such integrated approach that will make it possible to increase the WD course prediction accuracy and personalize therapeutic strategies.

Despite the lack of direct correlation between the genotype and the WD age of onset, the analysis conducted has shown that the liver damage severity depends on the nature of nucleotide variants. The use of NGS methods in clinical practice significantly simplifies and accelerates the diagnosis of WD, which allows for the prompt initiation of anti-copper therapy.

CONCLUSIONS

The study involving the use of next-generation sequencing (NGS) in the cohort of Russian patients with Wilson's disease (WD) revealed 31 pathogenic variants in the gene *ATP7B*, among which c.3207C>A (p.His1069Gln), c.3190G>A (p.Glu1064Lys), and c.3402delC (p.Ala1135fs) were the most common. We identified a correlation between the nucleotide sequences causing severe ATP7B protein abnormalities (nonsense, frameshift, and splice site variants) and adverse clinical manifestations of WD (severe liver damage, severe cirrhosis, decreased cholinesterase levels), while homozygosity for the c.3207C>A (p.His1069Gln) variant was not correlated to the disease severity. The data obtained confirm high diagnostic efficacy of NGS in WD and emphasize promise of further research focused on genotype-phenotype interactions for therapy personalization and patient management improvement.

References

1. Ferenci P, Caca K, Loudianos G, et al. Diagnosis and phenotypic classification of Wilson disease: A European reference network for rare liver diseases (ERN RARE-LIVER) expert consensus statement. J Hepatol. 2023; 79 (2): 508–21. DOI: 10.1016/j.jhep.2023.04.011.
2. Chang IJ, Hahn SH. The genetics of Wilson disease. Handb Clin Neurol. 2017; 142: 19–34. DOI: 10.1016/B978-0-444-63625-6.00003-3.
3. Przybyłkowski A, Gromadzka G, Członkowska A. Genotype-phenotype correlation in Wilson's disease. J Neurol. 2014; 261 (8): 1467–473. DOI: 10.1007/s00415-014-7391-3.
4. Couchonnal E, Bouchard N, Poupon J, et al. Genotype–phenotype correlations in a large cohort of Wilson disease patients in France. J Hepatol. 2024; 80 (3): 416–25. DOI: 10.1016/j.jhep.2023.11.020.
5. Xie JJ, Wu ZY. Wilson's disease in China. Neurosci Bull. 2017; 33 (3): 323–30. DOI: 10.1007/s12264-017-0100-8.
6. Lepori MB, Zappu A, Incollu S, et al. Mutation analysis of the ATP7B gene in a new group of Wilson's disease patients: contribution to diagnosis. Mol Cell Probes. 2012; 26 (4): 147–50. DOI: 10.1016/j.mcp.2012.03.007.
7. Lu Y, Zhang J, Li R, et al. Genotype-phenotype correlation in 1337 patients with Wilson disease. Liver Int. 2023; 43 (8): 1745–56. DOI: 10.1111/liv.15627.
8. Ryzhkova OP, Kardymon OL, Prohorchuk EB, Konovalov FA, Maslennikov AB, Stepanov VA, i dr. Rukovodstvo po interpretacii dannyh posledovatel'nosti DNK cheloveka, poluchennyh metodami massovogo parallel'nogo sekvenirovaniya (MPS) (redakciya 2018, versiya 2). Medicinskaya genetika. 2019; 18 (2): 3–23. Russian.
9. Richards S, Aziz N, Bale S, Bick D, Das S, Gastier-Foster J, et al. Standards and guidelines for the interpretation of sequence variants: a joint consensus recommendation of the American College of Medical Genetics and Genomics and the Association for Molecular Pathology. Genet Med. 2015; 17 (5): 405–24. DOI: 10.1038/gim.2015.30.
10. Tuluzanovskaya IG, Balashova MS, ZHuchenko NA, Rozina TP, Starostina EE, Glotov OS, i dr. Kliniko-geneticheskaya baza dannyh pacientov s bolezn'yu Vil'sona–Konovalova. Svidetel'stvo o gosudarstvennoj registracii bazy dannyh RF № 2024626180. 19.12.2024. Russian.
11. Balashova MS, Tuluzanovskaya IG, Glotov OS, Glotov AS, Barbitoff YA, Fedyakov MA, et al. The spectrum of pathogenic variants of the ATP7B gene in Wilson disease in the Russian Federation. J Trace Elem Med Biol. 2020; 59: 126420. DOI: 10.1016/j.jtemb.2019.126420. Epub 2019 Oct 25.
12. Socha P, Janczyk W, Dhawan A, Baumann U, D'Antiga L, Tanner S, et al. Wilson's Disease in Children: A Position Paper by the Hepatology Committee of the European Society for Paediatric Gastroenterology, Hepatology and Nutrition. J Pediatr Gastroenterol Nutr. 2018; 66 (2): 334–44. DOI: 10.1097/MPG.0000000000001787.
13. EASL Clinical Practice Guidelines on Wilson disease. J Hepatol. 2022; 77 (2): 545–71. DOI: 10.1016/j.jhep.2022.04.010.
14. Ferenci P, Stremmel W, Członkowska A, et al. Age and sex but not ATP7B genotype effectively influence the clinical phenotype of Wilson disease. Hepatology. 2019; 69 (4): 1464–81. DOI: 10.1002/hep.30280.
15. Podymova SD. Bolezn' Vil'sona–Konovalova. Osobennosti debyuta, techeniya zabolevaniya, trudnosti diagnostiki, faktory progressirovaniya. Eksperimental'naya i klinicheskaya gastroenterologiya. 2022; 204 (8): 77–83. DOI: 10.31146/1682–8658-ecg-204–8–77–83. Russian.
16. Ganaraja VH, Holla VV, Pal PK. Current Management of Neurological Wilson's Disease. Tremor Other Hyperkinet Mov (NY). 2025; 15: 17. DOI: 10.5334/tohm.938.
17. Garbuz M, Ovchinnikova E, Ovchinnikova A, Vinokurova V, Aristarkhova Y, Kuziakova O, et al. Spectrum of Pathogenic Variants of the ATP7B Gene and Genotype-Phenotype Correlation in Eastern Eurasian Patient Cohorts with Wilson's Disease. Biomedicines. 2024; 12 (12): 2833. DOI: 10.3390/biomedicines12122833.
18. Ovchinnikova EV, Garbuz MM, Ovchinnikova AA, Kumeiko VV. Epidemiology of Wilson's Disease and Pathogenic Variants of the ATP7B Gene Leading to Diversified Protein Disfunctions. Int J Mol Sci. 2024; 25 (4): 2402. DOI: 10.3390/ijms25042402.
19. Human Genom Mutation Database. Available from: https://portal.biobaseinternational.com/hgmd/pro/start.php.
20. Gromadzka G, Schmidt HH, Genschel J, Bochow B, Rodo M, Tarnacka B, et al. Frameshift and nonsense mutations in the gene for ATPase7B are associated with severe impairment of copper metabolism and with an early clinical manifestation of Wilson's disease. Clin Genet. 2005; 68 (6): 524–32. DOI: 10.1111/j.1399-0004.2005.00528.x.
21. European Association for the Study of the Liver. EASL-ERN Clinical Practice Guidelines on Wilson's disease. J Hepatol. 2025: S0168-8278(24)02706-5. DOI: 10.1016/j.jhep.2024.11.007.
22. Litwin T, Gromadzka G, Członkowska A. Monozygotic twins with Wilson's disease: a detailed phenotypic description. Mov Disord. 2012; 27 (14): 1820–1. DOI: 10.1002/mds.25205/.
23. Sandahl TD, et al. The prevalence and spectrum of ATP7B mutations in a large cohort. Hepatology. 2022; 76 (3): 745–57. DOI: 10.1002/hep.32445
24. Stättermayer AF, et al. Genetic modifiers of clinical presentation in Wilson disease. Hepatology. 2022; 75 (4): 912–23. DOI: 10.1002/hep.32214.
25. Weiss KH, et al. MTHFR and COMMD1 polymorphisms influence age at diagnosis in Wilson disease. J Hepatol. 2023; 78: S213 (EASL abstract).
26. Pfeiffenberger J, et al. Sex-specific differences in presentation and outcome of Wilson disease. Liver Int. 2023; 43 (10): 2210–9. DOI: 10.1111/liv.15678.
27. Roberts EA, Schilsky ML. Environmental and dietary influences on copper toxicity and Wilson disease. Hepatology. 2022; 76 (6): 1625–37. DOI: 10.1002/hep.32645.
28. Dong Y, et al. Methodological issues in genotype-phenotype studies of Wilson disease. Hepatol Int. 2024; 18 (2): 412–20. DOI: 10.1007/s12072-023-10612-4.

Литература

1. Ferenci P, Caca K, Loudianos G, et al. Diagnosis and phenotypic classification of Wilson disease: A European reference network for rare liver diseases (ERN RARE-LIVER) expert consensus statement. J Hepatol. 2023; 79 (2): 508–21. DOI: 10.1016/j.jhep.2023.04.011.
2. Chang IJ, Hahn SH. The genetics of Wilson disease. Handb Clin Neurol. 2017; 142: 19–34. DOI: 10.1016/B978-0-444-63625-6.00003-3.
3. Przybyłkowski A, Gromadzka G, Członkowska A. Genotype-phenotype correlation in Wilson's disease. J Neurol. 2014; 261 (8): 1467–473. DOI: 10.1007/s00415-014-7391-3.
4. Couchonnal E, Bouchard N, Poupon J, et al. Genotype–phenotype correlations in a large cohort of Wilson disease patients in France. J Hepatol. 2024; 80 (3): 416–25. DOI: 10.1016/j.jhep.2023.11.020.
5. Xie JJ, Wu ZY. Wilson's disease in China. Neurosci Bull. 2017; 33 (3): 323–30. DOI: 10.1007/s12264-017-0100-8.
6. Lepori MB, Zappu A, Incollu S, et al. Mutation analysis of the ATP7B gene in a new group of Wilson's disease patients: contribution to diagnosis. Mol Cell Probes. 2012; 26 (4): 147–50. DOI: 10.1016/j.mcp.2012.03.007.
7. Lu Y, Zhang J, Li R, et al. Genotype-phenotype correlation in 1337 patients with Wilson disease. Liver Int. 2023; 43 (8): 1745–56. DOI: 10.1111/liv.15627.
8. Рыжкова О. П., Кардымон О. Л., Прохорчук Е. Б., Коновалов Ф. А., Масленников А. Б., Степанов В. А., и др. Руководство по интерпретации данных последовательности ДНК человека, полученных методами массового параллельного секвенирования (MPS) (редакция 2018, версия 2). Медицинская генетика. 2019; 18 (2): 3–23.
9. Richards S, Aziz N, Bale S, Bick D, Das S, Gastier-Foster J, et al. Standards and guidelines for the interpretation of sequence

variants: a joint consensus recommendation of the American College of Medical Genetics and Genomics and the Association for Molecular Pathology. Genet Med. 2015; 17 (5): 405–24. DOI: 10.1038/gim.2015.30.
10. Тулузановская И. Г., Балашова М. С., Жученко Н. А., Розина Т. П., Старостина Е. Е., Глотов О. С., и др. Клинико-генетическая база данных пациентов с болезнью Вильсона–Коновалова. Свидетельство о государственной регистрации базы данных РФ № 2024626180. 19.12.2024.
11. Balashova MS, Tuluzanovskaya IG, Glotov OS, Glotov AS, Barbitoff YA, Fedyakov MA, et al. The spectrum of pathogenic variants of the ATP7B gene in Wilson disease in the Russian Federation. J Trace Elem Med Biol. 2020; 59: 126420. DOI: 10.1016/j.jtemb.2019.126420. Epub 2019 Oct 25.
12. Socha P, Janczyk W, Dhawan A, Baumann U, D'Antiga L, Tanner S, et al. Wilson's Disease in Children: A Position Paper by the Hepatology Committee of the European Society for Paediatric Gastroenterology, Hepatology and Nutrition. J Pediatr Gastroenterol Nutr. 2018; 66 (2): 334–44. DOI: 10.1097/MPG.0000000000001787.
13. EASL Clinical Practice Guidelines on Wilson disease. J Hepatol. 2022; 77 (2): 545–71. DOI: 10.1016/j.jhep.2022.04.010.
14. Ferenci P, Stremmel W, Członkowska A, et al. Age and sex but not ATP7B genotype effectively influence the clinical phenotype of Wilson disease. Hepatology. 2019; 69 (4): 1464–81. DOI: 10.1002/hep.30280.
15. Подымова С. Д. Болезнь Вильсона–Коновалова. Особенности дебюта, течения заболевания, трудности диагностики, факторы прогрессирования. Экспериментальная и клиническая гастроэнтерология. 2022; 204 (8): 77–83. DOI: 10.31146/1682–8658-ecg-204–8–77–83.
16. Ganaraja VH, Holla VV, Pal PK. Current Management of Neurological Wilson's Disease. Tremor Other Hyperkinet Mov (NY). 2025; 15: 17. DOI: 10.5334/tohm.938.
17. Garbuz M, Ovchinnikova E, Ovchinnikova A, Vinokurova V, Aristarkhova Y, Kuziakova O, et al. Spectrum of Pathogenic Variants of the ATP7B Gene and Genotype-Phenotype Correlation in Eastern Eurasian Patient Cohorts with Wilson's Disease. Biomedicines. 2024; 12 (12): 2833. DOI: 10.3390/biomedicines12122833.
18. Ovchinnikova EV, Garbuz MM, Ovchinnikova AA, Kumeiko VV. Epidemiology of Wilson's Disease and Pathogenic Variants of the ATP7B Gene Leading to Diversified Protein Disfunctions. Int J Mol Sci. 2024; 25 (4): 2402. DOI: 10.3390/ijms25042402.
19. Human Genom Mutation Database. Available from: https://portal.biobaseinternational.com/hgmd/pro/start.php.
20. Gromadzka G, Schmidt HH, Genschel J, Bochow B, Rodo M, Tarnacka B, et al. Frameshift and nonsense mutations in the gene for ATPase7B are associated with severe impairment of copper metabolism and with an early clinical manifestation of Wilson's disease. Clin Genet. 2005; 68 (6): 524–32. DOI: 10.1111/j.1399-0004.2005.00528.x.
21. European Association for the Study of the Liver. EASL-ERN Clinical Practice Guidelines on Wilson's disease. J Hepatol. 2025: S0168-8278(24)02706-5. DOI: 10.1016/j.jhep.2024.11.007.
22. Litwin T, Gromadzka G, Członkowska A. Monozygotic twins with Wilson's disease: a detailed phenotypic description. Mov Disord. 2012; 27 (14): 1820–1. DOI: 10.1002/mds.25205/.
23. Sandahl TD, et al. The prevalence and spectrum of ATP7B mutations in a large cohort. Hepatology. 2022; 76 (3): 745–57. DOI: 10.1002/hep.32445
24. Stättermayer AF, et al. Genetic modifiers of clinical presentation in Wilson disease. Hepatology. 2022; 75 (4): 912–23. DOI: 10.1002/hep.32214.
25. Weiss KH, et al. MTHFR and COMMD1 polymorphisms influence age at diagnosis in Wilson disease. J Hepatol. 2023; 78: S213 (EASL abstract).
26. Pfeiffenberger J, et al. Sex-specific differences in presentation and outcome of Wilson disease. Liver Int. 2023; 43 (10): 2210–9. DOI: 10.1111/liv.15678.
27. Roberts EA, Schilsky ML. Environmental and dietary influences on copper toxicity and Wilson disease. Hepatology. 2022; 76 (6): 1625–37. DOI: 10.1002/hep.32645.
28. Dong Y, et al. Methodological issues in genotype-phenotype studies of Wilson disease. Hepatol Int. 2024; 18 (2): 412–20. DOI: 10.1007/s12072-023-10612-4.

A RELIABLE AND REPRODUCIBLE MULTIPLEX RT-QPCR ASSAY FOR *mTOR* GENE EXPRESSION ANALYSIS

Kornilov DO[1] ✉, Simarzina VM[1], Bekhter AA[1], Maslakov GP[2], Nechaeva DM[1], Kariakina AE[1], Fadeev FA[1,3], Voroshilina ES[1,4], Zornikov DL[1]

[1] Ural State Medical University, Yekaterinburg, Russia

[2] Institute of Cytology of the Russian Academy of Sciences, Saint Petersburg, Russia

[3] State Autonomous Health Institution of the Sverdlovsk Region "Center for Specialized Types of Medical Care 'Institute of Medical Cellular Technologies'", Yekaterinburg, Russia

[4] Medical Center "Garmoniya", Yekaterinburg, Russia

The PI3K/AKT/mTOR signaling pathway is a key regulator of cell growth, and its dysregulation is involved in oncogenesis. Existing methods for assessing *mTOR* activity have design flaws. The aim of this work was to develop and validate a novel multiplex RT-qPCR assay for relative quantification of *mTOR* gene expression normalized to *RPLP0* and *TBP*. Primers and probes were designed *in silico*. Validation was performed using the human SCP-1 cell line. Specificity was assessed in 10 separate and 10 multiplex runs. Analytical sensitivity and efficiency were determined from 27 technical replicates using a protocol without an elongation step. Specificity of amplification was assessed by agarose gel electrophoresis, and quantitative analysis was performed in real-time PCR using FAM (*mTOR*), HEX (*RPLP0*), and ROX (*TBP*) fluorescence channels. The assay showed 100% specificity. Stable detection was achieved at 125,000 cells/mL. Amplification efficiencies were 73–81%. The variation of *mTOR* expression normalized to *RPLP0* ranged from –21.5% to 26.4%, and normalized to *TBP* from –14.3% to 19.2%. Normalization to the geometric mean of both reference genes provided the best reproducibility, with an interquartile range from –9% to 23.4%. The developed assay demonstrates high specificity, sensitivity, and reproducibility, making it a reliable tool for subsequent clinical research.

Keywords: gene expression profiling, molecular diagnostics, multiplex polymerase chain reaction, reproducibility of results, reverse transcriptase polymerase chain reaction, TOR serine-threonine kinases

Acknowledgments: The authors express their gratitude to the staff of the Laboratory of Enteral Viral Infections, Federal Budgetary Institution of Science "Federal Scientific Research Institute of Viral Infections 'Virome'" of Rospotrebnadzor, for their assistance in organizing the work.

Author contribution: Kornilov DO — conceptualization, methodology, writing — original draft; Simarzina VM — investigation, methodology, visualization; Bekhter AA — investigation, visualization; Maslakov GP — investigation, software, validation; Nechaeva DM — methodology, writing — review and editing; Kariakina AE — methodology, writing — review and editing; Fadeev FA — resources, writing — review and editing; Voroshilina ES — supervision, project administration; Zornikov DL — supervision, visualization, formal analysis, writing — review and editing.

Compliance with ethical standards: The study was approved by the Local Ethical Committee of the Ural State Medical University, Yekaterinburg, Russia (Protocol No. 6 dated October 18, 2024). Informed consent was not applicable, as commercial cell lines were used.

✉ **Correspondence should be addressed:** Daniil O. Kornilov
Klyuchevskaya, 17, Yekaterinburg, 620109, Russia; danilovkornil@gmail.com

Received: 11.03.2026 **Accepted:** 25.03.2026 **Published online:** 31.03.2026

DOI: 10.24075/brsmu.2026.011

НАДЕЖНАЯ И ВОСПРОИЗВОДИМАЯ МУЛЬТИПЛЕКСНАЯ ОТ-ПЦР-РВ ТЕСТ-СИСТЕМА ДЛЯ КОЛИЧЕСТВЕННОЙ ОЦЕНКИ ЭКСПРЕССИИ ГЕНА *mTOR*

Д. О. Корнилов[1] ✉, В. М. Симарзина[1], А. А. Бехтер[1], Г. П. Маслаков[2], Д. М. Нечаева[1], А. Е. Карякина[1], Ф. А. Фадеев[1,3], Е. С. Ворошилина[1,4], Д. Л. Зорников[1]

[1] Уральский государственный медицинский университет, Екатеринбург, Россия

[2] Институт цитологии Российской академии наук, Санкт-Петербург, Россия

[3] Центр специализированных видов медицинской помощи «Институт медицинских клеточных технологий, Екатеринбург, Россия

[4] Медицинский центр «Гармония», Екатеринбург, Россия

Сигнальный путь PI3K/AKT/mTOR — ключевой регулятор роста клеток, его дисрегуляция вовлечена в онкогенез. Существующие способы оценки активности *mTOR* имеют недостатки дизайна. Целью работы было разработать и провести валидацию новой мультиплексной ОТ-ПЦР-РВ-тест-системы для относительного количественного анализа экспрессии гена *mTOR* с нормализацией на гены *RPLP0* и *TBP*. Праймеры и зонды сконструированы *in silico*. Валидацию проводили на клеточной линии стромальных клеток костного мозга человека SCP-1. Специфичность оценивали в 10 сепарированных и 10 мультиплексных постановках. Аналитическую чувствительность и эффективность определяли по 27 техническим повторам с использованием протокола без элонгации. Специфичность амплификации оценивали с помощью электрофореза в агарозном геле, а количественный анализ выполняли в режиме реального времени по каналам флуоресценции FAM (*mTOR*), HEX (*RPLP0*) и ROX (*TBP*). Тест показал 100%-ю специфичность. Стабильная детекция достигалась при 125 тыс. клеток/мл. Эффективность амплификации составила 73–81%. Вариация экспрессии *mTOR*, нормализованной на *RPLP0,* составила от –21,5 до 26,4%, по *TBP* от –14,3 до 19%. Нормализация на среднее геометрическое двух генов обеспечила лучшую воспроизводимость от –9 до 23,4%. Разработанный тест отличается высокой специфичностью, чувствительностью и воспроизводимостью, что делает его надежным инструментом для последующих клинических исследований.

Ключевые слова: профилирование экспрессии генов, молекулярная диагностика, мультиплексная полимеразная цепная реакция, воспроизводимость результатов, полимеразная цепная реакция с обратной транскрипцией, TOR-серин-треониновые киназы

Благодарности: авторы выражают благодарность сотрудникам лаборатории энтеральных вирусных инфекций ФБУН ФНИИВИ «Виром» Роспотребнадзора за помощь в организации работы.

Вклад авторов: Д. О. Корнилов — разработка концепции, методология, написание рукописи; В. М. Симарзина — проведение экспериментов, методология, визуализация; А. А. Бехтер — проведение экспериментов, визуализация; Г. П. Маслаков — проведение экспериментов, программное обеспечение, валидация; Д. М. Нечаева, А. Е. Карякина — методология, рецензирование и редактирование рукописи; Ф. А. Фадеев — ресурсы, рецензирование и редактирование рукописи; Е. С. Ворошилина — научное руководство, администрирование проекта; Д. Л. Зорников — научное руководство, визуализация, формальный анализ, рецензирование и редактирование рукописи.

Соблюдение этических стандартов: исследование одобрено этическим комитетом ФГБОУ ВО «Уральский государственный медицинский университет» Минздрава России, г. Екатеринбург (протокол № 6 от 18 октября 2024 г.). В работе использовали коммерческие клеточные линии.

✉ **Для корреспонденции:** Даниил Олегович Корнилов
ул. Ключевская, д. 17, г. Екатеринбург, 620109; danilovkornil@gmail.com

Статья получена: 11.03.2026 **Статья принята к печати:** 25.03.2026 **Опубликована онлайн:** 31.03.2026

DOI: 10.24075/vrgmu.2026.011

The phosphoinositide 3-kinase (PI3K)/protein kinase B (AKT)/mammalian target of rapamycin (mTOR) signaling pathway is a crucial regulator of cellular processes like proliferation and metabolism, with mTOR kinase acting as its central hub [1, 2]. Its dysregulation is implicated in a wide spectrum of pathologies, ranging from progeria and tuberous sclerosis to neurological disorders and cancer, including breast cancer [1, 3–5]. Consequently, the study of mTOR signaling attracts significant interest from diverse scientific fields, including oncology, aging research, and neurobiology [6–8].

This central role makes mTOR a high-priority target for novel therapeutics to restore pathway homeostasis. The broader scientific community actively pursues this direction [9]. In our previous work, miR-162a suppressed osteosarcoma cell proliferation and viability, suggesting potential *mTOR* inhibition [10]. The lack of a reliable *mTOR* expression assay prevented direct confirmation of this mechanism, motivating the development of the assay presented.

The high interest in studying mTOR regulation and its functions drives the demand for reliable methods to assess its activity. While established methods like Western blot [11] and luminescence microscopy [12] are reliable, they suffer from high cost, complexity, and operator-dependence.

An alternative method for evaluating protein activity is to assess the level of gene expression (mRNA quantity) using reverse transcription quantitative real-time polymerase chain reaction (RT-qPCR) with relevant reference genes, typically housekeeping genes which are stably expressed in most cells under normal and pathological conditions, for example Glyceraldehyde-3-Phosphate Dehydrogenase (*GAPDH*), Beta-Actin (*ACTB*), Beta-2-Microglobulin (*B2M*), as well as some of the most stable ones — *TATA-binding protein* (*TBP*) and *Ribosomal protein P0* (*RPLP0*) [13–14].

A multiplex PCR assay for mTOR expression analysis was previously developed by Quidville et al. [15], utilizing the reference genes *TBP* and *RPLP0*, which are among the most stable known to date [14]. However, a fundamental flaw in its design — specifically, a probe-primer overlap for the *TBP* gene — renders this system unreliable and highlights the critical need for a properly constructed alternative [13, 15, 16].

The aim of this study was to develop and validate a new multiplex RT-qPCR assay for the relative quantitative analysis of *mTOR* expression normalized to the reference genes *TBP* and *RPLP0*.

METHODS

In silico development and analysis of the PCR assay

Target gene mRNA sequences (FASTA) were retrieved from the NCBI Nucleotide database (https://www.ncbi.nlm.nih.gov/nucleotide/) [Accessed 2024 Sep 23]. Transcripts were annotated using the Assemble by CDS tool in Geneious Prime 2019.2.1 software (Biomatters Ltd., USA). Primers and probes were designed using the PrimerQuest Tool web service (Integrated DNA Technologies, Inc., USA; https://www.idtdna.com/pages/tools/primerquest) [Accessed 2024 Sep 23]. The following selection criteria were used for primer design [17]:

– Specificity — primers complementary to a single region.
– Primer length of approximately 20 nucleotides.
– Guanine-cytosine (GC) content of approximately 50%.
– At least one guanine-cytosine base pair at the primer ends.
– No complementary regions between primers.
– Primer melting temperature (Tm) between 55 °C and 65 °C.

The following requirements were applied to the probes:

– Length of approximately 20 nucleotides.
– GC content of approximately 50%.
– No more than four consecutive guanine or cytosine repeats.
– The probe must be located as close as possible to the primers but must not overlap them.
– The probe Tm must be 8–10 °C higher than the primer Tm.

Analysis of primer specificity, flanking, and spanning was performed in Geneious Prime 2019.2.1 software using the BLAST algorithm. Primer dimer formation was checked using the OligoAnalyzer Tool web service (Integrated DNA Technologies, Inc., USA; https://www.idtdna.com/pages/tools/oligoanalyzer) [Accessed 2024 Sep 23] [17].

In vitro validation of the PCR assay

Cell line

The study used the human bone marrow stromal cell line SCP-1, which was obtained from the Cell Culture Collection of the Ural State Medical University (Yekaterinburg, Russia). Cells were cultured in T-25 flasks (Sarstedt, Germany) with an adhesive coating in a medium containing 94% LoSera basal medium (HiMedia, India), 5% Fetal Bovine Serum (FBS) (HiMedia, India), 0.01% L-glutamine (Servicebio, China), and 0.01% (1 : 1 : 1) solution of penicillin, streptomycin, and amphotericin B (Servicebio, China), in a CO_2 incubator (Panasonic (Sanyo) MCO-15A, Japan) at 5% CO_2 and 37 °C [10]. Upon reaching 90–100% confluency, cells were passaged by removing the spent medium, washing twice with Hanks' Balanced Salt Solution (HBSS) without Ca and Mg ions (Servicebio, China), and then adding 2.5 mL of 0.25% trypsin-EDTA solution (Servicebio, China). The solution was removed after 10 seconds of exposure. The flask was placed in the CO_2 incubator for 1 minute 30 seconds. After adding fresh medium with serum, detached cells were collected, centrifuged at 350g for 3 minutes, resuspended, and distributed to new flasks at a 1 : 3 ratio [18]. For this study, a cell suspension was prepared as described, and cells were counted in a Goryaev chamber using the trypan blue exclusion method.

Nucleic acid extraction

For total RNA extraction, containing the mRNA fraction, the cell suspension (1 million cells/mL) was placed in a 1.5 mL Eppendorf tube and titrated with twofold dilutions in normal saline to obtain samples with concentrations of 1 million, 500 thousand, 250 thousand, 125 thousand and 62,5 thousand cells/mL. RNA was extracted from all dilutions to calculate the analytical parameters of the PCR assay.

RNA extraction from cell culture samples was performed using the «Proba-NK» reagent kit («DNA-Technology» LLC, Russia) according to the manufacturer's protocol. After the RNA extraction, total RNA from the 1 million cells/mL suspension was serially twofold diluted in normal saline to obtain samples with the matrix concentrations of 1, 1 : 2, 1 : 4, 1 : 8 and 1 : 16. All RNA matrix concentration variants were used for amplification to validate the PCR assay and calculate PCR efficiency.

Amplification

To analyze the specificity of the amplification product, 10 separate RT-qPCR technical repeats for each gene were performed using the BioMaster RT-qPCR SYBR Blue reagent kits («Biolabmix» LLC, Russia). Undiluted RNA matrix

from a suspension of 1 million cells/mL was used. Primers, according to the designed sequences, were synthesized by «DNK-sintez» LLC, Russia. According to the manufacturer's protocol, reaction mixtures were prepared from 12.5 µl of "Reaction Buffer" (containing dNTP mix, Mg ions and SYBR Green), 1 µl of "Master Mix" (containing genetically modified Moloney Murine Leukemia Virus reverse transcriptase and recombinant Taq DNA polymerase inactivated by specific monoclonal antibodies), 5 µl of a mixture with probe, forward and reverse primers (each at 0.12 µmol/L, 3 pmol/reaction), and 6.5 µl of RNA matrix. The final reaction volume was 25 µl. Additionally, 10 multiplex technical repeats (amplification of the target gene and normalizers in one tube) were performed using the BioMaster RT-qPCR reagent kits («Biolabmix» LLC, Russia). Reaction mixtures were prepared as above, except that the reaction buffer lacked an intercalating dye. Detection was performed by endpoint analysis using horizontal agarose gel electrophoresis.

The assay's analytical performance was assessed using the comprehensive dilution scheme as described in the section Nucleic Acid Extraction. This scheme incorporated both pre-analytical (cell concentration) and analytical (RNA dilution) variables, enabling simultaneous evaluation of amplification efficiency, analytical sensitivity, and technical reproducibility. All resulting RNA samples — from the five different cell concentrations and the four serial dilutions — were analyzed in triplicate using the multiplex RT-qPCR protocol described (Fig. 1). Three negative control replicates were included. This design resulted in a total of 27 individual reactions (9 unique sample types × 3 replicates). The results from these 27 technical repeats formed the primary dataset for all subsequent calculations of PCR efficiency, reference gene stability, and technical variability.

The amplification protocol consisted of reverse transcription for 30 minutes at 45 °C, initial denaturation for 5 minutes at 95 °C, followed by 45 cycles of denaturation (15 seconds at 95 °C) and primer annealing (30 seconds at 68 °C). The elongation step was excluded from the amplification protocol to limit DNA amplification [19]. For real-time detection of *mTOR*, *RPLP0*, and *TBP* amplification products, the fluorescent channels FAM, HEX, and ROX were selected, respectively.

Real-time detection was performed, and the Crossing Point (*Cp*) value was determined by the instrument's software as the cycle number at the maximum of the second derivative of the fluorescence growth curve [20]. As this study focused on the relative quantification of gene expression using the comparative method, no external calibration curves were run alongside the experimental samples. Results were considered valid if the *Cp* value was detected before the 31st amplification cycle. This threshold was established experimentally: when using a protocol that included an elongation step, additional amplification products appeared starting from cycle 31, which upon electrophoretic analysis corresponded in length to a fragment amplified from genomic DNA (574 bp, the size of the intron). Exclusion of the elongation step from the protocol eliminated this nonspecific amplification, and no signals were detected after the 31st cycle. Thus, the 31-cycle threshold was set as the limit beyond which no contribution from genomic DNA amplification is guaranteed to occur.

All runs used the «DTprime» thermal cycler («DNA-Technology» LLC, Russia) with the manufacturer's software.

Agarose gel electrophoresis

A 2,5% agarose gel was prepared using 2,5 g agarose powder (Helicon, Russia) in 100 mL 1x TBE buffer («Biolabmix» LLC, Russia) with the addition of 3 µL ethidium bromide (Servicebio, China). Electrophoresis ran at 100 V/A in a Sub-Cell GT Cell horizontal electrophoresis chamber (Bio-Rad, USA) for 40 minutes. Results were analyzed on a UV table transilluminator (Vilber, France) using a 10–25 DNA marker (Servicebio, China) [25, 26]. Images were captured digitally and processed in Adobe Photoshop CC 26.11 software (Adobe Inc., USA).

Statistical analysis

The expression value was determined based on the *Cp* value using the "Fold Change" (*FC*) formula presented by Livak and Schmittgen [22]. The formula was as follows:

$$FC = 2^{-\Delta Cp},\ \Delta Cp = Cp_{target} - Cp_{reference},$$

where Cp_{target} is *Cp* value of the target gene and $Cp_{reference}$ is *Cp* value of the normalizer.

For the analysis, the Δ*Cp* value was calculated using each normalizer individually (*RPLP0* or *TBP*) and, additionally,

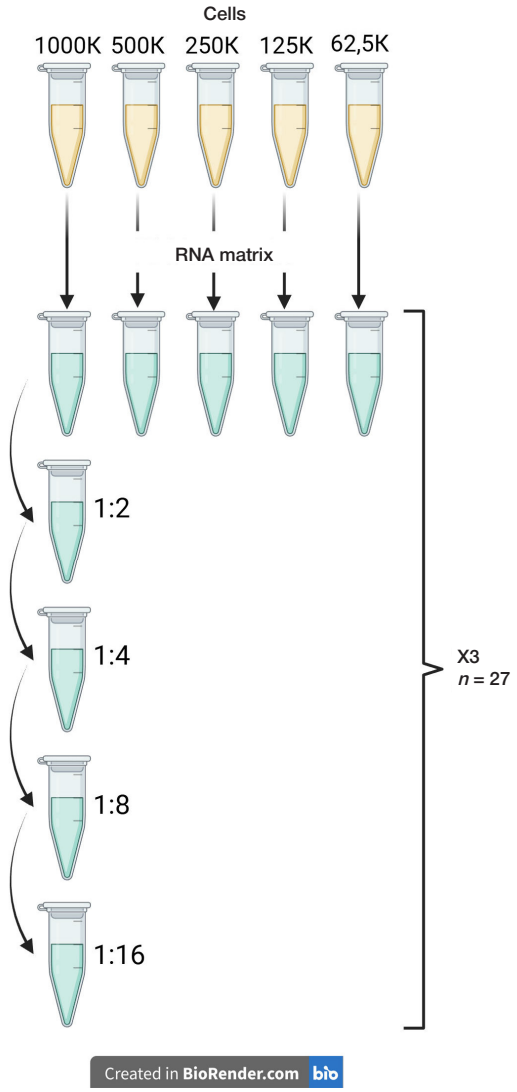

Fig. 1. Experimental design for multiplex RT-qPCR assay validation. The scheme illustrates the two independent dilution series used to assess assay performance. The pre-analytical series (*yellow*) involved total RNA isolation from SCP-1 cells at five different starting concentrations. The analytical series (*blue*) was created by twofold serial dilution of the RNA isolated from the highest cell concentration. Each resulting RNA sample (n = 9) was analyzed in triplicate, totaling 27 individual reactions for the evaluation of PCR efficiency, analytical sensitivity, and technical reproducibility

Table. Oligonucleotide characteristics for the multiplex RT-qPCR assay

Type	Gene name	Sequence, 5' → 3'	Amplicon length, bp	Melting T, °C	GC%	Detection
F-primer	*mTOR*	GCCCAGGCCGCATTGTCTCTAT	84	68	59.1	FAM
R-primer		GCAGTAAATGCAGGTAGTCATCCAGGTT		73	60.0	
Probe		TGGCTGCAATCCAGCTGTTTGGCGC		68	46.4	
F-primer	*RPLP0*	GGCGACCTGGAAGTCCAACTA	149	66	57.1	HEX
R-primer		CCATCAGCACCACAGCCTTC		65	60.0	
Probe		ATCTGCTGCATCTGCTTGGAGCCCA		72	56.0	
F-primer	*TBP*	CACGAACCACGGCACTGATT	89	65	55.0	ROX
R-primer		TTTTCTTGCTGCCAGTCTGGAC		65	50.0	
Probe		TGTGCACAGGAGCCAAGAGTGAAGA		69	52.0	

Note: F — forward; R — reverse. Gene symbols refer to mammalian target of rapamycin (*mTOR*), ribosomal protein lateral stalk subunit P0 (*RPLP0*), and TATA-box binding protein (*TBP*). All primers and probes were designed to meet standard criteria for multiplex real-time PCR, including amplicon size (<150 bp), matched melting temperatures within each set, optimal GC-content, and distinct, non-overlapping fluorescent detection channels

using the geometric mean of both normalizers *Cp* values as a combined reference value.

PCR efficiency for the *mTOR* gene and reference genes was assessed using linear regression of the *Cp* value dependence on the $\log_2$ of Cell Equivalent (*CE*). This metric, expressed in cell equivalents, represents the theoretical number of cells from which the RNA in the reaction was derived, accounting for both cell suspension dilution and RNA dilution. The correlation between the *CE* in the sample and the *Cp* value was assessed using Spearman's correlation coefficient (p, considered statistically significant at $p < 0.05$). The amplification efficiency (E) for each gene was calculated based on the slope (b) of the linear regression line plotted for the dependence of the *Cp* value on the $\log_2$ of the *CE*. Regression analysis yielded the following equation for each gene:

$$y = a - b \cdot x,$$

where y is the predicted *Cp* value, a is the y-intercept, b is the slope of the regression line, and x is $\log_2(N)$, with N being the calculated *CE*.

The *CE* was calculated as:

$$CE = \text{initial cell concentration} \div \text{cell dilution} \div \text{matrix dilution}.$$

The stability of the reference genes was assessed by analyzing the distribution of the *mTOR* expression value normalized to each reference gene (*FC*) and described by the median with the 0.25 and 0.75 percentiles.

Technical variability of the *mTOR FC* for a corresponding reference gene(s) was represented as median with the 0.25 and 0.75 percentiles of variability value, which had been calculated according to the formula:

$$\text{variability value} = 1 - (\text{mTOR FC sample value} / \text{mean mTOR FC value}).$$

mTOR FC values were calculated for the corresponding normalization strategy (normalized to *RPLP0*, *TBP*, or the geometric mean of both).

All analyses and graphs were performed in the R environment, version 4.5.2.

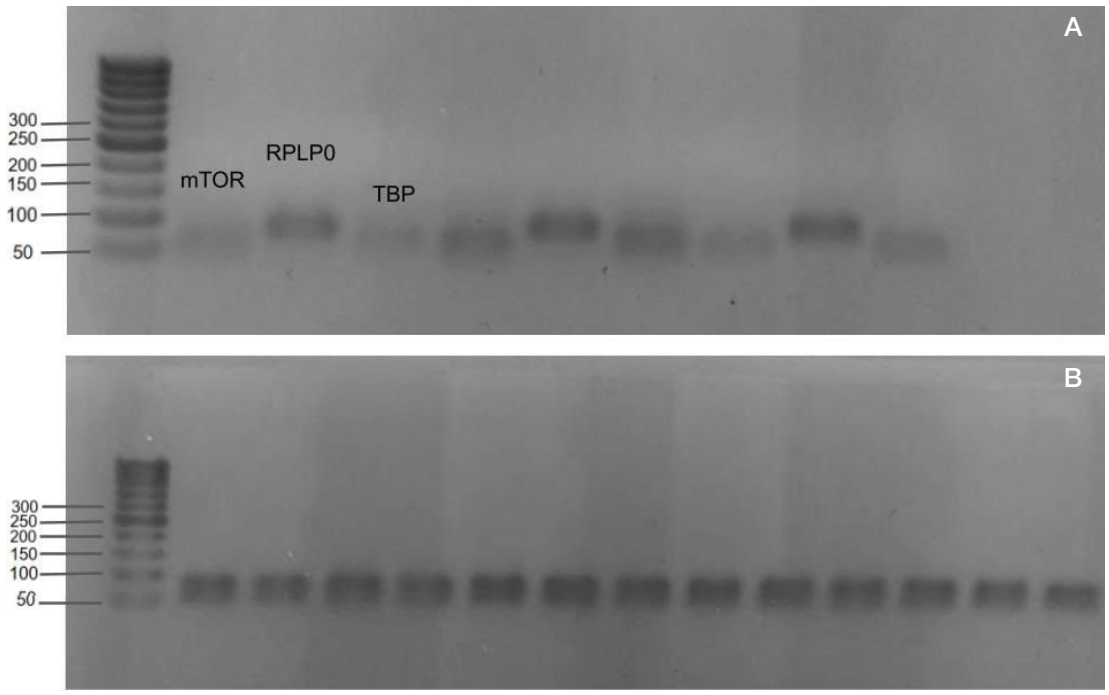

Fig. 2. Results of amplification product specificity analysis by agarose gel electrophoresis. **A**. Separate RT-qPCR technical repeats for each target gene. **B**. Multiplex RT-qPCR technical repeats amplifying all three targets simultaneously. Lanes for each gene show a single amplicon corresponding to the expected size, confirming high assay specificity

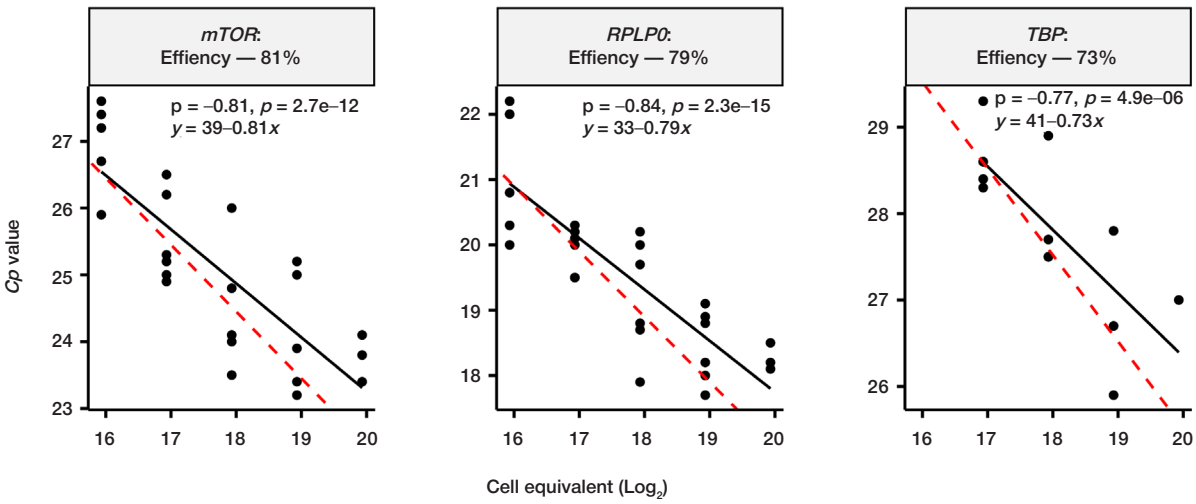

Fig. 3. Amplification efficiency of the target gene *mTOR* and reference genes *RPLP0* and *TBP*. Amplification efficiency analysis for *mTOR*, *RPLP0*, and *TBP* genes showing linear regression plots of *Cp* values versus $\log_2$ of the Cell Equivalent. Experimental amplification efficiencies were 81% for *mTOR* (regression equation: $y = 39 – 0.81x$), 79% for *RPLP0* ($y = 33 – 0.79x$), and 73% for *TBP* ($y = 41 – 0.73x$). The dashed *red line* represents theoretical 100% amplification efficiency (slope = –1), when *Cp* value decreases by one for each twofold increase of cell concentration, while *solid black lines* show actual regression lines, and *black dots* indicate individual data points from multiplex RT-qPCR technical repeats

RESULTS

In silico development and analysis of the PCR assay

Available methods to exclude genomic DNA amplification include "spanning" — positioning one of the primers or the probe to span two exons — and "flanking" — positioning primers on exons separated by a large intron.

To subsequently check the primers for meeting this condition, sequences (FASTA) of the *mTOR* (NM_004958.4), *RPLP0* (NM_001002.4), and *TBP* (NM_003194.5) genes were retrieved. Data from human chromosomes 1 (NC_000001.11), 12 (NC_000012.12), and 6 (NC_000006.12), where the target genes are located, respectively, were used as reference sequences, which were then annotated to highlight introns and exons.

Using obtained exons sequences of the genes, the primer pairs and probes for the *mTOR* and *RPLP0* genes, described previously [16], were verified and their effectiveness was confirmed. 10 primer-probe sets for *TBP* were designed, and the most specific and suitable combination was selected (Table). Primer and probe sequences and parameters are presented in Table.

The proposed normalization strategies and oligonucleotide designs were verified in silico. For the *mTOR* and *RPLP0* genes, primer flanking of exon-exon junctions was confirmed (exons 21–22 and 2–3, respectively, flanking strategy), and for the *TBP* gene, probe spanning of the intron between exons 5 and 6 was confirmed (spanning strategy), which guarantees the absence of genomic DNA amplification. According to NCBI reference sequences (NM_004958.4, NM_001002.4, NM_003194.5), the primers and probes are localized on the CDS as follows: for *mTOR* — forward primer 3381–3402, probe 3411–3435, reverse primer 3437–3464; for *RPLP0* — forward primer 95–115, probe 181–205, reverse primer 224–243; for *TBP* — forward primer 863–882, probe 902–926, reverse primer 930–951.

The primers for *mTOR*, *RPLP0*, and *TBP* did not form stable dimers, indicating a low risk of nonspecific amplification products.

In vitro validation of the PCR assay

When assessing the specificity of amplification products in all separate ($n = 10$) and all multiplex ($n = 10$) technical repeats, a single clear amplification product was obtained for each of the target genes — mTOR, RPLP0, and TBP. All amplicon lengths matched the calculated values (Table). Side or nonspecific bands were not observed when analyzing amplification products by gel electrophoresis (Fig. 2). The analytical specificity of the PCR assay was 100%. To assess analytical sensitivity, various cell dilutions were used; stable detection of all three genes was maintained at a minimum concentration of 125 thousand cells/mL.

A linear regression plot between *Cp* and the *CE* ($\log_2$) was constructed for all three genes (Fig. 3).

Spearman correlation coefficients for the relationship between *Cp* and the *CE* ($\log_2$) were –0.81, –0.84, and –0.77 for *mTOR*, *RPLP0*, and *TBP*, respectively ($p < 0.05$ in all cases), indicating a strong and statistically significant inverse correlation between the number of investigated cells and the *Cp* value for each target.

Amplification efficiency was calculated for each gene from the slope of the linear regression. For the *mTOR* gene, the efficiency was 81%, for *RPLP0* — 79%, for *TBP* — 73%. All efficiency values were obtained based on the deviation of the slope of the experimental regression from the theoretical slope corresponding to 100% efficiency (slope = –1). The obtained values indicate high amplification efficiency of the investigated primers, with the slopes of the experimental lines close to –1 ($y = 39 – 0.81x$ for *mTOR*, $y = 33 – 0.79x$ for *RPLP0*, $y = 41 – 0.73x$ for *TBP*).

The stability of the reference genes was assessed in 27 multiplex technical repeats by analyzing *FC* of mTOR normalized to RPLP0 and TBP. The median *FC* value of *mTOR* normalized to *RPLP0* was 0.02 (0.02 – 0.03), indicating a consistently higher expression level of the *RPLP0* gene compared to *mTOR* in the studied samples. When normalized to *TBP*, the median *FC* of *mTOR* was 9.85 (8.57 – 12.13), indicating a consistently lower expression level of *TBP* relative to mTOR (Fig. 4).

To assess variability between technical replicates, the *mTOR FC* deviation from the mean value was calculated for each sample. The median variability value for *mTOR FC* when normalized to *RPLP0* was –2.3% (–21.5 – 26.4%). The median variability value for *mTOR FC* when normalized to *TBP* was 7.2% (–14.3 – 19.2%). When normalizing *mTOR FC* to both reference genes, the median *mTOR FC* value was 4.9% (–9 – 23.4%) (Fig. 5). In this case, the narrower interquartile range indicates higher reproducibility of results when using the geometric mean of the two reference genes for normalization.

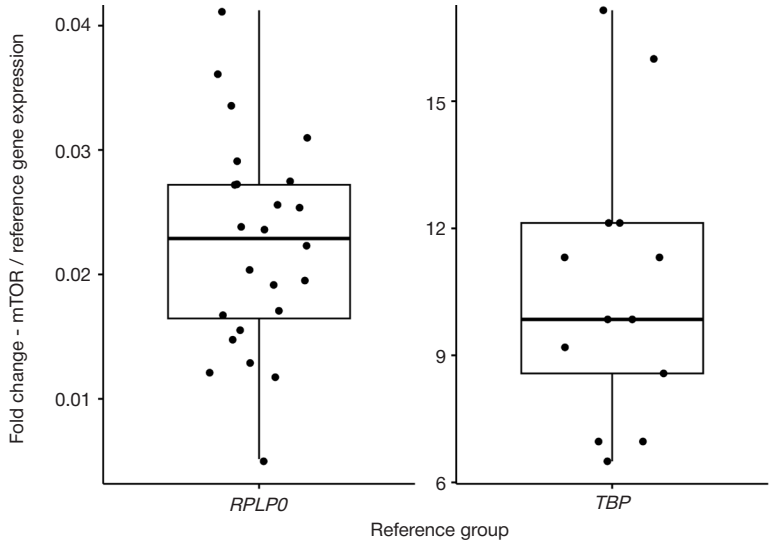

Fig. 4. Analysis of *mTOR* expression relative to reference genes *RPLP0* and *TBP*. The expression of *mTOR* was consistently lower than *RPLP0* and higher than *TBP* in the SCP-1 cell line

DISCUSSION

In this study, we successfully developed and validated a multiplex PCR assay for determining the expression level of the *mTOR* gene normalized to the reference genes *TBP* and *RPLP0*. The in silico analysis stage involved careful selection and verification of primers and probes based on specificity, thermodynamic parameters, and the absence of stable dimer formation. A crucial achievement was the elimination of a drawback of the previously published assay [15] — the overlap between the probe and primer sequences for the *TBP* gene, which had called into question the reliability of the results obtained with it. Our proposed assay completely solves this problem.

Preclinical validation of the PCR assay confirmed high analytical specificity: 100% analytical specificity was achieved with the detection of a single, clearly defined amplification product for each target gene in the complete absence of nonspecific products. Furthermore, the developed PCR assay demonstrated reliable analytical sensitivity, providing stable detection at a minimum concentration of 125 thousand cells/mL.

There was stability of the expression ratios of both reference genes *RPLP0* and *TBP*, regardless of cell concentration or matrix RNA concentration, combined with low median variability between technical replicates. This indicates the high reliability and reproducibility of the developed multiplex PCR assay for analyzing *mTOR* expression levels.

The amplification efficiency for all three genes ranged from 73 to 81%. This range is attributable to two key methodological choices made to ensure the assay's clinical relevance. First, we validated the protocol using a widely adopted RNA extraction kit to reflect real-world diagnostic conditions; the resulting RNA purity, while representative, can modestly impact efficiency [23]. Second, to mitigate the risk of amplifying contaminating genomic DNA — a residue not fully removed by even advanced kits — we omitted the elongation step from the amplification protocol [19]. This precaution is particularly relevant given the high processivity of modern Taq polymerases [24]. Despite these necessary trade-offs, assay specificity remained uncompromised [22]. Future work may focus on fine-tuning primer concentrations to further improve efficiency.

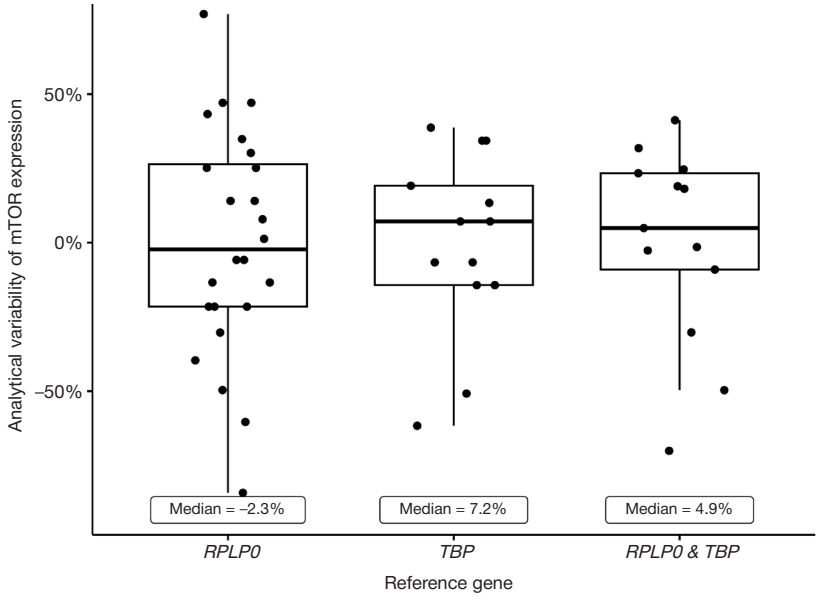

Fig. 5. Assessment of analytical reproducibility using different normalization strategies. The percentage deviation of *FC* values for each sample from the overall median. The reproducibility of results when *mTOR* expression normalized to *RPLP0*, *TBP*, and their geometric mean (*RPLP0* and *TBP*). The reduced variability (narrower interquartile range) achieved by using two reference genes simultaneously

Despite good median values, the interquartile ranges remain relatively wide. This is explained by the use of the Fold Change metric, based on an exponential formula, which amplifies the influence of even small changes in expression levels on the magnitude of percentage variability, which is an expected result for relative quantitative PCR analysis. The original *Cp* differences varied within a one-cycle range.

Such ranges of analytical *FC* variation fully correspond to the data from most published studies on the development of relative quantitative PCR kits without the use of absolute standards and are consistent with the results of fundamental works [22, 25]. In the study by Gentle et al. [26], the authors report technical *FC* variation values from 23 to 52%, depending on the number of technical replicates [26].

A key advantage of this study is the performance of rigorous analytical validation on a standardized cell line. The use of SCP-1 cells provided a homogeneous and controlled system, free from the pre-analytical variables inherent in clinical samples (such as tissue heterogeneity or variable RNA quality). This allowed us to accurately determine the intrinsic analytical parameters of the PCR assay — specificity, sensitivity, and reproducibility — without the influence of confounding biological factors. The demonstrated robustness of this PCR assay is a prerequisite for its successful application in the analysis of more complex biomaterial types, such as human tumor tissues, which will be the next step in our research.

Our multiplex RT-qPCR assay provides a direct and reproducible tool for assessing *mTOR* expression, capturing the integrated activity of the PI3K/AKT/mTOR pathway [27] and representing a promising objective alternative to operator-dependent methods like immunohistochemistry [28]. Unlike detecting mutations in genes like *BRCA1/2* or *PIK3CA* — which, despite their clinical utility, are limited to specific patient subgroups and provide information on predisposition or disease aggressiveness rather than serving as true diagnostic tools — our method quantifies pathway output directly. Given the role of mTOR overexpression in breast cancer [1, 6, 28], this assay holds significant potential for integration into future diagnostic and research strategies.

A limitation of this study is the use of a standardized cell line (SCP-1), which does not reflect the full heterogeneity of clinical tumor samples and does not account for the influence of pre-analytical variables [30]. Furthermore, assay performance is inextricably linked to the specific reagents and protocols employed in this work. Therefore, the clinical applicability of the developed test system for assessing mTOR expression in breast cancer diagnosis and stratification must be established through future studies on representative tissue cohorts. Such studies will determine its diagnostic accuracy (sensitivity, specificity, AUC) and evaluate the potential for implementation into routine clinical practice. It should also be noted that increased mTOR expression is observed not only in oncological but also in other diseases (e.g., rheumatic pathologies); therefore, the interpretation of results will depend on the type of biological material studied and the clinical study design. Depending on the specific task, future applications may require either the establishment of diagnostic thresholds for particular sample types (e.g., tumor biopsies) or the introduction of additional markers (e.g., RILP) to differentiate conditions with similar mTOR expression profiles. Despite the need for further research, the developed PCR assay represents a promising foundational tool for advancing molecular diagnostics in breast cancer.

CONCLUSIONS

In this study, we designed and validated a novel multiplex RT-qPCR assay for the relative quantification of *mTOR* gene expression normalized to *RPLP0* and *TBP*. A critical flaw of the the previously described design, which consisted of overlapping sequences of the probe and primer for the *TBP* gene was eliminated in the developed assay through the correct design of oligonucleotides, verification of the absence of primer-dimer interactions, and the use of optimal strategies to prevent genomic DNA amplification. The assay demonstrated 100% analytical specificity and a sensitivity of 125 thousand cells/mL. The amplification efficiency was 73% for *TBP*, 79% for *RPLP0*, and 81% for *mTOR*. In the SCP-1 cell line, the expression of *mTOR* was substantially higher than that of *TBP* but lower than *RPLP0*. Normalization to the geometric mean of both reference genes yielded the highest reproducibility, with a median Fold Change deviation of 4.9% between technical replicates. The developed PCR assay allows to overcome a critical design flaw of a previously published assay and, given the role of *mTOR* overexpression in carcinogenesis, is a promising tool for advancing molecular diagnosis in breast cancer.

References

1. Miricescu D, Totan A, Stanescu-Spinu II, Badoiu SC, Stefani C, Greabu M. PI3K/AKT/mTOR Signaling Pathway in Breast Cancer: From Molecular Landscape to Clinical Aspects. Int J Mol Sci. 2020; 22: 173.
2. Kornilov DO, Tryapicyn MA, Grebnev DYu. MTOR: signalizaciya, regulyaciya, vliyanie na metabolizm, rol' v regulyacii prodolzhitel'nosti zhizni i opuholevogo rosta. Izvestiya Komi nauchnogo centra URO RAN. 2021; 5: 104–115. Russian.
3. Luo C, Ye WR, Shi W, Yin P, Chen C, He YB, et al. Perfect match: mTOR inhibitors and tuberous sclerosis complex. Orphanet J Rare Dis. 2022; 17: 106.
4. Spilman P, Podlutskaya N, Hart MJ, Debnath J, Gorostiza O, Bredesen D, et al. Inhibition of mTOR by Rapamycin Abolishes Cognitive Deficits and Reduces Amyloid-β Levels in a Mouse Model of Alzheimer's Disease. PLoS One. 2010; 5 (4): e9979.
5. Zhu K, Wu Y, He P, Fan Y, Zhong X, Zheng H, et al. PI3K/AKT/mTOR-Targeted Therapy for Breast Cancer. Cells. 2022; 11 (16): 2508.
6. Xue QL, Yang H, Li HF, Abadir PM, Burks TN, Koch LG, et al. Rapamycin increases grip strength and attenuates age-related decline in maximal running distance in old low capacity runner rats. Aging (Albany NY). 2016; 8: 769–76.
7. Bitto A, Ito TK, Pineda VV, LeTexier NJ, Huang HZ, Sutlief E, et al. Transient rapamycin treatment can increase lifespan and healthspan in middle-aged mice. Elife. 2016; 5: e16351.
8. López-Otín C, Blasco MA, Partridge L, Serrano M, Kroemer G. The Hallmarks of Aging. Cell. 2013; 153: 1194–217.
9. Tang L, Fu Y, Song J, Hu T, Li K, Li Z. mTOR inhibition by TAK-228 is effective against growth, survival and angiogenesis in preclinical retinoblastoma models. Pharmacol Res Perspect. 2022; 10: e00930.
10. Grebnev DYu, Maklakova IYu, Kornilov DO, Simarzina VM, Tryapicyn MA, Kazancev YU. A., et al. Ingibirovanie opuholevogo rosta v kletochnoj kul'ture osteosarkomy s pomoshch'yu mikroRNK mir162a. Patologicheskaya fiziologiya i eksperimental'naya terapiya. 2023; 67 (1): 48–55. Russian.
11. Xu C, Gao Q, Wu Z, Lou W, Li X, Wang M, et al. Combined HASPIN and mTOR inhibition is synergistic against KRAS-driven carcinomas. Transl Oncol. 2022; 26: 101540.
12. Wei Z, Xia K, Zheng D, Gong C, Guo W. RILP inhibits tumor

progression in osteosarcoma via Grb10-mediated inhibition of the PI3K/AKT/mTOR pathway. Mol Med. 2023; 29: 106.
13. Kirschneck C, Batschkus S, Proff P, Köstler J, Spanier G, Schröder A. Valid gene expression normalization by RT-qPCR in studies on hPDL fibroblasts with focus on orthodontic tooth movement and periodontitis. Sci Rep. 2017; 7: 14739.
14. Hounkpe BW, Chenou F, de Lima F, De Paula EV. HRT Atlas v1.0 database: redefining human and mouse housekeeping genes and candidate reference transcripts by mining massive RNA-seq datasets. Nucleic Acids Res. 2021; 49: D947–D955.
15. Quidville V, Alsafadi S, Goubar A, Commo F, Scott V, Pioche-Durieu C, et al. Targeting the Deregulated Spliceosome Core Machinery in Cancer Cells Triggers mTOR Blockade and Autophagy. Cancer Res. 2013; 73: 2247–58.
16. Kornilov DO, Simarzina VM, Tryapicyn MA, Maslakov GP, Bekhter AA, Zornikov DL. Razrabotka mul'tipleksnoj PCR test-sistemy dlya analiza ekspressii protoonkogena mTOR. Ekaterinburg: FGBOU VO UGMU Minzdrava Rossii; 2024 Apr. Doklad na IX Mezhdunarodnoj nauchno-prakticheskoj konferencii molodyh uchenyh i studentov «Aktual'nye voprosy sovremennoj medicinskoj nauki i zdravoohraneniya». Russian.
17. Rodríguez A, Rodríguez M, Córdoba JJ, Andrade MJ. Design of Primers and Probes for Quantitative Real-Time PCR Methods. In: Basu C, editor. PCR Primer Design. New York, NY: Humana Press, 2015; 31–56.
18. Grigorev SS, Kozmenko AN, Gajnetdinov MR, Kornilov DO, Zornikov DL. Sravnitel'nyj analiz citotoksichnosti silerov dlya provedeniya plombirovaniya kornevyh kanalov (in vitro). Problemy stomatologii. 2023; 4: 44–49. Russian.
19. Kaur R, Sodhi M, Sharma A, Sharma VL, Verma P, Swami SK, et al. Selection of suitable reference genes for normalization of quantitative RT-PCR (RT-qPCR) expression data across twelve tissues of riverine buffaloes (Bubalus bubalis). PLoS One. 2018; 13: e0191558.
20. Meijerink J, Mandigers C, van de Locht L, Tönnissen E, Goodsaid F, Raemaekers J. A novel method to compensate for different amplification efficiencies between patient DNA samples in quantitative real-time PCR. J Mol Diagn. 2001; 3 (2): 55–61.
21. Figueroa S, Freire-Paspuel B, Vega-Mariño P, Velez A, Cruz M, Cardenas WB, et al. High sensitivity-low cost detection of SARS-CoV-2 by two steps end point RT-PCR with agarose gel electrophoresis visualization. Sci Rep. 2021; 11: 21234.
22. Livak KJ, Schmittgen TD. Analysis of Relative Gene Expression Data Using Real-Time Quantitative PCR and the 2-ΔΔCT Method. Methods. 2001; 25: 402–8.
23. Nolan T, Hands RE, Bustin SA. Quantification of mRNA using real-time RT-PCR. Nat Protoc. 2006; 1 (3): 1559–82.
24. BioMaster RT-qPCR – Standard (2×) one-step RT-qPCR reagent kit. Novosibirsk: «Biolabmix» LLC, 2024. Cat. No: RM03-80.
25. Dragon AH, Rowe CJ, Rhodes AM, Pak OL, Davis TA, Ronzier E. Systematic Identification of the Optimal Housekeeping Genes for Accurate Transcriptomic and Proteomic Profiling of Tissues following Complex Traumatic Injury. Methods Protoc. 2023; 6: 22.
26. Gentle A, Anastasopoulos F, McBrien NA. High-Resolution Semi-Quantitative Real-Time PCR without the Use of a Standard Curve. BioTechniques. 2001; 31: 502–8. Available from: https://doi.org/10.2144/01313st03.
27. Kołodziej P, Nicoś M, Krawczyk PA, Bogucki J, Karczmarczyk A, Zalewski D, et al. The Correlation of Mutations and Expressions of Genes within the PI3K/Akt/mTOR Pathway in Breast Cancer — A Preliminary Study. Int J Mol Sci. 2021; 22: 2061.
28. Jaglan P, Dass R, Duhan M. Breast Cancer Detection Techniques: Issues and Challenges. J Inst Eng India Ser B. 2019; 100: 379–86.
29. Madsen RR, Erickson EC, Rueda OM, Robin X, Caldas C, Toker A, et al. Positive correlation between transcriptomic stemness and PI3K/AKT/mTOR signaling scores in breast cancer, and a counterintuitive relationship with PIK3CA genotype. PLoS Genet. 2021; 17: e1009876.
30. Hensler M, Vančurová I, Becht E, Palata O, Strnad P, Tesařová P, et al. Gene expression profiling of circulating tumor cells and peripheral blood mononuclear cells from breast cancer patients. Oncoimmunology. 2016; 5: e1102827.

Литература

1. Miricescu D, Totan A, Stanescu-Spinu II, Badoiu SC, Stefani C, Greabu M. PI3K/AKT/mTOR Signaling Pathway in Breast Cancer: From Molecular Landscape to Clinical Aspects. Int J Mol Sci. 2020; 22: 173.
2. Корнилов Д. О., Тряпицын М. А., Гребнев Д. Ю. MTOR: сигнализация, регуляция, влияние на метаболизм, роль в регуляции продолжительности жизни и опухолевого роста. Известия Коми научного центра УРО РАН. 2021; 5: 104–15.
3. Luo C, Ye WR, Shi W, Yin P, Chen C, He YB, et al. Perfect match: mTOR inhibitors and tuberous sclerosis complex. Orphanet J Rare Dis. 2022; 17: 106.
4. Spilman P, Podlutskaya N, Hart MJ, Debnath J, Gorostiza O, Bredesen D, et al. Inhibition of mTOR by Rapamycin Abolishes Cognitive Deficits and Reduces Amyloid-β Levels in a Mouse Model of Alzheimer's Disease. PLoS One. 2010; 5 (4): e9979.
5. Zhu K, Wu Y, He P, Fan Y, Zhong X, Zheng H, et al. PI3K/AKT/mTOR-Targeted Therapy for Breast Cancer. Cells. 2022; 11 (16): 2508.
6. Xue QL, Yang H, Li HF, Abadir PM, Burks TN, Koch LG, et al. Rapamycin increases grip strength and attenuates age-related decline in maximal running distance in old low capacity runner rats. Aging (Albany NY). 2016; 8: 769–76.
7. Bitto A, Ito TK, Pineda VV, LeTexier NJ, Huang HZ, Sutlief E, et al. Transient rapamycin treatment can increase lifespan and healthspan in middle-aged mice. Elife. 2016; 5: e16351.
8. López-Otín C, Blasco MA, Partridge L, Serrano M, Kroemer G. The Hallmarks of Aging. Cell. 2013; 153: 1194–217.
9. Tang L, Fu Y, Song J, Hu T, Li K, Li Z. mTOR inhibition by TAK-228 is effective against growth, survival and angiogenesis in preclinical retinoblastoma models. Pharmacol Res Perspect. 2022; 10: e00930.
10. Гребнев Д. Ю., Маклакова И. Ю., Корнилов Д. О., Симарзина В. М., Тряпицын М. А., Казанцев Ю. А., и др. Ингибирование опухолевого роста в клеточной культуре остеосаркомы с помощью микроРНК mir162a. Патологическая физиология и экспериментальная терапия. 2023; 67 (1): 48–55.
11. Xu C, Gao Q, Wu Z, Lou W, Li X, Wang M, et al. Combined HASPIN and mTOR inhibition is synergistic against KRAS-driven carcinomas. Transl Oncol. 2022; 26: 101540.
12. Wei Z, Xia K, Zheng D, Gong C, Guo W. RILP inhibits tumor progression in osteosarcoma via Grb10-mediated inhibition of the PI3K/AKT/mTOR pathway. Mol Med. 2023; 29: 106.
13. Kirschneck C, Batschkus S, Proff P, Köstler J, Spanier G, Schröder A. Valid gene expression normalization by RT-qPCR in studies on hPDL fibroblasts with focus on orthodontic tooth movement and periodontitis. Sci Rep. 2017; 7: 14739.
14. Hounkpe BW, Chenou F, de Lima F, De Paula EV. HRT Atlas v1.0 database: redefining human and mouse housekeeping genes and candidate reference transcripts by mining massive RNA-seq datasets. Nucleic Acids Res. 2021; 49: D947–D955.
15. Quidville V, Alsafadi S, Goubar A, Commo F, Scott V, Pioche-Durieu C, et al. Targeting the Deregulated Spliceosome Core Machinery in Cancer Cells Triggers mTOR Blockade and Autophagy. Cancer Res. 2013; 73: 2247–58.
16. Корнилов Д. О., Симарзина В. М., Тряпицын М. А., Маслаков Г. П., Бехтер А. А., Зорников Д. Л. Разработка мультиплексной ПЦР тест-системы для анализа экспрессии протоонкогена mTOR. Екатеринбург: ФГБОУ ВО УГМУ Минздрава России; 2024 Апр. Доклад на IX Международной научно-практической конференции молодых ученых и студентов «Актуальные вопросы современной медицинской науки и здравоохранения».
17. Rodríguez A, Rodríguez M, Córdoba JJ, Andrade MJ. Design of Primers and Probes for Quantitative Real-Time PCR Methods. In: Basu C, editor. PCR Primer Design. New York, NY: Humana Press, 2015; 31–56.

18. Григорьев С. С., Козьменко А. Н., Гайнетдинов М. Р., Корнилов Д. О., Зорников Д. Л. Сравнительный анализ цитотоксичности силеров для проведения пломбирования корневых каналов (in vitro). Проблемы стоматологии. 2023; 4: 44–49.
19. Kaur R, Sodhi M, Sharma A, Sharma VL, Verma P, Swami SK, et al. Selection of suitable reference genes for normalization of quantitative RT-PCR (RT-qPCR) expression data across twelve tissues of riverine buffaloes (Bubalus bubalis). PLoS One. 2018; 13: e0191558.
20. Meijerink J, Mandigers C, van de Locht L, Tönnissen E, Goodsaid F, Raemaekers J. A novel method to compensate for different amplification efficiencies between patient DNA samples in quantitative real-time PCR. J Mol Diagn. 2001; 3 (2): 55–61.
21. Figueroa S, Freire-Paspuel B, Vega-Mariño P, Velez A, Cruz M, Cardenas WB, et al. High sensitivity-low cost detection of SARS-CoV-2 by two steps end point RT-PCR with agarose gel electrophoresis visualization. Sci Rep. 2021; 11: 21234.
22. Livak KJ, Schmittgen TD. Analysis of Relative Gene Expression Data Using Real-Time Quantitative PCR and the 2-ΔΔCT Method. Methods. 2001; 25: 402–8.
23. Nolan T, Hands RE, Bustin SA. Quantification of mRNA using real-time RT-PCR. Nat Protoc. 2006; 1 (3): 1559–82.
24. Набор реагентов БиоМастер ОТ-ПЦР-РВ (2×). Новосибирск: ООО «Биолабмикс», 2024. Кат. номер: RM03-80.
25. Dragon AH, Rowe CJ, Rhodes AM, Pak OL, Davis TA, Ronzier E. Systematic Identification of the Optimal Housekeeping Genes for Accurate Transcriptomic and Proteomic Profiling of Tissues following Complex Traumatic Injury. Methods Protoc. 2023; 6: 22.
26. Gentle A, Anastasopoulos F, McBrien NA. High-Resolution Semi-Quantitative Real-Time PCR without the Use of a Standard Curve. BioTechniques. 2001; 31: 502–8. Available from: https://doi.org/10.2144/01313st03.
27. Kołodziej P, Nicoś M, Krawczyk PA, Bogucki J, Karczmarczyk A, Zalewski D, et al. The Correlation of Mutations and Expressions of Genes within the PI3K/Akt/mTOR Pathway in Breast Cancer — A Preliminary Study. Int J Mol Sci. 2021; 22: 2061.
28. Jaglan P, Dass R, Duhan M. Breast Cancer Detection Techniques: Issues and Challenges. J Inst Eng India Ser B. 2019; 100: 379–86.
29. Madsen RR, Erickson EC, Rueda OM, Robin X, Caldas C, Toker A, et al. Positive correlation between transcriptomic stemness and PI3K/AKT/mTOR signaling scores in breast cancer, and a counterintuitive relationship with PIK3CA genotype. PLoS Genet. 2021; 17: e1009876.
30. Hensler M, Vančurová I, Becht E, Palata O, Strnad P, Tesařová P, et al. Gene expression profiling of circulating tumor cells and peripheral blood mononuclear cells from breast cancer patients. Oncoimmunology. 2016; 5: e1102827.

LARGE HEPATOCELLULAR ADENOMA OF THE LIVER IN A WOMAN OF REPRODUCTIVE AGE

Chichelnitsky AK[1], Savchenko DA[1], Kostina AS[1], Raklov DA[1], Zhuk ER[2], Buimova ES[2], Negodaeva AI[1], Ivanenko AO[1]✉, Aduchieva VI[3]

[1] Rostov State Medical University, Rostov-on-Don, Russia

[2] Gorky Donetsk State Medical University, Donetsk, Russia

[3] Razumovsky Saratov State Medical University, Saratov, Russia

Hepatocellular adenoma is a rare benign liver tumor with the potentially unfavorable course due to the risk of hemorrhage and malignant transformation. Treatment depends on the mass subtype and size. Here we present a clinical case of hepatocellular adenoma in a woman of reproductive age developed against the background of the long-term use of oral contraceptives. The tumor sized 8 cm was detected accidentally during instrumental examination; morphological and immunohistochemistry assessment confirmed that it was a benign one without β-catenin mutation. Liver resection was performed. The case highlights the importance of careful monitoring of the patients during the long-term use of oral contraceptives, as well as of the timely surgical interventions in individuals with large hepatocellular adenomas to prevent hemorrhage and malignization.

Keywords: hepatocellular adenoma, liver tumors, estrogen-containing drugs, liver resection

Author contribution: Chichelnitsky AK, Savchenko DA — manuscript writing and editing; Zhuk ER, Buimova ES — literature review, data analysis, manuscript writing; Kostina AS, Raklov DA — literature review, data acquisition, manuscript writing; Negodaeva AI, Ivanenko AO — concept and design, literature review, manuscript writing; Aduchieva VI — literature review, manuscript writing and editing.

Compliance with ethical standards: the patient submitted the informed consent for publication of anonymized personal medical information.

✉ **Correspondence should be addressed:** Anastasia O. Ivanenko
Alma-Atinskaya, 24, Rostov-on-Don, 344009, Russia; ivanenko.anastasiya.01@mail.ru

Received: 12.02.2026 **Accepted:** 10.03.2026 **Published online:** 28.03.2026

DOI: 10.24075/brsmu.2026.010

КРУПНАЯ ГЕПАТОЦЕЛЛЮЛЯРНАЯ АДЕНОМА ПЕЧЕНИ У ЖЕНЩИНЫ РЕПРОДУКТИВНОГО ВОЗРАСТА

А. К. Чичельницкий[1], Д. А. Савченко[1], А. С. Костина[1], Д. А. Раклов[1], Е. Р. Жук[2], Е. С. Буймова[2], А. И. Негодаева[1], А. О. Иваненко[1]✉, В. И. Адучиева[3]

[1] Ростовский государственный медицинский университет, Ростов-на-Дону, Россия

[2] Донецкий государственный медицинский университет имени М. Горького, Донецк, Россия

[3] Саратовский государственный медицинский университет имени В. И. Разумовского, Саратов, Россия

Гепатоцеллюлярная аденома является редкой доброкачественной опухолью печени с потенциально неблагоприятным течением, обусловленным риском кровоизлияния и злокачественной трансформации. Лечение зависит от подтипа и размеров образования. Представлено клиническое наблюдение гепатоцеллюлярной аденомы у женщины репродуктивного возраста на фоне длительного применения оральных контрацептивов. Опухоль размером 8 см была случайно выявлена при инструментальном обследовании; морфологическое и иммуногистохимическое исследование подтвердили доброкачественный характер без мутации β-катенина. Выполнена резекция печени. Случай подчеркивает важность внимательного наблюдения за пациентками на фоне длительного приема гормональных контрацептивов и своевременного хирургического вмешательства при крупных гепатоцеллюлярных аденомах с целью профилактики риска кровоизлияний и малигнизации.

Ключевые слова: гепатоцеллюлярная аденома, опухоли печени, эстрогенсодержащие препараты, резекция печени

Вклад авторов: А. К. Чичельницкий, Д. А. Савченко — написание и редактирование статьи; Е. Р. Жук, Е. С. Буймова — обзор литературы, анализ данных, написание статьи; А. С. Костина, Д. А. Раклов — обзор литературы, сбор данных, написание статьи; А. И. Негодаева, А. О. Иваненко — концепция и дизайн, обзор литературы, написание статьи; В. И. Адучиева — обзор литературы, написание и редактирование статьи.

Соблюдение этических стандартов: пациент подписал добровольное информированное согласие на публикацию персональной медицинской информации в обезличенной форме.

✉ **Для корреспонденции:** Анастасия Олеговна Иваненко
ул. Алма-Атинская, д. 24, г. Ростов-на-Дону, 344009, Россия; ivanenko.anastasiya.01@mail.ru

Статья получена: 12.02.2026 **Статья принята к печати:** 10.03.2026 **Опубликована онлайн:** 28.03.2026

DOI: 10.24075/vrgmu.2026.010

Hepatocellular adenoma (HCA) is a rare benign liver tumor diagnosed mainly in women of reproductive age [1, 2]. The long-term use of oral contraceptives (for more than 5 years) is the leading risk factor of HCA. The incidence of HCA in the general population is uncertain, there are reports of o 0.001–0.004%. According to the literature data [3], adenomas are considerably more often diagnosed in women using oral contraceptives for the long term (3.4 cases per 100,000 population), while the rate among women not using such drugs varies between 1–1.3 per 100,000 population. There is a direct relationship between the duration of using contraceptives and the increase in the rate of developing HCA and severity of HCA clinical manifestations (patients' complaints) [3]. In recent decades, the female-to-male ratio has decreased from 11 : 1 to 4 : 1, which is associated with the increasing use of anabolic steroids [4]. Additional risk factors include glycogenosis, obesity, metabolic syndrome, alcohol abuse, and endocrine disorders, including Klinefelter syndrome, type 3 diabetes (MODY), and polycystic

ovary syndrome [5, 6]. In recent years, the HCA association with the use of clomiphene and barbiturates has been shown [4, 7].

The main HCA complications include spontaneous hemorrhage reported in 27% of cases of detecting masses sized over 5 cm [4] and malignant transformation. Hemorrhage can be intratumoral, intrahepatic or intraperitoneal; intraperitoneal hemorrhage is associated with the development of acute hemorrhagic syndrome fraught with high risk of hemorrhagic shock and fatality [5].

Male sex, β-catenin mutations (exon 3), and the tumor size over 5 cm are associated with the increased risk of HCA malignization [8, 9].

In terms of morphology, HCAs consisting of hepatocytes without portal tracts and bile ducts are supplied by arteries only [2]. Due to the limited diagnostic information content of standard histological examination, especially when used for differential diagnosis of subtypes of HCA and hepatocellular carcinoma, immunohistochemistry and molecular genetic methods become increasingly important [10–12]. In 2007, the key immunohistochemistry markers for HCA classification were proposed, including L-FABP, β-catenin, glutamine synthetase, and serum amyloid A [13]. However, these proteins can be expressed in other benign and malignant liver lesions. Therefore, it is necessary to assess the nature of their distribution in the context of the background liver tissue [2]. Thus, the HCA diagnosis requires consistent, comprehensive assessment of clinical data, instrumental testing results, as well as morphological and immunohistochemical verification of the mass.

In 2017, the analysis of more than 500 HCA cases showed the correlation of molecular and immunohistochemical subtypes with the risk of hemorrhage, tumor growth, and malignant transformation [4]. The authors expanded classification to eight subtypes, including different variants of β-catenin-activated adenomas, mixed forms, sonic Hedgehog signaling adenoma (sh-HCA), associated with intratumoral hemorrhage [4, 14]. In total, novel and unclassified subtypes constitute about one third of all HCAs.

Thus, the current data emphasize the importance of comprehensive approach to the HCA diagnosis and risk stratification including clinical assessment, instrumental tests (MRI, CT, ultrasonography), and immunohistochemistry, which directly reflects the patient management strategy presented in this case study.

Clinical case

Patient M. aged 28 presented with the right hypochondrial pain, pressure in her epigastric region, and cough with a small amount of sputum that emerged after acute respiratory viral infection. She had a history of gastro-esophageal reflux disease and the long-term (more than 10-year) use of combined oral contraceptives. She had no family history of cancer of liver disease. The patient denied occupational hazards and the exposure to adverse production factors.

Assessment performed in a medical institution in Donetsk occasionally revealed a liver mass. The patient contacted the oncologic dispensary in Rostov-on-Don on her own for further diagnosis and comprehensive assessment.

Assessment data

According to the abdominal magnetic resonance imaging (03.10.2025, revision 05.10.2025), the liver is enlarged, with an uneven outline; bilobar dimensions 208 × 186 mm. A solid mass sized at least 65 × 76 × 80 mm in the S5–S6 segments is visible, which is comparable with the intact liver parenchyma based on signal intensity, with contrast uptake. When performing differential diagnosis, we considered focal nodular hyperplasia, hepatocellular adenoma, and hepatocellular carcinoma. The diagnostic interpretation was difficult due to technical limitations of the study (low signal-to-noise ratio, no full-fledged arterial phase and wash-in/wash-out phases). No ascites detected, bone structures without signs of abnormality.

The clinical and laboratory tests conducted revealed no abnormality. The alpha-fetoprotein (AFP) level of 2.36 ng/mL was within the reference range.

Due to the patient's young age, no liver cirrhosis, AFP within the reference range, the presence of the large solid mass, and inability to reliably rule out both benign and malignant nature of the tumor based on radiological data, it was decided to perform trephine biopsy in order to morphologically verify the diagnosis, which was of fundamental importance for determination of further treatment tactics.

The biopsy specimen histological examination (19.10.2025) revealed hepatocytes showing signs of focal protein (granular) dystrophy; some cells were deformed and atrophic. There were no portal tracts. Morphological features corresponded to hepatocellular adenoma (ICD-10: D13.4). Considering the need for malignization risk stratification, immunohistochemistry (IHC) assessment aimed at estimating proliferation activity and detecting β-catenin mutation was recommended.

According to IHC data (19.10.2025), the Ki-67 index was 2%, which suggests low proliferation activity of tumor cells. There was no nuclear β-catenin expression, which allowed us to rule out the β-catenin-activated adenoma subtype associated with high risk of malignization. Thus, IHC assessment confirmed that the mass was benign and belonged to the group of low cancer risk.

The morphological and immunophenotyping data obtained (no signs of β-catenin activation and low Ki-67 index) allowed us to consider the tumor as benign. At the same time, considerable tumor size (over 5 cm), risk of spontaneous bleeding, and the long-term use of oral contraceptives as a potential etiological factor made surgical treatment feasible.

On 07.11.2025 the patient underwent elective surgery with endotracheal anesthesia and intraoperative monitoring of vital functions. Midline laparotomy with layer-by-layer dissection of the anterior abdominal wall tissues was performed. After dissection the abdominal cavity was thoroughly revised: no free fluid was detected, no signs of tumor dissemination or peritoneal lesion were found. The liver was enlarged, in the projection of segments VI–VII there was a soft elastic mass with a diameter up to 8–9 cm (Fig.). Considering the tumor localization and size, anatomic resection of the liver segments VI–VII was performed using an ultrasonic scalpel and waterjet dissector, within the limits of visually intact tissues. The liver wound was treated using an argon plasma coagulator and hemostatic sponge (Tachocomb, Austria). A drainage tube made of polyvinyl chloride was installed in the subhepatic space. The abdominal cavity was sutured layer by layer. The radical surgery was performed without any technical complications.

The resected material morphological examination has shown that the mass is partially encapsulated and has uneven outline. It is represented by beams formed by two cell layers surrounded by the well-developed reticulin framework; there are no portal tracts. Morphological features correspond to hepatocellular adenoma.

The data obtained has confirmed that the resected liver mass was the HCA showing no signs of nuclear β-catenin activity.

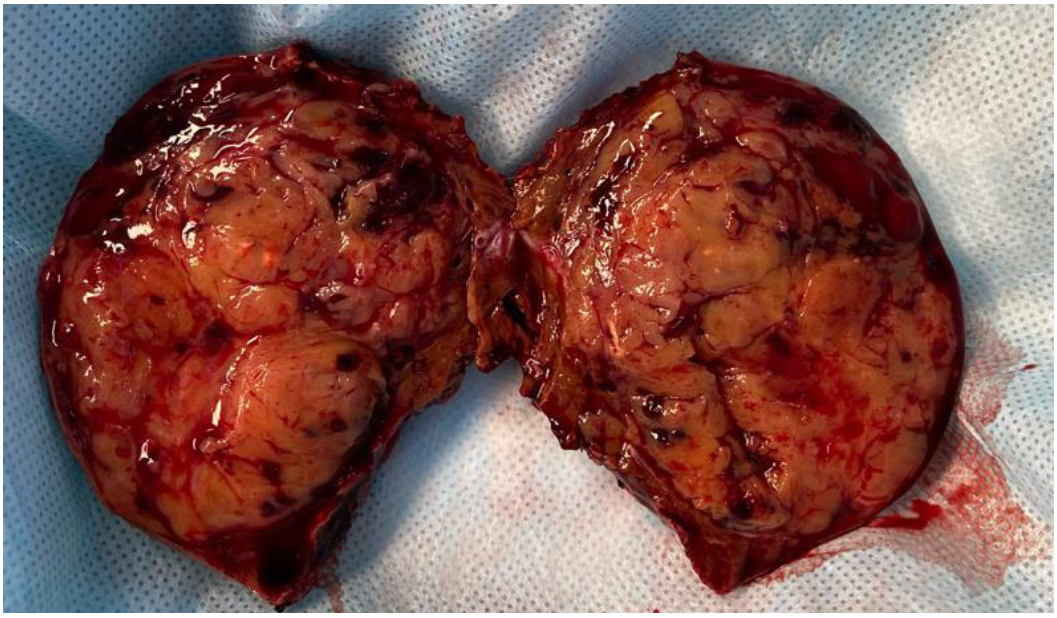

Fig. Gross specimen. Liver tissue fragment sized 8 × 8 × 7 cm, at a distance of 1 cm from the nearest resection margin

Morphological verification of biopsy and resected materials revealed typical HCA architecture with the beams of two cell layers, well-developed reticulin framework, and the lack of portal tracts. According to the immunophenotyping results, the Ki-67 index is 2%, there is no nuclear β-catenin activity, which corresponds to the group at low risk of malignization. These signs that are prognostically favorable confirm the tumor benign nature.

The postoperative period was uneventful, the patient was discharged on day 7 after surgery in satisfactory condition.

Clinical case discussion

Modern concepts emphasize heterogeneity of this group of neoplasms, differences between their molecular subtypes, and variability of prognostic characteristics. In the literature, the long-term use of oral contraceptives is considered as one of the factors associated with HCA in women of child-bearing age. In the case reported, the patient received hormonal contraceptives throughout 10 years, which can be considered a significant predisposing factor. However, the case report descriptive nature does not allow us to draw causal conclusions. The long-term hormonal exposure is associated with the increased expression of proliferative and metabolic pathways in hepatocytes, contributing to the development of adenomatous nodules. The tumor size over 5 cm remains the key prognostic criterion associated with the increased likelihood of hemorrhagic complications, regardless of the molecular subtype. It is also characterized by high risk of rupture, especially in pregnancy and during menstruation, which results in life-threatening complications [4, 9]. In large-scale clinical trials, the rate of rupture with intraperitoneal hemorrhage reached 17.5% [11].

In the clinical case reported, the patient's tumor size reached 8 cm, which corresponded to the critical size associated with the increased risk of intrahepatic and intraperitoneal hemorrhage, especially during hormonal stimulation. Immunohistochemistry assessment revealed the lack of the β-catenin, reducing the risk of malignant transformation, but the large tumor size itself represents an indication for surgical intervention.

Establishing the final diagnosis became possible due to coherent and comprehensive assessment of clinical data, radiological test results, and morphological and immunohistochemistry verification of the mass. Integration of clinical/instrumental and pathomorphological data enabled substantiated differential diagnosis of a focal liver lesion and determination of rational treatment tactics.

CONCLUSION

HCA is a rare benign liver tumor characterized by the risk of hemorrhagic complications and malignization. The long-term use of oral contraceptives by women of child-bearing age is considered as a significant etio-pathogenetic fator, which results in the need for personalized approach to management of patients and regular monitoring of benign focal liver masses. The tumor size ≥ 5 cm is an independent predictor of unfavorable course and indication for surgery, regardless of the β-catenin mutation status. Anatomic resection of the liver in individuals with large HCAs represents a rational treatment strategy aimed at reducing the risk of life-threatening conditions and achieving favorable treatment outcomes.

The case focuses on the need for increased clinical suspicion of liver tumors in women of reproductive age, especially in cases of the long-term use of hormonal contraceptives. The lack of specific clinical and laboratory manifestations does not preclude the existence of the tumor and requires in-depth assessment with morphological verification in cases of diagnostic uncertainty.

References

1. Bioulac-Sage P, Blanc JF, Rebouissou S, Balabaud C, Zucman-Rossi J. Genotype–phenotype classification of hepatocellular adenoma. World Journal of Gastroenterology. 2007; 13 (19): 2649–54. DOI: 10.3748/wjg.v13.i19.2649.
2. Kim H, Park YN. Hepatocellular adenomas: recent updates. Journal of Pathology and Translational Medicine. 2021; 55 (3): 171–80. DOI: 10.4132/jptm.2021.02.27.
3. Bonder A, Afdhal N. Evaluation of liver lesions. Clin Liver Dis. 2012;16 (2): 271–83. DOI: 10.1016/j.cld.2012.03.001.
4. Nault JC, Couchy G, Balabaud C, et al. Molecular classification of hepatocellular adenoma associates with risk factors, bleeding, and malignant transformation. Gastroenterology. 2017; 152 (4): 880–94. DOI: 10.1053/j.gastro.2016.11.042.
5. Aalten SM, Man RA, Ijzermans JN, Terkivatan T. Systematic review of haemorrhage and rupture of hepatocellular adenomas. British Journal of Surgery. 2012; 99 (7): 911–16. DOI: 10.1002/bjs.8762.
6. Shreenath AP, Grant LM, Kahloon A. Hepatocellular Adenoma. 2024 May 6. In: StatPearls [Internet]. Treasure Island (FL): StatPearls Publishing; doi.org/10.1093/bjr/tqae180.
7. Gautam S, Zhang L, Lee C, Arnaoutova I, Chen HD, Resaz R, et al. Molecular mechanism underlying impaired hepatic autophagy in glycogen storage disease type Ib. Human Molecular Genetics. 2023; 32 (2): 262–75. DOI: 10.1093/hmg/ddac197.
8. Fu J, Wang T, Zhai X, Xiao X. Primary hepatocellular adenoma due to biallelic HNF1A mutations and its co-occurrence with MODY 3: case report and review of the literature. Endocrine. 2020; 67 (3): 544–51. DOI: 10.1007/s12020-019-02138-x.
9. Margolskee E, Bao F, de Gonzalez AK, Moreira RK, Lagana S, Sireci AN, et al. Hepatocellular adenoma classification: a comparative evaluation of immunohistochemistry and targeted mutational analysis. Diagnostic Pathology. 2016; 11: 27. DOI: 10.1186/s13000-016-0475-5.
10. LiverTox: Clinical and Research Information on Drug-Induced Liver Injury [Internet]. Bethesda (MD): National Institute of Diabetes and Digestive and Kidney Diseases, 2012.
11. Thomeer MG, Broker M, Verheij J, Doukas M, Terkivatan T, Bijdevaate D, et al. Hepatocellular adenoma: when and how to treat? Update of current evidence. Therapeutic Advances in Gastroenterology. 2016; 9 (6): 898–912. DOI: 10.1177/1756283X16663882.
12. Poté N, Caruso S, Calderaro J, Cauchy F, Lagadec F, Couchy G, et al. Borderline hepatocellular adenomas: a practical diagnostic approach based on pathologic and molecular features. Modern Pathology. 2023; 36 (9): 100211. DOI: 10.1016/j.modpat.2023.100211.
13. Bioulac-Sage P, Rebouissou S, Thomas C, Blanc JF, Saric J, Sa Cunha A, et al. Hepatocellular adenoma subtype classification using molecular markers and immunohistochemistry. Hepatology. 2007; 46 (3): 740–8. DOI: 10.1002/hep.21743.
14. Bioulac-Sage P, Sempoux C, Balabaud C. Hepatocellular adenoma: classification, variants and clinical relevance. Seminars in Diagnostic Pathology. 2017; 34 (2): 112–25. DOI: 10.1053/j.semdp.2016.12.007.

Литература

1. Bioulac-Sage P, Blanc JF, Rebouissou S, Balabaud C, Zucman-Rossi J. Genotype–phenotype classification of hepatocellular adenoma. World Journal of Gastroenterology. 2007; 13 (19): 2649–54. DOI: 10.3748/wjg.v13.i19.2649.
2. Kim H, Park YN. Hepatocellular adenomas: recent updates. Journal of Pathology and Translational Medicine. 2021; 55 (3): 171–80. DOI: 10.4132/jptm.2021.02.27.
3. Bonder A, Afdhal N. Evaluation of liver lesions. Clin Liver Dis. 2012;16 (2): 271–83. DOI: 10.1016/j.cld.2012.03.001.
4. Nault JC, Couchy G, Balabaud C, et al. Molecular classification of hepatocellular adenoma associates with risk factors, bleeding, and malignant transformation. Gastroenterology. 2017; 152 (4): 880–94. DOI: 10.1053/j.gastro.2016.11.042.
5. Aalten SM, Man RA, Ijzermans JN, Terkivatan T. Systematic review of haemorrhage and rupture of hepatocellular adenomas. British Journal of Surgery. 2012; 99 (7): 911–16. DOI: 10.1002/bjs.8762.
6. Shreenath AP, Grant LM, Kahloon A. Hepatocellular Adenoma. 2024 May 6. In: StatPearls [Internet]. Treasure Island (FL): StatPearls Publishing; doi.org/10.1093/bjr/tqae180.
7. Gautam S, Zhang L, Lee C, Arnaoutova I, Chen HD, Resaz R, et al. Molecular mechanism underlying impaired hepatic autophagy in glycogen storage disease type Ib. Human Molecular Genetics. 2023; 32 (2): 262–75. DOI: 10.1093/hmg/ddac197.
8. Fu J, Wang T, Zhai X, Xiao X. Primary hepatocellular adenoma due to biallelic HNF1A mutations and its co-occurrence with MODY 3: case report and review of the literature. Endocrine. 2020; 67 (3): 544–51. DOI: 10.1007/s12020-019-02138-x.
9. Margolskee E, Bao F, de Gonzalez AK, Moreira RK, Lagana S, Sireci AN, et al. Hepatocellular adenoma classification: a comparative evaluation of immunohistochemistry and targeted mutational analysis. Diagnostic Pathology. 2016; 11: 27. DOI: 10.1186/s13000-016-0475-5.
10. LiverTox: Clinical and Research Information on Drug-Induced Liver Injury [Internet]. Bethesda (MD): National Institute of Diabetes and Digestive and Kidney Diseases, 2012.
11. Thomeer MG, Broker M, Verheij J, Doukas M, Terkivatan T, Bijdevaate D, et al. Hepatocellular adenoma: when and how to treat? Update of current evidence. Therapeutic Advances in Gastroenterology. 2016; 9 (6): 898–912. DOI: 10.1177/1756283X16663882.
12. Poté N, Caruso S, Calderaro J, Cauchy F, Lagadec F, Couchy G, et al. Borderline hepatocellular adenomas: a practical diagnostic approach based on pathologic and molecular features. Modern Pathology. 2023; 36 (9): 100211. DOI: 10.1016/j.modpat.2023.100211.
13. Bioulac-Sage P, Rebouissou S, Thomas C, Blanc JF, Saric J, Sa Cunha A, et al. Hepatocellular adenoma subtype classification using molecular markers and immunohistochemistry. Hepatology. 2007; 46 (3): 740–8. DOI: 10.1002/hep.21743.
14. Bioulac-Sage P, Sempoux C, Balabaud C. Hepatocellular adenoma: classification, variants and clinical relevance. Seminars in Diagnostic Pathology. 2017; 34 (2): 112–25. DOI: 10.1053/j.semdp.2016.12.007.

CHANGES IN EXPRESSION OF HOMOLOGOUS RECOMBINATION GENES IN CHEMOTHERAPY-INDUCED TUMORS *IN VIVO*

Tsyganov MM[1,2] ✉, Tsydenova IA[1], Loos DM[1], Ibragimova MK[1,2]

[1] Cancer Research Institute, Tomsk National Research Medical Center of the Russian Academy of Sciences, Tomsk, Russia
[2] Siberian State Medical University, Tomsk, Russia

Studying molecular mechanisms of carcinogenesis, including abnormalities of the homologous recombination (HR) system, is an important objective when studying malignization. Dysfunction of HR genes, such as *BRCA1/2*, contributes to genomic instability and the development of more aggressive tumor clones. The use of chemical carcinogens, such as dimethylbenz(a)anthracene (DMBA), allows one to simulate tumorigenesis processes and assess changes in expression of repair genes. It is important to study such changes to understand the mechanisms underlying adaptation of tumor cells to genotoxic stress and develop personalized approaches to cancer treatment. The study aimed to assess the expression of major HR genes in chemotherapy-induced carcinogenesis in mice. The study involved female outbred ICR laboratory mice (CD-1; $n = 20$). Two groups of animals were formed: the control group and the treatment group that was administered DMBA. Histological analysis of autopsy specimens was conducted to identify tumors. Gene expression levels were assessed using RT-PCR, and testing for chromosomal aberrations was performed using digital PCR. Tumors were found in four animals. Zero expression of the genes *Brca1, Brca2, Cdk12, Chek2, Palb2, Bard1, Brip1* and *Rad* paralogues was observed in three tumor samples. One sample showed high expression of the genes *Cdk12* (14.3), *Chek1* (27.6), *Rad51d* (38.5). Predominance of deletions in the test genes was reported in the majority of cases. Thus, tumorigenesis is associated with the decrease in expression of major repair genes, chromosomal aberration formation, which can contribute to the emergence of more aggressive clones and increase sensitivity to chemotherapy drugs.

Keywords: chemotherapy-induced carcinogenesis; homologous recombination genes, *Brca1*; expression; dimethylbenzanthracene

Funding: the study was supported by the Russian Science Foundation (grant No. 22-15-00169-П).

Acknowledgements: to D.Zh. Bulatova, animal care specialist (Cancer Research Institute, Tomsk), and P.E. Nikiforov, laboratory research assistant (Goldberg Research Institute of Pharmacology and Regenerative Medicine, Tomsk) for assistance in planning and conducting experiments involving model animals.

Author contribution: Tsyganov MM — manuscript writing; Tsydenova IA — acquisition of the data for analysis; Loos DM — acquisition of the data for analysis, imaging; Ibragimova MK — editing.

Compliance with ethical standards: the study was approved by the Ethics Committee of the Cancer Research Institute, Tomsk National Research Medical Center of the Russian Academy of Sciences (protocol No. 21 dated 14 October 2022). Animals were handled in accordance with the European Convention for the Protection of Vertebrate Animals Used for Experimental and Other Scientific Purposes (ETS No. 123).

✉ **Correspondence should be addressed:** Matvey M. Tsyganov
Kooperativnaya 5, Tomsk, 634050, Russia; tsyganovMM@yandex.ru

Received: 17.03.2026 **Accepted:** 08.04.2026 **Published online:** 19.04.2026

DOI: 10.24075/brsmu.2026.014

ИЗМЕНЕНИЯ В ЭКСПРЕССИИ ГЕНОВ ГОМОЛОГИЧНОЙ РЕКОМБИНАЦИИ В ХИМИЧЕСКИ ИНДУЦИРОВАННЫХ ОПУХОЛЯХ *IN VIVO*

М. М. Цыганов[1,2] ✉, И. А. Цыденова[1], Д. М. Лоос[1], М. К. Ибрагимова[1,2]

[1] Научно-исследовательский институт онкологии, Томский национальный научно-исследовательский медицинский центр, Томск, Россия
[2] Сибирский государственный медицинский университет, Томск, Россия

Изучение молекулярных механизмов канцерогенеза, включая нарушение в системе гомологичной рекомбинации (ГР), является важной задачей при изучении процесса малигнизации. Дисфункция генов ГР, таких как *BRCA1/2*, способствует геномной нестабильности и развитию более агрессивных опухолевых клонов. Использование химических канцерогенов, таких как диметилбенз(а)антрацен (ДМБА), позволяет моделировать процессы опухолеобразования и анализировать изменения экспрессии генов репарации. Изучение этих изменений важно для понимания механизмов адаптации опухолевых клеток к генотоксическому стрессу и разработки персонализированных подходов к терапии рака. Целью работы было оценить экспрессию основных генов ГР при химиоиндуцированном канцерогенезе у мышей. Исследование проводили на самках аутбредных лабораторных мышей ICR (CD-1; $n = 20$). Сформировано две группы животных: контрольная и группа исследования с введением ДМБА. Для идентификации опухолей аутопсийный материал подвергали гистологическому анализу. Уровень экспрессии генов оценивали при помощи ОТ-ПЦР, наличие хромосомных аберраций — посредством цифровой ПЦР. Наличие опухолей установлено у четырех животных. В трех образцах опухоли наблюдали нулевую экспрессию *Brca1, Brca2, Cdk12, Chek2, Palb2, Bard1, Brip1* и паралогов *Rad*. У одного образца зафиксированы высокие уровни генов *Cdk12* (14,3), *Chek1* (27,6), *Rad51d* (38,5). В большинстве случаев зафиксировано преобладание делеций в исследуемых генах. Таким образом, при опухолеобразовании происходит снижение экспрессии основных генов репарации, формирование хромосомных аберраций, что может способствовать появлению более агрессивных клонов, а также увеличивать чувствительность к химиопрепаратам.

Ключевые слова: химиоиндуцированный канцерогенез, гены гомологичной рекомбинации, *Brca1*, экспрессия, диметилбензантрацен

Финансирование: работа выполнена при финансовой поддержке Российского научного фонда (грант № 22-15-00169-П).

Благодарности: работнику по уходу за животными Д. Ж. Булатовой (НИИ онкологии, г. Томск) и лаборанту-исследователю П. Е. Никифорову (НИИ фармакологии и регенеративной медицины им. Е. Д. Гольдберга, г. Томск) за помощь в планировании и проведении эксперимента на модельных животных.

Вклад авторов: М. М. Цыганов — написание текста статьи; И. А. Цыденова — получение данных для анализа; Д. М. Лоос — получение данных для анализа, визуализация; М. К. Ибрагимова — редактирование.

Соблюдение этических стандартов: исследование одобрено этическим комитетом НИИ онкологии Томского национального научно-исследовательского медицинского центра Российской академии наук (протокол № 21, от 14 октября 2022 г.). Содержание, уход и все манипуляции с животными проводили в соответствии с Европейской конвенцией о защите позвоночных животных, используемых в экспериментальных и других научных целях (ETS № 123).

✉ **Для корреспонденции:** Матвей Михайлович Цыганов
ул. Кооперативная, д. 5, г. Томск, 634050, Россия; tsyganovMM@yandex.ru

Статья получена: 17.03.2026 **Статья принята к печати:** 08.04.2026 **Опубликована онлайн:** 19.04.2026

DOI: 10.24075/vrgmu.2026.014

Studying the mechanisms underlying the emergence and progression of solid tumors remains one of the most urgent tasks of modern biomedicine [1]. Alteration of homologous recombination system genes involved in double-stranded DNA breakrepair, cell cycle regulation, and other cellular processes can be one of the key events underlying carcinogenesis [2]. Such alterations can manifest itself as dysfunction (accumulation of mutations, major chromosomal rearrangements, changes in expression, etc.) of the key homologous recombination genes, specifically *BRCA1* and *BRCA2*. Dysfunction leads to deficiency of the repair of double-stranded DNA breaks, or homologous recombination deficiency (HRD) [3]. At the same time, the expression levels of *BRCA1/2* and other HR system genes represent the major ultimate factors determining not only the genetic and functional dysfunction extent, but also the tumor cell sensitivity to various chemotherapeutic agents.

According to the working hypothesis of the present study, the mechanisms underlying the development of homologous recombination deficiency are enhanced, increasing genetic instability during the tumor transformation, growth, and progression. From an evolutionary perspective, it is "beneficial" for the tumor to form a mutator phenotype, primarily through the homologous recombination dysregulation. Moreover, the mechanisms underlying the development of HRD in tumor cells have to be enhanced through the increase of the rate and expansion of the range of abnormalities. Baseline mutations in the HR genes can be complemented by deletions, methylation, gene repression, etc., which should lead to generation of more aggressive clones. However, this process remains practically unexplored. The study of the process will help predict the risk of malignant transformation for precancerous disorders and the aggressiveness of early-stage tumors.

Chemicals that cause mutations and other genotoxic changes are particularly valuable for carcinogenesis modeling, since these are direct triggers of tumor development. The 7,12-dimethylbenz[a]anthracene (DMBA) having the pronounced carcinogenic properties and widely used in pre-clinical trials for simulation of tumorigenesis processes *in vivo* and *in vitro* is one of the most common polycyclic aromatic hydrocarbons in our environment [4, 5]. Currently, the data on expression profiles of the tumor genes induced by specific chemical carcinogens remain scarce. The available data suggest the association between the effects of chemicals and the homologous recombination abnormalities. For example, it has been shown that the exposure to the PAH doses appropriate to the environmental conditions results in the dose-dependent *BRCA1* expression decrease in breast cancer cells [6]. The earlier research showed that PAH also suppressed *BRCA1 in vitro* and *in vivo* [7]. In this context, the use of mouse models has become a powerful instrument for *in vivo* assessment of cancer etiology and progression. However, studying the homologous recombination suppression effects *in vivo* is still a challenging task, especially in the context of chemotherapy-induced carcinogenesis. For example, it has been shown that the *Rad51* mutations strongly predispose mice to lymphomas, while the *Brca1* mutations contribute to the development of tumors of other types [8]. Mouse models with the partial loss of *Brca2* function also show increased carcinogenesis levels with predispodition to lymphomas [9]. In addition to the *BRCA1* and *BRCA2* key HR genes, other components of the pathways play an important role in both DNA repair and carcinogenesis. The mouse model studies have shown that the decrease in activity of the same *Rad51* gene in vivo does not contribute to tumor development, but rather ensures protection against the tumor. These data suggest that the *Rad51*-mediated repair can contribute to tumor progression rather than function as a tumor suppressor [10, 11]. Other HR genes with low penetrance, including *ATM*, *CHEK2*, *BRIP1*, and *BARD1*, have been extensively studied in the context of human breast carcinogenesis [12]. However, their function and contribution to tumorigenesis in mouse models are still poorly understood. Today, the data on the regulation of these genes in mouse models are limited, which hinders full understanding of their role in DNA repair and carcinogenesis [12]. That is why the analysis of the HR gene expression changes during carcinogenesis can make it possible to determine, how the cells respond to genotoxic stress and how these processes can be disrupted in tumor tissues [13]. Understanding of these dynamic changes can determine the tumor cell sensitivity to DNA-damaging agents, which is important for personalized cancer treatment. Thus, the present study aimed to assess the expression of the key homologous recombination system genes in chemotherapy-induced carcinogenesis in mice.

METHODS

Animals

Chemotherapy-induced carcinogenesis was assessed in 20 female outbred ICR laboratory mice (CD-1). The animals were handled in accordance with the European Convention for the Protection of Vertebrate Animals Used for Experimental and Other Scientific Purposes (ETS N 123). The animals were kept in standard conditions at a temperature of 22 ± 2 °C, relative humidity of 50–60%, with the 12-h light/dark cycle (8:00 to 20:00). Food and water were provided freely. All the procedures involving animals were conducted in the morning (9:00 to 11:00 local time) in accordance with the rules and guidelines on humane treatment of animals used for experimental and other scientific purposes. The health and behavioral aspects were monitored daily, and any signs of discomfort or illness were immediately eliminated by specialists.

Experimental design

The design was developed in accordance with the 3R principles, reducing the number of animals to the necessary minimum and minimizing discomfort. Two groups of animals were formed for the experiment. Weighing and randomization (based on the mean body weight, mean ± 10%) were used to divide the animals into the control (n = 10) and treatment (n = 10) groups. The mean body weight was 27.2 ± 0.62 g in the control group and 26.4 ± 0.56 g in the treatment group. Dimethylbenz(a)anthracene (DMBA) (100 mg, 1,3-dimethylbutylamine, 98%, Sigma-Aldrich #108-09-8) was used as a chemical agent possessing direct or indirect genotoxicity to induce carcinogenesis.

Dose selection

Since DMBA is not soluble in water, but is well soluble in organic solvents, when preparing the working solution, 100 mg of the substance was dissolved in 10 mL of toluene until completely dissolved, thereby obtaining a matrix solution with the substance concentration of 1 mg per 0.1 mL (100 μL) of the solvent. A total of 0.07 mg (70 μg) of the substance was taken for the course. Recalculated on the solution: 70 μL of the substance dissolved in toluene were adjusted to 30 ml of vegetable oil. With this dilution, the substance dose was 23 μg/kg, provided that 0.25 mL of the solution per 25 g of live weight would be administered. The resulting solution was

intragastrically administered weekly throughout 3 months. It should be noted that according to published data, toluene can have a toxic effect on behavioral characteristics of laboratory animals and some body's molecular parameters [14]. However, with minimal toluene doses cytochrome P4502A13 can effectively metabolize this substance in the body [15] without any negative effects.

Euthanasia

Humane euthanasia of animals was accomplished using the CO_2 camera with the gradually increasing gas concentration. Autopsy of the animals aimed at identifying the tumor was performed in accordance with the method for laboratory animal autopsy and organ harvesting [16]. After harvesting the tissue was placed in the RNAlater solution (Thermo Fisher Scientific, USA). After the 24-h incubation at +4 °C the tissue samples were stored at a temperature of –80 °C for further DNA and RNA extraction.

Morphological examination

To assess the pattern of morphological changes and confirm the presence of tumor tissue in the samples, the tissue fragments removed from the suspected tumor site, as well as metastases, were examined. The tissue fragments sized 5 mm^3 were placed in the 10% pH-neutral formalin (6.5–7.5). The duration of fixation was 18–24 h. Then the material was processed in accordance with the standard method and paraffin embedded. The 4–5 μm thick serial sections were prepared from paraffin blocks [17]. Slides were stained using the hematoxylin and eosin solutions prepared in accordance with the generally accepted protocols. Morphological examination was performed using the Axio Scope.A1 light microscope (Karl Zeiss, Germany). Microscopic evaluation was carried out according to the generally accepted criteria [18].

DNA and RNA extraction

RNA and DNA were extracted from the tumor tissue using the RNeasy Plus mini Kit and QIAamp DNA mini Kit (Qiagen, Germany), respectively, in accordance with the manufacturer's instructions.

Real-time qPCR

Expression levels of the homologous recombination genes *Brca1, Brca2, Atm, Bard1, Brip1, Cdk12, Chek1, Chek2, Fancl, Palb2, Ppp2r2a, Rad51b, Rad51c, Rad51d, Rad54l, Parp1* were assessed using the reverse transcription quantitative PCR in the real-time mode (RT-qPCR) based on the TaqMan technology in the Rotor-Gene-6000 thermal cycler (Qiagen, Germany), as previously reported [19]. Two genes were used as reference ones: *Gapdh* (glyceraldehyde 3-phosphate dehydrogenase) and *Actb* (beta-actin); expression levels of these genes were normalized with respect to normal expression values of the genes and measured in arbitrary units. The gene relative expression was assessed by the Pfaffl method [5]. RNA extracted from the normal tissue was used for calibration.

Digital PCR

Digital PCR in the QIAcuity Digital PCR System (Qiagen, Germany) was used as a method to analyze the *Brca1, Brca2, Cdk12, Chek1, Parp1*, and *Rad51c* gene copy number. The copy number variation analysis involved determination of the number of targets and reference loci by duplex amplification. The *Ap3b1* (adaptor related protein complex 3 subunit beta 1) gene recommended by the manufacturer was selected as a reference gene.

Statistical processing of the results

Statistical data processing was performed using the Statistica 8.0 software package (StatSoft Inc., USA).

RESULTS

In the first phase of the study, we assessed the dynamic changes in body weight in the studied groups of animals between 30 December 2023 and 16 November 2025 (Fig. 1). Animals of the control group showed no changes in body weight during the follow-up period. DMBA administration caused significant changes in the animals' body weight within six weeks (Fig. 1). In particular, the mean body weight of animals of the control group in this period was 30.5 ± 0.84 compared to that of the DMBA group (28.3 ± 0.54; $p = 0.05$). In three weeks, the differences became more pronounced ($p = 0.02$), with the body weight of the DMBA group (28.7 ± 0.69) and that of the control group (31.4 ± 1.07), respectively. Later the upward trend of the animals' body weight was observed in both control and experimental groups. However, no significant differences were reported throughout the experiment.

Upon palpating (and visually examining), tumors were found in four animals on weeks 46, 55, 56, and 61 of the experiment (Fig. 1).

After euthanasia, autopsy of the animals was performed, as well as testing for tumors and metastasis to distant organs (if any). A total of four mice out of 10 developed tumors. No tumors were found in the control group. Analysis of specimen obtained from the laboratory animal No. 7, which was located subcutaneously in the cervical region, revealed a morphological pattern of a pleomorphic cellular tumor with the invasive structure forming solid areas, variously sized sockets and cords, as well as trabecular and glandular structures, composed of moderately polymorphic cells of medium size with the moderately pronounced eosinophilic cytoplasm and rounded, hyperchromatic nuclei. Multiple tumor necrosis foci were found in the central areas of glandular structures. The stroma was moderately pronounced. It was represented by various-sized strands of mature fibrous connective tissue with hyalinosis and uneven lymphoplasmacytic infiltration. There was an extremely small fragment of skin with the subcutaneous fat along the edge of the fragment (Fig. 2A). Tumors with similar morphological structure, but localized in the stomach area on the peritoneum, were found in another two laboratory mice (specimens No. 8 and No. 9). Subtotal tissue fragments were represented by necrosis with signs of active inflammation. Structures of the invasive tumor described above were found along the periphery of a tissue fragment in some fields of view (specimen No. 7). The signs of uneven moderate inflammatory infiltration with the presence of neutrophils and corpuscular purulenta were seen throughout the fragment. There were sporadic small calcifications in the thickness of necrotic areas (Fig. 2B and C).

In one more laboratory animal (No. 6), the tumor was localized in the lung tissue (Fig. 2D). Morphological examination revealed lung tissue fragments subtotally substituted with the tumor of polymorphic structure within the slide. A large part of the tumor was represented by merged solid

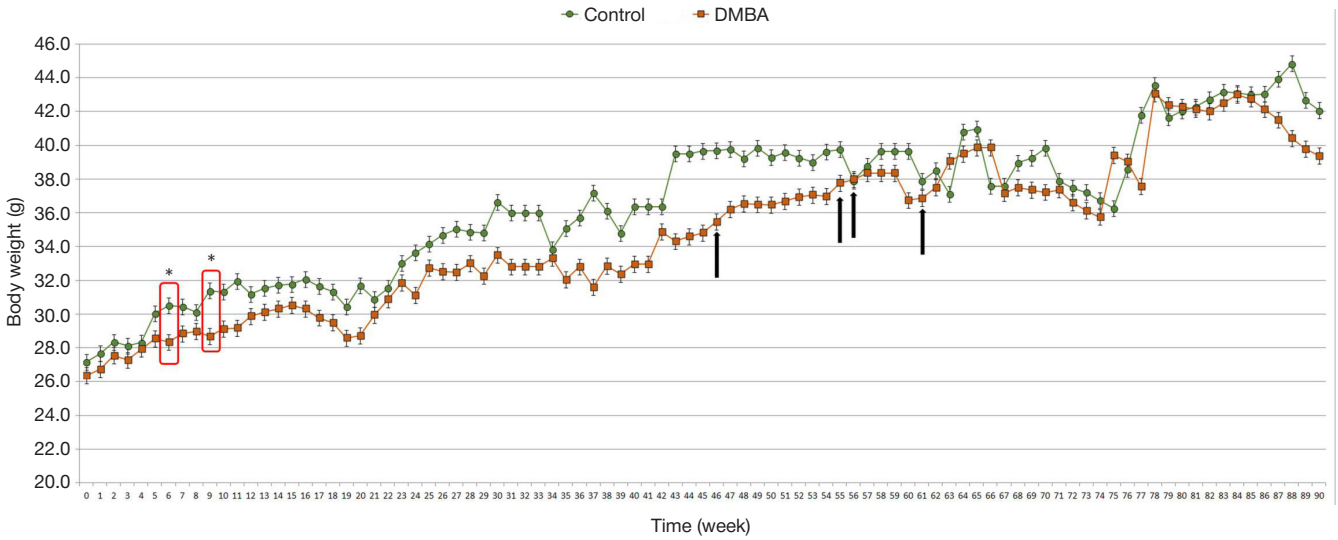

Fig. 1. Dynamic changes in body weight in the studied groups of animals during the follow-up period. DMBA — group of animals administered dimethylbenz[a] anthracene; * — significant differences; the time of tumor emergence in the studied group of animals is marked with *arrows*

areas of moderately polymorphic, moderately sized cells with moderately pronounced eosinophilic cytoplasm and rounded, hyperchromatic nuclei. In some fields of view, the tumor consisted of the acinar structures composed of medium and small sized relatively monomorphic cells. In some foci, the tumor formed pseudovascular fissures; a few small foci of necrosis were found. The moderately pronounced tumor stroma was represented by strands of the mature fibrous connective tissue with mild lymphoid infiltration.

In the next phase of the study, we assessed the expression of homologous recombination genes in the tumor tissue specimens collected (Fig. 3).

In particular, high expression of the genes Brca1 (2.06 AU); *Atm* (6.81 AU), *Bard1* (5.62 AU), *Cdk12* (14.36 AU), *Chek1* (27.68 AU), *Fancl* (5.82 AU), *Rad51d* (38.57 AU) was found for the tumor tissue specimen collected from the laboratory mouse No. 6 (Fig. 3A), which suggests that the homologous recombination system and its potential DNA damage repair activity were preserved in this tumor. It should be also noted that testing for chromosomal aberrations using digital PCR revealed the *Brca1* gene amplification (Table). Low expression of the test genes was observed in other tumor tissue specimens. In particular, in the laboratory mouse No. 7, normal expression was found typical only for *Parp1* (1.001 AU), and hyperexpression was reported only for *Rad51c* (2.9 AU). All other genes, including *Brca1/2*, showed zero or very low expression (Fig. 3B). Similar results were typical for another two samples. In the tumor specimen from the mouse No. 8, zero expression was typical for 8 test genes out of 16 (*Brca1, Brca2, Cdk12, Chek2, Palb2, Rad51b, Rad51c, Rad51d*). In the tumor of mouse No. 9, zero values were reported for 12/16 genes (*Brca1, Brca2, Atm, Bard1, Brip1, Chek2, Fancl, Palb2, Ppp2r2a, Rad51b, Rad51d*,

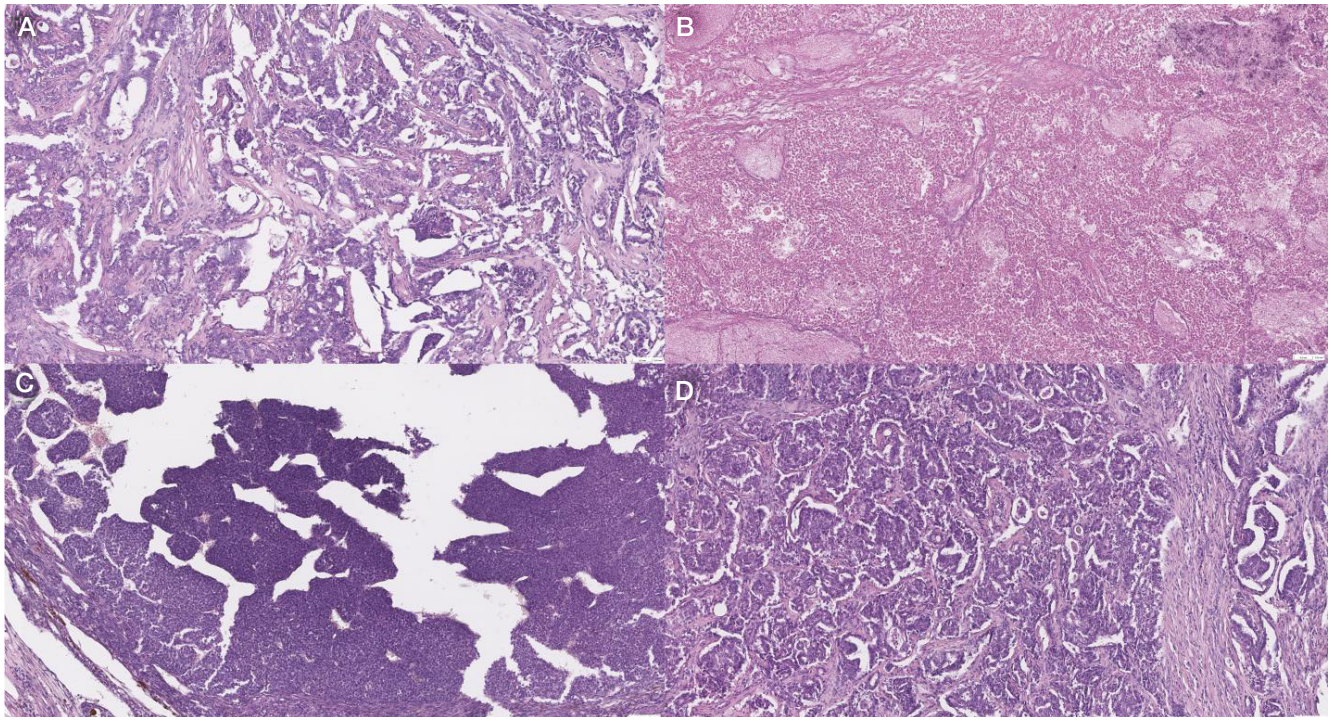

Fig. 2. Microphotographs of the sections of tumor specimens obtained from laboratory animals No. 7 (**A**), No. 8 (**B**), No. 9 (**C**), and No. 6 (**D**), 10× magnification. Hematoxylin and eosin stain

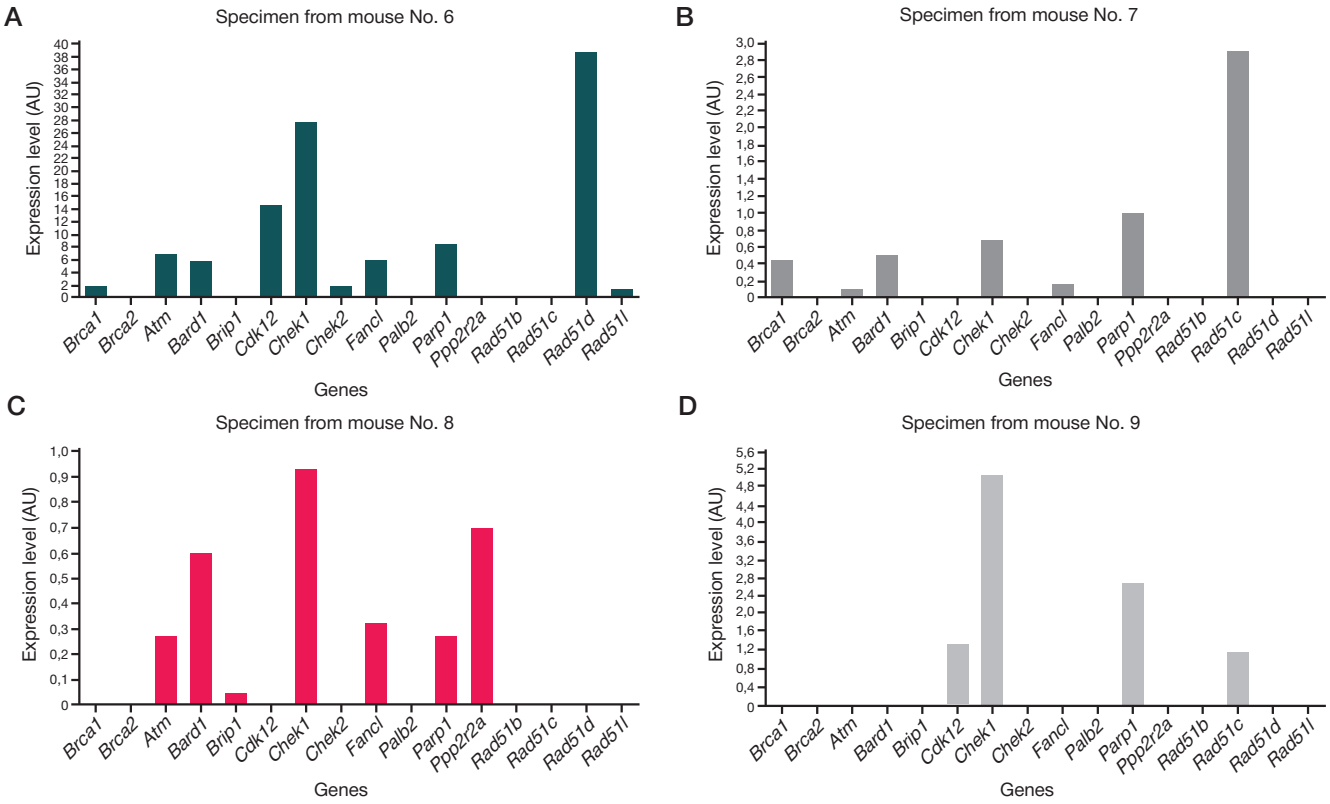

Fig. 3. Homologous recombination gene expression levels in the group of mice administered carcinogen (DMBA)

Rad51l) (Fig. 3C and D). The deletion in the *Brca1* was reported for all specimens. Furthermore, Table 1 provides the data of the analysis of chromosomal rearrangements in some test genes in tumor specimens. The analysis results demonstrate high genomic rearrangement heterogeneity. In particular, in the specimen No. 6, amplification is reported for the genes *Cdk12*, *Chek1*, *Parp1*, along with *Brca1*, and only two deletions are reported for the genes *Brca2* and *Rad51c*. Predominance of deletions in the test genes or normal gene copy number was observed in other specimens. In general, this suggests that the emergence of major chromosomal rearrangements and the DNA repair gene activity decrease can represent one of the carcinogenesis primary events. Furthermore, the fact of identifying amplification and/or normal gene copy number is correlated with high expression of the gene, which is in line with the literature data [20].

Thus, considering the experimental data, it has been found that disturbances of the homologous recombination mechanisms lead to the accumulation of genomic abnormalities and decreased reparative activity, thereby increasing the risk of tumors. However, if the tumor already exists, such disturbances make it more susceptible to DNA-damaging agents. This has been shown in clinical material, where the presence of the deletion and low *BRCA1* expression affected the efficacy of chemotherapy with platinum-based drugs in patients with breast cancer [21], as well as metastasis-free survival of patients with non-small cell lung cancer [22]. The studies of animal models show that such alterations (in HR genes) can contribute to both the increase in the number of tumor cases and the emergence of various tumor clones with different molecular genetic characteristics.

DISCUSSION

Homologous recombination responsible for the repair of double-strand DNA breaks plays an important role in maintaining genomic stability and preventing of carcinogenesis [8]. However, when exposed to carcinogens, such as DMBA, the HR system can show reduced activity, resulting in accumulation of mutations and, therefore, to tumorigenesis [23]. Our study demonstrates hyperexpression of the genes *Cdk12, Brca1, Atm, Bard1, Fancl, Chek1*, and *Parp1*. Furthermore, according to the literature data, disturbances in *Cdk12* functional activity lead to DNA repair abnormalities, causing

Table. Presence of the homologous recombination gene DNA copy number aberrations in tumor specimens

Genes/samples	Tumor specimen from animal No. 6	Tumor specimen from animal No. 7	Tumor specimen from animal No. 8	Tumor specimen from animal No. 9
Brca1	Gain	Loss	Loss	Loss
Brca2	Loss	Loss	Loss	Loss
Cdk12	Gain	Loss	Loss	Loss
Chek1	Gain	n	n	n
Parp1	Gain	n	n	Gain
Rad51c	Loss	Gain	Loss	n

Note: the table provides the data on the presence of major chromosomal rearrangemens for some homologous recombination genes, where gain — amplification; *n* — normal gene copy number; loss — deletion

genomic instability and the decrease in expression of some homologous recombination genes, such as *Brca1*, *Fanci*, and *Fancd2* [21, 22]. Moreover, hyperexpression of the test genes was observed in one specimen, which is not consistent with the hypothesis provided. Unfortunately, since the expression at the mRNA level is not always positively correlated with the quantity and activity of appropriate proteins, the actual functional activity of HR system in tumor cells may differ from the data obtained. This phenomenon can be explained by the influence of post-transcriptional regulatory mechanisms, such as mRNA degradation, alternative splicing, microRNA influence, post-translational modifications of proteins, etc., which can considerably modify the ultimate activity of genes in tumor cells [24]. This emphasizes the need for further research, including the study of HR system activity at the level of post-transcriptional factors.

Special attention was paid to the *Brca1* gene, the expression of which was significantly decreased in tumor tissues. Cases have been reported, when mutant mice with *Brca1* defects (*Brca1tr/tr*) developed tumors of various types, including breast cancer and lymphomas, without any additional genetic alterations, such as *Trp53* gene inactivation. Our data confirm these results and suggest the importance of *Brca1* dysfunction for the mechanism of carcinogenesis [10]. Moreover, assessment of the *Brca1* gene copy number using digital PCR revealed the *Brca1* gene deletion in three animals and amplification and the gene expression level of 2.06 in one animal. Low expression of this gene in tumor tissues was observed in the presence of the *Brca1* gene deletion. We also revealed hyperexpression of the genes *Rad51d* and *Rad51c* in three tumor specimens (Fig. 3). It can be assumed that upregulation of those in tumors can represent a compensatory mechanism in the context of *Brca1/2* dysfunction [25]. A number of studies confirm this hypothesis [10, 11]. As for *Bard1*, it has been shown that the *Bard1* inactivation induces basal-like carcinomas of the breast with the rate, latency, and histopathological characteristics indistinguishable from those observed in mice with the *Brca1* mutation or double *Bard1/Brca1* mutation [13]. Such results suggest that *Bard1* functions as the key tumor suppressor gene, along with *Brca1*, and that the *Brca1*-mediated tumor suppression is largely dependent on the *Bard1/Brca1* heterodimer. However, the question remains, why high *Bard1* expression is observed despite the decreased *Brca1* expression. In our previous *in vitro* study, it was found that when continuously exposed to cytostatic agents, the cell lines with *BRCA1* dysfunction acquired genetic alterations characterized by the HR gene amplification (including *BARD1*) and increased expression [14].

Among the genes tested, it is also important to highlight the *Rad51* gene paralogues that are involved in attracting *Rad51* to the sites of DNA damage [26] and contribute to formation and stabilization of the *Rad51* nucleoprotein filament. However, the exact role of each paralogue is not yet fully defined. Nevertheless, none of the *RAD51* mutations are associated with predisposition to cancer, which constitutes the "*RAD51* paradox" [25]. One potential explanation of the "*RAD51* paradox" is that the mutations affecting the mediator genes/accessory genes (such as *BRCA1* or *BRCA2*) in cancer result in the lack of *RAD51* in damaged DNA, leaving access to alternative, exclusively mutagenic repair processes [25]. Thus, it has been shown in the mouse model that decreasing the *Rad51* activity in vivo not only contributes to tumorigenesis, but also protects against tumors. These data suggest that the *Rad51*-controlled repair is not a tumor suppressor, but rather contributes to tumor progression [10, 11].

CONCLUSIONS

Thus, carcinogenesis is accompanied by developing the homologous recombination deficiency, and the related repair gene abnormalities are enhanced at early stages of transformation and tumor progression. We found significant changes in the copy number and expression profiles of the genes involved in biotransformation of xenobiotics, apoptosis, and cell proliferation. The findings emphasize the need for comprehensive analysis of the homologous recombination gene aberrant states aimed at understanding the carcinogenesis mechanisms and suggest potential directions for the development of novel diagnostic and therapeutic strategies in oncology. Understanding of abnormalities in the test genes, their homo- or heterogeneity can contribute to the development of the algorithms to determine the tumor chemosensitivity to DNA-damaging agents in the future. Such an approach will shed more light on the role of genetic instability in carcinogenesis and open new avenues for treatment methods.

References

1. Smith MT, Guyton KZ, Kleinstreuer N, Borrel A, Cardenas A, Chiu WA, et al. The key characteristics of carcinogens: relationship to the hallmarks of cancer, relevant biomarkers, and assays to measure them. Cancer Epidemiology, Biomarkers & Prevention. 2020; 29 (10): 1887–903.
2. Barnes JL, Zubair M, John K, Poirier MC, and Martin FL. Carcinogens and DNA damage. Biochemical Society Transactions. 2018; 46 (5): p. 1213–24.
3. Turner N, Reis-Filho J, Russell A, Springall R, Ryder K, Steele D, et al. BRCA1 dysfunction in sporadic basal-like breast cancer. Oncogene. 2007; 26 (14): p. 2126–32.
4. Morales-Herrero M and Ortega-Medina I. Experimental carcinogenesis with 7, 12-dimethylbenz (a) anthrazene (DMBA) and its inhibition with isothi-ocyanates. J oral res (Impresa). 2022: p. 1–13.
5. Allam AM, Abubakr HO, Yassin AM, Abdel-Razek AS, Khattab MS Gouda EM, et al. Potential chemopreventive effects of Broccoli extract supplementation against 7, 12 dimethyl Benz (a) anthracene (DMBA)-induced toxicity in female rats. Scientific reports. 2023; 13 (1): p. 1–19.
6. Davidson CJ, Svenson D, Hannigan JH, Perrine SA, and Bowen SE. A novel preclinical model of environment-like combined benzene, toluene, ethylbenzene, and xylenes (BTEX) exposure: Behavioral and neurochemical findings. Neurotoxicology and teratology. 2022; 91: 1–11.
7. Sahay D, Lloyd SE, Rivera JA, Jezioro J, Mcdonald JD, Pitiranggon M, et al. Prenatal polycyclic aromatic hydrocarbons, altered ERα pathway-related methylation and expression, and mammary epithelial cell proliferation in offspring and grandoffspring adult mice. Environmental research. 2021; 196: 1–15.
8. Xu X, Qiao W, Linke SP, Cao L, Li W-M, Furth PA, et al. Genetic interactions between tumor suppressors Brca1 and p53 in apoptosis, cell cycle and tumorigenesis. Nature genetics. 2001; 28 (3): 266–71.
9. Yossepowitch O, Olvera N, Satagopan JM, Huang H, Jhanwar S, Rapaport B, et al. BRCA1 and BRCA2 germline mutations in lymphoma patients. Leukemia & lymphoma. 2003; 44 (1): 127–31.
10. Matos-Rodrigues G, Barroca V, Muhammad AA, Dardillac E, Allouch A, Koundrioukoff S, et al. In vivo reduction of RAD51-mediated homologous recombination triggers aging but impairs oncogenesis. The EMBO journal. 2023; 42 (20): 1–21.

11. Kuznetsov SG, Haines DC, Martin BK, and Sharan SK. Loss of Rad51c leads to embryonic lethality and modulation of Trp53-dependent tumorigenesis in mice. Cancer research. 2009; 69 (3): 863–72.
12. Yamamoto H and Hirasawa A. Homologous recombination deficiencies and hereditary tumors. International journal of molecular sciences. 2021; 23 (1): 1–18.
13. Coates PJ, Lorimore SA, and Wright EG. Cell and tissue responses to genotoxic stress. The Journal of Pathology: A Journal of the Pathological Society of Great Britain and Ireland. 2005; 205 (2): 221–35.
14. Cruz SL, Rivera-García MT, and Woodward JJ. Review of toluene action: clinical evidence, animal studies and molecular targets. Journal of drug and alcohol research. 2014; 3: 1–15.
15. Fukami T, Katoh M, Yamazaki H, Yokoi T, and Nakajima M. Human cytochrome P450 2A13 efficiently metabolizes chemicals in air pollutants: naphthalene, styrene, and toluene. Chemical research in toxicology. 2008; 21 (3): 720–5.
16. Rathnamali K. Dissection of laboratory animal and sample collection for histology. International Journal of Scientific and Applied Research (IJSAR), eISSN: 2583–0279. 2022; 2 (3): 1–12.
17. Sadeghipour A and Babaheidarian P. Making formalin-fixed, paraffin embedded blocks. Biobanking: Methods and Protocols. 2018: 253–68.
18. Greenberg AK, Yee H, and Rom WN. Preneoplastic lesions of the lung. Respiratory research. 2002; 3: 1–10.
19. Tsyganov MM, Bulatova DZ, Fedorenko AA, Loos DM, Nikiforov PE, Tsydenova IA, et al. Assessment of Homologous Recombination System Gene Expression in Chemologically Induced Carcinogenesis In Vivo Models. Current Issues in Molecular Biology. 2026; 48 (3): 1–17.
20. Myhre S, Lingjærde O-C, Hennessy BT, Aure MR, Carey MS, Alsner J, et al. Influence of DNA copy number and mRNA levels on the expression of breast cancer related proteins. Molecular oncology. 2013; 7 (3): 704–18.
21. Tsyganov MM, Ibragimova MK, Garbukov EY, Bragina OD, Karchevskaya AA, Usynin EA, et al. Determination of BRCAness Phenotype in Breast Tumors for the Appointment of Neoadjuvant Chemotherapy Based on Platinum and Taxanes. International journal of molecular sciences. 2022; 24 (1): 1–13.
22. Tsyganov MM, Ibragimova MK, Tsydenova IA, Kravtsova EA, Bayanbaeva AA, Sharipkhanova Zh, Rodionov EO, Bragina OD, Mokh AA, Miller SV. Influence of DNA copy number aberrations and changes in the expression level of homologous recombination genes on the survival of primary operable non-small cell lung cancer patients. Acta Biomedica Scientifica.2026; 10 (6): 112–22.
23. Hollander MC, Kovalsky O, Salvador JM, Kim KE, Patterson AD, Haines DC, et al. Dimethylbenzanthracene carcinogenesis in Gadd45a-null mice is associated with decreased DNA repair and increased mutation frequency. Cancer research. 2001; 61 (6): 2487–91.
24. Verta J-P and Jacobs A. The evolutionary significance of post-transcriptional gene regulation. Heredity. 2024; 132 (3): 117–9.
25. Lopez BS. RAD51-mediated homologous recombination is a pro-tumour driver pathway. Oncogene. 2025; 44 (42): 4006–16.
26. Garcin EB, Gon S, Sullivan MR, Brunette GJ, Cian AD, Concordet J-P, et al. Differential requirements for the RAD51 paralogs in genome repair and maintenance in human cells. PLoS Genetics. 2019; 15 (10): 1–29.

Литература

1. Smith MT, Guyton KZ, Kleinstreuer N, Borrel A, Cardenas A, Chiu WA, et al. The key characteristics of carcinogens: relationship to the hallmarks of cancer, relevant biomarkers, and assays to measure them. Cancer Epidemiology, Biomarkers & Prevention. 2020; 29 (10): 1887–903.
2. Barnes JL, Zubair M, John K, Poirier MC, and Martin FL. Carcinogens and DNA damage. Biochemical Society Transactions. 2018; 46 (5): p. 1213–24.
3. Turner N, Reis-Filho J, Russell A, Springall R, Ryder K, Steele D, et al. BRCA1 dysfunction in sporadic basal-like breast cancer. Oncogene. 2007; 26 (14): p. 2126–32.
4. Morales-Herrero M and Ortega-Medina I. Experimental carcinogenesis with 7, 12-dimethylbenz (a) anthrazene (DMBA) and its inhibition with isothi-ocyanates. J oral res (Impresa). 2022: p. 1–13.
5. Allam AM, Abubakr HO, Yassin AM, Abdel-Razek AS, Khattab MS Gouda EM, et al. Potential chemopreventive effects of Broccoli extract supplementation against 7, 12 dimethyl Benz (a) anthracene (DMBA)-induced toxicity in female rats. Scientific reports. 2023; 13 (1): p. 1–19.
6. Davidson CJ, Svenson D, Hannigan JH, Perrine SA, and Bowen SE. A novel preclinical model of environment-like combined benzene, toluene, ethylbenzene, and xylenes (BTEX) exposure: Behavioral and neurochemical findings. Neurotoxicology and teratology. 2022; 91: 1–11.
7. Sahay D, Lloyd SE, Rivera JA, Jezioro J, Mcdonald JD, Pitiranggon M, et al. Prenatal polycyclic aromatic hydrocarbons, altered ERα pathway-related methylation and expression, and mammary epithelial cell proliferation in offspring and grandoffspring adult mice. Environmental research. 2021; 196: 1–15.
8. Xu X, Qiao W, Linke SP, Cao L, Li W-M, Furth PA, et al. Genetic interactions between tumor suppressors Brca1 and p53 in apoptosis, cell cycle and tumorigenesis. Nature genetics. 2001; 28 (3): 266–71.
9. Yossepowitch O, Olvera N, Satagopan JM, Huang H, Jhanwar S, Rapaport B, et al. BRCA1 and BRCA2 germline mutations in lymphoma patients. Leukemia & lymphoma. 2003; 44 (1): 127–31.
10. Matos-Rodrigues G, Barroca V, Muhammad AA, Dardillac E, Allouch A, Koundrioukoff S, et al. In vivo reduction of RAD51-mediated homologous recombination triggers aging but impairs oncogenesis. The EMBO journal. 2023; 42 (20): 1–21.
11. Kuznetsov SG, Haines DC, Martin BK, and Sharan SK. Loss of Rad51c leads to embryonic lethality and modulation of Trp53-dependent tumorigenesis in mice. Cancer research. 2009; 69 (3): 863–72.
12. Yamamoto H and Hirasawa A. Homologous recombination deficiencies and hereditary tumors. International journal of molecular sciences. 2021; 23 (1): 1–18.
13. Coates PJ, Lorimore SA, and Wright EG. Cell and tissue responses to genotoxic stress. The Journal of Pathology: A Journal of the Pathological Society of Great Britain and Ireland. 2005; 205 (2): 221–35.
14. Cruz SL, Rivera-García MT, and Woodward JJ. Review of toluene action: clinical evidence, animal studies and molecular targets. Journal of drug and alcohol research. 2014; 3: 1–15.
15. Fukami T, Katoh M, Yamazaki H, Yokoi T, and Nakajima M. Human cytochrome P450 2A13 efficiently metabolizes chemicals in air pollutants: naphthalene, styrene, and toluene. Chemical research in toxicology. 2008; 21 (3): 720–5.
16. Rathnamali K. Dissection of laboratory animal and sample collection for histology. International Journal of Scientific and Applied Research (IJSAR), eISSN: 2583–0279. 2022; 2 (3): 1–12.
17. Sadeghipour A and Babaheidarian P. Making formalin-fixed, paraffin embedded blocks. Biobanking: Methods and Protocols. 2018: 253–68.
18. Greenberg AK, Yee H, and Rom WN. Preneoplastic lesions of the lung. Respiratory research. 2002; 3: 1–10.
19. Tsyganov MM, Bulatova DZ, Fedorenko AA, Loos DM, Nikiforov PE, Tsydenova IA, et al. Assessment of Homologous Recombination System Gene Expression in Chemologically Induced Carcinogenesis In Vivo Models. Current Issues in Molecular Biology. 2026; 48 (3): 1–17.
20. Myhre S, Lingjærde O-C, Hennessy BT, Aure MR, Carey MS, Alsner J, et al. Influence of DNA copy number and mRNA levels on the expression of breast cancer related proteins. Molecular oncology. 2013; 7 (3): 704–18.
21. Tsyganov MM, Ibragimova MK, Garbukov EY, Bragina OD, Karchevskaya AA, Usynin EA, et al. Determination of BRCAness Phenotype in Breast Tumors for the Appointment of Neoadjuvant

Chemotherapy Based on Platinum and Taxanes. International journal of molecular sciences. 2022; 24 (1): 1–13.
22. Цыганов М., Ибрагимова М., Цыденова И., Кравцова Е., Баянбаева А., Шарипханова Ж., и др. Влияние наличия аберраций числа копий ДНК и изменений в уровне экспрессии генов гомологичной рекомбинации на выживаемость больных первично-операбельным немелкоклеточным раком легкого. Acta Biomedica Scientifica. 2026; 10 (6): 112–22.
23. Hollander MC, Kovalsky O, Salvador JM, Kim KE, Patterson AD, Haines DC, et al. Dimethylbenzanthracene carcinogenesis in Gadd45a-null mice is associated with decreased DNA repair and increased mutation frequency. Cancer research. 2001; 61 (6): 2487–91.
24. Verta J-P and Jacobs A. The evolutionary significance of post-transcriptional gene regulation. Heredity. 2024; 132 (3): 117–9.
25. Lopez BS. RAD51-mediated homologous recombination is a pro-tumour driver pathway. Oncogene. 2025; 44 (42): 4006–16.
26. Garcin EB, Gon S, Sullivan MR, Brunette GJ, Cian AD, Concordet J-P, et al. Differential requirements for the RAD51 paralogs in genome repair and maintenance in human cells. PLoS Genetics. 2019; 15 (10): 1–29.

USING INTERACTIVE TECHNOLOGIES FOR REHABILITATION FOLLOWING REVISION KNEE ARTHROPLASTY

Minasov BSh[1], Yakupov RR[1], Akbashev VN[1] ✉, Bilyalov AR[1], Evgrafov IO[1], Karimov KK[2], Minasov IB[1], Akhmeldinova AA[1], Salimyanova MR[1]

[1] Bashkir State Medical University, Republic of Bashkortostan, Ufa, Russia
[2] Avicenna Tajik State Medical University, Dushanbe, Tajikistan

A chronic periprosthetic infection after knee replacement typically requires two-stage treatment. However, the inter-stage rehabilitation protocol for patients with an articulating spacer has not been adequately developed. This study aimed to determine whether adding interactive biofeedback walking training on the Walker View treadmill enhances the effectiveness of a standard recovery program following the first stage of two-stage revision treatment. The prospective randomized controlled trial included 87 patients who had undergone removal of their endoprostheses and placement of articulating spacers. The treatment group (n = 43) had the standard 21-day rehabilitation program combined with Walker View sessions, while the control group (n = 44) only followed the program. We assessed knee joint movement volume, quadriceps EMG amplitude, stride length, walking speed, postural stability, and SF-36, WOMAC, and KSS scores. By the end of the rehabilitation course, the results registered in the treatment group were better than in the control group: flexion — 78 ± 6° versus 71 ± 7° (p = 0.01); EMG amplitude — 179 ± 16 versus 165 ± 16 μV (p = 0.01); step length — 54.2 ± 5.0 versus 49.5 ± 5.0 cm (p = 0.01); walking speed — 0.70 ± 0.05 versus 0.65 ± 0.05 m/s (p = 0.02); overall stability — 80 ± 8% versus 72 ± 7% (p = 0.01); physical component SF-36 — 51 ± 8 versus 47 ± 7 points (p = 0.01). The differences in WOMAC and KSS scores were insignificant (p = 0.06 and p = 0.07). The inclusion of Walker View sessions in the inter-stage rehabilitation program yields more pronounced improvements in mobility, neuromuscular function, walking, and balance restoration.

Keywords: revision arthroplasty, knee joint, periprosthetic infection, rehabilitation, biofeedback, Walker View, two-stage revision arthroplasty, articulating spacer

Author contribution: Minasov BS — study concept and design, research supervision, editing; Yakupov RR — study design, data analysis, text preparation; Akbashev VN — study concept, interpretation of results, editing; Bilyalov AR — collection of clinical material, examination of patients, preparation of materials for analysis; Yevgrafov IO — rehabilitation program, collection and systematization of clinical data; Karimov KK — methodological support of the study, technical support, analysis of the obtained data; Minasov IB — interpretation of the results, text preparation and editing; Akhmeldinova AA — statistical data processing, registration of the results of the study; Salimyanova MR — literature analysis, preparation and registration of the manuscript.

Compliance with ethical standards: the study was approved by the Ethics Committee of the Bashkir State Medical University of the Ministry of Health of the Russian Federation (Minutes #2 of February 03, 2025). All procedures were performed in accordance with the requirements of the 2013 World Medical Association Declaration of Helsinki. All patients signed a voluntary informed consent form for participation in the study.

✉ **Correspondence should be addressed:** Vladislav N. Akbashev
Lenina, 3, Ufa, 450008, Russia; vlad-akb@mail.ru

Received: 21.03.2026 **Accepted:** 10.04.2026 **Published online:** 27.04.2026

DOI: 10.24075/brsmu.2026.018

ИСПОЛЬЗОВАНИЕ ИНТЕРАКТИВНЫХ ТЕХНОЛОГИЙ В ВОССТАНОВИТЕЛЬНОМ ЛЕЧЕНИИ ПОСЛЕ РЕВИЗИОННОЙ АРТРОПЛАСТИКИ КОЛЕННОГО СУСТАВА

Б. Ш. Минасов[1], Р. Р. Якупов[1], В. Н. Акбашев[1] ✉, А. Р. Билялов[1], И. О. Евграфов[1], К. К. Каримов[2], И. Б. Минасов[1], А. А. Ахмельдинова[1], М. Р. Салимьянова[1]

[1] Башкирский государственный медицинский университет, Республика Башкортостан, Уфа, Россия
[2] Таджикский государственный медицинский университет имени Абуали ибни Сино, Душанбе, Таджикистан

Хроническая перипротезная инфекция после эндопротезирования коленного сустава требует двухэтапного лечения, однако межэтапная реабилитация пациентов с артикулирующим спейсером разработана недостаточно. Целью работы было определить, повышает ли включение интерактивной тренировки ходьбы с биологической обратной связью на комплексе Walker View эффективность стандартной восстановительной программы после первого этапа двухэтапной ревизии. В проспективное рандомизированное контролируемое исследование включили 87 пациентов после удаления эндопротеза и установки артикулирующего спейсера. Основная группа (n = 43) проходила стандартную реабилитацию в сочетании с тренировкой на Walker View, контрольная (n = 44) — только стандартную программу; курс составил 21 день. Оценивали объем движений в коленном суставе, амплитуду ЭМГ четырехглавой мышцы, длину шага, скорость ходьбы, постуральную устойчивость, показатели SF-36, WOMAC и KSS. К окончанию курса в основной группе достигнуты лучшие результаты: сгибание 78 ± 6° против 71 ± 7° (p = 0,01), амплитуда ЭМГ 179 ± 16 против 165 ± 16 мкВ (p = 0,01), длина шага 54,2 ± 5,0 против 49,5 ± 5,0 см (p = 0,01), скорость ходьбы 0,70 ± 0,05 против 0,65 ± 0,05 м/с (p = 0,02), общая стабильность 80 ± 8% против 72 ± 7% (p = 0,01), физический компонент SF-36 — 51 ± 8 против 47 ± 7 баллов (p = 0,01). Различия по WOMAC и KSS были статистически незначимы (p = 0,06 и p = 0,07). Включение Walker View в межэтапную реабилитацию обеспечивает более выраженное восстановление подвижности, нейромышечной функции, ходьбы и равновесия.

Ключевые слова: ревизионная артропластика, коленный сустав, перипротезная инфекция, реабилитация, биологическая обратная связь, Walker View, двухэтапное ревизионное эндопротезирование, артикулирующий спейсер

Вклад авторов: Б. Ш. Минасов — концепция и дизайн исследования, научное руководство, редактирование; Р. Р. Якупов — дизайн исследования, анализ данных, подготовка текста; В. Н. Акбашев — концепция исследования, интерпретация результатов, редактирование; А. Р. Билялов — сбор клинического материала, обследование пациентов, подготовка материалов для анализа; И. О. Евграфов — реабилитационные мероприятия, сбор и систематизация клинических данных; К. К. Каримов — методическое обеспечение исследования, техническое сопровождение, анализ полученных данных; И. Б. Минасов — интерпретация результатов, подготовка и редактирование текста; А. А. Ахмельдинова — статистическая обработка данных, оформление результатов исследования; М. Р. Салимьянова — анализ литературы, подготовка и оформление рукописи.

Соблюдение этических стандартов: исследование одобрено этическим комитетом ФГБОУ ВО «Башкирский государственный медицинский университет» Минздрава России (протокол № 2 от 03 февраля 2025 г.). Все процедуры проведены в соответствии с требованиями Хельсинкской декларации Всемирной медицинской ассоциации (2013 г.). Все пациенты подписали добровольное информированное согласие на участие.

✉ **Для корреспонденции:** Владислав Николаевич Акбашев
ул. Ленина, д. 3, г . Уфа, 450008, Россия; vlad-akb@mail.ru

Статья получена: 21.03.2026 **Статья принята к печати:** 10.04.2026 **Опубликована онлайн:** 27.04.2026

DOI: 10.24075/vrgmu.2026.018

The rising prevalence of destructive and dystrophic musculoskeletal diseases has increased the frequency of large joint replacement surgery. According to federal statistics, the incidence of osteoarthritis in Russia rose from 546.9 cases per 100,000 population in 2015 to 650.0 in 2024, an 18% increase [1]. Knee replacement is the most effective surgery for destructive and dystrophic joint lesions. In modern orthopedics, it is the gold standard, considerably improving patients' quality of life and life expectancy. However, the implants placed are limited functionally, and over time, the components of the endoprosthesis wear out. It is projected that by 2030, more than 260,000 revision knee surgeries will be performed annually in the United States [2]. Over the years, tension force vectors in the bone and connective tissue around the endoprosthesis shift, leading to a biomechanical conflict with the supporting structures. As a result, aseptic instability, metallosis, and osteolysis can develop, as well as periprosthetic infection (PPI) if microbial factors are involved.

PPI is one of the most severe complications of knee replacement. Large-scale cohort studies report the incidence of PPI as 1–2% after primary arthroplasty, and up to 4% after revision surgeries [3]. PPI is the leading cause of revision intervention, more common than aseptic instability and wear of polyethylene [4]. Chronic periprosthetic knee joint infection causes soft tissue and bone destruction, impairing limb function. It often requires two-stage revision arthroplasty with a temporary antibiotic spacer.

Two-stage revision arthroplasty remains the most recognized treatment for chronic PPI. The first stage is aimed at rehabilitating the infection site, stabilizing soft tissue and bone structures, and partially preserving limb function when using an articulating spacer. The key factor in the effectiveness of the two-stage approach is the quality of recovery during the period between the stages, which usually ranges from 6 to 12 weeks [5]. The rehabilitation itself commonly includes early mobilization of the joint and physical therapy [6]. The use of articulating spacers allows patients to start recovery activities in the early postoperative period [7]. However, it is not yet fully clear which rehabilitation methods are optimal under these conditions. Some authors recommend a gentle regimen to prevent spacer dislocation, while others emphasize the need for early activation to prevent muscular atrophy [8].

In recent years, biofeedback technologies have been increasingly integrated into musculoskeletal rehabilitation. The Walker View platform (TecnoBody, Italy) is a treadmill with an integrated 3D motion analysis system and a touchscreen that allows real-time evaluation of temporal and spatial gait parameters, step symmetry, and joint kinematics [9, 10]. The technology has been proven effective in post-knee replacement rehabilitation [11], but there is no information about its efficacy in the context of a two-stage revision arthroplasty that involves a temporary spacer [12].

Thus, the relevance of this study stems from the availability of data on the effectiveness of interactive biofeedback technology in rehabilitation after primary knee joint arthroplasty, coupled with the lack of evidence on its use between stages of revision surgery with an articulating spacer.

This study aimed to evaluate the effectiveness of a comprehensive rehabilitation program that includes interactive biofeedback sessions on a Walker View treadmill in comparison with the standard rehabilitation protocol followed after the first stage of two-stage revision knee arthroplasty undertaken to treat PPI.

METHODS

This study was a prospective, randomized controlled trial designed to evaluate the effectiveness of comprehensive rehabilitation following the first stage of two-stage revision knee arthroplasty in patients with chronic periprosthetic joint infection. In the context of the study, we compared a standard rehabilitation program and an extended program that incorporates the use of interactive biofeedback technology.

Inclusion criteria: age 55–75 years, diagnosed chronic knee periprosthetic infection (ICD-10 code T84.5), absence of significant somatic diseases that could hinder rehabilitation, and informed consent to participate in the study.

Exclusion criteria: acute infectious diseases at the time of enrollment; severe comorbidities in the decompensation stage, such as class III–IV cardiovascular insufficiency (NYHA classification); diabetes mellitus with glycated hemoglobin (HbA1c) > 8.5%; severe chronic obstructive pulmonary disease with forced expiratory volume in 1 second (FEV1) <50% of predicted; end-stage chronic kidney disease (glomerular filtration rate < 15 mL/min/1.73 m^2 or dialysis dependence); patient's refusal to participate; cognitive impairments preventing completion of the rehabilitation program (MMSE score < 24 points).

Sample characteristics

The study included 87 patients hospitalized for chronic periprosthetic knee infection who underwent the first stage of two-stage revision arthroplasty with an articulating spacer (made in BSMU's Additive Technologies Laboratory; Eurasian Application No. 202492817).

The sample size was calculated using the G*Power 3.1.9.7 program. Based on the expected difference in the range of 10° knee joint motion (control group average: 70° ± 15°; treatment group average: 80° ± 15°), with 80% study power and a significance level of $\alpha = 0.05$, each group should have included at least 36 patients. Since it was assumed that 15% of the participants would drop out, the plan was to invite 44 patients to each group, for a total sample size of 88. Eventually, 87 patients were included (one patient refused to participate before the beginning of the rehabilitation). The mean age of the sample was 65.4 ± 5.2 years. Gender distribution: 51 female (58.6%) and 36 male (41.4%). The sample was randomized by the block randomization method (block size 4) using a random number generator: treatment group, $n = 43$; control group, $n = 44$.

The patients were divided into groups after the first stage of surgery. Blinding of patients and rehabilitation specialists was not possible due to the nature of the intervention. The functional outcomes and statistical data were analyzed by specialists who were uninvolved in the rehabilitation program and unaware of the patients' group affiliations. The groups were comparable in age and gender ($p > 0.05$).

Rehabilitation program

The rehabilitation program began on the first day after the first stage of revision arthroplasty. It lasted for 21 days, and the patients remained in the hospital throughout its duration. The program included two consecutive stages: the early postoperative period stage (days 1–4) and the core rehabilitation stage (days 5–21).

Early postoperative period stage (days 1–4)

In the early postoperative period, patients performed gentle isometric exercises to prevent thromboembolic complications, maintain muscle tone, and preserve basic motor activity.

Table 1. The standard medical rehabilitation program

Component	Brief description of the intervention	Parameters	Intended goal
Cryotherapy	Local cooling of the knee joint area	15-20 minutes, 2-3 times a day; t° –5...+5 °C	Reduction of pain and swelling, control of inflammation
Continuous passive motion (CPM)	Mechanical passive joint mobilization using the Artromot device with a gradual increase in amplitude	20–30 minutes, 2–3 times a day; increase of 5–10° a day	Contracture prevention, ROM maintenance
Pneumocompression lymphatic drainage	Sequential pneumocompression of the lower limb	30 minutes, 1–2 times a day; pressure 40–60 mmHg	Reduction of edema, improvement of lymphovenous drainage
Physical therapy	Active exercises for the muscles of the thigh, lower leg, buttocks using resistance bands and body weight	30–40 minutes a day; 2–3 sets of 10–15 repetitions	Restoration of strength and weight-bearing ability
Electrical muscle stimulation	Neuromuscular electrical stimulation of *m. quadriceps femoris* and *m. gastrocnemius*	Frequency 30–50 Hz, pulse duration 250–300 microseconds, 15–20 minutes	Prevention of atrophy, activation
Soft tissue massage	Classical and lymphatic drainage massage of the thigh and lower leg muscles	15–20 minutes a day, a course of 10–14 procedures	Improved microcirculation, decreased muscle tone
Graded walking	Learning walking techniques with the distance gradually increasing	10–15 minutes, 2 times a day; weight-bearing intensity as allowed by the spacer protocol	Normalization of walking patterns, early mobilization

The set included the following.

1. Isometric exercises for the thigh muscles — static tension of the quadriceps femoris and adductor muscles with a gradual increase in the duration of tension from 5 to 10–15 seconds, followed by 10-second relaxation; 10 repetitions, 3 times a day.
2. Active movements of the ankle joints — flexion and extension of the foot, circular movements; 15–20 repetitions of each exercise, 4–5 times a day to stimulate venous outflow.
3. Straight leg lift while supine: knee extension followed by lifting the straightened leg 15–20 cm from the bed surface, with a 5-second hold; 8–10 repetitions, twice daily, emphasizing the anterior thigh muscles.
4. Knee joint passive flexion and extension — performed within the permissible range of motion (usually 0–30 ° on the first day), taking into account the features of the installed spacer and muscle balance; 5–10 repetitions, 2 times a day.
5. Respiratory exercises — diaphragmatic breathing, chest expander exercises to prevent congestion in the lungs.

Core rehabilitation stage (days 5–21)

On days 5–7 post-surgery, once the patients' condition had stabilized and provided there were no signs of inflammatory complications and the postoperative wound was satisfactory, they advanced to the core rehabilitation stage. Table 1 presents the standard rehabilitation program followed in both groups.

Interactive rehabilitation program (treatment group)

In the treatment group, the standard rehabilitation program was extended to include sessions on the Walker View 3.0 SCX system (TecnoBody S.r.l., Italy). This integrated platform features a treadmill with load sensors, an optical 3D motion analysis array with four cameras, a touch surface for assessing weight-bearing distribution, and real-time gait analysis software.

The Walker View sessions took place every day starting from days 5–7 post-surgery, provided that the postoperative wound had healed and there were no signs of an active inflammatory process. Each session lasted for 20–30 minutes. The patients held onto a support bar at all times. On days 5–10, they walked on the treadmill while resting their weight on the side rails of the Walker View platform, which ensured a stable position and prevented loss of balance. The load on the operated limb was controlled according to an individual protocol, based on the type of articulating spacer implanted and the postoperative wound condition. As patients regained the ability to bear their own weight and gained walking confidence, handrail support was gradually reduced. The axial load was monitored using Walker View's built-in pressure sensors. These enabled real-time control of load distribution across the limbs and prevented exceeding the safe load limit on the operated side.

Each session included three consecutive stages.

Stage one — basic gait analysis: patients performed a standard walking test to record baseline parameters at a comfortable pace. "The system automatically recorded the following parameters: step length and symmetry between the operated and contralateral limbs; duration of the weight-bearing and transfer phases; movement speed and cadence; spatial parameters of pelvis and trunk motion (lateral shifts and rotation); kinematic characteristics of the hip and knee joints (sagittal-plane movement amplitude); and load distribution between the limbs. The data obtained was used to determine the individual targets for the current training session.

Stage two — Gait Trainer module, interactive learning involving real-time visual biofeedback: the patients saw the target parameters of the step and the walking cycle phases on the screen in front of them. The training included the following components.

1. Step length symmetry correction — visualization of the difference in step length between the operated and healthy limbs to equalize the metrics.
2. Walking phases optimization — gradual increase of weight-bearing time on the operated limb, normalization of the push-off moment.
3. Control trunk's lateral motions and rotation of the pelvis — visualization of deviations of the center of mass from the midline with feedback on the accuracy of the trajectory.
4. Restoration of the axis of the lower limb — stabilization of the knee joint in the sagittal plane and correction of varus/valgus deviations.
5. Kinematic exercises — execution of movements with visualization of the angular parameters of the knee joint to restore the amplitude of flexion and extension.
6. Load distribution normalization — control of symmetry in the load response recorded by the platform's pressure sensors.

To ensure physiological accuracy and safety of movements, we used SCX Speed Control technology, which automatically adapts treadmill speed to the patient's pace. The technology eliminated the need to maintain the set speed and reduced the risk of loss of balance.

Stage 3 — session report. At the end of the training, the patient received a summary visual assessment of the achieved changes in key parameters: step length, phase symmetry, movement speed, lateral stability, and angular kinematics of the joints. These data were stored in the system and used for subsequent adjustment of training tasks.

We used the interactive Walker View program to establish a physiological gait pattern early on, reduce limb movement asymmetry, improve neuromuscular control, and restore the limb's supporting function while using the articulating spacer.

Efficacy assessment methods

The efficacy of the rehabilitation program was assessed based on a comprehensive analysis of the functional state of the operated limb, kinematic characteristics of gait, neuromuscular activity, parameters of postural stability, and quality of life indicators (Table 2). The patients were examined twice: on the day after the first stage of revision arthroplasty (before active rehabilitation) and after completing the three-week inpatient rehabilitation program. All methods were standardized, with an identical examination protocol for both groups. Procedures were performed by a qualified specialist trained in the equipment used.

Knee joint range of motion assessment

The amplitude of knee joint flexion and extension was determined on an Arthromot ORMED FLEX-F01 Active complex (Ormed LLC, Russia). For the assessment, the patient lay supine with the hip joint fixed at 90° flexion to prevent compensatory movements. We measured the maximum angles of active flexion and extension that the patient could tolerate without a marked increase in pain. Each measurement was performed in triplicate, and the average was used for analysis. The measurement error was ±1°.

Electromyographic examination

The functional state of the lower extremity muscles was assessed using surface electromyography on a Neuro-MVP-4 device (NPP Medical Computer Technology, Russia). Biopotentials were recorded from the quadriceps femoris (rectus femoris) and gastrocnemius (medial head) muscles on the operated side. The electrodes were placed over the muscular abdomen, with the specific position selected based on anatomical landmarks; the skin was pre-treated with an alcohol solution. We analyzed the amplitude (in mV) of voluntary muscle contractions using standardized isometric tests: knee extension against resistance (quadriceps muscle) and standing on tiptoes (gastrocnemius muscle). The recording duration was 5 seconds, the gain — 1000 mV/div. The measurements were taken in triplicate, with an interval of 30 seconds.

Analysis of temporal and spatial gait parameters

The kinematic and temporal-spatial characteristics of gait were evaluated using the Walker View 3.0 SCX system (TecnoBody S.r.l., Italy). The patients walked at a comfortable self-selected pace on an instrumented treadmill 150 cm long. We recorded the following parameters: step length (cm), movement speed (m/s), load phase duration for the operated limb (ms), transfer phase duration for the operated limb (ms), and step symmetry coefficient between the operated and contralateral limbs.

The testing began after a two-minute adaptation to the treadmill. The parameters were registered for 30 seconds of continuous walking. The average values from stable walking cycles (at least 10 consecutive steps) were used for the analysis.

Stabilometric study

Postural stability and equilibrium reactions were assessed using the Huber 360 stabilometric complex (LPG Systems, France). The study included the following tests:

1) static test — recording of center of pressure (CP) deviations during 30-second quiet stance on two legs with eyes open;

2) statodynamic test — assessing stability limits during forward, backward, and sideways torso bending.

We recorded the following parameters: the area of the CP scattering ellipse (mm^2), the amplitude of trunk motions in the frontal and sagittal planes (mm), the integral index of overall stability (%), and the stability limit (% of the maximum possible bending). The stabilometric study served only diagnostic purposes, and Huber 360 was not used for rehabilitation.

Clinical questionnaires

The clinical efficacy of rehabilitation and its impact on the quality of life were assessed using validated Russian-language versions of the following questionnaires.

1. Medical Outcomes Study 36-Item Short-Form Health Survey (SF-36): comprehensive assessment of quality of life's physical and mental components. We analyzed the total score of the physical component as the most sensitive to changes in motor function in the early postoperative period.

2. Western Ontario and McMaster Universities Osteoarthritis Index (WOMAC): assessment of the severity of pain (5 questions), stiffness (2 questions) of the knee joint, and its physical function (17 questions). We used the Likert III version of the index (0-4 points); the maximum possible total score was 96 (the higher the score, the worse the condition).

3. Knee Society Score scale (KSS): assessment of the clinical status of the knee joint (Knee Score, maximum 100 points) and its functional state (Function Score, maximum 100 points).

All questionnaires were filled out by patients independently under the supervision of a researcher.

Standardization of measurements

To minimize variability in data processing, all studies and examinations were conducted by one certified specialist who was not involved in the rehabilitation. The equipment used was calibrated as prescribed by the manufacturer before each test/study. All quantitative indicators were measured in triplicate (or more); for statistical analysis, we used the arithmetic mean. All patients underwent a specific test or study in the same time of day (morning or afternoon).

The endpoints of the study

The primary endpoint was the knee joint active flexion index after 21 days of inpatient rehabilitation. The secondary endpoints were the index of active extension, the amplitude of EMG of m.quadriceps femoris, step length, walking speed, load phase duration, integral indicators of postural stability, as well as the data collected using the SF-36, WOMAC, and KSS questionnaires.

Statistical data processing

IBM SPSS Statistics 26.0 (IBM Corp., USA) was used for statistical processing of the data. Normality of distribution of

Table 2. Rehabilitation results assessment methods

Method	Measured parameters	Tool / equipment	Purpose
Range of motion (ROM) assessment	Angle of active flexion and extension of the knee joint	Arthromot ORMED FLEX-F01 Active (Russia)	Assessment of mobility restoration and contracture prevention
Electromyography (EMG)	The amplitude of arbitrary contractions of *m. quadriceps femoris* and *m. gastrocnemius*	Neuro-MVP-4 (Russia)	Analysis of neuromuscular activation and muscle tone
Gait analysis	Step length, movement speed, load phase duration, step symmetry coefficient	Walker View 3.0 SCX (Italy)	Assessment of recovery of motor patterns and gait parameters
Stabilometry	Pressure center, oscillation amplitude, stability limit, integral stability	Huber 360 (France)	Diagnosis of postural stability (not included in the rehabilitation program)
Clinical questionnaires	SF-36: quality of life; WOMAC: pain, stiffness, function; KSS: clinical and functional parameters of the joint.	Paper forms	Comprehensive assessment of clinical efficacy and functional status

the quantitative data was assessed using the Shapiro-Wilk test. We calculated the mean and standard deviation (M ± SD) for normally distributed data and the median and interquartile range (Me [Q_1; Q_3]) for non-normal data. The intergroup differences between the treatment and control groups were assessed using the independent Student's *t*-test for normally distributed quantitative data; the Mann–Whitney test for quantitative data without a normal distribution; and Pearson's χ^2 test or Fisher's exact test for categorical variables.

To assess dynamics within the groups (before and after rehabilitation), we used the paired *t*-test when differences were normally distributed and the Wilcoxon test otherwise.

The differences were considered significant at $p < 0.05$. The hypothesis testing at the primary endpoint was confirmatory. The analysis of secondary endpoints was exploratory; the obtained *p*-values were interpreted with adjustment for the multiplicity of compared indicators. To minimize systematic errors, all calculations were performed by one specialist who was not involved in the rehabilitation and clinical examination of patients.

RESULTS

The mean service life of the first endoprosthesis before the development of periprosthetic infection was 7.2 ± 2.8 years in the treatment group and 7.5 ± 3.1 years in the control group ($p = 0.64$). We confirmed the diagnosis of chronic periprosthetic infection in all participants according to the Musculoskeletal Infection Society (MSIS) criteria. The distribution of patients according to the Cierny-Mader classification did not differ between the groups ($p = 0.78$).

The initial values of all assessed indicators (range of motion, electromyographic parameters, gait parameters, stabilometry, quality of life) were statistically comparable between the treatment and control groups at baseline (all $p > 0.05$), enabling accurate evaluation of the rehabilitation programs' effectiveness.

Range of motion and neuromuscular activity

At the end of the three-week rehabilitation course, the knee joint motion amplitude has increased significantly in both groups (Table 3). In the treatment group, flexion increased by 30% from baseline, compared to 22% in the control group. Extension improved by 6% and 5%, respectively. The intergroup differences in the final values of flexion and extension were significant ($p = 0.010$ and $p = 0.040$ respectively).

Electromyographic study revealed that the amplitude of voluntary muscle contractions of *m. quadriceps femoris* has grown in both groups. The relative increase was 17.8% in the treatment group and 11.5% in the control group ($p = 0.010$ between the groups). A similar trend was observed for *m. gastrocnemius*, but the intergroup difference was smaller. The recorded increase in the amplitude of biopotentials indicates restoration of neuromuscular activation after surgery.

Gait parameters

The dynamics of temporal and spatial characteristics of gait were positive in both groups. The step length increased by 18% in the treatment group and by 12.5% in the control group ($p = 0.010$). Movement speed increased by 14.8% and 10.2%, respectively ($p = 0.020$).

The duration of load on the operated limb decreased in both groups ($p < 0.001$), which reflects the restoration of confidence in the functionality of that limb. The transfer phase shortened from 412 ± 38 ms to 371 ± 34 ms in the treatment group and from 415 ± 40 ms to 390 ± 37 ms in the control group ($p = 0.040$ between groups). This indicates improved movement control without load. The step symmetry coefficient (ratio of the operated limb's step length to that of the contralateral limb) improved from 0.82 to 0.94 in the treatment group and from 0.81 to 0.89 in the control group ($p = 0.015$ between groups).

Postural stability

The integral indicators of stabilometry significantly increased in both groups. Overall stability increased by 21% in the treatment group and 12.5% in the control group ($p = 0.010$). The stability limit increased by 24.6% and 13.3%, respectively ($p = 0.010$).

Meanwhile, local parameters (amplitude of pressure center fluctuations and pressure center deviation) did not differ significantly between groups ($p = 0.070$ and 0.080). This may indicate that the accuracy characteristics of postural control require a longer recovery period than the integral indicators.

Quality of life and functional status

The SF-36 score demonstrated an improvement in the physical component of the quality of life in both groups. The absolute increase was 10 points in the treatment group and 8 points in the control group ($p = 0.010$ between the groups).

The WOMAC score decreased by 30% in the treatment group and by 20% in the control group, indicating an improvement in condition. However, the intergroup differences in the final values did not reach statistical significance ($p = 0.060$). A similar trend was observed for the KSS score: both groups exhibited clinical status improvement, but the intergroup differences were insignificant ($p = 0.070$). This lack of significance may stem from the load limitation associated with

Table 3. Post-rehabilitation functional state assessment

Indicator	Treatment group (before)	Treatment group (before)	Control group (before)	Control group (before)	*p* between groups
Knee joint flexion, °	60 ± 7	78 ± 6	58 ± 8	71 ± 7	0.01
Knee joint extension, °	166 ± 4	176 ± 2	165 ± 5	173 ± 3	0.04
Quadriceps EMG, mV	152 ± 17	179 ± 16	148 ± 18	165 ± 16	0.01
Operated limb's step length, cm	46 ± 5	54.2 ± 5	44 ± 5	49.5 ± 5	0.01
Walking speed, m/s	0.61 ± 0.06	0.70 ± 0.05	0.59 ± 0.07	0.65 ± 0.05	0.02
Operated limb's load phase, ms	767 ± 49	690 ± 51	762 ± 52	714 ± 48	0.01
Operated limb's transfer phase, ms*	412 ± 38	371 ± 34	415 ± 40	390 ± 37	0.04
Step symmetry coefficient	0.82 ± 0.06	0.94 ± 0.04	0.81 ± 0.07	0.89 ± 0.05	0.015
Pressure center deviation, mm	23 ± 4	18 ± 3	22 ± 4	20 ± 3	0.08
Oscillation amplitude, mm	12 ± 2	10.8 ± 2	11 ± 2	10 ± 2	0.07
Overall stability, %	66 ± 9	80 ± 8	64 ± 9	72 ± 7	0.01
Limit of stability, %	61 ± 7	76 ± 7	60 ± 7	68 ± 7	0.01
SF-36, points	41 ± 7	51 ± 8	39 ± 8	47 ± 7	0.01
WOMAC, points	66 ± 8	46 ± 11	65 ± 9	52 ± 10	0.06
KSS, points	56 ± 9	81 ± 8	55 ± 9	76 ± 8	0.07

Note: the knee extension index is represented as the value of the external angle; full extension is 180°. The increase in the indicator reflects a decrease in the extension deficit. *p* — the level of statistical significance of intergroup differences; EMG — electromyography.

the spacer, and from insufficient sensitivity of instruments in the early postoperative period.

DISCUSSION

The data obtained reflect the features of the functional recovery dynamics observed in patients after the first stage of two-stage knee revision arthroplasty. Both groups exhibited extending motion amplitudes and increasing muscle activity indicators, which aligns with the recovery expectations. However, the differences between the groups reveal that the magnitude of these changes is not similar. An increase in the amplitude of flexion and extension may be associated with both a gradual reduction of postoperative pain and adaptation of periarticular tissues to new biomechanical conditions [13]. The observed post-rehabilitation intergroup differences suggest that the selection of patterns of motor activity in this context may affect the recovered range of motion [14].

The interpretation of the results of this study should factor in the specifics of the period after the first stage of two-stage revision arthroplasty. Unlike patients after primary arthroplasty, those with an articulating temporary spacer naturally have limited functional restoration. This stems from the need for gentle exercise, preservation of postoperative soft tissue integrity, and gradual increases in range of motion. In this regard, it seems natural to expect an earlier response in the objective motor parameters (range of motion, EMG, and temporal-spatial gait indicators), while WOMAC and KSS clinical scales may be less sensitive during the early post-revision period.

Changes in electromyography parameters indicate a gradual restoration of neuromuscular activation. The increase in the amplitude of quadriceps biopotentials in both groups reflects reinnervation and normalization of muscle tone after surgery [15–17]. Statistical differences between groups after treatment suggest that exercise type and motor activity nature influence muscle group recruitment patterns, which in turn affect motor response development. Post-rehabilitation intergroup differences allow considering different rehabilitation models as a factor influencing the rate of change in kinematic characteristics [18–19].

Compared to gait and ROM parameters, the dynamics of stability indicators was less drastic. This may be explained by the compensatory action of intact components that help maintain posture after the first stage of revision arthroplasty [20].

The changes registered with the quality-of-life scales were also unidirectional; they revealed gradual improvement of the functional state. The differences in final SF-36 scores between groups reflect how motor activity influences patients' subjective perceptions of daily function. At the same time, the lack of statistically significant differences in WOMAC and KSS scores may stem from the limited workload imposed by the temporary spacer, as well as these scales' greater sensitivity in later rehabilitation stages [21].

The dynamics of temporal and spatial characteristics of gait were rather similar. Growing step length, movement speed, and a shortening load phase reflect the gradual restoration of basic parameters in the cyclic motor stereotype [22].

With an articulating spacer, such parameters are closely related to the specifics of load distribution and the degree of participation of the operated limb in the transfer of body weight.

Individual parameters (general stability, stability limit) were different between the groups, while local indicators (amplitude of fluctuations, deviation of the pressure center) remained comparable. This aligns with the faster changes in integral stability indicators during the early post-surgery period, while precision and local stabilization parameters take longer to recover [23].

A comprehensive interpretation of the results suggests that motor parameters — ROM, EMG, gait characteristics — are more susceptible to changes in the early recovery period. Postural stability and clinical scales exhibit different dynamics, reflecting the heterogeneity of recovery processes with an articulating spacer and the need for a differentiated approach to assessing rehabilitation effectiveness.

The results are comparable with data from previous studies, confirming the importance of a multi-level restorative approach in revision arthroplasty. Comparison with literature data shows that the observed range of motion (71–78° of flexion) corresponds to values expected in patients with an articulating temporal spacer during the early postoperative period [7]. They are slightly lower than after implantation of the final endoprosthesis (usually 90–110°), due to the design of the temporary implant and the need to limit loading during the interim period.

The present study has a number of limitations. Firstly, it was conducted in a single clinical center, which may limit the generalizability of the results. Secondly, the follow-up period was 21 days of inpatient rehabilitation; long-term outcomes, including after the second stage of revision arthroplasty, were not evaluated. Third, the relatively small sample size (87 patients) could be insufficient to identify intergroup differences on the WOMAC and KSS clinical scales, which are typically less sensitive in the early stages. Despite the blindness in assessing the primary outcomes, complete blindness of patients and researchers regarding the type of rehabilitation program was not possible due to the specifics of the intervention.

CONCLUSIONS

We conducted a prospective randomized controlled trial comparing a comprehensive rehabilitation program incorporating interactive biofeedback technology (Walker View) with a standard program in patients undergoing the interval phase between the two stages of revision knee arthroplasty for chronic periprosthetic joint infection. After the three-week interstage rehabilitation period, the treatment group showed significantly greater range of motion, neuromuscular activity, temporal-spatial gait characteristics, and overall postural stability indicators than the control group. Local stabilometry parameters and the WOMAC and KSS scores were not significantly different between groups. The data reveal distinct recovery dynamics depending on the rehabilitation model used, highlighting the need for a differentiated approach to assessing functional state with a temporary spacer. Further research could focus on assessing long-term outcomes after the second stage of surgery, evaluating how rehabilitation models affect complication rates, and developing criteria for readiness for final replacement.

References

1. CHililov A, Mihajlova Yu, Zelenova O, Sterlikov S, Oskov Yu. Epidemiologiya osteoartrozov v Rossijskoj Federacii i prognoz ee razvitiya v postkovidnyj period. Social'nye aspekty zdorov'ya naseleniya. 2025; 71 (2): 21–21, DOI: 10.21045/2071-5021-2025-71-2-21. Russian.
2. Alrayes MM, Sukeik M. Two-stage revision in periprosthetic knee joint infections. World J Orthop. 2023; 14 (3): 113–22. DOI: 10.5312/wjo.v14.i3.113.
3. Ayoade F, Li D, Mabrouk A, Todd JR. Periprosthetic Joint Infection. StatPearls, Treasure Island (FL): StatPearls Publishing, 2025. (Просмотрено: 21 февраль 2026 г.) Available from: http://www.ncbi.nlm.nih.gov/books/NBK448131/.
4. Lakpriya S, De C, Tahir M, Sanka SK, Pierce TP, Gwam C. Etiology of Failure in Revision Total Knee Arthroplasty: A Systematic Review and Meta-Analysis. J Arthroplasty. 2025; S0883-5403(25)00836–8. DOI: 10.1016/j.arth.2025.06.085.
5. Iorio R, et al. A Modified Technique for Two-Stage Revision in Knee PJI Treatment. J Clin Med. 2023; 12 (23): 7323. DOI: 10.3390/jcm12237323.
6. Kulchitskaya DB, Fesyun AD, Samoilov A., Kolbakhova SN. The Physical Factors Application in Rehabilitation Programs for Patients after Total Knee Replacement. Bull Rehabil Med. 2022; 21 (2): 46–52. DOI: 10.38025/2078-1962-2022-21-2-46-52.
7. Kim YS, Bae KC, Cho CH, Lee KJ, Sohn E, Kim BS. Two-stage revision using a modified articulating spacer in infected total knee arthroplasty. Knee Surg Relat Res. 2013; 25 (4): 180–85. DOI: 10.5792/ksrr.2013.25.4.180.
8. Irani JL, et al. Clinical practice guidelines for enhanced recovery after colon and rectal surgery from the American Society of Colon and Rectal Surgeons and the Society of American Gastrointestinal and Endoscopic Surgeons. Surg Endosc. 2023; 37 (1): 5–30. DOI: 10.1007/s00464-022-09758-x.
9. Castellarin G, Merlini M, Bettinelli G, Riso R, Bori E, Innocenti B. Effect of an Innovative Biofeedback Insole on Patient Rehabilitation after Total Knee Arthroplasty. Appl Sci. 2022; 12 (5): 2456. DOI: 10.3390/app12052456.
10. Karaborklu Argut S, Celik D, Yasacı Z. Effectiveness of therapeutic electromyographic biofeedback after orthopedic knee surgeries: a systematic review. Disabil Rehabil. 2022; 44 (14): 3364–72. DOI: 10.1080/09638288.2020.1867904.
11. Bravi M, et al. Validity Analysis of WalkerViewTM Instrumented Treadmill for Measuring Spatiotemporal and Kinematic Gait Parameters. Sensors. 2021; 21 (14): 4795. DOI: 10.3390/s21144795.
12. Su S, He J, Wang R, Chen Z, Zhou F. The Effectiveness of Virtual Reality, Augmented Reality, and Mixed Reality Rehabilitation in Total Knee Arthroplasty: A Systematic Review and Meta-Analysis. J Arthroplasty. 2024; 39 (3): 582–90.e4. DOI: 10.1016/j.arth.2023.08.051.
13. Mizner RL, Petterson SC, Stevens JE, Vandenborne K, Snyder-Mackler L. Early quadriceps strength loss after total knee arthroplasty. The contributions of muscle atrophy and failure of voluntary muscle activation. J Bone Joint Surg Am. 2005; 87 (5): 1047–53. DOI: 10.2106/JBJS.D.01992.
14. Bade MJ, Stevens-Lapsley JE. Early high-intensity rehabilitation following total knee arthroplasty improves outcomes. J Orthop Sports Phys Ther. 2011; 41 (12): 932–41. DOI: 10.2519/jospt.2011.3734.
15. Stevens-Lapsley JE, et al. Relationship between intensity of quadriceps muscle neuromuscular electrical stimulation and strength recovery after total knee arthroplasty. Phys Ther. 2012; 92 (9): 1187–96. DOI: 10.2522/ptj.20110479.
16. Sklempe Kokic I, Vuksanic M, Kokic T, Peric I, Duvnjak I. Effects of Electromyographic Biofeedback on Functional Recovery of Patients Two Months after Total Knee Arthroplasty: A Randomized Controlled Trial. J Clin Med. 2022; 11 (11): 3182. DOI: 10.3390/jcm11113182.
17. Armshaw B, Vaidya M, Mehta S. Surface electromyography-based biofeedback can facilitate recovery from total knee arthroplasty. J Appl Behav Anal. 2024; 57 (3): 560–73. DOI: 10.1002/jaba.1076.
18. Bravi M, et al. Supervised versus unsupervised rehabilitation following total knee arthroplasty: A systematic review and meta-analysis. The Knee. 2023. 40: 71–89. DOI: 10.1016/j.knee.2022.11.013.
19. Monsegue AP, Emans PC, Van Loon LJ, Verdijk LB. Resistance exercise training to improve post-operative rehabilitation in knee arthroplasty patients: A narrative review. Eur J Sport Sci. 2024; 24 (7): 938–49. DOI: 10.1002/ejsc.12114.
20. Szczypiór-Piasecka K, Adamczewska P, Kołodziej Ł, Ziętek P. The Temporal–Spatial Parameters of Gait After Total Knee Arthroplasty. J Clin Med. 2025; 14 (13): 4548. DOI: 10.3390/jcm14134548.
21. Tsed AN, Kozhevin AA, Mushtin NE. Current trends in early rehabilitation of patients after total hip and knee replacement. Grek Bull Surg. 2024; 183 (1): 60–65. DOI: 10.24884/0042-4625-2024-183-1-60-65.
22. Bezgodkov YA, Kornilov NN, Petukhov AI, et al. Biomechanical indicators of standing and walking in patients after total knee arthroplasty using computer navigation. Traumatology and Orthopedics of Russia. 2011; 4: 11–17. EDN: NLEHPE.
23. Sekirin AB. Protocol of early rehabilitation after arthroplasty of major joints (literature review). Bull Rehabil Med. 2019; 2: 51–57. EDN: VEYUBF.

Литература

1. Чилилов А., Михайлова Ю., Зеленова О., Стерликов С., Осков Ю. Эпидемиология остеоартрозов в Российской Федерации и прогноз ее развития в постковидный период. Социальные аспекты здоровья населения. 2025; 71 (2): 21–21, DOI: 10.21045/2071-5021-2025-71-2-21.
2. Alrayes MM, Sukeik M. Two-stage revision in periprosthetic knee joint infections. World J Orthop. 2023; 14 (3): 113–22. DOI: 10.5312/wjo.v14.i3.113.
3. Ayoade F, Li D, Mabrouk A, Todd JR. Periprosthetic Joint Infection. StatPearls, Treasure Island (FL): StatPearls Publishing, 2025. (Просмотрено: 21 февраль 2026 г.) Available from: http://www.ncbi.nlm.nih.gov/books/NBK448131/.
4. Lakpriya S, De C, Tahir M, Sanka SK, Pierce TP, Gwam C. Etiology of Failure in Revision Total Knee Arthroplasty: A Systematic Review and Meta-Analysis. J Arthroplasty. 2025; S0883-5403(25)00836–8. DOI: 10.1016/j.arth.2025.06.085.
5. Iorio R, et al. A Modified Technique for Two-Stage Revision in Knee PJI Treatment. J Clin Med. 2023; 12 (23): 7323. DOI: 10.3390/jcm12237323.
6. Kulchitskaya DB, Fesyun AD, Samoilov A., Kolbakhova SN. The Physical Factors Application in Rehabilitation Programs for Patients after Total Knee Replacement. Bull Rehabil Med. 2022; 21 (2): 46–52. DOI: 10.38025/2078-1962-2022-21-2-46-52.
7. Kim YS, Bae KC, Cho CH, Lee KJ, Sohn E, Kim BS. Two-stage revision using a modified articulating spacer in infected total knee arthroplasty. Knee Surg Relat Res. 2013; 25 (4): 180–85. DOI: 10.5792/ksrr.2013.25.4.180.
8. Irani JL, et al. Clinical practice guidelines for enhanced recovery after colon and rectal surgery from the American Society of Colon and Rectal Surgeons and the Society of American Gastrointestinal and Endoscopic Surgeons. Surg Endosc. 2023; 37 (1): 5–30. DOI: 10.1007/s00464-022-09758-x.
9. Castellarin G, Merlini M, Bettinelli G, Riso R, Bori E, Innocenti B. Effect of an Innovative Biofeedback Insole on Patient Rehabilitation after Total Knee Arthroplasty. Appl Sci. 2022; 12 (5): 2456. DOI: 10.3390/app12052456.
10. Karaborklu Argut S, Celik D, Yasacı Z. Effectiveness of therapeutic electromyographic biofeedback after orthopedic knee surgeries: a systematic review. Disabil Rehabil. 2022; 44 (14): 3364–72. DOI: 10.1080/09638288.2020.1867904.
11. Bravi M, et al. Validity Analysis of WalkerViewTM Instrumented Treadmill for Measuring Spatiotemporal and Kinematic Gait Parameters. Sensors. 2021; 21 (14): 4795. DOI: 10.3390/s21144795.
12. Su S, He J, Wang R, Chen Z, Zhou F. The Effectiveness of Virtual Reality, Augmented Reality, and Mixed Reality Rehabilitation in Total Knee Arthroplasty: A Systematic Review and Meta-Analysis. J Arthroplasty. 2024; 39 (3): 582–90.e4. DOI: 10.1016/j.arth.2023.08.051.
13. Mizner RL, Petterson SC, Stevens JE, Vandenborne K, Snyder-Mackler L. Early quadriceps strength loss after total knee arthroplasty. The contributions of muscle atrophy and failure of voluntary muscle activation. J Bone Joint Surg Am. 2005; 87 (5): 1047–53. DOI: 10.2106/JBJS.D.01992.
14. Bade MJ, Stevens-Lapsley JE. Early high-intensity rehabilitation following total knee arthroplasty improves outcomes. J Orthop Sports Phys Ther. 2011; 41 (12): 932–41. DOI: 10.2519/jospt.2011.3734.
15. Stevens-Lapsley JE, et al. Relationship between intensity of quadriceps muscle neuromuscular electrical stimulation and strength recovery after total knee arthroplasty. Phys Ther. 2012; 92 (9): 1187–96. DOI: 10.2522/ptj.20110479.
16. Sklempe Kokic I, Vuksanic M, Kokic T, Peric I, Duvnjak I. Effects of Electromyographic Biofeedback on Functional Recovery of Patients Two Months after Total Knee Arthroplasty: A Randomized Controlled Trial. J Clin Med. 2022; 11 (11): 3182. DOI: 10.3390/jcm11113182.
17. Armshaw B, Vaidya M, Mehta S. Surface electromyography-based biofeedback can facilitate recovery from total knee arthroplasty. J Appl Behav Anal. 2024; 57 (3): 560–73. DOI: 10.1002/jaba.1076.
18. Bravi M, et al. Supervised versus unsupervised rehabilitation following total knee arthroplasty: A systematic review and meta-analysis. The Knee. 2023. 40: 71–89. DOI: 10.1016/j.knee.2022.11.013.
19. Monsegue AP, Emans PC, Van Loon LJ, Verdijk LB. Resistance exercise training to improve post-operative rehabilitation in knee arthroplasty patients: A narrative review. Eur J Sport Sci. 2024; 24 (7): 938–49. DOI: 10.1002/ejsc.12114.
20. Szczypiór-Piasecka K, Adamczewska P, Kołodziej Ł, Ziętek P. The Temporal–Spatial Parameters of Gait After Total Knee Arthroplasty. J Clin Med. 2025; 14 (13): 4548. DOI: 10.3390/jcm14134548.
21. Tsed AN, Kozhevin AA, Mushtin NE. Current trends in early rehabilitation of patients after total hip and knee replacement. Grek Bull Surg. 2024; 183 (1): 60–65. DOI: 10.24884/0042-4625-2024-183-1-60-65.
22. Bezgodkov YA, Kornilov NN, Petukhov AI, et al. Biomechanical indicators of standing and walking in patients after total knee arthroplasty using computer navigation. Traumatology and Orthopedics of Russia. 2011; 4: 11–17. EDN: NLEHPE.
23. Sekirin AB. Protocol of early rehabilitation after arthroplasty of major joints (literature review). Bull Rehabil Med. 2019; 2: 51–57. EDN: VEYUBF.

ELECTRICAL MYOSTIMULATION EFFECTS ON NEUROMUSCULAR CONDUCTION AND FUNCTIONAL STATE OF MUSCLES AFTER COMPONENT SEPARATION

Demin NA[1,2], Achkasov EE[1], Polyaev BA[2], Shishkin AA[2], Medvedeva AI[3], Ostanin OE[2] ✉

[1] Sechenov First Moscow State Medical University (Sechenov University), Moscow, Russia
[2] Pirogov Russian National Research Medical University (Pirogov University), Moscow, Russia
[3] Patrice Lumumba Peoples' Friendship University of Russia (RUDN University), Moscow, Russia

Muscular dysfunction of the anterior abdominal wall persists in many patients post component separation due to postoperative ventral hernia. Electrical myostimulation can contribute to better recovery, but its efficacy after such surgical procedures is poorly understood. The study aimed to assess the effect of the postoperative electrical myostimulation on the neuromuscular conduction and functional activity of the rectus abdominis muscles. A total of 128 patients (average age 47.9 ± 8.6 years) post component separation were included in a prospective controlled non-randomized study. The index group (n = 64) received electrical myostimulation starting from day 10 (12 sessions, 5–10 min each, 3 times a week, COMPEX SP-2.0® muscle stimulator, Switzerland), and the control one (n = 64) received no electrical myostimulation. Electroneuromyography of the rectus abdominis muscles was performed before and after the course using the Synapsis system (Neurotech, Russia). In the index group, the latency period reduced from 10.1 to 7.9 ms (by 21.8%; $p < 0.001$), and in the control group it reduced from 9.7 to 9.2 ms (by 5.2%; $p < 0.001$); the intergroup difference $p = 0.002$. The M-response amplitude improved in both groups (index group: from 8.4 to 8.9 mV, +5.6%, $p < 0.001$; control group: from 8.2 to 8.8 mV, +6.8%, $p < 0.001$), without any intergroup differences ($p = 0.295$). The induced muscle contraction velocity changed minimally in the index group (from 45.0 to 45.4 m/s, $p = 0.049$) and did not change in the control group ($p = 0.316$); in 89.1% of patients, the values were still below normal. Conclusions: postoperative electrical myostimulation significantly accelerates the neuromuscular conduction restoration, but does not affect the muscular response amplitude. It is reasonable to include electrical myostimulation in rehabilitation programmes.

Keywords: electrical myostimulation, postoperative rehabilitation, ventral hernia, hernioplasty, neuromuscular conduction, electroneuromyography

Author contribution: Demin NA — implementation of the main stages of the pilot study, manuscript writing; Achkasov EE — study design, academic editing, expert control; Polyaev BA — academic editing, expert control; Shishkin AA — statistical data processing; Medvedeva AI — manuscript writing, clinical data collection; Ostanin OE — clinical data collection, statistical processing.

Compliance with ethical standards: the study was approved by the Ethics Committee of the Sechenov University (protocol No. 08-19 dated 05 June 2019). All subjects submitted the informed consent. No personally identifiable information is disclosed.

✉ **Correspondence should be addressed:** Oleg E. Ostanin
Ostrovityanova, 1, Moscow, 117513, Russia; ostanin.oleg2011@yandex.ru

Received: 29.03.2026 **Accepted:** 16.04.2026 **Published online:** 28.04.2026

DOI: 10.24075/brsmu.2026.020

ВЛИЯНИЕ ЭЛЕКТРОМИОСТИМУЛЯЦИИ НА НЕРВНО-МЫШЕЧНУЮ ПРОВОДИМОСТЬ И ФУНКЦИОНАЛЬНОЕ СОСТОЯНИЕ МЫШЦ ПОСЛЕ СЕПАРАЦИОННОЙ ГЕРНИОПЛАСТИКИ

Н. А. Демин[1,2], Е. Е. Ачкасов[1], Б. А. Поляев[2], А. А. Шишкин[2], А. И. Медведева[3], О. Е. Останин[2] ✉

[1] Первый Московский государственный медицинский университет имени И. М. Сеченова (Сеченовский Университет), Москва, Россия
[2] Российский национальный исследовательский медицинский университет имени Н. И. Пирогова (Пироговский Университет), Москва, Россия
[3] Российский университет дружбы народов имени Патриса Лумумбы (РУДН), Москва, Россия

После сепарационной герниопластики по поводу послеоперационных вентральных грыж у многих пациентов сохраняется мышечная дисфункция передней брюшной стенки. Электромиостимуляция может улучшить восстановление, но ее эффективность после таких операций изучена недостаточно. Целью исследования было оценить влияние послеоперационной электромиостимуляции на нервно-мышечную проводимость и функциональную активность прямых мышц живота. В проспективное контролируемое нерандомизированное исследование включили 128 пациентов (средний возраст 47,9 ± 8,6 лет), перенесших сепарационную герниопластику. Основная группа (n = 64) получала электромиостимуляцию с 10-х суток (12 сеансов по 5–10 мин, 3 раза в неделю, аппарат COMPEX SP-2.0®, Швейцария), контрольная (n = 64) — нет. Электронейромиографию прямых мышц живота проводили до и после курса на аппарате «Synapsis» (ООО НМФ «Нейротех», Россия). В основной группе латентный период сократился с 10,1 до 7,9 мс (на 21,8%; $p < 0,001$), в контрольной — с 9,7 до 9,2 мс (на 5,2%; $p < 0,001$); межгрупповое различие $p = 0,002$. Амплитуда М-ответа улучшилась в обеих группах (основная: с 8,4 до 8,9 мВ, +5,6%, $p < 0,001$; контрольная: с 8,2 до 8,8 мВ, +6,8%, $p < 0,001$) без различий между группами ($p = 0,295$). Скорость индуцированного мышечного сокращения в основной группе изменилась минимально (с 45,0 до 45,4 м/с, $p = 0,049$), в контрольной — нет ($p = 0,316$); у 89,1% пациентов показатель оставался ниже нормы. Выводы: послеоперационная электромиостимуляция достоверно ускоряет восстановление нервно-мышечной проводимости, но не влияет на амплитуду мышечного ответа. Включение электромиостимуляции в реабилитационные программы целесообразно.

Ключевые слова: электромиостимуляция, послеоперационная реабилитация, вентральные грыжи, герниопластика, нервно-мышечная проводимость, электронейромиография

Вклад авторов: Н. А. Демин — проведение основных этапов пилотного исследования, написание статьи; Е. Е. Ачкасов — дизайн исследования, научное редактирование, экспертный контроль; Б. А. Поляев — научное редактирование, экспертный контроль; А. А. Шишкин — статистическая обработка данных; А. И. Медведева — написание статьи, сбор клинических данных; О. Е. Останин — сбор клинических данных, статистическая обработка.

Соблюдение этических стандартов: исследование одобрено этическим комитетом Сеченовского Университета (протокол № 08-19 от 05 июня 2019 г.). Все участники подписали информированное добровольное согласие. Данные, позволяющие идентифицировать личность, не раскрываются.

✉ **Для корреспонденции:** Олег Евгеньевич Останин
ул. Островитянова, д. 1, г. Москва, 117513, Россия; ostanin.oleg2011@yandex.ru

Статья получена: 29.03.2026 **Статья принята к печати:** 16.04.2026 **Опубликована онлайн:** 28.04.2026

DOI: 10.24075/vrgmu.2026.020

In recent decades, surgery for postoperative ventral hernias (PHR) has fundamentally changed. Widespread introduction into world's clinical practice of separation hernioplasty techniques, such as the anterior component separation according to Ramirez, posterior component separation with the transversus abdominis release (TAR), and their combination, has made it possible to radically reduce the incidence of recurrence and severe postoperative complications even in patients with giant and repeatedly recurring hernias [1, 2]. The possibility of adequate anterior abdominal wall defect closure with restoration of the anterior abdominal wall structural integrity and functional framework has transformed the formerly palliative interventions into full-fledged reconstructive surgical procedures. However, despite the obvious progress in surgical techniques, the problem of full functional rehabilitation of patients post component separation has not been finally resolved.

Extensive mobilization of the muscular-aponeurotic layers, which is inevitable with separation techniques, is associated with the severe surgical soft tissue injury, intersection of intermuscular neurovascular bundles, and creation of extensive wound surfaces. This results in a complex of pathophysiological alterations in the anterior abdominal wall muscles, primarily in the rectus abdominis muscles. Intraoperative damage to the terminal branches of the intercostal nerves innervating the rectus abdominis muscles, as well as the development of local inflammatory edema and ischemia in the operated site underlie the neuromuscular conduction impairment [3]. The above factors cause temporary denervation of muscle fibers, the clinical manifestations of which are the nerve conduction slowdown and muscle contractility reduction. A significant proportion of patients show signs of muscle dysfunction in the postoperative period, even with the technically flawless surgery: structural atrophy of muscle fibers, decreased muscle fiber contractility, nerve conduction slowdown in motor fibers [4]. Clinical manifestations of such impairment include persistent abdominal weakness, persistent pain, limitation of daily physical activity, and, as a result, significant deterioration of the patients' quality of life for weeks or even months after hospital discharge [5]. Thus, there is an objective need to develop effective and pathogenetically substantiated postoperative rehabilitation methods aimed at accelerating the abdominal wall muscle functional state restoration.

Today, various approaches to rehabilitation of patients post hernioplasty are used, including therapeutic exercises, breathing exercises, manual therapy, kinesiotaping, and physiotherapy treatments. However, the effectiveness of many of these methods in terms of restoring neuromuscular conduction remains insufficiently proven, and the terms of prescription and optimal exposure parameters are not standardized [6]. In particular, active physical exercise in the early postoperative period is often limited due to pain and the risk of suture failure, which dictates the need to search for alternative, passive methods of muscle activity stimulation.

Instrumental electrical myostimulation (EMS) represents one of the most promising and physiological methods of impact onto the neuromuscular system in the context of forced hypokinesia. The EMS therapeutic effect is based on artificial generation of electrical impulses, which reach motor neuron terminals and muscle fibers, causing depolarization and subsequent contraction of the latter. This enables simulation of the physiological voluntary muscle contraction process, maintains tissue trophism, and prevents the development of neurogenic atrophy during periods, when active movement is limited due to pain or the risk of suture failure [7]. Experimental studies involving the use of hernioplasty models have clearly demonstrated that the use of EMS of the anterior abdominal wall muscles contributes to the significant decrease in the postoperative muscle fiber atrophy severity, microcirculation improvement in the operated area, and faster return of muscle activity functional parameters back to normal [8].

Despite the compelling theoretical and experimental basis, the clinical use of EMS in rehabilitation programmes after hernioplasty due to PVH is still poorly understood. The clinical data available in the literature are fragmentary, often contradictory and do not allow for the development of unambiguous guidelines for practical healthcare [9]. In particular, questions remain about optimal time intervals for the beginning of stimulation in the early postoperative period, most effective electric current parameters (frequency, pulse duration, intensity), as well as differentiated EMS effects on the outcomes of various types of reconstructive interventions on the anterior abdominal wall, depending on the traumatic nature of the procedure [10, 11]. The lack of standardized protocols and evidence base hinders the widespread implementation of this method into routine clinical practice of abdominal surgeons and medical rehabilitation specialists.

The study aimed to assess the effect of postoperative EMS on the restoration of neuromuscular conduction and functional activity of the rectus abdominis muscles in patients post component separation due to ventral hernia.

METHODS

A prospective controlled non-randomized study was conducted at the Department of Surgery of the Vorokhobov City Clinical Hospital, Moscow, between Sepember 2019 and March 2022. The study design was compliant with the CONSORT guidelines for non-randomized interventional studies [12].

Selection of patients

Of 207 patients post elective open component separation due to postoperative ventral hernias (PVH), 128 individuals (71 females, 57 males) age 28–83 years (average age 47.9 ± 8.6 years) were included in the study after applying the selection criteria. The follow-up period was 6–10 months (median follow-up period 8 months).

Inclusion criteria: age over 18 years; elective open component separation with the retromuscular polypropylene implant installation; submitted informed consent to take part in the study; remote communication capability for protocol execution monitoring; body mass index (BMI) ≤ 39.9 kg/m^2.

Non-inclusion criteria (assessed before patient enrollment): refusal of submitting the informed consent; history of recurrent PVH; pacemaker installed; decompensated somatic disorder (decompensated diabetes mellitus, NYHA functional class III–IV chronic heart failure, grade II–III chronic respiratory failure); active cancer or cancer treatment finished less than 6 months before; clinically significant musculoskeletal disorder limiting the performance of test exercises; mental disorder impeding the protocol execution; personal circumstances making participation impossible.

Exclusion criteria (applied after patient enrollment): postoperative complications requiring the rehabilitation tactics modification (wound infection, hematoma requiring drainage, thromboembolic complications, pneumonia, recurrent hernia during follow-up); informed consent revocation by the patient; identification of a previously undiagnosed condition meeting the non-inclusion criteria during follow-up.

Characteristics of hernias

The following parameters were analyzed to assess comparability of the groups based on the hernial defect baseline characteristics: hernia orifice size (cm), localization according to the European Hernia Society (EHS) guidelines, presence of the loss of domain (determined based on the computed tomography (CT) data as a ratio of hernia sac volume to abdominal cavity volume > 20%). The above characteristics are provided in Table 1. No significant intergroup differences in these parameters were revealed ($p > 0.05$).

Surgical technique

All the patients underwent open posterior component separation with the transversus abdominis release (TAR) in combination with the retromuscular polypropylene implant placement. The term "combination" reflects the combination of a separation component (mobilization of the muscular aponeurotic layers) with the prosthetic reconstruction. All interventions were performed by the same surgical team in accordance with the standardized protocol. The average hernial defect area calculated based on CT data was 150.4 ± 38.1 см^2 (range 103.0–351.3 cm^2). The implant size was selected individually in order to ensure complete defect closure capturing at least 5 cm of healthy tissue in each direction.

Group formation

The patients were divided into two groups, 64 individuals per group, depending on the postoperative rehabilitation protocol. The index group was through the course of electrical myostimulation (EMS) starting from day 10 after surgery; the control group was through standard rehabilitation without EMS.

Justification for the timing of the electrical myostimulation start and duration

The EMS course was started on day 10 after surgery due to the fact that the acute phase of postoperative inflammation was over by this time, severe pain was relieved, and no surgical wound dehiscence was observed, which enabled safe electrode placement on the rectus abdominis muscles without any risk of tissue infection or damage. The course duration of 12 sessions (4 weeks) was selected based on the earlier published experimental data, according to which the minimal time necessary for the clinically significant changes in neuromuscular conduction under exposure to EMS was at least 10–12 sessions [6]. The frequency of procedures (3 sessions per week with an interval of at least 48 h) ensured the optimal balance of the stimulating effect and the time necessary for restoration of muscle fibers after applying electrical load.

Electrical myostimulation protocol

The COMPEX SP-2.0® 6-channel muscle stimulator (Compex Medical SA, Switzerland) was used for EMS. Stimulation was conducted with the pulse current frequency of 5.0–30.0 Hz and pulse duration of 50.0–100.0 μs. The course consisted of 12 sessions (3 sessions per week with an interval of at least 48 h), 5–10 min each. The procedure was conducted in a supine position; in a number of cases, the patient was asked to perform slight flexion of the neck and bring the chin to the chest for additional tension in the rectus abdominis muscles to enhance the effect (Fig.).

Fig. Electrical muscles myostimulation of the anterior abdominal wall (10th day after hernioplasty)

Assessment methods

The main instrumental method for assessing the neuromuscular system functional state was electroneuromyography (ENMG) of the rectus abdominis muscles performed with the 4-channel Synapsis system (Neurotech, Russia) using the following settings: operating sampling frequency — 40.0 kHz, stimulation amplitude — 0–100.0 mA, signal measurement range — 0.1–200.0 mV. The following parameters were analyzed: latency period (LP, normal range 5.0–7.0 ms) reflecting the nerve conduction time; M-response amplitude (normal range 5.0–10.0 mV) characterizing the total muscle fiber activity; induced muscle contraction measure (IMR, normal range 50.0–75.0 m/s) estimating the rate of muscle fiber contraction in response to the electrical stimulus. Parameters were recorded twice: at the baseline (before the EMS course in the index group and in comparable terms in the control group) and after the end of the 4-week rehabilitation course.

Statistical data processing was performed using the StatTech v.4.8.0 software package (StatTech, Russia). The quantitative data distribution was tested for normality using the Shapiro–Wilk data. The normally distributed data were presented as the mean (M) ± standard deviation (SD); Student's t-test was used to compare such data in two groups, and the paired t-test was used to compare the data obtained before and after the intervention. The non-normally distributed data were described using the median (Me) and interquartile range (Q_1–Q_3); the Mann–Whitney *U*-test (for unrelated samples) and Wilcoxon test (for related samples) were used for comparison. Categorical data were presented as absolute values (*n*) and percentage (%). The differences were considered significant at $p < 0.05$.

RESULTS

When conducting electroneuromyography before the beginning of the electrical myostimulation course, there were no significant differences in latency period values between the index and control groups ($p = 0.639$). The intergroup differences became significant after the end of the electrical myostimulation course ($p = 0.002$) (Table 1).

The best latency period values were recorded in the group of patients, who received postoperative EMS: the median latency period reduced from 10.1 ms to 7.9 ms, i.e. by 21.8%

Table 1. Dynamic changes in neuromyography latency period values (ms)

Group	Follow-up stages				*p*
	LP before		LP after		
	Me	Q_1–Q_3	Me	Q_1–Q_3	
No EMS	9.7	8.3–12.0	9.2	8.0–11.3	< 0.001*
EMS	10.1	8.2–11.9	7.9	7.0–9.9	< 0.001*
p	0.639		0.002*		–

Note: * — significant differences ($p < 0.05$), the following methods were used: Mann–Whitney *U*-test, Wilcoxon test.

Table 2. Dynamic changes in neurographic muscle motor response amplitude values (mV)

Group	Follow-up stages				*p*
	M-response before		M-response after		
	Me	Q_1–Q_3	Me	Q_1–Q_3	
No EMS	8.2	7.5–9.1	8.8	8.0–9.3	< 0.001*
EMS	8.4	7.8–9.3	8.9	8.1–9.8	< 0.001*
p	0.139		0.295		–

Note: * — significant differences ($p < 0.05$), the following methods were used: Mann–Whitney *U*-test, Wilcoxon test.

($p < 0.001$). In the control group, the median latency period reduced from 9.7 ms to 9.2 ms, which corresponded to reduction by 5.2% ($p < 0.001$).

The analysis of the M-response amplitude revealed no significant differences between groups both before the beginning ($p = 0.139$) and after the end ($p = 0.295$) of the EMS course. At the same time, the parameter improvement relative to baseline was reported in both groups. In the control group, the mean M-response amplitude four weeks after surgery was 8.8 mV, which was 6.8% higher compared to the baseline value of 8.2 mV ($p < 0.001$). In the index group, the amplitude increased from 8.4 mV to 8.9 mV, i.e. by 5.6% ($p < 0.001$) (Table 2).

There were no significant intergroup differences in the induced muscle contraction rate, neither before, nor after the rehabilitation course. In 89.1% of subjects, the values of this parameter remained below the reference value of 50.0 m/s throughout the follow-up period. In the index group, the minimal, but significant increase in the induced muscle contraction rate was reported: the median increased from 45.0 m/s to 45.4 m/s ($p = 0.049$). There were no dynamic changes in this parameter in the control group ($p = 0.316$) (Table 3).

DISCUSSION

The study conducted has shown that postoperative EMS of the anterior abdominal wall muscles in patients post component separation significantly improves neuromuscular conduction, which is most clearly manifested by the latency period reduction. In the index group, the latency period reduced by 21.8%, while in the control group it reduced by 5.2% only ($p = 0.002$). These data suggest that EMS accelerates the physiological neuromuscular function restoration in the early postoperative period.

Such a pronounced latency period reduction under the exposure to EMS can be explained by several mechanisms. First, rhythmic electrical stimulation contributes to microcirculation improvement in the operated area, thereby accelerating the postoperative edema resorption and reducing the nerve fiber compression. Second, passive muscle fiber contraction under the exposure to electrical impulses maintains activity of the sodium-potassium pumps in the sarcolemma and prevents the development of denervation hypersensitivity. Third, regular stimulation of motor units prevents atrophy of the fast (type II) muscle fibers most vulnerable in the context of postoperative immobilization.

The M-response amplitude improved to approximately equal extent in both groups (by 5.6% in the index group and 6.8% in the control group), which suggests natural processes of the muscle tissue postoperative regeneration that do not depend on the use of EMS. The findings are consistent with the fact that EMS primarily affects neurogenic mechanisms underlying the muscle activity regulation, rather than the actual contractile properties of muscle fibers [13]. Similar conclusions were drawn by other authors, who showed that the neuromuscular conduction values improved faster, than the muscle strength and volume increased after the EMS course [14].

The induced muscle contraction rate remained low in the vast majority of patients (89.1%), although in the index group the minimal, but significant increase in this value (from 45.0 to 45.4 m/s, $p = 0.049$) was reported. The fact, that in most patients the induced muscle contraction rate did not reach normal values even after the rehabilitation course completion, suggests the postoperative muscle dysfunction severity and

Table 3. Dynamic changes in neurographic induced muscle contraction values (m/s)

Group	Follow-up stages				*p*
	IMR before		IMR after		
	M ± SD	95% CI	M ± SD	95% CI	
No EMS	45.6 ± 1.9	45.1–46.2	45.8 ± 2.2	45.1–46.4	0.316
EMS	45.0 ± 2.0	44.6–45.8	45.4 ± 2.0	44.8–46.0	0.049*
p	0.293		0.436		–

Note: * — significant differences ($p < 0.05$), the following method was used: Student's *t*-test.

the need for longer recovery period. It is likely that the longer rehabilitation course or combining EMS with other physical therapy methods, such as therapeutic and breathing exercises is needed to bring this parameter back to normal. Our findings are consistent with the data showing that the use of EMS after extensive abdominal surgery made it possible to reduce the muscle mass loss by 20–25%, but did not ensure complete restoration of functional parameters during the 4-week follow-up period [15]. Furthermore, our data are correlated to the experimental results obtained using the hernioplasty model that has shown that EMS accelerates restoration of the muscle bioelectrical activity, but longer time is required to achieve full functional recovery [6].

Clinical significance of the findings lies in the fact that even a relatively short EMS course can considerably accelerate the neuromuscular conduction restoration, which can contribute to earlier activation of patients, decreased risk of developing abnormal motor stereotypes, and, finally, to improved quality of life in the postoperative period. It is important to note that the EMS procedure was well tolerated by patients; it caused no complications and did not require the patients' active involvement, which made it especially valuable in the early postoperative period, when the opportunities for active physical activity were limited.

Limitations of this study include the lack of blinding design, the relatively short follow-up period (four weeks of intervention), and the lack of assessment of long-term outcomes. Furthermore, clinical outcomes, such as quality of life and pain severity, were not assessed. These may become the subject of further research. Assessment of the impact of various EMS parameters (frequency, pulse duration, intensity) on the muscle function recovery rate and development of personalized rehabilitation protocols depending on the surgery extent and baseline characteristics of the patient also seem to be a promising area.

CONCLUSIONS

The study conducted has demonstrated a significant positive effect of postoperative EMS on the functional recovery of the anterior abdominal wall muscles in patients post open component separation due to PVH. The ENMG analysis revealed a significant improvement of the neuromuscular conduction parameters in the group that received EMS, with the significant LP reduction by 21.8% relative to baseline (from 10.1 to 7.9 ms; $p < 0.001$). In the control group that did not receive EMS, the dynamics of LP restoration was 5.2%. However, the M-response amplitude changes in both groups were comparable, which suggests natural processes of postoperative muscle function restoration that do not depend on the use of EMS. Of special interest is the identified trend towards IMR improvement in the EMS group, despite the fact that absolute values of this parameters remained below normal. The findings confirm the feasibility of including EMS in postoperative rehabilitation programmes, which could potentially contribute to the more rapid neuromuscular conduction restoration and serve as a preventative measure for prolonged muscle atony among patients post hernioplasty for PVH. Thus, EMS is a promising postoperative rehabilitation instrument. However, further studies with the longer follow-up period and assessment of the long-term outcomes depending on the hernioplasty type and other parameters of the patient are required for optimization of protocols.

References

1. Pochhammer J, Ibald C, Weller MP, et al. Retromuscular, periprosthetic drainage after hernioplasty with sublay mesh reinforcement in ventral hernias results in less retromuscular fluid collections but longer hospital stay and analgetic use with unclear effect on clinical outcome — a randomized controlled trial. Langenbecks Arch Surg. 2024; 409 (1): 334. DOI: 10.1007/s00423-024-03522-6.
2. Serafio-Gómez JL, Aragón-Quintana C, Bustillos-Ponce M, et al. Effective Management of Giant Ventral Hernias: A Comprehensive Approach Combining Preoperative Botulinum Toxin Application, Modified Ramírez's Component Separation, and Rives-Stoppa Hernioplasty. Cureus. 2023; 15 (11): e48967. DOI: 10.7759/cureus.48967.
3. Zabolotskikh IB, Lebedinskiy KM, Belkin AA, Butrov AV, Kondratev AN, Lubnin AYu, et. al. Perioperatsionnoe vedenie patsientov s nervno-myshechnymi zabolevaniyami (proekt klinicheskikh rekomendatsiy FAR Rossii). Regionarnaya anesteziya i lechenie ostroy boli. 2014; (2): 56-75. DOI: 10.17816/RAOL43254. Russian.
4. Daes J, Oma E, Jorgensen LN. Changes in the abdominal wall after anterior, posterior, and combined component separation. Hernia. 2022; 26 (1): 17–27. DOI: 10.1007/s10029-021-02535-0.
5. Ciomperlik H, Dhanani NH, Cassata N, et al. Patient quality of life before and after ventral hernia repair. Surgery. 2021; 169 (5): 1158–63. DOI: 10.1016/j.surg.2020.11.003.
6. Petrushko SI, Portnyagin EV, Michurov EI, Repina EV, Sagynaliev AS, Rozhina AV. Reabilitatsiya bol'nykh posle gernioplastiki v rannem posleoperatsionnom periode. Trudnyi patsient. 2020; 18 (3): 46–48. DOI: 10.24411/2074-1995-2020-10020.
7. Da Mota Moreira I, Krause A, Memmert D. Effects of electromyostimulation on physiological determinants of endurance-performance in healthy subjects: a systematic review. J Sports Med Phys Fitness. 2022; 62 (12): 1654–61. DOI: 10.23736/S0022-4707.22.13428-6.
8. Demin NA, Achkasov EE, Karkischenko VN, et al. Possibilities of physical rehabilitation using myostimulation after ventral hernia repair retro-rectus. Clinical and Experimental Surgery. Petrovsky Journal. 2022; 10 (3): 114–24. DOI: 10.33029/2308-1198-2022-10-3-114-124.
9. Ricci PA, Di Thommazo-Luporini L, Santos-de-Araújo AD, et al. Combining Whole-Body Electromyostimulation and Dynamic Exercise After Bariatric Surgery: A Randomized, Double-Blind, and Sham-Controlled Trial. Obes Surg. 2025. DOI: 10.1007/s11695-025-08107-w.
10. Christopher AN, Fowler C, Patel V, et al. Bilateral transversus abdominis release: Complex hernia repair without sacrificing quality of life. Am J Surg. 2022; 223 (2): 250–6. DOI: 10.1016/j.amjsurg.2021.03.020.
11. Cai X, Wang F, Zhu Y, et al. Application of bridging mesh repair in giant ventral incisional hernia. Updates Surg. 2024; 76 (6): 2411–20. DOI: 10.1007/s13304-024-01825-3.
12. Thabane L, Hopewell S, Lancaster GA, et al. Methods and processes for development of a CONSORT extension for reporting pilot randomized controlled trials. Pilot Feasibility Stud. 2016; 2: 25. DOI: 10.1186/s40814-016-0065-z.
13. Adams V. Electromyostimulation to fight atrophy and to build muscle: facts and numbers. J Cachexia Sarcopenia Muscle. 2018; 9 (4): 631–4. DOI: 10.1002/jcsm.12332.
14. Moreau D, Dubots P, Boggio V, et al. Effects of electromyostimulation and strength training on muscle soreness, muscle damage and sympathetic activation. J Sports Sci. 1995; 13 (2): 95–100. DOI: 10.1080/02640419508732216.
15. Hardy EJ, Hatt J, Doleman B, et al. Post-operative electrical muscle stimulation attenuates loss of muscle mass and function following major abdominal surgery in older adults: a split body randomised control trial. Age Ageing. 2022; 51 (10): afac234. DOI: 10.1093/ageing/afac234.

Литература

1. Pochhammer J, Ibald C, Weller MP, et al. Retromuscular, periprosthetic drainage after hernioplasty with sublay mesh reinforcement in ventral hernias results in less retromuscular fluid collections but longer hospital stay and analgetic use with unclear effect on clinical outcome — a randomized controlled trial. Langenbecks Arch Surg. 2024; 409 (1): 334. DOI: 10.1007/s00423-024-03522-6.
2. Serafio-Gómez JL, Aragón-Quintana C, Bustillos-Ponce M, et al. Effective Management of Giant Ventral Hernias: A Comprehensive Approach Combining Preoperative Botulinum Toxin Application, Modified Ramírez's Component Separation, and Rives-Stoppa Hernioplasty. Cureus. 2023; 15 (11): e48967. DOI: 10.7759/cureus.48967.
3. Заболотских И. Б., Лебединский К. М., Белкин А. А., Бутров А. В., Кондратьев А. Н., Лубнин А. Ю., и др. Периоперационное ведение пациентов с нервно-мышечными заболеваниями (проект клинических рекомендаций ФАР России). Региональная анастезия и лечение острой боли. 2014; 8 (2): 58–75.
4. Daes J, Oma E, Jorgensen LN. Changes in the abdominal wall after anterior, posterior, and combined component separation. Hernia. 2022; 26 (1): 17–27. DOI: 10.1007/s10029-021-02535-0.
5. Ciomperlik H, Dhanani NH, Cassata N, et al. Patient quality of life before and after ventral hernia repair. Surgery. 2021; 169 (5): 1158–63. DOI: 10.1016/j.surg.2020.11.003.
6. Petrushko SI, Portnyagin EV, Michurov EI, Repina EV, Sagynaliev AS, Rozhina AV. Reabilitatsiya bol'nykh posle gernioplastiki v rannem posleoperatsionnom periode. Trudnyi patsient. 2020; 18 (3): 46–48. DOI: 10.24411/2074-1995-2020-10020.
7. Da Mota Moreira I, Krause A, Memmert D. Effects of electromyostimulation on physiological determinants of endurance-performance in healthy subjects: a systematic review. J Sports Med Phys Fitness. 2022; 62 (12): 1654–61. DOI: 10.23736/S0022-4707.22.13428-6.
8. Demin NA, Achkasov EE, Karkischenko VN, et al. Possibilities of physical rehabilitation using myostimulation after ventral hernia repair retro-rectus. Clinical and Experimental Surgery. Petrovsky Journal. 2022; 10 (3): 114–24. DOI: 10.33029/2308-1198-2022-10-3-114-124.
9. Ricci PA, Di Thommazo-Luporini L, Santos-de-Araújo AD, et al. Combining Whole-Body Electromyostimulation and Dynamic Exercise After Bariatric Surgery: A Randomized, Double-Blind, and Sham-Controlled Trial. Obes Surg. 2025. DOI: 10.1007/s11695-025-08107-w.
10. Christopher AN, Fowler C, Patel V, et al. Bilateral transversus abdominis release: Complex hernia repair without sacrificing quality of life. Am J Surg. 2022; 223 (2): 250–6. DOI: 10.1016/j.amjsurg.2021.03.020.
11. Cai X, Wang F, Zhu Y, et al. Application of bridging mesh repair in giant ventral incisional hernia. Updates Surg. 2024; 76 (6): 2411–20. DOI: 10.1007/s13304-024-01825-3.
12. Thabane L, Hopewell S, Lancaster GA, et al. Methods and processes for development of a CONSORT extension for reporting pilot randomized controlled trials. Pilot Feasibility Stud. 2016; 2: 25. DOI: 10.1186/s40814-016-0065-z.
13. Adams V. Electromyostimulation to fight atrophy and to build muscle: facts and numbers. J Cachexia Sarcopenia Muscle. 2018; 9 (4): 631–4. DOI: 10.1002/jcsm.12332.
14. Moreau D, Dubots P, Boggio V, et al. Effects of electromyostimulation and strength training on muscle soreness, muscle damage and sympathetic activation. J Sports Sci. 1995; 13 (2): 95–100. DOI: 10.1080/02640419508732216.
15. Hardy EJ, Hatt J, Doleman B, et al. Post-operative electrical muscle stimulation attenuates loss of muscle mass and function following major abdominal surgery in older adults: a split body randomised control trial. Age Ageing. 2022; 51 (10): afac234. DOI: 10.1093/ageing/afac234.

EARLY ADMINISTRATION OF XENON-OXYGEN MIXTURE IN NEONATAL HYPOXIC-ISCHEMIC ENCEPHALOPATHY

Dementev IM[1,2], Gabitov MV[1] ✉, Timoshin SS[2], Kuzovlev AN[1], Grebenchikov OA[1]

[1] Negovsky Research Institute of General Reanimatology, Federal Research and Clinical Center of Intensive Care Medicine and Rehabilitology, Moscow, Russia
[2] Vladimirsky Moscow Regional Research Clinical Institute, Moscow, Russia

Hypoxic-ischemic encephalopathy remains a leading cause of neonatal mortality and disability. Experimental data suggest potential neuroprotective properties of xenon; however, the mechanisms and extent of its effect are not fully understood. The study aimed to evaluate the neuroprotective properties of a xenon-oxygen mixture in a neonatal ischemia-hypoxia rat model using MRI and follow-up neurological assessment. The experiment involved Wistar rat pups (n = 16). Neonatal ischemia-hypoxia was induced by the Rice–Vannucci method. Thirty minutes post-hypoxia, animals received the 60-min inhalation of either nitrogen-oxygen (control, n = 8), or 50/50 xenon-oxygen mixture (n = 8). Brain MRI was performed on day 7. In the xenon group, brain lesion volume was significantly reduced by 25% compared to controls on day 7 (p = 0.001). Neurological development was assessed from day 3 to 28 using a combination of behavioral tests. Xenon-treated animals demonstrated earlier formation of forelimb and hindlimb grasping reflexes (p = 0.025 and p = 0.005), better hindlimb placement and cliff avoidance on day 7 (p = 0.045 and p = 0.03), and better preserved auditory startle response on day 14 (p = 0.035). Thus, early administration of a xenon-oxygen mixture after ischemia-hypoxia exerts pronounced neuroprotection in newborn rats, confirmed by reduced brain damage and improved neurological outcomes.

Keywords: xenon, xenon-oxygen mixture, hypoxic-ischemic encephalopathy, neuroprotection, Rice–Vannucci model, rats

Funding: the work was carried out under the research project "Cytoprotective Effects of Inert Gases for the Prevention and Treatment of Organ Dysfunction in Critical Conditions" (No. FGWS-2025-0015).

Author contribution: Dementev IM — conducting the model experiment, analysis and discussion of results, manuscript writing; Gabitov MV — analysis of results, statistical analysis, manuscript writing and editing; Timoshin SS — discussion of results and manuscript editing; Kuzovlev AN — study planning, discussion of results, manuscript editing; Grebenchikov OA — approval of the study design, discussion of results, manuscript editing.

Compliance with ethical standards: the study was approved by the Ethics Committee of the Federal Research and Clinical Center of Intensive Care Medicine and Rehabilitology (Protocol No. 2/25/5 dated March 26, 2025). All animal procedures were performed in accordance with the principles of the European Convention for the Protection of Vertebrate Animals used for Experimental and Other Scientific Purposes (Strasbourg, 1986). The report of the study was prepared in accordance with the ARRIVE (Animal Research: Reporting of In Vivo Experiments) guidelines.

✉ **Correspondence should be addressed:** Mikhail V. Gabitov
Petrovka 25, str. 2, Moscow, 107031, mgabitov@fnkcrr.ru

Received: 25.02.2026 **Accepted:** 10.03.2026 **Published online:** 17.03.2026

DOI: 10.24075/brsmu.2026.009

РАННЕЕ ПРИМЕНЕНИЕ КСЕНОН-КИСЛОРОДНОЙ СМЕСИ ПРИ НЕОНАТАЛЬНОЙ ГИПОКСИЧЕСКОЙ ИШЕМИЧЕСКОЙ ЭНЦЕФАЛОПАТИИ

И. М. Дементьев[1,2], М. В. Габитов[1] ✉, С. С. Тимошин[2], А. Н. Кузовлев[1], О. А. Гребенчиков[1]

[1] Научно-исследовательский институт общей реаниматологии имени В. А. Неговского Федерального научно-клинического центра реаниматологии и реабилитологии, Москва, Россия
[2] Московский областной научно-исследовательский клинический институт имени М. Ф. Владимирского, Москва, Россия

Гипоксическая ишемическая энцефалопатия остается одной из ведущих причин неонатальной смертности и инвалидизации. Экспериментальные данные свидетельствуют о потенциальных нейропротекторных свойствах ксенона, однако механизмы и выраженность его эффекта изучены недостаточно. Целью работы было оценить нейропротекторные свойства ксенон-кислородной смеси на модели неонатальной ишемии-гипоксии у крыс с использованием МРТ и динамического анализа неврологического статуса. Экспериментальная работа выполнена на крысятах линии Wistar (n = 16). Неонатальную ишемию-гипоксию моделировали по методу Райса–Ванучи. Через 30 мин после гипоксии животные получали ингаляцию либо азот-кислородной смеси (контроль, n = 8), либо ксенон-кислородной смеси 50/50 (n = 8) в течение 60 мин. На 7-е сутки проводили МРТ головного мозга. В группе ксенона объем повреждения головного мозга на 7-е сутки был статистически значимо ниже на 25% по сравнению с контролем (p = 0,001). Неврологическое развитие оценивали с третьих по 28-е сутки с использованием комплекса поведенческих тестов. Животные группы Xe демонстрировали более раннее формирование хватательных рефлексов передних и задних конечностей (p = 0,025 и p = 0,005), лучшую постановку задних конечностей и более выраженную реакцию избегания обрыва на 7-е сутки (p = 0,045 и p = 0,03), а также более сохранную слуховую стартл-реакцию на 14-е сутки (p = 0,035). Таким образом, раннее применение ксенон-кислородной смеси после моделирования ишемии-гипоксии оказывает выраженный нейропротекторный эффект у новорожденных крыс, что подтверждается уменьшением объема повреждения головного мозга и улучшением неврологических показателей.

Ключевые слова: ксенон, ксенон-кислородная смесь, гипоксическая ишемическая энцефалопатия, нейропротекция, модель Rice-Vannucci, крысы

Финансирование: работа выполнена по теме НИР «Цитопротекторные эффекты инертных газов для профилактики и лечения органной дисфункции при критических состояниях» (No FGWS - 2025-0015).

Вклад авторов: И. М. Дементьев — проведение модельного эксперимента, анализ и обсуждение результатов, написание рукописи; М. В. Габитов — анализ результатов, статистический анализ, написание и редактирование рукописи, подготовка в печать; С. С. Тимошин — обсуждение результатов и редактирование рукописи; А. Н. Кузовлев — планирование исследования, обсуждение результатов, редактирование рукописи; О. А. Гребенчиков — утверждение дизайна исследования, обсуждение результатов, редактирование рукописи.

Соблюдение этических стандартов: исследование одобрено этическим комитетом Федерального научно-клинического центра реаниматологии и реабилитологии (протокол № 2/25/5 от 26 марта 2025 г.). Все процедуры с участием животных выполнены в соответствии с принципами Европейской конвенции о защите позвоночных животных, используемых для экспериментов или в иных научных целях (Страсбург, 1986). Отчет о проведенном исследовании подготовлен в соответствии с рекомендациями ARRIVE (Animal Research: Reporting of In Vivo Experiments).

✉ **Для корреспонденции:** Михаил Валерьевич Габитов
ул. Петровка, д. 25, стр. 2, г. Москва, 107031; mgabitov@fnkcrr.ru

Статья получена: 25.02.2026 **Статья принята к печати:** 10.03.2026 **Опубликована онлайн:** 17.03.2026

DOI: 10.24075/vrgmu.2026.009

The term "hypoxic-ischemic encephalopathy" refers to acute damage to the brain structures caused by perinatal asphyxia. The prevalence worldwide varies between 1 and 3 cases per 1000 live births in developed economies, while in resource-limited States the prevalence can be 10 times higher [1, 2]. In the Russian Federation the rate is 13.3 per 1000 newborns [3].

The hypoxic-ischemic encephalopathy pathogenesis is induced by the cerebral perfusion decrease resulting in hypoxia, ischemia, and energy deficiency, and the neurological outcome severity is correlated with gestational age and localization of the lesion [4]. Oxidative stress, neuroinflammation, excitotoxicity, apoptosis, and cell necrosis represent the key links of the complex pathophysiological cascades induced in the brain. However, the exact pathophysiological mechanisms underlying the development of hypoxic-ischemic encephalopathy are poorly understood [5, 6].

Today, therapeutic hypothermia remains the only evidence-based neuroprotection method used in hypoxic-ischemic encephalopathy [7–10]. However, the method efficacy is limited, since therapeutic hypothermia only partially reduces the risk of mortality and disability [11–13]. This encourages active search for new therapeutic strategies capable of enhancing the effects of hypothermia or having independent neuroprotective effects.

One promising direction is the use of noble gases, which, according to experimental data, possess pharmacological activity [14–16]. Xenon is of particular interest, its neuroprotective properties have been demonstrated in various brain damage models [17]. However, the results of clinical trials, such as the international TOBY-Xe trial, have revealed no significant improvement of outcomes when adding xenon to hypothermia in full-term newborns [18, 19]. This does not mean that there is no xenon potential, but rather points to the need for more thorough preclinical assessment of the xenon mechanisms of action, dosing regimens, and delayed effects. In particular, the xenon ability to influence functional maturation of the brain in the post-ischemic period, which can be assessed in experimental models using the long-term neuro-behavioral testing and brain imaging methods, needs to be clarified.

The study aimed to evaluate the neuroprotective properties of a xenon-oxygen mixture in a neonatal ischemia-hypoxia rat model and assess the extent of brain damage and some neurological status indicators.

METHODS

The experiment involved male and female Wistar rat pups with the body weight of 25–30 g (n = 16). The animals were simply randomized into groups using a random number generator. Animals that showed signs of disease in the initial phase based on the results of a standard examination and behavior assessment were excluded from the study, along with the ones that died due to complications from anesthesia or surgical intervention. The following data were the criteria for humane withdrawal from the experiment: postoperative wound infection, no startle response, weight loss of more than 20% in one day, manifestations of autoaggressive behavior, inability to self-feed and drink 24 h after the ischemia-hypoxia induction.

The study design provided for formation of two experimental series. Control group (group C, n = 8): within 30 min after the ischemia-hypoxia modeling the animals were subjected to the nitrogen-oxygen mixture inhalation (nitrogen 50%/oxygen 50%; InertGasMedical, Russia) for 60 min. Experimental group (group Xe, n = 8): within 30 min after the ischemia-hypoxia modeling the animals received the xenon-oxygen mixture (XenOx 50, xenon 50% /oxygen 50%; registration certificate No. LP-006493, InertGasMedical, Russia) for 60 min. Laboratory animals were euthanized through the anesthetic agent overdose after the end of the experiment.

Neonatal ischemia-hypoxia was simulated using the Rice–Vannucci model [20]. Isoflurane anesthesia (induction 3%, maintenance 1.5–2% in 100% O_2) on the hot bench (36 °C) was used. The anesthesia depth was regulated by monitoring the loss of corneal and interdigital reflexes. After microsurgical isolation and lygation of the left common carotid artery we perceived no distal pulse, and the wound was sutured. The rat pups were placed in a thermostat (36 °C, 60 min), then in a multi-gas incubator with the hypoxic mixture (8% O_2 / 92% N_2) for 90 min with temperature monitoring and visual control.

Within 30 min after the end of hypoxia induction, during which the animals had access to the mother, the rat pups were placed in a chamber for 60 min for inhalation of the control and experimental gas mixtures. N_2/O_2 50/50 or XenOx 50 was supplied continuously with the flow rate of 0.5–1 L/min. The temperature within the chamber was regulated at 36°C, with the relative humidity maintained between 40% and 60%. There were no more than five rat pups in the chamber at once; a layer of wood litter was introduced at the base to ensure biological fluid absorption. The contour was fitted with a desiccant (silica gel) and CO_2 adsorber (soda lime); recirculation was ensured by a fan. The animals' arousal level and motor activity were assessed after the end of the exposure.

Neurological status

The newborn rat pups' neurological development was assessed using 8 behavioral tests starting from day 3 after birth in accordance with the previously reported protocols [21–23].

The forelimb grasping reflex was assessed starting from the third day of life: a blunt rod was gently pressed to the forelimb palmar surface, which normally induced finger flexion and grasp. The reflex was considered to be completely developed with stable grasping with both front paws throughout two consecutive days. A three-point assessment scale was used, where score 0 corresponded to no reflex, score 1 corresponded to grasping with one front paw (with the side specified), and score 2 corresponded to grasping with both front paws. Similarly, the hindlimb grasping reflex was assessed by the same method starting from the third day: score 0 — no grasp, score 1— grasping with one hind limb, score 2 — grasping with both hind limbs.

The righting reflex was also tested starting from the third day: the rat pup was placed in a supine position with the limbs straightened, and then released, recording the time taken to return to a prone position. The maximum time allowed for the response to complete was 15 s. No prone position restoration within this time was scored 0, roll over on the side (with the side specified) or incorrect posture was scored 1, and complete roll over resulting in a physiologically correct posture (onto all four paws) was scored 2.

The hindlimb placement reflex was assessed starting from the fourth day of life: the rat pup was held vertically by the body and the edge of a hard surface was touched with the back of the hind paw. Normally, the animal pulled back its paw and placed it on the surface. No response was scored 0, placement of one limb (with the side specified) was scored 1, and placement of both limbs was scored 2.

The cliff avoidance response also assessed starting from the fourth day was tested by placing the rat pup with its front paws and muzzle over the edge of a horizontal surface; a soft

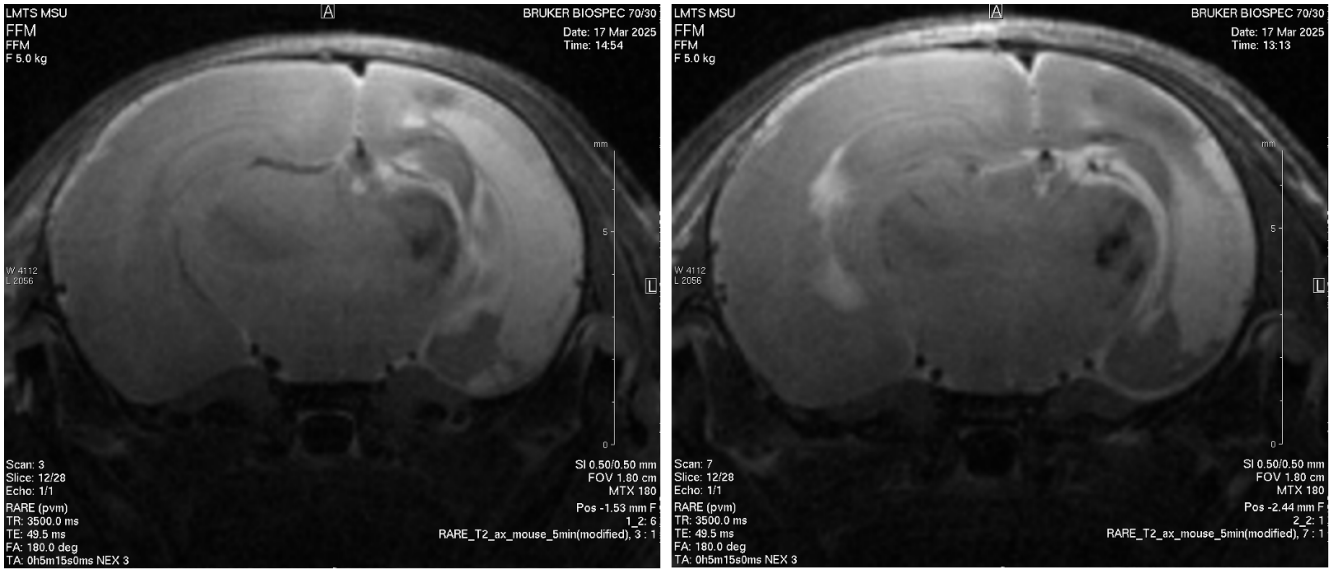

Fig. The animals' brain MRI scans on day 7. Group C — left, group Xe — right

pad was placed under the edge to prevent injury from fall. Reflexive avoidance manifested itself in turning away from the edge. No movement or fall was scored 0, an attempt to move away from the edge with dangling limbs was scored 1, and complete departure from the edge was scored 2.

The auditory startle response was assessed starting from the 10th day: a loud tone was presented just above the animal. Sudden movement or startle was considered as positive response and scored 1, no response was scored 0.

The nature of posture when moving on a non-slip surface was assessed starting from the 12th day of life. Not fully developed posture (dragging of the abdomen, the limbs perpendicular to the body) was scored 1, the fully developed posture (elevated abdomen, the limbs parallel) was scored 2; no movement corresponded to 0 points. At the same age, since day 12, eye opening was recorded: the eyelids fused shut corresponded to 0, opening of one eye (with the side specified) corresponded to 1 point, opening of both eyes corresponded to 2 points.

The limb sensorimotor function was assessed using the limb placement on support test. After three days of adaptation to hands the animals were through seven trials aimed at assessing the limb sensorimotor integration. The trials involved alternately moving the front and back paws off the edge of the table in different positions (with visual control, laterally, when pushing the body towards the edge, and when lowering to the surface by the tail). A three-point scale was used to assess performance in each trial: score 2 — normal performance, score 1 — slow or incomplete performance, score 0 — no response.

Magnetic resonance imaging

On day 7 after the ischemia-hypoxia modeling, the animals underwent *in vivo* MRI in the 7 T MRI scanner with the 105 mT/m gradient system (BioSpec 70/30; Bruker, Germany). After being anesthetized with isoflurane at a concentration of 1.5–2%, the animal was placed in a stereotactic fixation system with thermal control. A standard brain assessment protocol involving acquisition of T2-weighted images was used. A linear transmitter with the internal diameter of 72 mm was used to transmit the radio frequency signal; a surface receiver coil for the rat brain was used for signal detection. The RARE spin echo sequence had the following parameters: TR = 6000 ms, TE = 63.9 ms, slice thickness — 0.8 mm with an increment of 0.8 mm, matrix size — 256 × 384, resolution — 0.164 × 0.164 mm/pixel. The overall scan time per animal was about 30 min.

The extent of brain damage was assessed by planimetric analysis of MR images with subsequent calculation of the damaged tissue volume. The series of MRI scans was used to calculate the lesion area (mm^2) for each slice in ImageJ (National Institutes of Health, Bethesda, MD, USA). For that the areas of the intact tissue in the healthy (S_1) and damaged (S_2) hemispheres were isolated, and the lesion area for a slice was calculated using the following formula: $\Sigma S = S_1 - S_2$, where ΣS was the lesion area on a single slice (mm^2) [24]. The brain damage volume was calculated using the following formula: $V = \Sigma S_n \times d$, where d was the slice thickness (0.8 mm), ΣS_n was the sum of lesion areas on all slices (mm^2).

Statistical analysis

Statistical analysis was performed using SPSS Statistics 28.0.1 and GraphPad Prism 10.4.2. The distribution was tested for normality using the Shapiro–Wilk test. Since the indicators were ordinal scales and their distribution was non-normal, the data are provided as the median and interquartile range Me (Q_1; Q_3). Groups were compared using the Mann–Whitney *U*-test. The differences were considered significant with the two-tailed $p < 0.05$. To minimize the systematic error, the researcher, who conducted MRI and assessed the animals' neurological status in behavioral tests, was blinded; he/she was unaware of the rat pup distribution into groups.

RESULTS

According to the MRI imaging data obtained on day 7, the group of animals that received the xenon-oxygen mixture showed a significant brain damage volume reduction. This value was 25% lower, than in the control group ($p = 0.001$; Fig.).

The neurological status analysis revealed significant reflex formation acceleration in the rat pups of group Xe. On day 3, the median forelimb grasping reflex estimate of this group was significantly higher compared to that of the control group ($p = 0.025$; Table), which suggests a significant xenon-oxygen mixture neuroprotective effect in terms of motor functions. Similarly, even more pronounced dynamic changes were

Table. Neurological status indicators in rat pups of groups C and Xe

Day	Test	Group C (n = 8)	Group Xe (n = 8)	p-value
3	Forelimb grasping reflex	1 [0; 1]	1.5 [1; 2]	0.025
	Hindlimb grasping reflex	1 [1; 1]	1.5 [1; 2]	0.005
	Righting reflex	1 [0; 1]	1 [1; 2]	0.19
7	Hindlimb placement	0.5 [0; 1]	1.5 [1; 2]	0.045
	Cliff avoidance response	1 [0; 1]	1 [1; 2]	0.03
14	Startle response to tone	1 [0; 1]	1 [1; 2]	0.035
	Eye opening	1 [1; 2]	1 [1; 2]	0.1
28	Limb placement on support	12 [8; 13]	13 [12; 13.5]	0.08

reported for the hindlimb reflex (p = 0.005). The righting reflex test revealed no significant differences between the studied groups (p = 0.190).

On day 7, animals of group Xe showed significantly better performance in the hindlimb placement test (p = 0.045), as well as more pronounced cliff avoidance response compared to controls (p = 0.030).

By day 14, the significantly better preserved startle response to tone was reported in the rat pups, which received the xenon-oxygen mixture (p = 0.035). There were no significant differences in the terms of eye opening between groups (p = 0.100).

On day 28, sensorimotor integration assessment based on the limb placement on support test revealed no significant differences (p = 0.080).

DISCUSSION

The data obtained show that the xenon-oxygen mixture (50% Xe/50% O_2) inhalation in the early recovery period after ischemia-hypoxia has a pronounced neuroprotective effect in the Rice–Vannucci model rat model. A significant reduction of the brain lesion volume by 25% in the Xe group on day 7 based on the MRI data has become the key finding. This result is in line with the conclusions of the recent large-scale systematic review and meta-analysis showing that xenon reduced neurological deficit on average by 39.7% in mouse, rat, and swine pre-clinical hypoxic-ischemic encephalopathy models [25]. Our study confirms that even a single 60-minute application of xenon can significantly limit the development of brain infarction, as can be seen in T2-weighted images.

The improvement recorded in behavioral tests confirms morphological data and has a clear temporal logic. Improvement of grasping reflexes and the limb placement test results on days 3–7 suggests that xenon contributes to preservation of the sensorimotor pathways and cortical centers responsible for these reflexes. This is critically important since it is motor impairment that underlies such severe hypoxic-ischemic encephalopathy outcomes, as cerebral palsy. The preserved startle response to tone on day 14 suggests better functional state of the auditory systems and brainstem, which resonates with the data of the abovementioned review, in which the authors note the xenon capability of apoptosis reduction and neuroinflammation modulation [25]. The lack of significant differences in the limb placement on support test results on day 28 is likely to be associated with small sample size and high variability resulting from the immature brain's compensatory capacity.

Our findings fit well into modern concepts of the xenon mechanisms of action. The xenon neuroprotective effect is mediated by both NMDA receptor antagonism and pleiotropic effects: activation of two-pore-domain potassium channels, modulation of AMPA receptors, and, which is especially important for the neonate's brain, anti-apoptotic effect [26]. It has been shown that xenon reduces neuronal death and suppresses chronic neuroinflammation [27, 28]. Improvement of neurological outcomes in our experiment is likely to result from such a combined effect: limitation of primary lesion and creation of more favorable conditions for postnatal brain maturation.

Our preclinical data gain particular importance in the light of the results of clinical trials, such as TOBY-Xe. In this trial adding xenon to hypothermia in neonates did not result in improvement of outcomes, which the authors attribute, among other things, to the late start of therapy. In our study xenon was administered strictly 30 min after hypoxia, which emphasizes critical importance of the therapeutic window. According to other data, the maximum xenon efficacy is also achieved when therapy is initiated in the first hours after stroke [25].

Thus, the use of the xenon-oxygen mixture after modeling hypoxic-ischemic encephalopathy ensured neuroprotective effect in newborn rats, which allows us to consider the goal of the study as achieved. It is necessary to consider a number of limitations when interpreting the results obtained. The animal experiments did not involve therapeutic hypothermia being an essential component of modern clinical practice. Furthermore, the 28-day follow-up period is not equivalent to the complete life cycle, which leaves open the question of the long-term effectiveness of the drug.

CONCLUSIONS

The xenon-oxygen mixture (xenon 50%/oxygen 50%) administration in early neonatal ischemia-hypoxia ensures a pronounced neuroprotective effect in newborn Wistar rats, which is confirmed by significant brain lesion reduction by 25% on day 7 based on MRI data. The xenon-oxygen mixture contributes to acceleration of the central nervous system postnatal functional maturation: the earlier formation of grasping reflexes, improvement of sensorimotor responses, and preservation of auditory startle response have been reported in group Xe. The data obtained confirm the crucial role of early therapy initiation within the therapeutic window and substantiate the need for further exploration of optimal xenon dosing regimens, as well as xenon potential synergism with therapeutic hypothermia for optimization of hypoxic-ischemic encephalopathy treatment in newborns.

References

1. Ranjan AK, Gulati A. Advances in Therapies to Treat Neonatal Hypoxic-Ischemic Encephalopathy. Journal of Clinical Medicine. 2023; 12: 6653.
2. Bruschettini M, Romantsik O, Moreira A, Ley D, Thébaud B. Stem cell-based interventions for the prevention of morbidity and mortality following hypoxic-ischaemic encephalopathy in newborn infants. Cochrane Database Syst Rev. 2020; 8 (8): CD013202.
3. Ionov OV, Balashova EN, Degtyarev DN, Burov AA, Gorev VV, Gorelik KD i dr. Klinicheskie rekomendacii «Gipoksicheskaya ishemicheskaya encefalopatiya novorozhdennogo vsledstvie perenesennoj asfiksii pri rodah». M.: Rossijskoe obshchestvo neonatologov, ASPM. 2025; 72 s. Russian.
4. Modisett AK, Patel RM, Jernigan SM, Figueroa J, Sewell EK, Hamrick SEG. Patterns of acute kidney and hepatic injury and association with adverse outcomes in infants undergoing therapeutic hypothermia for hypoxic ischemic encephalopathy. J. Perinatol. 2022; 42 (1): 1361–7.
5. Yang M, Wang K, Liu B, Shen Y, Liu G. Hypoxic-Ischemic Encephalopathy: Pathogenesis and Promising Therapies. Molecular Neurobiology. 2024; (62): 2105–22.
6. Greco P, Nencini G, Piva I, Scioscia M, Volta C, Spadaro S et al. Pathophysiology of hypoxic–ischemic encephalopathy: a review of the past and a view on the future. Acta Neurologica Belgica. 2020; 120: 277–88.
7. Eldarov ChM, Starodubceva NL, Shevcova YuA, Goryunov KV, Ionov OV, Silachev DN. Ocenka effekta gipotermii posle modelirovannoj ishemicheskoj gipoksicheskoj encefalopatii po metabolomu krovi. Vestnik RGMU. 2024; 6: 144–51. Russian.
8. Acun C, Lavu R, Liu W, Nicoletti N, Ramsey J, Aly H. Therapeutic hypothermia in mild hypoxic ischemic encephalopathy: A clinical dilemma with uncertain long-term outcomes. Early Hum Dev. 2026; 212: 106427.
9. Zadvornov AA, Grigorev EV. Celevoe upravlenie temperaturoĭ u novorozhdennyh pri provedenii obshcheĭ terapevticheskoĭ gipotermii. Anesteziologiya i reanimatologiya. 2022; (3) 55–57. Russian.
10. Butrov AV, Torosyan BD, Cheboksarov DV, Mahmutova GR. Terapevticheskaya gipotermiya pri porazheniyah golovnogo mozga razlichnogo geneza. Vestnik intensivnoj terapii imeni A.I. Saltanova. 2019; 2: 75–81. Russian.
11. Rodríguez M, Valez V, Cimarra C, Blasina F, Radi R. Hypoxic-Ischemic Encephalopathy and Mitochondrial Dysfunction: Facts, Unknowns, and Challenges. Antioxidants Redox Signaling. 2020; 33 (4): 247–62.
12. Abate BB, Bimerew M, Gebremichael B, Mengesha KA, Kassaw M, Gebremeskel T, et al. Effects of therapeutic hypothermia on death among asphyxiated neonates with hypoxic-ischemic encephalopathy: A systematic review and meta-analysis of randomized control trials. PLoS One. 2021; 16 (2); e0247229.
13. Caramelo I, Coelho M, Rosado M, Cardoso CMP, Dinis A, Duarte CB, et al. Biomarkers of hypoxic-ischemic encephalopathy: a systematic review. World J Pediatr. 2023; 19: 505–48.
14. Beda EE, Gabitov MV, Redkin IV, Kryukov IA, Grebenchikov OA. Vliyanie ksenona na soderzhanie GSK-3β, NF-κB i Nrf2 v golovnom mozge krys (eksperimental'noe issledovanie). Obshchaya reanimatologiya. 2025; 21 (3): 26–31. Russian.
15. Antonova VV, Kujdin DV, Gabitov MV, Kryukov IA, Redkin IV, CHerpakov RA i dr. Vliyanie kripton-kislorodnoj smesi na nevrologicheskij status krys posle modelirovaniya otkrytoj CHMT. Patologicheskaya fiziologiya i eksperimental'naya terapiya. 2025; 69 (4): 79–88. Russian.
16. Boeva EA, Grebenchikov OA. Organoprotektivnye svojstv argona (obzor). Obshchaya reanimatologiya. 2022; 18 (5): 44–59. Russian.
17. Maze M, Laitio T. Neuroprotective properties of xenon. Mol Neurobiol. 2020; 57: 118–24.
18. Azzopardi D, Robertson NJ, Bainbridge A, Cady E, Charles-Edwards G, Deierl A. et al. Moderate hypothermia within 6 h of birth plus inhaled xenon versus moderate hypothermia alone after birth asphyxia (TOBY-Xe): a proof-of-concept, open-label, randomised controlled trial. Lancet Neurol. 2016; 15 (2): 145–53.
19. Azzopardi D, Chew AT, Deierl A, Huertas A, Robertson NJ, Tusor N et al. Prospective qualification of early cerebral biomarkers in a randomised trial of treatment with xenon combined with moderate hypothermia after birth asphyxia. EBioMedicine. 2019; 47: 484–91.
20. Vannucci SJ, Back SA. The Vannucci Model of Hypoxic-Ischemic Injury in the Neonatal Rodent: 40 years Later. Dev Neurosci. 2022; 44 (4–5): 186–93.
21. Penny TR, Oorschot DE, Reynolds ML, Waldvogel HJ, Faull RLM, Ozanne SE et al. Optimization of behavioral testing in a long-term rat model of neonatal hypoxic-ischemic brain injury. Dev Neurosci. 2021; 43 (5): 281–94.
22. Kumar AJ, Gomez MS, Santos FP, Almeida RS, Ferreira TB, Carvalho SM et al. Sensorimotor development and neurological reflex assessment in neonatal Wistar rats subjected to anoxia. Dev Psychobiol. 2022; 64 (8): e22291.
23. Schallert T, Fleming S, Leasure J, Tillerson J, Bland S. CNS plasticity and assessment of forelimb sensorimotor outcome in unilateral rat models of stroke, cortical ablation, parkinsonism and spinal cord injury. Neuropharmacology. 2000; 39: 777–87.
24. Silachev DN, Uchevatkin AA, Pirogov YA, Zorov DB, Isaev NK. Comparative Evaluation of Two Methods for Studies of Experimental Focal Ischemia: Magnetic Resonance Tomography and Triphenyltetrazoleum Detection of Brain Injuries. Bull Exp Biol Med. 2009; 147: 269–72.
25. Barros M, Liang M, Iannucci N, Dickinson R. Xenon and Argon as Neuroprotective Treatments for Perinatal Hypoxic-Ischemic Brain Injury: A Preclinical Systematic Review and Meta-Analysis. Anesth Analg. 2025; 141 (2): 327–42.
26. McGuigan S, Marie DJ, O'Bryan LJ, Flores FJ, Evered L, Silbert B et al. The cellular mechanisms associated with the anesthetic and neuroprotective properties of xenon: a systematic review of the preclinical literature. Front Neurosci. 2023; 17: 1225191.
27. Ma D, Hossain M, Chow A, Arshad M, Battson RM, Sanders RD et al. Xenon and hypothermia combine to provide neuroprotection from neonatal asphyxia. Ann Neurol. 2005; 58 (2): 182–93.
28. Campos-Pires R, Onggradito H, Ujvari E, Karimi S, Valeo F, Aldhoun J et al. Xenon treatment after severe traumatic brain injury improves locomotor outcome, reduces acute neuronal loss and enhances early beneficial neuroinflammation: a randomized, blinded, controlled animal study. Crit Care. 2020; 24: 667.

Литература

1. Ranjan AK, Gulati A. Advances in Therapies to Treat Neonatal Hypoxic-Ischemic Encephalopathy. Journal of Clinical Medicine. 2023; 12: 6653.
2. Bruschettini M, Romantsik O, Moreira A, Ley D, Thébaud B. Stem cell-based interventions for the prevention of morbidity and mortality following hypoxic-ischaemic encephalopathy in newborn infants. Cochrane Database Syst Rev. 2020; 8 (8): CD013202.
3. Ионов О. В., Балашова Е. Н., Дегтярев Д. Н., Буров А. А., Горев В. В., Горелик К. Д. и др. Клинические рекомендации «Гипоксическая ишемическая энцефалопатия новорожденного вследствие перенесенной асфиксии при родах». М.: Российское общество неонатологов, АСПМ. 2025; 72 с.
4. Modisett AK, Patel RM, Jernigan SM, Figueroa J, Sewell EK, Hamrick SEG. Patterns of acute kidney and hepatic injury and association with adverse outcomes in infants undergoing therapeutic hypothermia for hypoxic ischemic encephalopathy. J. Perinatol. 2022; 42 (1): 1361–7.
5. Yang M, Wang K, Liu B, Shen Y, Liu G. Hypoxic-Ischemic Encephalopathy: Pathogenesis and Promising Therapies. Molecular Neurobiology. 2024; (62): 2105–22.
6. Greco P, Nencini G, Piva I, Scioscia M, Volta C, Spadaro S et al. Pathophysiology of hypoxic–ischemic encephalopathy: a review

of the past and a view on the future. Acta Neurologica Belgica. 2020; 120: 277–88.
7. Эльдаров Ч. М., Стародубцева Н. Л., Шевцова Ю. А., Горюнов К. В., Ионов О. В., Силачев Д. Н. Оценка эффекта гипотермии после моделированной ишемической гипоксической энцефалопатии по метаболому крови. Вестник РГМУ. 2024; 6: 144–51.
8. Acun C, Lavu R, Liu W, Nicoletti N, Ramsey J, Aly H. Therapeutic hypothermia in mild hypoxic ischemic encephalopathy: A clinical dilemma with uncertain long-term outcomes. Early Hum Dev. 2026; 212: 106427.
9. Задворнов А. А., Григорьев Е. В. Целевое управление температурой у новорожденных при проведении общей терапевтической гипотермии. Анестезиология и реаниматология. 2022; (3) 55–57.
10. Бутров А. В., Торосян Б. Д., Чебоксаров Д. В., Махмутова Г. Р. Терапевтическая гипотермия при поражениях головного мозга различного генеза. Вестник интенсивной терапии имени А.И. Салтанова. 2019; 2: 75–81.
11. Rodríguez M, Valez V, Cimarra C, Blasina F, Radi R. Hypoxic-Ischemic Encephalopathy and Mitochondrial Dysfunction: Facts, Unknowns, and Challenges. Antioxidants Redox Signaling. 2020; 33 (4): 247–62.
12. Abate BB, Bimerew M, Gebremichael B, Mengesha KA, Kassaw M, Gebremeskel T, et al. Effects of therapeutic hypothermia on death among asphyxiated neonates with hypoxic-ischemic encephalopathy: A systematic review and meta-analysis of randomized control trials. PLoS One. 2021; 16 (2); e0247229.
13. Caramelo I, Coelho M, Rosado M, Cardoso CMP, Dinis A, Duarte CB, et al. Biomarkers of hypoxic-ischemic encephalopathy: a systematic review. World J Pediatr. 2023; 19: 505–48.
14. Беда Е. Е., Габитов М. В., Редкин И. В., Крюков И. А., Гребенчиков О. А. Влияние ксенона на содержание ГСК-3β, NF-κB и Nrf2 в головном мозге крыс (экспериментальное исследование). Общая реаниматология. 2025; 21 (3): 26–31.
15. Антонова В. В., Куйдин Д. В., Габитов М. В., Крюков И. А., Редкин И. В., Черпаков Р. А. и др. Влияние криптон-кислородной смеси на неврологический статус крыс после моделирования открытой ЧМТ. Патологическая физиология и экспериментальная терапия. 2025; 69 (4): 79–88.
16. Боева Е. А., Гребенчиков О. А. Органопротективные свойств аргона (обзор). Общая реаниматология. 2022; 18 (5): 44–59.
17. Maze M, Laitio T. Neuroprotective properties of xenon. Mol Neurobiol. 2020; 57: 118–24.
18. Azzopardi D, Robertson NJ, Bainbridge A, Cady E, Charles-Edwards G, Deierl A. et al. Moderate hypothermia within 6 h of birth plus inhaled xenon versus moderate hypothermia alone after birth asphyxia (TOBY-Xe): a proof-of-concept, open-label, randomised controlled trial. Lancet Neurol. 2016; 15 (2): 145–53.
19. Azzopardi D, Chew AT, Deierl A, Huertas A, Robertson NJ, Tusor N et al. Prospective qualification of early cerebral biomarkers in a randomised trial of treatment with xenon combined with moderate hypothermia after birth asphyxia. EBioMedicine. 2019; 47: 484–91.
20. Vannucci SJ, Back SA. The Vannucci Model of Hypoxic-Ischemic Injury in the Neonatal Rodent: 40 years Later. Dev Neurosci. 2022; 44 (4–5): 186–93.
21. Penny TR, Oorschot DE, Reynolds ML, Waldvogel HJ, Faull RLM, Ozanne SE et al. Optimization of behavioral testing in a long-term rat model of neonatal hypoxic-ischemic brain injury. Dev Neurosci. 2021; 43 (5): 281–94.
22. Kumar AJ, Gomez MS, Santos FP, Almeida RS, Ferreira TB, Carvalho SM et al. Sensorimotor development and neurological reflex assessment in neonatal Wistar rats subjected to anoxia. Dev Psychobiol. 2022; 64 (8): e22291.
23. Schallert T, Fleming S, Leasure J, Tillerson J, Bland S. CNS plasticity and assessment of forelimb sensorimotor outcome in unilateral rat models of stroke, cortical ablation, parkinsonism and spinal cord injury. Neuropharmacology. 2000; 39: 777–87.
24. Silachev DN, Uchevatkin AA, Pirogov YA, Zorov DB, Isaev NK. Comparative Evaluation of Two Methods for Studies of Experimental Focal Ischemia: Magnetic Resonance Tomography and Triphenyltetrazoleum Detection of Brain Injuries. Bull Exp Biol Med. 2009; 147: 269–72.
25. Barros M, Liang M, Iannucci N, Dickinson R. Xenon and Argon as Neuroprotective Treatments for Perinatal Hypoxic-Ischemic Brain Injury: A Preclinical Systematic Review and Meta-Analysis. Anesth Analg. 2025; 141 (2): 327–42.
26. McGuigan S, Marie DJ, O'Bryan LJ, Flores FJ, Evered L, Silbert B et al. The cellular mechanisms associated with the anesthetic and neuroprotective properties of xenon: a systematic review of the preclinical literature. Front Neurosci. 2023; 17: 1225191.
27. Ma D, Hossain M, Chow A, Arshad M, Battson RM, Sanders RD et al. Xenon and hypothermia combine to provide neuroprotection from neonatal asphyxia. Ann Neurol. 2005; 58 (2): 182–93.
28. Campos-Pires R, Onggradito H, Ujvari E, Karimi S, Valeo F, Aldhoun J et al. Xenon treatment after severe traumatic brain injury improves locomotor outcome, reduces acute neuronal loss and enhances early beneficial neuroinflammation: a randomized, blinded, controlled animal study. Crit Care. 2020; 24: 667.

BIOMECHANICAL EVALUATION OF MANDIBULAR SPLINTING METHOD FOR FRACTURES WITHIN THE DENTAL ARCH

Darawsheh HM[1], Mellin RV[2], Akulinichev EA[1], Moiseev DA[3]✉, Snezhko OV[4], Kopetskiy IS[3], Vasiliev YuL[1]

[1] Sechenov First Moscow State Medical University (Sechenov University), Moscow, Russia

[2] Lobachevsky State University of Nizhny Novgorod, Nizhny Novgorod, Russia

[3] Pirogov Russian National Research Medical University (Pirogov University), Moscow, Russia

[4] Novosibirsk State Medical University, Novosibirsk, Russia

Treatment of mandibular fractures remains a pressing issue in maxillofacial surgery. This paper presents a novel single-jaw splinting technique (RF patent No. 2735258) for the immobilization of bone fragments in fractures located within the dental arch. Mathematical modeling using the finite element method (FEM), based on computed tomography data from one volunteer, was performed to assess its biomechanical efficiency. A 3D model of the mandible with the fixation construct and an indenter (simulating occlusal load up to 50 N) was constructed. The modeling results showed that the relative movement between the fragments was approximately 25 μm, which is comparable with literature data for two-titanium-plate osteosynthesis. The maximum equivalent stress values in the metal splint reached 100 MPa, and in the splint these reached 3 MPa. The developed method ensures stable fixation without involvement of the maxilla. The analysis involved only a single model and no experimental validation; therefore, confirmation in further research is required. Nevertheless, the obtained data suggest that the method is promising as an alternative to existing immobilization techniques.

Keywords: mandibular fracture, bone fragment immobilization, finite element method, single-jaw splinting, biomechanics

Author contribution: Darawsheh HM, Mellin RV, Akulinichev EA — research procedure; Darawsheh HM, Mellin RV — data analysis; Darawsheh HM, Mellin RV, Akulinichev EA, Moiseev DA, Snezhko OV — manuscript writing; Kopetskiy IS, Vasiliev YuL, Moiseev DA — manuscript editing.

Compliance with ethical standards: the study was approved by the ethics committee of the Sechenov First Moscow State Medical University (protocol No. 16–24 dated 20 June 2024).

✉ **Correspondence should be addressed:** Denis A. Moiseev
Ostrovityanova 1, str. 9, Moscow, 117997, Russia; moiseev_da@rsmu.ru

Received: 03.03.2026 **Accepted:** 13.04.2026 **Published online:** 23.04.2026

DOI: 10.24075/brsmu.2026.015

БИОМЕХАНИЧЕСКАЯ ОЦЕНКА МЕТОДА ШИНИРОВАНИЯ НИЖНЕЙ ЧЕЛЮСТИ ПРИ ПЕРЕЛОМАХ В ПРЕДЕЛАХ ЗУБНОГО РЯДА

Х. М. Дарауше[1], Р. В. Меллин[2], Е. А. Акулиничев[1], Д. А. Моисеев[3] ✉, О. В. Снежко[4], И. С. Копецкий[3], Ю. Л. Васильев[1]

[1] Первый московский государственный медицинский университет имени И. М. Сеченова (Сеченовский Университет), Москва, Россия

[2] Национальный исследовательский Нижегородский государственный университет имени Н. И. Лобачевского, Нижний Новгород, Россия

[3] Российский национальный исследовательский медицинский университет имени Н. И. Пирогова (Пироговский Университет), Москва, Россия

[4] Новосибирский государственный медицинский университет, Новосибирск, Россия

Лечение переломов нижней челюсти остается актуальной проблемой челюстно-лицевой хирургии. В исследовании представлен новый метод одночелюстного шинирования (патент РФ №2735258) для иммобилизации отломков при переломах в пределах зубного ряда. Для оценки его биомеханической эффективности использовали математическое моделирование методом конечных элементов (МКЭ) на основе компьютерной томографии одного добровольца. Построена трехмерная модель нижней челюсти с фиксирующей конструкцией и импактором, имитирующим жевательную нагрузку до 50 Н. Результаты моделирования показали, что относительное смещение между отломками составляет около 25 мкм, что сопоставимо с данными литературы по остеосинтезу двумя титановыми пластинами. Максимальные эквивалентные напряжения в металлической шине достигают 100 МПа, в каппе — до 3 МПа. Разработанный метод обеспечивает стабильную фиксацию без вовлечения верхней челюсти. Анализ выполнен на единственной модели без экспериментальной валидации, что требует подтверждения в дальнейших работах. Тем не менее, полученные данные свидетельствуют о перспективности метода как альтернативы существующим способам иммобилизации.

Ключевые слова: перелом нижней челюсти, иммобилизация отломков, метод конечных элементов, одночелюстное шинирование, биомеханика

Вклад авторов: Х. М. Дарауше, Р. В. Меллин, Е. А. Акулиничев — проведение исследования; Х. М. Дарауше, Р. В. Меллин — анализ данных; Х. М. Дарауше, Р. В. Меллин, Е. А. Акулиничев, Д. А. Моисеев, О. В. Снежко — написание статьи; И. С. Копецкий, Ю. Л. Васильев, Д. А. Моисеев — редактирование статьи.

Соблюдение этических стандартов: исследование одобрено локальным этическим комитетом ФГАОУ ВО Первый МГМУ им. И. М. Сеченова Минздрава России (протокол № 16-24 от 20 июня 2024 г.).

✉ **Для корреспонденции:** Денис Александрович Моисеев
ул. Островитянова, д. 1, с. 9, г. Москва, 117997, Россия; moiseev_da@rsmu.ru

Статья получена: 03.03.2026 **Статья принята к печати:** 13.04.2026 **Опубликована онлайн:** 23.04.2026

DOI: 10.24075/vrgmu.2026.015

Mandibular fractures hold a significant position in maxillofacial surgery worldwide and represent one of the most prevalent types of jaw injuries [1]. Treatment of mandibular fractures should be aimed at preserving the integrity of the anatomical structures and stabilizing bone fragments in a fixed position until healing, while restoring the correct occlusal relationship and maintaining the proportions of the lower third of the face.

In recent years, surgical intervention using bone fixation with various types of bone plates has become widely adopted. However, there is debate regarding their rigidity and stability, as well as depending on the clinical case: the location of the fracture (within or outside the dental arch), displaced mandibular fractures depending on the severity of the injury, and the increase in the cost of medical services provided [2, 3].

An important condition for the provision of qualified medical care is the physician's level of training and valid manual skills, which allow correct screw positioning, a competent approach to plate selection considering tissue resources and the type of injury, and consideration of the clinical and anatomical features of the mandibular structures, including abnormalities. In the absence of these factors, dangerous precedents of deficiencies in the provision of medical care or harm are created, which, under local legislation, may be considered a criminally punishable act.

Conservative treatment methods for fractures using intermaxillary fixation with dental splints and elastic tension are also accepted. Along with a large number of advantages, these methods have a number of disadvantages, the most significant of which are a marked decrease in oral hygiene and the patient's quality of life during the period of bite fixation [4, 5].

It should be noted that splinting remains a compromise method for treating mandibular fractures in areas with low population density or complex geographic landscape. Moreover, an important role in the care provision protocol is played by factors such as the clinic's material and technical resources, the professional skills of healthcare staff, etc.

In terms of prevalence, mandibular fractures account for 57–82% of all facial bone fractures [6]. According to a large epidemiological study by Morris et al. (2015), fractures of the mandibular body are the most common (16.8%) [7]. Similar patterns have been reported for the Russian population: according to Shashkov et al. (2021) [8], fractures of the mandibular body were distributed as follows: in the incisor area — 3.9%, in the canine and premolar area — 15.9%, and in the molar area — 15.3%. Such fractures significantly decrease patients' quality of life, including influencing their socialization and eating habits, the alteration of which may worsen the comprehensive rehabilitation process. We should also note the deterioration of dental health resulting from treatment with splints of previous generations: according to the literature, there is an increase in the rate of carious lesions of hard dental tissues and inflammatory diseases of periodontal tissues, which is associated with difficulties in hygiene when using classic dental splints [9, 10].

In this regard, the development of new methods for fragment immobilization in mandibular fractures remains an urgent problem and requires further solution; therefore, we have developed a novel single-jaw splinting technique for mandibular fractures (RF invention patent No. 2735258 dated 29.10.20).

For null hypothesis testing, the use of mathematical modeling by the finite element method, widely used in physical and mathematical modeling, would be a rational solution. Such an approach is an important experimental instrument that makes it possible to assess the efficacy of the planned treatment method. The main purpose of finite element analysis in medicine, as in other fields, is to analyze the effects of force on a given structure, evaluate the stability and resistance of the structure to pressure, force, and other external influences [11]. Today, this method allows us to effectively assess biomechanical stability, calculate the stress between bone fragments of the facial skull, and their fixation strength in the context of specific mandibular injuries [12, 13]. The data obtained that confirm the null hypothesis can be transferred into clinical practice without fear of adverse effects on biological tissues, thereby increasing the quality of skilled care provision in the field of maxillofacial surgery.

This study aimed to perform a finite element analysis of the efficacy of a novel mandibular fracture fixation method.

METHODS

Data

Computer modeling and the finite element method (FEM) were used to simulate the stress-strain state (SSS) of two configurations of the fractured mandible: with the proposed fixation construct and with the conventional treatment approach using osteosynthesis, the results of which were reported in a previous study [14]. The jaw and teeth were segmented on multiplanar reconstruction from dental CBCT data (KaVo ORTHOPANTOMOGRAPH OP300 Maxio cone beam computed tomography scanner, 312 slices, pixel size 250 μm) of a volunteer (male, born in 1989) with no pathological changes detected in the mandibular region, using a trial version of the software (Inobitec PRO 2.10, Voronezh, Russia) (Fig. 1A).

Routine segmentation in three projections was performed for each anatomical structure. The contours obtained were used to generate a voxel model, which was then converted into an STL model (Fig. 1B).

NURBS modeling

Reverse engineering of the STL models was performed in SolidWorks (Dassault Systèmes SE, Vélizy-Villacoublay, France). The ScanTo3D utility was used to generate NURBS models (NURBS — Non-uniform rational B-spline) of the mandible and teeth (Fig. 2A). In the STL model of the dental arch, each tooth was segmented and converted into a NURBS model (Fig. 2B). Using the basic tools of SolidWorks, a linear fracture region with a gap of 0.1 mm, corresponding to a simple uncomplicated fracture, was modeled between teeth 44 and 45, along with a pair of temporomandibular joints, a fixation construct, and an indenter mimicking food (Fig. 2).

Pre-processing of the NURBS model for finite element analysis was performed in HyperMesh (Altair Engineering Inc., Troy, Michigan, USA). A tetrahedral mesh was generated for each anatomical structure (two mandibular segments, 15 teeth, two temporomandibular joints), the indenter, and the fixation construct. Mesh quality was controlled using the Jacobian (threshold ≥ 0.1) and Tet collapse (threshold ≤ 0.1) metrics. At least 98% of the elements met these criteria; elements that failed the test were rebuilt manually. The final mesh contained 800,604 elements (Fig. 3) [15]. The resulting finite element models were imported as orphan meshes into Abaqus CAE (Simulia, Johnston, Rhode Island, USA) to assign mechanical properties to materials and to set boundary conditions for biomechanical analysis of the model [16].

Assumptions and mathematical formulation of the problem

From a mathematical point of view, a static problem in elasticity theory was solved in each of the locally homogeneous

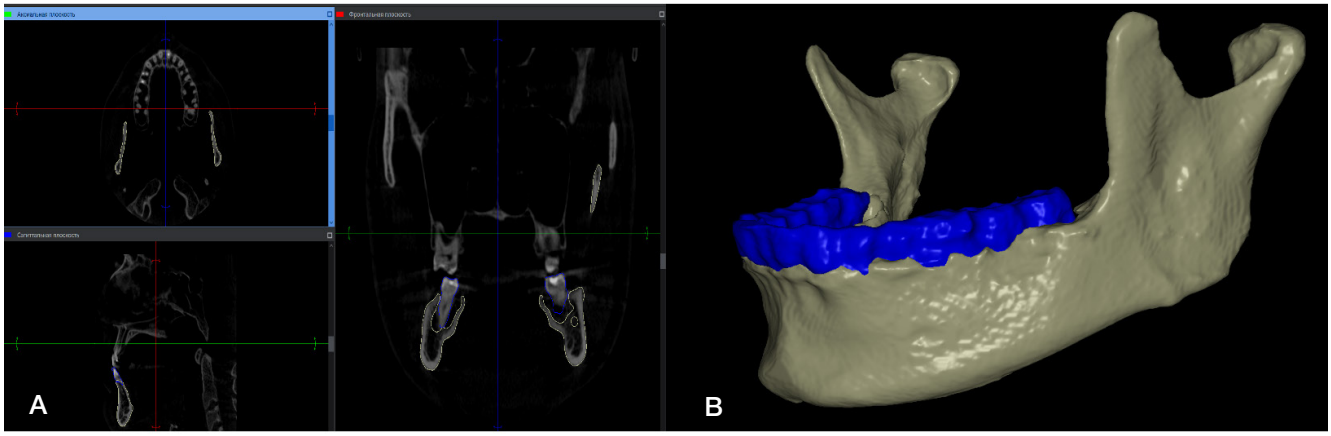

Fig. 1. A. Interface of the Inobitec PRO software for segmentation of medical images: multiplanar reconstruction with highlighted contours of the zone of interest. **B**. Segmentation result in the form of voxel 3D model of the mandible and dental arch

subregions of the heterogeneous functional element of the model, considering the effect of a moment of force to simulate the indentation of the fixed jaw segments into the elastic indenter. To connect the jaw segments and teeth, the joints and condylar processes, the mouthguard and the wire, multiple contact without relative movement was employed, which constitutes a critical assumption within the model. Contacts between the jaw segments, teeth and mouthguard, and between the mouthguard and the indenter were set as tangential with a friction coefficient of 0.1 and normal "hard contact" behavior. The upper surface of the fixator and the temporomandibular joints were rigidly fixed (no degrees of freedom for any node on the surface). The masseteric tuberosity regions (Fig. 4, highlighted in pink) were kinematically connected at the mental protuberance (Fig. 4, RP-3), to which a moment of force was applied, linearly increasing to 500 N·mm (0.5 N·m). An isotropic linear elastic material model was used for all materials [17, 18]. The mechanical characteristics taken from the literature are provided in the Table.

In this study, a deterministic finite element analysis was performed; no statistical processing was applied, because the analysis was based on a single model.

RESULTS

The finite element method was used to obtain the stress-strain state (SSS) of the mandibular segments with a fracture and a fixation construct. It was found that the relative displacement in the proposed configuration increases linearly with a linearly increasing load. Under a load of 50 N, a relative displacement of 25 μm was achieved between the fragments. The results were compared with those of the two-plate fragment immobilization method in two different configurations [14] (Fig. 5). Outliers on the graph are associated with an increase in the solver increment. The contact pressure between the fragments is shown in Fig. 6A and reaches 2 MPa. In the deformed configuration, the relative displacement is marked with a dotted line.

The maximum stress in the entire configuration is concentrated on the metal splint (Fig. 6B) and reaches 100 MPa. In turn, the maximum stress on the mouthguard is distributed over the fracture area (Fig. 6B), reaching a value of 3 MPa.

The finite element analysis has shown that the proposed fixation method demonstrates satisfactory displacement between the fragments of about 25 μm with a linear increase in the indenter load (mimicking food) to 50 N. The relative displacement achieved with the proposed method is comparable to the displacement obtained from the finite element calculation for the fixation construct with two titanium plates.

DISCUSSION

The present study has a number of limitations. First, the finite element analysis was performed based on CT data from a single volunteer whose clinical and anatomical characteristics met the indications for the use of the developed splinting device, which does not allow for consideration of anatomical variability.

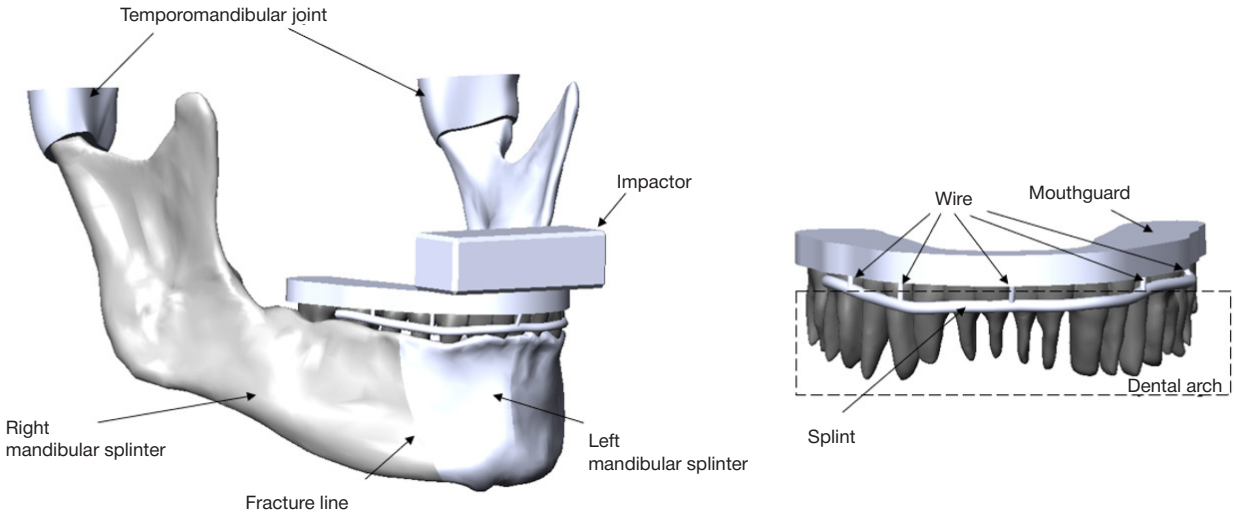

Fig. 2. NURBS model of the mandible with the fixing construct and impactor

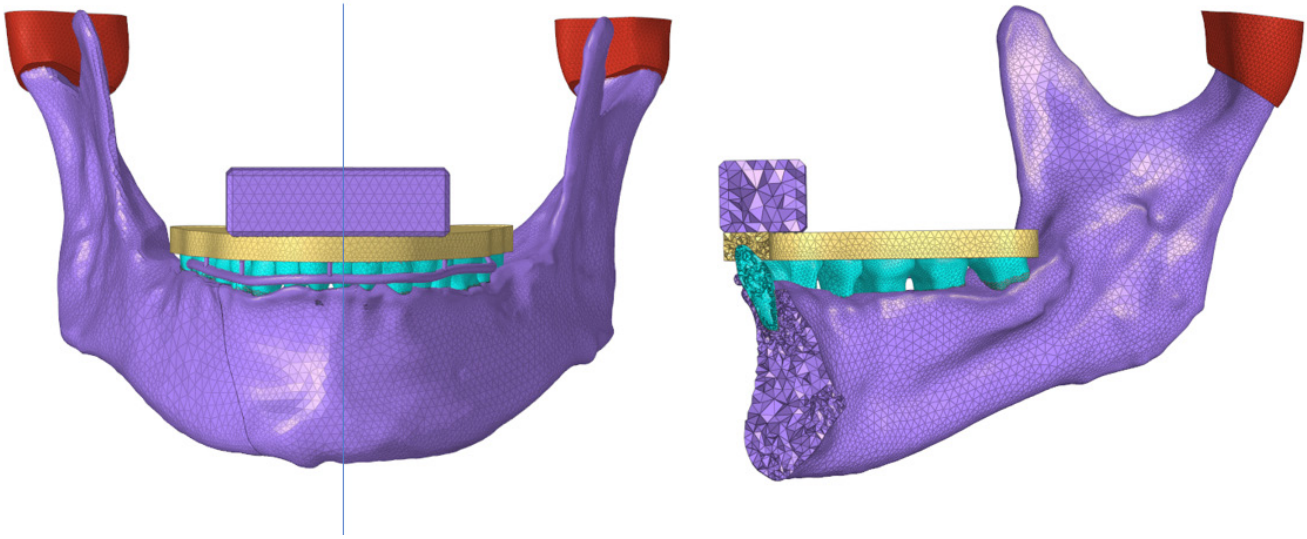

Fig. 3. Finite element model of the estimated area: left — frontal view, right — cutaway model (midsagittal plane)

Second, the model was not validated in a field experiment, either on synthetic jaw models or on biological material. Third, the efficacy of the developed splint was compared with literature data on condylar process fixation using two plates [14], which is not a direct analogue due to the lack of valid literature data on similar constructs. Further research involving an expanded sample of virtual models and experimental verification is required to obtain more reliable data.

As previously stated in the modeling methods, multiple contact without relative movement was used for dentoalveolar structures, which is justified by the strategy of uniform load redistribution over the entire surface of the splinting construct and between the fragments.

Rigid tooth–splint contact (μ = 0.1, slip-free) reflects the clinical stability of dental splinting with multiple supports (4–6 teeth) in adult patients, ensuring uniform load redistribution without relative movement of the fragments [25]. Microdisplacement (< 0.1 mm) does not exceed the physiological mobility of the periodontium and does not affect fracture consolidation.

All mandibular fracture treatment methods are aimed at fixing bone fragments until they fuse and the masticatory load provided by several muscle groups is restored. Due to the complex anatomy of the mandible, which is determined by its functions, the application of forces to the fracture line or to the selected fixation system (plates) may inadequately affect the restoration of physiological load. Indeed, there is ongoing debate in the literature regarding the selection of the most appropriate fixation system for each specific case. Some surgeons prefer to use mini-plates and screws, while others prefer titanium plates to stabilize fractures, believing that such a system ensures sufficient rigidity and minimizes resistance to physiological load. Furthermore, two-jaw dental splints can be used for stabilization and fixation of the fracture during healing. These splints have a specific design that helps maintain the correct position of the jaw and prevents unwanted movement or displacement of the fracture. Experimental data obtained by Claes et al. [26] using a sheep model of metatarsal osteotomy with an adjustable gap size and interfragmentary movement show that with a gap of 1–2 mm and interfragmentary movement of up to 0.5 mm (500 μm), successful fusion with high mechanical stability (bending rigidity > 20 Nm/mm) is achieved. The authors note that it is not the quantity but the quality of the forming bone callus that determines the healing outcome. In our study, the interfragmentary displacement was only 25 μm, which is an order of magnitude lower than the values at which stable fusion was observed in that study. Thus, the results obtained can be extrapolated to our data, as they indicate sufficient stability of the developed splinting construct, ensuring fracture consolidation.

According to the generalized results of experimental studies and clinical trials, when the gap between bone fragments is no more than 3 mm, the interfragmentary displacement range optimal for stimulation of bone fusion is 0.15–0.4 mm, and the threshold exceeded by more than 1.0 mm is associated with the risk of fusion failure [26–29]. In our study, the displacement of splinters relative to each other under the load of 50 N was as small as 0.025 mm (25 μm), which was almost an order of magnitude below the optimal range lower limit.

Given the results, the fixation system for the mandibular bone splinters should be selected based on the clinical anatomy, fracture type, patient's condition, and the aim of surgery. It is important for the surgeon to select the most appropriate fixation system, which would ensure the splinters' stability without altering the physiological load on the jaw, based on his/her experience and knowledge.

In the study, we used the one-jaw splinting method for mandibular fractures we had developed, designed for fixation of

Table. Mechanical characteristics of the anatomical structures being parts of the segment asessed

Anatomical sructure	Young's modulus E (MPa)	Poisson's ratio	Element type	Reference
Bone	15 000	0.3	C3-D4	[19, 20]
Teeth	18 600	0.31	C3-D4	[21]
Temporomandibular joints	10.4	0.4	C3-D4	[22]
Impactor	0.1	0.45	C3-D4	
Mouth guard (Ftorax)	1860	0.3	C3-D4	[23]
Wire (aluminum)	71 000	0.33	C3-D4	[24]

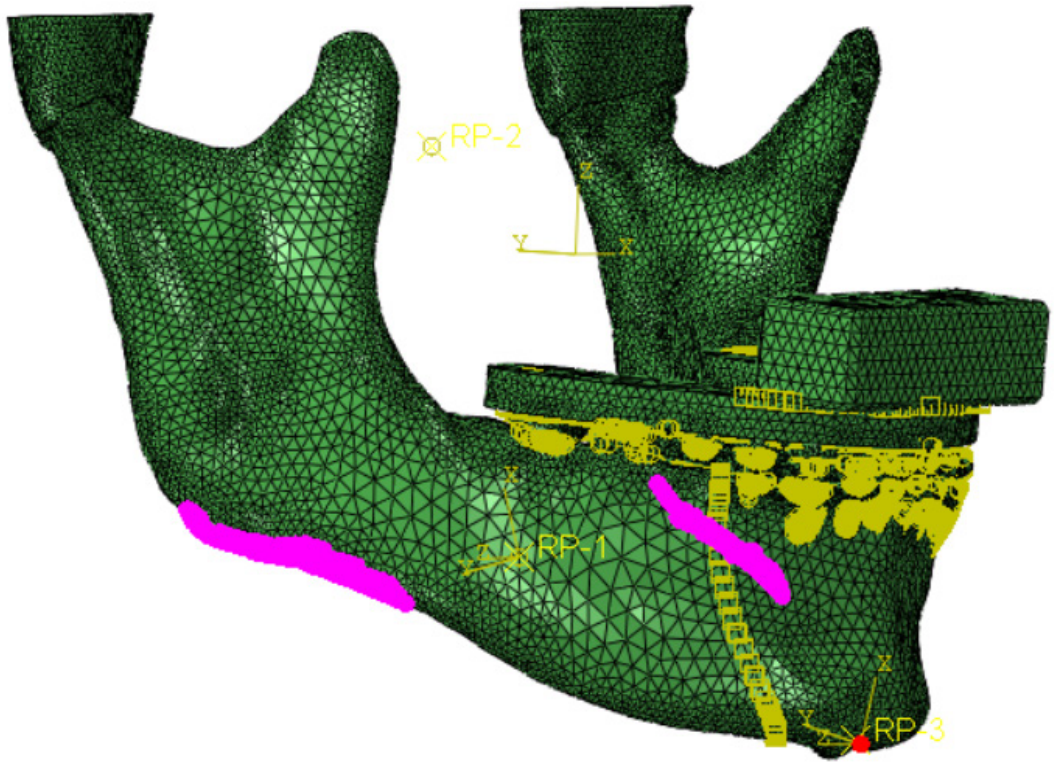

Fig. 4. Determination of contact interactions in the Abaqus CAE 6.14 software

fractures within the dental arch, which seems to be an optimal solution for the distant regions and FAS, where high-tech medical care is not always available in the required quantities and with the necessary urgency.

The limits of force applied to various parts of the mandible have been reported. Thus, in the symphysis zone the value was 82 MPa with the mouth closed and 117 MPa with the mouth open, which allows one to predict the position of the jaws clenched more beneficial in terms of the fracture prognosis [30]. The angle, at which force is applied, is of great importance. According to some data, the condylar process (in case of direct injury to the body) or angle of the jaw is a common area of fracture [31].

In the literature, papers can be found focusing on non-removable treatment techniques, in which, among other findings, conclusions are drawn about the advantages of splinting constructs for the rehabilitation of patients with maxillofacial injuries [32–34]. Nevertheless, despite good planning, detailed analysis of force loads, and fracture prediction, there is very little information in the literature on the finite element analysis of removable appliances. Our study showed that the proposed fixation method demonstrates satisfactory fragment displacement of about 25 μm with a linear increase in indenter load to 50 N, which is comparable to the displacement obtained from the finite element calculation for a fixation construct with two titanium plates.

Summarizing and generalizing the data, we can state that the developed splinting construct is physiological and comparable in its characteristics to non-removable devices. The findings of Graillon et al. [35], who concluded that mini-plates have a traumatic effect, altering mandibular biomechanics and even leading to more complex fractures, support the method we propose. The developed method may be considered a promising alternative to existing immobilization techniques, provided it is further clinically evaluated.

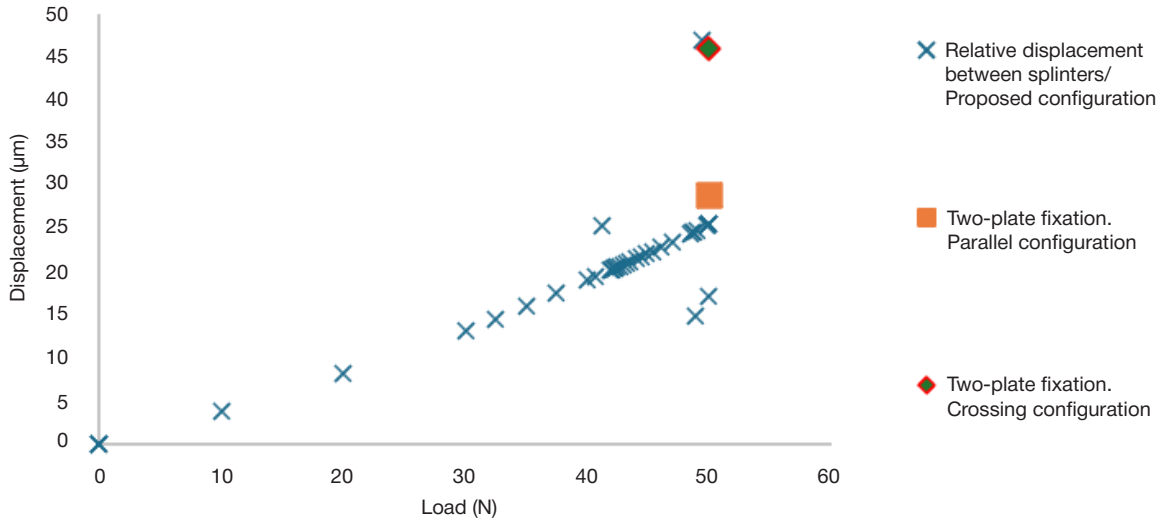

Fig. 5. Relative displacement between splinters as a function of the load applied to the mandibular segment

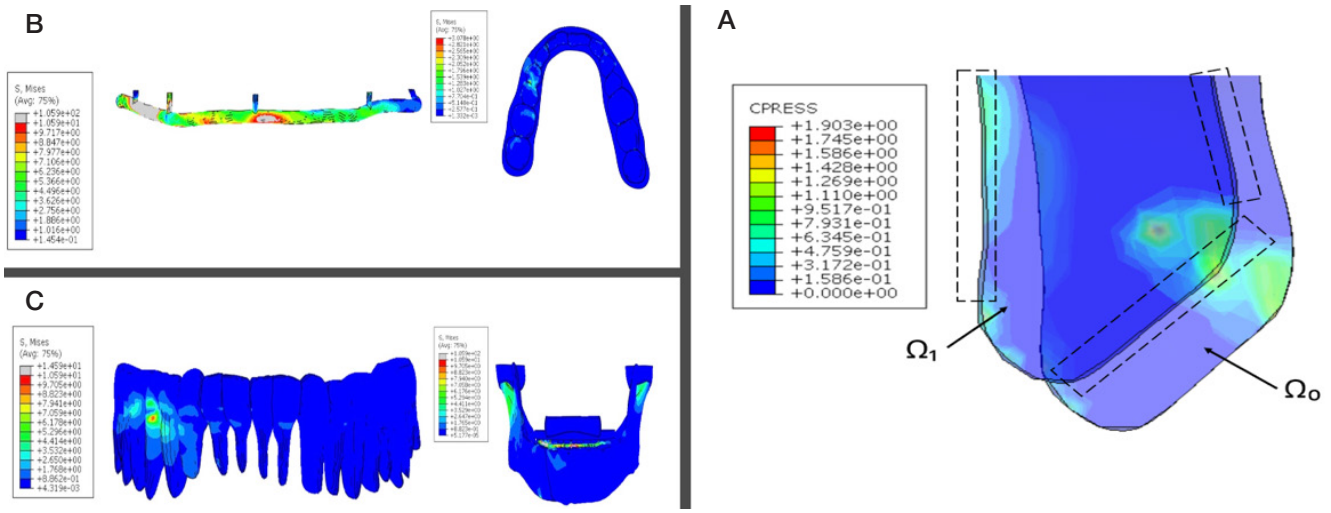

Fig. 6. A. Diagram of the contact pressure distribution in the fracture area. Ω_0 — unloaded configuration, Ω_1 — loaded configuration, areas of displacement between splinters are highlighted with the dotted line. **B**. Diagrams of the stress distribution across splinters of the mandible fixed using the construct proposed. **C**. Diagrams of the stress distribution across splinters of the mandible fixed using the construct proposed, and across the teeth

CONCLUSIONS

This paper presents a finite element analysis of the efficacy of a novel single-jaw splinting method for mandibular fractures within the dental arch. The developed splinting construct ensures a relative displacement of the bone fragments of about 25 μm with a linear increase in masticatory load to 50 N, which is comparable to fixation with two titanium plates and is far below the threshold critical for fracture consolidation (150–400 μm). This provides reliable apposition of the mandibular fragments without involving the maxilla in immobilization. The maximum equivalent stress values in the metal splint are 100 MPa, and in the mouthguard these reach 3 MPa, which does not exceed the tensile strength of the materials used. Immobilization is achieved without maxillary involvement, thereby improving oral hygiene and the patient's quality of life during treatment. The proposed method may represent an effective and safe alternative to conventional osteosynthesis, especially in settings with limited access to high-tech surgery and in patients with contraindications to open reduction. However, validation of the results is necessary in field experiments using synthetic and biological models, as well as in clinical trials with an expanded sample, to confirm long-term stability and optimize the construct.

References

1. Hesham A, Geiger J, Alshamrani Y, Sawatari Y. Can the Mechanism of Injury Impact the Location of a Mandibular Fracture? A Systematic Review. J Maxillofac Oral Surg. 2024; 23 (2): 363–70. DOI: 10.1007/s12663-022-01750-1. Epub 2022 Jul 31. PMID: 38601229; PMCID: PMC11001800.
2. Savelev AL, Samutkina MG. Sovremennyj podhod k lecheniyu pacientov s perelomami nizhnej chelyusti. Operativnaya hirurgiya i klinicheskaya anatomiya (Pirogovskij nauchnyj zhurnal). 2021; 5 (1): 29–34. Dostupno po ssylke: https://doi.org/10.17116/operhirurg2021501129. Russian.
3. Vitkos EN, Papadopoulos KA, Dimasis P, Weissinger C, Kyrgidis A. One miniplate versus two miniplates in the fixation of mandibular angle fractures. An updated systematic review and meta-analysis. J Stomatol Oral Maxillofac Surg. 2022; 123 (6): e865–e873. DOI: 10.1016/j.jormas.2022.07.008. Epub 2022 Jul 21. PMID: 35872351.
4. Tsolov R, Firkova EI. Periodontal status in patients with mandibular fractures. J of IMAB. 2022; 28 (1): 4247–50. DOI: https://doi.org/10.5272/jimab.2022281.4247.
5. Jain A, Rai A. Is the Use of Intermaxillary Fixation Screws an Alternative to Erich Arch Bars for Maxillomandibular Fixation During Management of Maxillofacial Fractures? A Systematic Review and Meta-Analysis. Craniomaxillofac Trauma Reconstr. 2021; 14 (3): 236–45. Available from: https://doi.org/10.1177/1943387520971410.
6. Nasser M, Pandis N, Fleming PS, Fedorowicz Z, Ellis E, Ali K. Interventions for the management of mandibular fractures. Cochrane Database Syst Rev. 2013; 2013 (7): CD006087. Available from: https://doi.org/10.1002/14651858.CD006087.pub3.
7. Morris C, Bebeau NP, Brockhoff H, Tandon R, Tiwana P. Mandibular fractures: an analysis of the epidemiology and patterns of injury in 4,143 fractures. J Oral Maxillofac Surg. 2015; 73 (5): 951.e1–951.e12. DOI: 10.1016/j.joms.2015.01.001. Epub 2015 Jan 13. PMID: 25883009.
8. SHashkov VA, Gajvoronskij IV, Gajvoronskaya MG, Iordanishvili AK, Rodionov AA, Nichiporuk GI. Rasprostranennost' razlichnyh vidov perelomov nizhnej chelyusti u vzroslyh. Vyatskij medicinskij vestnik. 2021; 1 (69): 41–47. DOI: 10.24411/2220-7880-2021-10149. Russian.
9. Akkina SR, Bevans SE, Johnson AW. Techniques for maxillomandibular fixation: old and new. Curr Opin Otolaryngol Head Neck Surg. 2025; 33 (4): 216–21. Available from: https://doi.org/10.1097/MOO.0000000000001043.
10. Johnson AW, Akkina SR, Bevans SE. Maxillomandibular Fixation: Understanding the Risks and Benefits of Contemporary Techniques in Adults. Facial Plastic Surgery & Aesthetic Medicine. 2025; 27 (1): 98–105. DOI: 10.1089/fpsam.2024.0113.
11. Pigolkin YuI, Kislov MA, Krupin KN. Matematicheskoe modelirovanie s pomoshch'yu konechno-elementnogo analiza v sudebno-medicinskoj ekspertize. Sudebno-medicinskaya ekspertiza. 2023; 66 (1): 9–13. Dostupno po ssylke: https://doi.org/10.17116/sudmed2023660119. Russian.
12. Xu X, Cheng Kj, Liu Yf, et al. Experimental validation of finite element simulation of a new custom-designed fixation plate to treat mandibular angle fracture. BioMed Eng OnLine. 2021; 20 (15). Available from: https://doi.org/10.1186/s12938-021-00851-1.
13. Daqiq O, Roossien CC, Wubs FW, van Minnen B. Biomechanical assessment of mandibular fracture fixation using finite element analysis validated by polymeric mandible mechanical testing. Sci Rep. 2024; 14 (1): 11795. Available from: https://doi.org/10.1038/s41598-024-62011-4.

14. Aquilina P, Chamoli U, Parr WC, Clausen PD, Wroe S. Finite element analysis of three patterns of internal fixation of fractures of the mandibular condyle. Br J Oral Maxillofac Surg. 2013; 51 (4): 326–31. Available from: https://doi.org/10.1016/j.bjoms.2012.08.007.
15. Mańkowski J, Piękoś J, Dominiak K, Klukowski P, Fotek M, Zawisza M, Żach P. A Mandible with the Temporomandibular Joint-A New FEM Model Dedicated to Strength and Fatigue Calculations of Bonding Elements Used in Fracture and Defect Surgery. Materials (Basel). 2021; 14 (17): 5031. DOI: 10.3390/ma14175031. PMID: 34501120; PMCID: PMC8434464.
16. Darawsheh HM, Safronova AA, Vasilev YL, Makarova NI, Diachkova EY, Saleeva GT, et al. Choosing the optimal mandible position for inferior alveolar nerve block (IANB) using finite element analysis. Ann Anat. 2023; 247: 152055. DOI: 10.1016/j.aanat.2023.152055. Epub 2023 Jan 22. PMID: 36696926.
17. Panagiotopoulou O, Iriarte-Diaz J, Wilshin S, Dechow PC, Taylor AB, Mehari Abraha H, et al. In vivo bone strain and finite element modeling of a rhesus macaque mandible during mastication. Zoology (Jena). 2017; 124: 13–29. DOI: 10.1016/j.zool.2017.08.010. Epub 2017 Sep 1. PMID: 29037463; PMCID: PMC5792078.
18. Tomioka Takahiro, Ito Daisuke, Murai Takato, Takeda Arisa, Nakamura Mami , Koshinuma Shinya, et al. Analysis of Mechanisms of Mandible Fractures by Lateral Impact: A Biomechanical Approach Using Finite Element Models. Applied Sciences. 2025; 15: 1205. Available from: https://doi.org/10.3390/app15031205.
19. Pinheiro M, Willaert R, Khan A, Krairi A, Van Paepegem W. Biomechanical evaluation of the human mandible after temporomandibular joint replacement under different biting conditions. Sci Rep. 2021; 11 (1): 14034. Available from: https://doi.org/10.1038/s41598-021-93564-3.
20. Hedeşiu M, Pavel DG, Almăşan O, Pavel SG, Hedeşiu H, Rafiroiu D. Three-Dimensional Finite Element Analysis on Mandibular Biomechanics Simulation under Normal and Traumatic Conditions. Oral. 2022; 2, 221–237. Available from: https://doi.org/10.3390/oral2030021.
21. Sarrafpour B, Swain M, Li Q, Zoellner H. Tooth eruption results from bone remodelling driven by bite forces sensed by soft tissue dental follicles: a finite element analysis. PLoS One. 2013; 8 (3): e58803. Available from: https://doi.org/10.1371/journal.pone.0058803
22. Mengoni M. Biomechanical modelling of the facet joints: a review of methods and validation processes in finite element analysis. Biomech Model Mechanobiol. 2021; 20 (2): 389–401. DOI: 10.1007/s10237-020-01403-7. Epub 2020 Nov 22. PMID: 33221991; PMCID: PMC7979651.
23. Raszewski Z, Nowakowska D. Mechanical Properties of Hot Curing Acrylic Resins after Reinforced with Different Kinds of Fibers. Int J Biomed Mater Res. 2013; 1 (1): 9–13. Available from: https://doi.org/10.11648/j.ijbmr.20130101.12.
24. Anderson K, Weritz J, Kaufman JG, editors. ASM Handbook, Volume 2B: Properties and Selection of Aluminum Alloys. ASM International. 2019.
25. Klinicheskie rekomendacii «Perelom nizhnej chelyusti». Utv. Minzdravom Rossii 2021. Dostupno po ssylke: https://www.garant.ru/products/ipo/prime/doc/402775975/ (data obrashcheniya: 22.03.2026).
26. Claes L, Augat P, Suger G, Wilke HJ. Influence of size and stability of the osteotomy gap on the success of fracture healing. J Orthop Res. 1997; 15 (4): 577–84. DOI: 10.1002/jor.1100150414. PMID: 9379268.
27. Ng BW, Abdul Wahab AH, Abdul Wahid AM, Abdullah NNAA, Abdul Kadir MR, Ammarullah MI, et al. Finite element analysis and clinical evaluation of cross locking external fixator configuration for distal third tibia fracture. Sci Rep. 2025; 15 (1): 13310. DOI: 10.1038/s41598-025-97090-4. PMID: 40247025; PMCID: PMC12006471.
28. Glatt V, Evans CH, Tetsworth K. A Concert between Biology and Biomechanics: The Influence of the Mechanical Environment on Bone Healing. Front Physiol. 2017; 7: 678. DOI: 10.3389/fphys.2016.00678. PMID: 28174539; PMCID: PMC5258734.
29. Bowers KM, Anderson DE. Delayed Union and Nonunion: Current Concepts, Prevention, and Correction: A Review. Bioengineering (Basel). 2024; 11 (6): 525. DOI: 10.3390/bioengineering11060525. PMID: 38927761; PMCID: PMC11201148.
30. Sancar B, Çetiner Y, Dayı E. Evaluation of the pattern of fracture formation from trauma to the human mandible with finite element analysis. Part 1: Symphysis region. Dent Traumatol. 2023; 39 (4): 352–60. Available from: https://doi.org/10.1111/edt.12825.
31. Sancar B, Çetiner Y, Dayı E. Evaluation of the pattern of fracture formation from trauma to the human mandible with finite element analysis. Part 2: The corpus and the angle regions. Dent Traumatol. 2023; 39 (5): 437–47. Available from: https://doi.org/10.1111/edt.12841.
32. Kahveci K, Ayranci F. Finite element analysis of different internal fixation methods for the treatment of atrophic mandible fractures. J Stomatol Oral Maxillofac Surg. 2023; 124 (1S): 101276. Available from: https://doi.org/10.1016/j.jormas.2022.08.019.
33. Jindal P, Worcester F, Walia K, Gupta A, Breedon P. Finite element analysis of titanium alloy-graphene based mandible plate. Comput Methods Biomech Biomed Engin. 2019; 22 (3): 324–30. Available from: https://doi.org/10.1080/10255842.2018.1555244.
34. Krennmair S, Winterhalder P, Hunger S, Rupperti S, Holberg C. The effects of frontal trauma on 4 interforaminal dental implants: a 3-dimensional finite element analysis comparing splinted and unsplinted implant configurations. J Oral Maxillofac Surg. 2020; 78 (6): 961–72. Available from: https://doi.org/10.1016/j.joms.2019.12.007.
35. Graillon N, Foletti JM, Godio-Raboutet Y, Guyot L, Varazzani A, Thollon L. Mandibular titanium miniplates change the biomechanical behaviour of the mandible in the case of facial trauma: a three-dimensional finite element analysis. Bioengineering (Basel). 2023; 10 (9): 994. Available from: https://doi.org/10.3390/bioengineering10090994.

Литература

1. Hesham A, Geiger J, Alshamrani Y, Sawatari Y. Can the Mechanism of Injury Impact the Location of a Mandibular Fracture? A Systematic Review. J Maxillofac Oral Surg. 2024; 23 (2): 363–70. DOI: 10.1007/s12663-022-01750-1. Epub 2022 Jul 31. PMID: 38601229; PMCID: PMC11001800.
2. Савельев А. Л., Самуткина М. Г. Современный подход к лечению пациентов с переломами нижней челюсти. Оперативная хирургия и клиническая анатомия (Пироговский научный журнал). 2021; 5 (1): 29–34. Доступно по ссылке: https://doi.org/10.17116/operhirurg2021501129.
3. Vitkos EN, Papadopoulos KA, Dimasis P, Weissinger C, Kyrgidis A. One miniplate versus two miniplates in the fixation of mandibular angle fractures. An updated systematic review and meta-analysis. J Stomatol Oral Maxillofac Surg. 2022; 123 (6): e865–e873. DOI: 10.1016/j.jormas.2022.07.008. Epub 2022 Jul 21. PMID: 35872351.
4. Tsolov R, Firkova EI. Periodontal status in patients with mandibular fractures. J of IMAB. 2022; 28 (1): 4247–50. DOI: https://doi.org/10.5272/jimab.2022281.4247.
5. Jain A, Rai A. Is the Use of Intermaxillary Fixation Screws an Alternative to Erich Arch Bars for Maxillomandibular Fixation During Management of Maxillofacial Fractures? A Systematic Review and Meta-Analysis. Craniomaxillofac Trauma Reconstr. 2021; 14 (3): 236–45. Available from: https://doi.org/10.1177/1943387520971410.
6. Nasser M, Pandis N, Fleming PS, Fedorowicz Z, Ellis E, Ali K. Interventions for the management of mandibular fractures. Cochrane Database Syst Rev. 2013; 2013 (7): CD006087. Available from: https://doi.org/10.1002/14651858.CD006087.pub3.
7. Morris C, Bebeau NP, Brockhoff H, Tandon R, Tiwana P. Mandibular fractures: an analysis of the epidemiology and patterns of injury in 4,143 fractures. J Oral Maxillofac Surg. 2015; 73 (5): 951.e1–951.e12. DOI: 10.1016/j.joms.2015.01.001. Epub 2015 Jan 13. PMID: 25883009.
8. Шашков В. А., Гайворонский И. В., Гайворонская М. Г., Иорданишвили А. К., Родионов А. А., & Ничипорук Г. И. Распространенность различных видов переломов нижней челюсти у взрослых. Вятский медицинский вестник. 2021; 1 (69): 41–47. DOI: 10.24411/2220-7880-2021-10149.
9. Akkina SR, Bevans SE, Johnson AW. Techniques for maxillomandibular fixation: old and new. Curr Opin Otolaryngol

Head Neck Surg. 2025; 33 (4): 216–21. Available from: https://doi.org/10.1097/MOO.0000000000001043.
10. Johnson AW, Akkina SR, Bevans SE. Maxillomandibular Fixation: Understanding the Risks and Benefits of Contemporary Techniques in Adults. Facial Plastic Surgery & Aesthetic Medicine. 2025; 27 (1): 98–105. DOI: 10.1089/fpsam.2024.0113.
11. Пиголкин Ю. И., Кислов М. А., Крупин К. Н. Математическое моделирование с помощью конечно-элементного анализа в судебно-медицинской экспертизе. Судебно-медицинская экспертиза. 2023; 66 (1): 9–13. Доступно по ссылке: https://doi.org/10.17116/sudmed2023660119.
12. Xu X, Cheng Kj, Liu Yf, et al. Experimental validation of finite element simulation of a new custom-designed fixation plate to treat mandibular angle fracture. BioMed Eng OnLine. 2021; 20 (15). Available from: https://doi.org/10.1186/s12938-021-00851-1.
13. Daqiq O, Roossien CC, Wubs FW, van Minnen B. Biomechanical assessment of mandibular fracture fixation using finite element analysis validated by polymeric mandible mechanical testing. Sci Rep. 2024; 14 (1): 11795. Available from: https://doi.org/10.1038/s41598-024-62011-4.
14. Aquilina P, Chamoli U, Parr WC, Clausen PD, Wroe S. Finite element analysis of three patterns of internal fixation of fractures of the mandibular condyle. Br J Oral Maxillofac Surg. 2013; 51 (4): 326–31. Available from: https://doi.org/10.1016/j.bjoms.2012.08.007.
15. Mańkowski J, Piękoś J, Dominiak K, Klukowski P, Fotek M, Zawisza M, Żach P. A Mandible with the Temporomandibular Joint-A New FEM Model Dedicated to Strength and Fatigue Calculations of Bonding Elements Used in Fracture and Defect Surgery. Materials (Basel). 2021; 14 (17): 5031. DOI: 10.3390/ma14175031. PMID: 34501120; PMCID: PMC8434464.
16. Darawsheh HM, Safronova AA, Vasilev YL, Makarova NI, Diachkova EY, Saleeva GT, et al. Choosing the optimal mandible position for inferior alveolar nerve block (IANB) using finite element analysis. Ann Anat. 2023; 247: 152055. DOI: 10.1016/j.aanat.2023.152055. Epub 2023 Jan 22. PMID: 36696926.
17. Panagiotopoulou O, Iriarte-Diaz J, Wilshin S, Dechow PC, Taylor AB, Mehari Abraha H, et al. In vivo bone strain and finite element modeling of a rhesus macaque mandible during mastication. Zoology (Jena). 2017; 124: 13–29. DOI: 10.1016/j.zool.2017.08.010. Epub 2017 Sep 1. PMID: 29037463; PMCID: PMC5792078.
18. Tomioka Takahiro, Ito Daisuke, Murai Takato, Takeda Arisa, Nakamura Mami , Koshinuma Shinya, et al. Analysis of Mechanisms of Mandible Fractures by Lateral Impact: A Biomechanical Approach Using Finite Element Models. Applied Sciences. 2025; 15: 1205. Available from: https://doi.org/10.3390/app15031205.
19. Pinheiro M, Willaert R, Khan A, Krairi A, Van Paepegem W. Biomechanical evaluation of the human mandible after temporomandibular joint replacement under different biting conditions. Sci Rep. 2021; 11 (1): 14034. Available from: https://doi.org/10.1038/s41598-021-93564-3.
20. Hedeşiu M, Pavel DG, Almăşan O, Pavel SG, Hedeşiu H, Rafiroiu D. Three-Dimensional Finite Element Analysis on Mandibular Biomechanics Simulation under Normal and Traumatic Conditions. Oral. 2022; 2, 221–237. Available from: https://doi.org/10.3390/oral2030021.
21. Sarrafpour B, Swain M, Li Q, Zoellner H. Tooth eruption results from bone remodelling driven by bite forces sensed by soft tissue dental follicles: a finite element analysis. PLoS One. 2013; 8 (3): e58803. Available from: https://doi.org/10.1371/journal.pone.0058803
22. Mengoni M. Biomechanical modelling of the facet joints: a review of methods and validation processes in finite element analysis. Biomech Model Mechanobiol. 2021; 20 (2): 389–401. DOI: 10.1007/s10237-020-01403-7. Epub 2020 Nov 22. PMID: 33221991; PMCID: PMC7979651.
23. Raszewski Z, Nowakowska D. Mechanical Properties of Hot Curing Acrylic Resins after Reinforced with Different Kinds of Fibers. Int J Biomed Mater Res. 2013; 1 (1): 9–13. Available from: https://doi.org/10.11648/j.ijbmr.20130101.12.
24. Anderson K, Weritz J, Kaufman JG, editors. ASM Handbook, Volume 2B: Properties and Selection of Aluminum Alloys. ASM International. 2019.
25. Клинические рекомендации «Перелом нижней челюсти». Утв. Минздравом России 2021. Доступно по ссылке: https://www.garant.ru/products/ipo/prime/doc/402775975/ (дата обращения: 22.03.2026).
26. Claes L, Augat P, Suger G, Wilke HJ. Influence of size and stability of the osteotomy gap on the success of fracture healing. J Orthop Res. 1997; 15 (4): 577–84. DOI: 10.1002/jor.1100150414. PMID: 9379268.
27. Ng BW, Abdul Wahab AH, Abdul Wahid AM, Abdullah NNAA, Abdul Kadir MR, Ammarullah MI, et al. Finite element analysis and clinical evaluation of cross locking external fixator configuration for distal third tibia fracture. Sci Rep. 2025; 15 (1): 13310. DOI: 10.1038/s41598-025-97090-4. PMID: 40247025; PMCID: PMC12006471.
28. Glatt V, Evans CH, Tetsworth K. A Concert between Biology and Biomechanics: The Influence of the Mechanical Environment on Bone Healing. Front Physiol. 2017; 7: 678. DOI: 10.3389/fphys.2016.00678. PMID: 28174539; PMCID: PMC5258734.
29. Bowers KM, Anderson DE. Delayed Union and Nonunion: Current Concepts, Prevention, and Correction: A Review. Bioengineering (Basel). 2024; 11 (6): 525. DOI: 10.3390/bioengineering11060525. PMID: 38927761; PMCID: PMC11201148.
30. Sancar B, Çetiner Y, Dayı E. Evaluation of the pattern of fracture formation from trauma to the human mandible with finite element analysis. Part 1: Symphysis region. Dent Traumatol. 2023; 39 (4): 352–60. Available from: https://doi.org/10.1111/edt.12825.
31. Sancar B, Çetiner Y, Dayı E. Evaluation of the pattern of fracture formation from trauma to the human mandible with finite element analysis. Part 2: The corpus and the angle regions. Dent Traumatol. 2023; 39 (5): 437–47. Available from: https://doi.org/10.1111/edt.12841.
32. Kahveci K, Ayranci F. Finite element analysis of different internal fixation methods for the treatment of atrophic mandible fractures. J Stomatol Oral Maxillofac Surg. 2023; 124 (1S): 101276. Available from: https://doi.org/10.1016/j.jormas.2022.08.019.
33. Jindal P, Worcester F, Walia K, Gupta A, Breedon P. Finite element analysis of titanium alloy-graphene based mandible plate. Comput Methods Biomech Biomed Engin. 2019; 22 (3): 324–30. Available from: https://doi.org/10.1080/10255842.2018.1555244.
34. Krennmair S, Winterhalder P, Hunger S, Rupperti S, Holberg C. The effects of frontal trauma on 4 interforaminal dental implants: a 3-dimensional finite element analysis comparing splinted and unsplinted implant configurations. J Oral Maxillofac Surg. 2020; 78 (6): 961–72. Available from: https://doi.org/10.1016/j.joms.2019.12.007.
35. Graillon N, Foletti JM, Godio-Raboutet Y, Guyot L, Varazzani A, Thollon L. Mandibular titanium miniplates change the biomechanical behaviour of the mandible in the case of facial trauma: a three-dimensional finite element analysis. Bioengineering (Basel). 2023; 10 (9): 994. Available from: https://doi.org/10.3390/bioengineering10090994.

CLINICAL AND MORPHOLOGICAL ASSESSMENT OF BONE QUALITY IN THE DENTAL IMPLANTATION ZONE IN PATIENTS WITH OSTEOPOROSIS

Akkalaev AB[1]✉, Abdullaeva RR[1], Aliev MR[1], Mustafaev RG[1], Bedoeva AA[1], Mironova AA[1], Khugaeva VF[1], Kadieva LM[2], Munapova KKh[2]

[1] North Ossetian State Medical Academy, Vladikavkaz, Russia

[2] Khetagurov North Ossetian State University, Vladikavkaz, Russia

Systemic osteoporosis is one of the most significant systemic factors capable of worsening bone tissue quality and affect osseointegration of dental implants. The increase in the number of patients of older age groups in need of implant treatment determines high clinical significance of preoperative assessment of the implant bed condition in this category of patients. The study aimed to assess clinical and morphological features of bone tissue in the dental implantation zone in patients with osteoporosis and determine the correlation of those with the primary stability of implants and early marginal bone remodeling. A total of 84 patients aged 55–75 were included in a prospective pilot study, who were planned for implantation in the areas of maxillary and mandibular premolars and molars: 42 with the confirmed systemic osteoporosis and 42 having no signs of osteoporosis. All the patients underwent CBCT with the bone quality and type determination in accordance with the Lekholm and Zarb classification; histological and histomorphometric analysis of bone biopsy specimens was performed in a subgroup of 32 patients. Primary stability was assessed by the resonance frequency analysis; clinical monitoring was conducted after 2, 6, and 12 months. The D3–D4 type bones were more often found in patients with osteoporosis, along with lower bone density and implant stability quotient (ISQ) values, reduced bone volume fraction (BV/TV), trabecular thinning, and increased RANKL/OPG ratio. There was a positive correlation between the BV/TV, radiological bone density, and primary stability of implants. Systemic osteoporosis degrades the implant bed quality, therefore, the implantation protocol personalization and comprehensive preoperative assessment are required.

Keywords: dental implantation, osteoporosis, bone quality, histomorphometry, primary implant stability, cone-beam computed tomography

Author contribution: Akkalaev AB — study concept and design, academic advising, manuscript editing; Abdullaeva RR, Aliev MR, Mustafaev RG — clinical material collection, literature review, manuscript writing; Bedoeva AA, Mironova AA, Khugaeva VF — morphological material processing, analysis and statistical processing of the results; Kadieva LM, Munapova KKh — clinical support of patients, preparation of materials, manuscript writing.

Compliance with ethical standards: the study was approved by the Ethics Committee of the North Ossetian State Medical Academy (protocol No. 2 dated 12 February 2026). All the subjects submitted the informed consent for participation in the study, diagnostic and invasive procedures, and personal data processing.

✉ **Correspondence should be addressed:** Albert B. Akkalaev
Pushkinskaya, 40, Vladikavkaz, 362019, Russia; asp358888@yandex.ru

Received: 19.03.2026 **Accepted:** 15.04.2026 **Published online:** 25.04.2026

DOI: 10.24075/brsmu.2026.017

КЛИНИКО-МОРФОЛОГИЧЕСКАЯ ОЦЕНКА КАЧЕСТВА КОСТИ В ЗОНЕ ДЕНТАЛЬНОЙ ИМПЛАНТАЦИИ У ПАЦИЕНТОВ С ОСТЕОПОРОЗОМ

А. Б. Аккалаев[1]✉, Р. Р. Абдуллаева[1], М. Р. Алиев[1], Р. Г. Мустафаев[1], А. А. Бедоева[1], А. А. Миронова[1], В. Ф. Хугаева[1], Л. М. Кадиева[2], К. Х. Мунапова[2]

[1] Северо-Осетинская государственная медицинская академия, Владикавказ, Россия

[2] Северо-Осетинский государственный университет имени К. Л. Хетагурова, Владикавказ, Россия

Системный остеопороз — один из наиболее значимых системных факторов, способных ухудшать качество костной ткани и влиять на условия остеоинтеграции дентальных имплантатов. Увеличение числа пациентов старших возрастных групп, нуждающихся в имплантологическом лечении, определяет высокую клиническую значимость предоперационной оценки состояния костного ложа у этой категории больных. Целью исследования было оценить клинико-морфологические особенности костной ткани в зоне дентальной имплантации у пациентов с остеопорозом и определить их связь с первичной стабильностью имплантатов и ранней маргинальной ремоделяцией кости. В проспективное пилотное исследование включены 84 пациента 55–75 лет, которым планировали выполнить имплантацию в области премоляров и моляров верхней и нижней челюсти: 42 с подтвержденным системным остеопорозом и 42 без признаков остеопороза. Всем пациентам выполняли КЛКТ с определением плотности кости и типа кости по Lekholm и Zarb; в подгруппе из 32 пациентов проводили гистологический и гистоморфометрический анализ костных биоптатов. Первичную стабильность оценивали методом резонансно-частотного анализа, клиническое наблюдение проводили через 2, 6 и 12 месяцев. У пациентов с остеопорозом чаще выявляли типы кости D3–D4, более низкие значения плотности кости и коэффициента стабильности имплантатов (ISQ), а также снижение объемной доли костной ткани (BV/TV), истончение трабекул и повышение отношения RANKL/OPG. Установлена положительная корреляция между BV/TV, рентгенологической плотностью кости и первичной стабильностью имплантатов. Системный остеопороз ухудшает качество костного ложа, что требует индивидуализации протокола имплантации и комплексной предоперационной оценки.

Ключевые слова: дентальная имплантация, остеопороз, качество костной ткани, гистоморфометрия, первичная стабильность имплантатов, конусно-лучевая компьютерная томография

Вклад авторов: А. Б. Аккалаев — концепция и дизайн исследования, научное руководство, редактирование рукописи; Р. Р. Абдуллаева, М. Р. Алиев, Р. Г. Мустафаев — сбор клинического материала, анализ литературы, подготовка текста; А. А. Бедоева, А. А. Миронова, В. Ф. Хугаева — морфологическая обработка материалов, анализ и статистическая обработка результатов; Л. М. Кадиева, К. Х. Мунапова — клиническое сопровождение пациентов, оформление материалов, подготовка рукописи.

Соблюдение этических стандартов: исследование одобрено этическим комитетом ФГБОУ ВО «Северо-Осетинская государственная медицинская академия» Минздрава России (протокол № 2 от 12 февраля 2026 г.). Все участники исследования подписали добровольное информированное согласие на участие в исследовании, выполнение диагностических и инвазивных процедур, а также на обработку персональных данных.

✉ **Для корреспонденции:** Альберт Борисович Аккалаев
ул. Пушкинская, д. 40, г. Владикавказ, 362019, Россия; asp358888@yandex.ru

Статья получена: 19.03.2026 **Статья принята к печати:** 15.04.2026 **Опубликована онлайн:** 25.04.2026

DOI: 10.24075/vrgmu.2026.017

Dental implantation has firmly taken the place of one of the basic orthopedic rehabilitation methods for the partially and completely edentulous patients. The implant treatment high clinical efficacy necessitates accurate evaluation of the recipient implant bed condition, including its morphological characteristics and radiodensity [1, 2].

The jawbone density quantification is considered as an important preoperative planning phase allowing one to predict primary stability of the implant and the risk of early complications [3]. Osteoporosis associated with the bone mineral density decrease and microstructure disruption represents one of the most significant factors capable of degrading the bone quality [4].

The bone quality is determined by not only bone volume, but also the cortical to trabecular bone ratio, degree of mineralization, and remodeling activity. Morphological assessment of implantation outcomes shows that the features of bone microstructure have a significant effect on the osseointegration course [5]. In clinical practice, the Lekholm and Zarb classification linking the radiological pattern to the implant bed surgical characteristics is widely used to approximately determine the bone type [6].

As the population ages and the number of patients with the postmenopausal and senile osteoporosis increases, the problem of choosing the optimal implantation protocol is becoming increasingly relevant. The issue of the impact of systemic osteoporosis on the implant survival, marginal bone loss, and early osseointegration phases is still a matter of debate, which is confirmed by the data of systematic reviews and meta-analyses [7, 8].

Modern concepts of bone quality include the analysis of histomorphometric parameters: bone volume fraction, trabecular thickness, number, and spacing. Matching morphometric indicators to the clinical and radiological assessment allows one to more accurately characterize the implant bed load-bearing capacity [9]. Additional opportunities for preoperative risk stratification are provided by the computed tomographic modification of the jawbone quality classification [10].

The bone remodeling imbalance, including alterations in the RANK/RANKL/OPG system and the decrease in bone formation efficiency, represents an important link of the osteoporosis pathogenesis. Morphological and histomorphometric testing in implant dentistry confirm the importance of such alterations for the formation of a stable contact between the implant and the bone [11]. According to the data of modern meta-analyses, a more thorough analysis of the early bone remodeling risk factors is required, even with the high overall survival of implants in patients with osteoporosis [12].

The study aimed to perform clinical and morphological assessment of bone quality in the dental implantation zone in patients with systemic osteoporosis and determine the correlation of morphological characteristics of the bone with the indicators of primary stability of implants and early results of their functioning.

METHODS

A prospective comparative pilot study of 84 patients of the older age group, who were planned for dental implantation in the areas of maxillar and mandibular premolars and molars, was conducted. The age range of 5–75 years was selected considering the maximum prevalence of the clinical postmenopausal and senile osteoporosis; when interpreting the results, the WHO approach to age was used, according to which elderly patients (60–74 years) were the main focus of clinical interest, and inclusion of patients aged 55–59 and 75 reflected the actual patient traffic. The index group consisted of 42 patients with the postmenopausal or senile osteoporosis confirmed based on the dual-energy X-ray absorptiometry data (T-score ≤ –2.5); the comparison group consisted of 42 patients without any signs of systemic osteoporosis. The patients' gender was considered as a clinical characteristic, but no separate gender-stratified analysis was conducted within the framework of the pilot design; similarly, the osteoporosis drug therapy was not singled out as an independent stratification factor, which was considered when interpreting the results.

The cone-beam computed tomography was performed before planning implantation in all cases. Only the lateral parts of the maxilla and mandible were scanned; localization of implantation was considered when performing the analysis, but no separate analysis stratified by the jaws was conducted due to small sample size. The alveolar ridge height and width, the cortical plate thickness, the radiological bone density in the proposed implantation area, and the bone type according to the Lekholm and Zarb classification were analyzed [6, 10]. The bone density was measured in the standardized areas of interest in the planned implant center, except the zones of artifacts.

In the subgroup of 32 patients (18 with osteoporosis and 14 without osteoporosis), a cylindrical bone fragment 2.0–2.5 mm in diameter was collected using a trephine drill, when shaping the bed for the implant. Biopsy specimens were fixed in the 10% neutral formalin, subjected to standard decalcification, paraffin embedded. Then serial longitudinal sections were made. The hematoxylin and eosin stain was used, along with the Masson stain.

Histomorphometric assessment involved determination of the bone volume fraction (BV/TV), trabecular thickness, trabecular number per unit of length, trabecular spacing, osteoid tissue area, relative osteoclast counts. In addition, immunohistochemistry assessment was performed using antibodies to osteocalcin and proteins of the RANK/RANKL/OPG system [9, 11].

Implants were installed in accordance with the standard surgical protocol with respect for the principles of atraumatic surgery and constant cooling of the instrument. Sequential dissection of the bed with a pilot drill followed by step-by-step expansion in accordance with the clinical situation and the manufacturer's recommendations was considered as the standard protocol. A full drilling protocol was implemented in the D1–D2 bone regions, while moderate underpreparation of the final stage was allowed for the D3–D4 bone to increase primary stability. The implant length and diameter were selected individually based on the CBCT data and the alveolar ridge parameters; comparative evaluation of various implant systems and surface characteristics was not the scope of this study. Primary stability was assessed by the resonance frequency analysis with the ISQ recording in the vestibulo-oral and mesiodistal directions and calculation of the mean.

Clinical monitoring was conducted 2, 6, and 12 months after the implant placement. Control within 2 months was selected for the early assessment of soft tissue healing, signs of inflammation, and primary stability prior to the functional load phase; the terms 6 and 12 months were used to assess the early marginal bone remodeling and clinical functioning of implants. The facts of having pain, signs of inflammation of peri-implant tissues, as well as implant mobility, mucous membrane condition, and marginal bone loss were assessed based on the targeted intraoral radiography data.

Statistical processing of the results was performed using the variation statistics methods. The distribution was tested for normality using the Shapiro–Wilk test. The mean and standard

deviation were calculated for quantitative characteristics; when the distribution was normal, the differences between groups were assessed using the Student's *t*-test for independent samples; when the distribution was non-normal, the Mann–Whitney *U*-test was used. Categorical traits were compared using the chi-squared test or Fischer's exact test. The correlation analysis involved calculation of the Pearson's or Spearman's coefficient, depending on the data distribution. The differences were considered significant at $p < 0.05$.

RESULTS

The comparative analysis showed that the share of regions with the D3–D4 bone type reached 78.6% in patients of the index group, while in the comparison group this value was 42.9%. The average radiological bone density in the implantation zone expressed in Hounsfield units (HU) was 452 ± 118 in patients with osteoporosis vs. 721 ± 146 in the comparison group ($p < 0.001$). The average implant stability quotient (ISQ) was also lower in the index group — 62.3 ± 5.1 vs. 71.4 ± 4.3, respectively ($p < 0.001$).

Histological assessment of biopsy samples confirmed the presence of the bone microstructure alterations typical for osteoporosis: trabecular thinning and sites of discontinuity in trabeculae, trabecular spacing increase, emergence of resorption lacunae and microcracks. According to histomorphometry data, the bone volume fraction (BV/TV) was 21.3 ± 4.2% in patients with osteoporosis, while in the comparison group it was 32.7 ± 5.1% ($p < 0.001$). At the same time, the trabecular thickness decrease and trabecular spacing increase were reported.

Immunohistochemistry assessment revealed the decrease in osteocalcin expression in patients of the index group, along with the increase in the RANKL/OPG ratio suggesting shifting the balance of remodeling towards resorption. We found a positive correlation between BV/TV and the ISQ value ($r = 0.62$; $p < 0.01$), as well as between the radiological bone density and primary implant stability ($r = 0.55$; $p < 0.01$).

The 12-month implant survival was 94.7% in the index group and 98.3% in the comparison group; given small sample size, this difference was considered as a clinical trend, not as an independent finite performance criterion. The clinically significant bone loss of more than 1.5 mm within the first year of functioning was significantly more often observed in patients with the lowest BV/TV and ISQ values.

DISCUSSION

The findings suggest that systemic osteoporosis is accompanied by not only bone mineral density decrease, but also severe impairment of its trabecular architecture in the implantation zone. This is consistent with the data of the systematic reviews emphasizing the role of local bone quality as one of the key factors of successful osseointegration in patients with osteoporosis [7, 8, 12].

The combination of CBCT-based assessment and histomorphometric analysis made it possible to match radiological signs of low bone density to certain morphological alterations: decreased BV/TV, trabecular thinning, and trabecular spacing increase. Such an approach enhancing the preoperative assessment diagnostic potential is in line with modern ideas about the relationship between tomographic and morphometric characteristics of the bone [9–11].

In practical terms, the findings confirm the fact that osteoporosis is not an absolute contraindication to dental implantation, but personalization of the surgical and orthopedic protocol is required. When spotting signs of the D3–D4 bone type, it is reasonable to more gently prepare the bed, as well as to use a differentiated approach to the finite dissection diameter, delayed functional load, and enhanced radiological monitoring in the early postoperative period [7, 8, 12].

A number of limitations of the study should be taken into account. The biopsy subgroup was relatively small, so morphometric and immunohitochemistry data should be considered as the pilot phase results. The study aimed at obtaining early results did not envisage stratification by gender, implant localization (maxilla/mandible), drug therapy of osteoporosis, and implant system type; no separate analysis of the impact of antiresorptive therapy was conducted, despite the fact that this factor is clinically significant due to the risk of the medication-related osteonecrosis of the jaw. In this regard, it is reasonable to interpret the differences in the 12-month survival of implants as a trend that should be confirmed in larger studies. Further monitoring should include the histomorphometric subgroup expansion, the analysis stratified by the anatomical localization and gender, consideration of antiresorptive therapy, and extension of the follow-up period to at least 24–36 months.

CONCLUSIONS

Patients with systemic osteoporosis significantly more often show signs of the D3–D4 bone type, decreased radiodensity, and deterioration of the bone histomorphometric characteristics in the dental implantation zone. The BV/TV decrease, trabecular thinning, and the RANKL/OPG ratio increase are associated with the lower primary stability of implants and higher risk of early marginal bone loss. The comprehensive preoperative assessment, including CBCT and morphological analysis (if possible), makes it possible to stratify the risk and personalize the implantation protocol in patients with osteoporosis.

References

1. Batishcheva NN, Korneeva EN, Kiseleva EV. Kliniko-morfologicheskaya otsenka kachestva kostnoi tkani chelyusti pri podgotovke k dental'noi implantatsii. Rossiiskaya stomatologiya. 2022; 8 (3): 25–31. Russian.
2. Senkina AYu, Voroshilova LA, Tishkin VV. Otsenka opticheskoi plotnosti kostnoi tkani pri dental'noi implantatsii. Rossiiskaya stomatologiya. 2023; 12 (3): 40–46. Russian.
3. Shevchenko AV, Zhukova IG, Loginov VA. Opredelenie plotnosti kostnoi tkani chelyustei pri dental'noi implantatsii. Meditsinskie novosti. 2020; (5): 52–57. Russian.
4. Martynova EV. Osteoporoz v dental'noi implantologii: eksperimental'noe modelirovanie i klinicheskaya diagnostika [dissertation]. M., 2024; 156 p. Russian.
5. Gil'mutdinova AF, Nurieva ER, Ziyatdinov KR. Morfologicheskaya otsenka rezul'tatov dental'noi implantatsii. Kazanskii meditsinskii zhurnal. 2023; 104 (4): 567–73. Russian.
6. Panov AA, Kuznetsov SV, Romanov PV. Otsenka rentgenologicheskoi plotnosti i tipa kostnoi tkani pri planirovanii dental'noi implantatsii. Sovremennaya stomatologiya. 2022; 2: 15–21. Russian.
7. Santiago Júnior JF, da Silva-Neto JP, Nary Filho H, et al. Dental implants in patients with osteoporosis: a systematic review with meta-analysis. Int J Oral Maxillofac Surg. 2020; 47 (4): 480–91.

8. Lemos CAA, de Oliveira AS, Faé DS, et al. Do dental implants placed in patients with osteoporosis have higher risks of failure and marginal bone loss compared to those in healthy patients? A systematic review with meta-analysis. Clin Oral Investig. 2023; 27 (3): 1301–14.
9. Oliveira MR, Gonçalves A, Gabrielli MAC, et al. Evaluation of alveolar bone quality: correlation between histomorphometric analysis and Lekholm and Zarb classification. J Oral Maxillofac Surg. 2020; 77 (5): 987–95.
10. Roze J, Boffano P, Viterbo S, et al. Revised, computed tomography-based Lekholm and Zarb jawbone quality classification. Int J Prosthodont. 2023; 31 (4): 342–5.
11. Koodaryan R, Hafezeqoran A, Jabbari S. Histomorphometric analysis of osseointegrated intraosseous dental implants: a scoping review. J Funct Biomater. 2022; 13 (11): 672–84.
12. Mohajerani H, Roozbeh N, Taherian S, et al. Impact of osteoporosis on dental implant survival, failure, and marginal bone loss: a systematic review and meta-analysis. J Clin Med. 2024; 13 (19): 6719.

Литература

1. Батищева Н. Н., Корнеева Е. Н., Киселева Е. В. Клинико-морфологическая оценка качества костной ткани челюсти при подготовке к дентальной имплантации. Российская стоматология. 2022; 8 (3): 25–31.
2. Сенькина А. Ю., Ворошилова Л. А., Тишкин В. В. Оценка оптической плотности костной ткани при дентальной имплантации. Российская стоматология. 2023; 12 (3): 40–46.
3. Шевченко А. В., Жукова И. Г., Логинов В. А. Определение плотности костной ткани челюстей при дентальной имплантации. Медицинские новости. 2020; 5: 52–57.
4. Мартынова Е. В. Остеопороз в дентальной имплантологии: экспериментальное моделирование и клиническая диагностика [диссертация]. М., 2024; 156 с.
5. Гильмутдинова А. Ф., Нуриева Э. Р., Зиятдинов К. Р. Морфологическая оценка результатов дентальной имплантации. Казанский медицинский журнал. 2023; 104 (4): 567–73.
6. Панов А. А., Кузнецов С. В., Романов П. В. Оценка рентгенологической плотности и типа костной ткани при планировании дентальной имплантации. Современная стоматология. 2022; 2: 15–21.
7. Santiago Júnior JF, da Silva-Neto JP, Nary Filho H, et al. Dental implants in patients with osteoporosis: a systematic review with meta-analysis. Int J Oral Maxillofac Surg. 2020; 47 (4): 480–91.
8. Lemos CAA, de Oliveira AS, Faé DS, et al. Do dental implants placed in patients with osteoporosis have higher risks of failure and marginal bone loss compared to those in healthy patients? A systematic review with meta-analysis. Clin Oral Investig. 2023; 27 (3): 1301–14.
9. Oliveira MR, Gonçalves A, Gabrielli MAC, et al. Evaluation of alveolar bone quality: correlation between histomorphometric analysis and Lekholm and Zarb classification. J Oral Maxillofac Surg. 2020; 77 (5): 987–95.
10. Roze J, Boffano P, Viterbo S, et al. Revised, computed tomography-based Lekholm and Zarb jawbone quality classification. Int J Prosthodont. 2023; 31 (4): 342–5.
11. Koodaryan R, Hafezeqoran A, Jabbari S. Histomorphometric analysis of osseointegrated intraosseous dental implants: a scoping review. J Funct Biomater. 2022; 13 (11): 672–84.
12. Mohajerani H, Roozbeh N, Taherian S, et al. Impact of osteoporosis on dental implant survival, failure, and marginal bone loss: a systematic review and meta-analysis. J Clin Med. 2024; 13 (19): 6719.

ORAL FLUID CHANGES IN XEROSTOMIA PATIENTS ON MEDICATIONS: CLINICAL AND LABORATORY CHARACTERISTICS

Khetagurov SK ✉, Sadaeva AA, Shovkhalova RU, Murzabekov BI, Dovletmurzaev ZS, Ozkan Zh-M, Sugaipova DA, Betersultanova DI, Oleinik II

North Ossetian State Medical Academy, Vladikavkaz, Russia

Drug-induced xerostomia is common among elderly patients taking multiple medications. The condition significantly affects dental health and quality of life. This study aimed to evaluate the clinical and laboratory characteristics of oral fluid (OF) in xerostomia patients taking xerogenic medications, and to assess associations between total xerogenic load, salivary flow rates, and OF composition. The study included 60 people aged 45–75 years. The treatment group consisted of 40 patients with at least 3 months of dry mouth history and routine intake of two or more medications with known xerogenic potential. The control group included 20 healthy individuals exhibiting no signs of xerostomia and not taking medications routinely. We used the Xerostomia Inventory questionnaire to collect data from the participants; they also underwent clinical dental examination and sialometry for unstimulated and stimulated oral fluid (OF). The fluid samples were examined in the laboratory to determine pH, buffer capacity, total protein content, alpha-amylase activity, glucose and lactate levels. Compared to the control group, patients in the treatment group showed marked hyposalivation, decreased OF pH and buffer capacity, increased total protein content and alpha-amylase activity, and tended more often to have multiple caries lesions, candidal stomatitis, and atrophic changes in the oral mucosa. Thus, drug-induced xerostomia is accompanied by pronounced quantitative and qualitative changes in OF as well dental health and quality of life deterioration. A comprehensive clinical and laboratory assessment of OF provides an objective measure of xerostomia severity and enables compilation of tailored prevention and treatment programs.

Keywords: xerostomia, hyposalivation, oral fluid, saliva, medications, sialometry, dental health status

Author contribution: Khetagurov SK — concept and design of the study, supervision, manuscript editing; Sadaeva AA, Shovkhalova RU, Murzabekov BI — collection of clinical material, patient survey, manuscript authoring; Betersultanova DI, Oleinik II — oral health examination, sialometry, and compilation of the primary database; Dovletmurzaev ZS, Ozkan Zh-M, Sugaipova DA — laboratory tests, statistical processing of results, manuscript formalization.

Compliance with ethical standards: the study was approved by the local Ethics Committee of North Ossetian State Medical Academy of the Ministry of Health of the Russian Federation (Minutes No. 5 of September 20, 2025). All participants have voluntarily signed informed consent forms. The study did not involve animal experiments.

✉ **Correspondence should be addressed:** Soslan Kazbekovich Khetagurov
Pushkinskaya, 40, Vladikavkaz, 362019, North Ossetia–Alania, Russia; asp358888@yandex.ru

Received: 19.03.2026 **Accepted:** 03.04.2026 **Published online:** 22.04.2026

DOI: 10.24075/brsmu.2026.016

КЛИНИКО-ЛАБОРАТОРНАЯ ХАРАКТЕРИСТИКА ИЗМЕНЕНИЙ РОТОВОЙ ЖИДКОСТИ У ПАЦИЕНТОВ С КСЕРОСТОМИЕЙ НА ФОНЕ ПРИЕМА ЛЕКАРСТВЕННЫХ ПРЕПАРАТОВ

С. К. Хетагуров ✉, А. А. Садаева, Р. У. Шовхалова, Б. И. Мурзабеков, З. С. Довлетмурзаев, Ж.-М. Озкан, Д. А. Сугаипова, Д. И. Бетерсултанова, И. И. Олейник

Северо-Осетинская государственная медицинская академия, Владикавказ, Россия

Медикаментозная ксеростомия широко распространена на фоне полипрагмазии у пациентов старших возрастных групп и существенно влияет на стоматологический статус и качество жизни. Целью исследования было оценить клинико-лабораторные характеристики ротовой жидкости (РЖ) у пациентов с ксеростомией, развившейся на фоне приема лекарственных препаратов (ЛП) с ксерогенным эффектом, и определить связь между суммарной ксерогенной нагрузкой, показателями слюноотделения и изменениями состава РЖ. В исследование включено 60 человек 45–75 лет. Основная группа — 40 пациентов с жалобами на сухость во рту продолжительностью не менее 3 месяцев при одновременном приеме двух и более ЛП с известным ксерогенным потенциалом. Контрольная группа — 20 здоровых лиц без признаков ксеростомии и без регулярного приема ЛП. Проводили анкетирование (опросник Xerostomia Inventory), клиническое стоматологическое обследование, сиалометрию нестимулированной и стимулированной РЖ, а также лабораторное исследование РЖ с определением pH, буферной емкости, общего содержания белка, активности альфа-амилазы, уровней глюкозы и лактата. У пациентов основной группы выявлены выраженная гипосаливация, снижение pH и буферной емкости РЖ, повышение общего содержания белка и активности альфа-амилазы, а также более высокая частота множественного кариеса, кандидозного стоматита и атрофических изменений слизистой оболочки полости рта по сравнению с контрольной группой. Таким образом, медикаментозная ксеростомия сопровождается выраженными количественными и качественными изменениями РЖ, ухудшением стоматологического статуса и снижением качества жизни. Комплексная клинико-лабораторная оценка РЖ позволяет объективизировать тяжесть ксеростомии и обосновать индивидуализированные программы профилактики и лечения.

Ключевые слова: ксеростомия, гипосаливация, ротовая жидкость, слюна, лекарственные препараты, сиалометрия, стоматологический статус

Вклад авторов: С. К. Хетагуров — концепция и дизайн исследования, научное руководство, редактирование рукописи; А. А. Садаева, Р. У. Шовхалова, Б. И. Мурзабеков — сбор клинического материала, анкетирование пациентов, написание рукописи; Д. И. Бетерсултанова, И. И. Олейник — проведение стоматологического обследования, сиалометрии и формирование базы первичных данных; З. С. Довлетмурзаев, Ж.-М. Озкан, Д. А. Сугаипова — лабораторный этап исследования, статистическая обработка результатов, оформление рукописи.

Соблюдение этических стандартов: исследование одобрено локальным этическим комитетом ФГБОУ ВО СОГМА Минздрава России (протокол № 5 от 20 сентября 2025 г.). Все участники исследования подписали добровольное информированное согласие на участие в исследовании. Исследование не включало эксперименты на животных.

✉ **Для корреспонденции:** Сослан Казбекович Хетагуров
ул. Пушкинская, д. 40, г. Владикавказ, 362019, Республика Северная Осетия – Алания; asp358888@yandex.ru

Статья получена: 19.03.2026 **Статья принята к печати:** 03.04.2026 **Опубликована онлайн:** 22.04.2026

DOI: 10.24075/vrgmu.2026.016

The physiology of salivation and the composition of oral fluid are fundamentally important for dental health. Normally, saliva moisturizes the mucous membranes, helps form the food bolus, supports remineralization of hard tooth tissues, regulates acid-base balance, and performs protective functions via its enzymes, mucins, and immune proteins [1, 2].

Xerostomia is a subjective feeling of dryness in the oral cavity; it can be concomitant with decreased salivation, qualitative changes in secretions, or impaired saliva distribution on the surface of the mucous membrane [3–5]. Dry mouth is a common complaint among adults, particularly older patients [6, 7].

The etiological factors of xerostomia are diverse and include autoimmune diseases, endocrine and metabolic disorders, chronic somatic pathology, radiation therapy in the head and neck area, as well as long-term drug therapy [5, 8–13]. Among medications, the most pronounced xerogenic potential has been described for antidepressants, anxiolytics, neuroleptics, antihypertensive agents, diuretics, antiarrhythmic drugs, and antihistamines [6, 11–13].

Clinical manifestations of drug-induced xerostomia include a constant feeling of dry mouth, thirst, difficulty swallowing dry food, speech disorders, changes in taste, burning of the mucous membranes and tongue, and reduced tolerance for removable dentures [4, 7, 12]. Prolonged hyposalivation increases the risk of multiple carious lesions, root caries, candidal mucosal lesions, and atrophic glossitis [4, 7, 12].

Diagnosis of xerostomia is based on a combination of clinical assessment and objective research methods. Standardized questionnaires, including the Xerostomia Inventory, are widely used to quantify subjective symptoms, while objective assessments of secretory function are performed using sialometry for unstimulated and stimulated oral fluid [14–16].

Laboratory examination of oral fluid enables measurement of saliva's pH, buffering capacity, protein composition, and enzymatic activity; this expands the possibilities for objectively assessing the degree of hyposalivation and the risk of dental complications [1, 2, 17]. In the context of polypharmacy, combined clinical and laboratory analysis of oral fluid appears to be the most informative [5, 6, 11–13, 18].

However, the relationship between total xerogenic drug load and specific oral fluid changes (detected via clinical and laboratory analysis) in xerostomia patients remains poorly understood.

This study aimed to evaluate the clinical and laboratory characteristics of oral fluid in xerostomia patients taking xerogenic medications, and to assess associations between total drug-related xerogenic load, salivary flow rates, and changes of the oral fluid composition.

METHODS

This was a single-stage, comparative observational study conducted at a dental clinic and the therapeutic department of a multidisciplinary hospital.

The study included 60 patients of both sexes aged 45–75 years. The treatment group consisted of 40 patients who had complained of dry mouth for at least 3 months and had routinely taken two or more potentially xerogenic medications for 6 months or longer. The control group included 20 practically healthy people of comparable age who did not complain of dry mouth, routinely take medications, or use anything beyond occasional non-narcotic analgesics and nonsteroidal anti-inflammatory drugs.

Based on the literature, the considered xerogenic drugs were antidepressants, anxiolytics, neuroleptics, the main groups of antihypertensive drugs, diuretics, antiarrhythmic medications, and antihistamines [8, 9, 11–13, 18]. Exclusion criteria: Sjogren's syndrome and other autoimmune diseases, decompensated diabetes mellitus, chronic renal or liver failure, previous radiation therapy of the head and neck, alcohol abuse, acute infectious and inflammatory diseases at the time of examination, pregnancy and lactation.

All patients underwent a standard dental examination. We evaluated their complaints, medical and life histories, drug therapy (including structure and duration), and examined the oral cavity, assessing the condition of the mucous membrane, tongue, lips, and gums, and noting any atrophy, erythema, cracks, erosions, plaques, or signs of candidal lesions. Dental health was described using the DMFT index calculated according to a generally accepted method.

The subjective severity of xerostomia was assessed using a modified Xerostomia Inventory (XI) [14, 15]. The patient filled out the questionnaire independently and asked for the doctor's help if necessary. A higher total score indicated more severe dry mouth syndrome, as perceived by the patient.

Unstimulated whole-saliva flow was quantitatively assessed using Navazesh sialometry [16]. The oral fluid was collected in the morning, no earlier than 2 hours after eating, drinking, smoking and hygiene procedures. The patient was seated, breathing through the nose, and spitting the generated saliva into a graduated tube every 30 seconds over a 5-minute period. The salivation rate was calculated in mL/min.

Stimulated salivation was measured after chewing a standard paraffin pellet (weight 1.0 g) for 5 minutes. The collected saliva was measured in a graduated cylinder to calculate stimulated flow rate. The accepted hyposalivation thresholds were 0.1 mL/min (unstimulated) and 0.5 ml/min (stimulated).

After collection, samples were centrifuged at 3000 rpm for 10 min; the supernatant was subjected to biochemical analysis no later than 2 h after sampling. Table gives the key analytical modes, reagents, and equipment used for the purpose.

To asses the drug load, we analyzed the prescribed therapy. Each xerogenic medication was assigned a conditional score depending on the severity of the effect on salivation according to literature data [11–13, 18]. The total score for each patient was considered as an integral indicator of the xerogenic load.

Statistical processing was performed using standard application software packages. The normality of distribution was assessed using the Shapiro-Wilk test. The results were presented as M ± SD for normally distributed data and as Me (Q_1; Q_3) for non-normal distributions. The Student's *t*-test or Mann–Whitney *U* test was used for quantitative variables between groups; for categorical variables, the chi-square test or Fisher's exact test. Correlation analysis was performed using the Pearson or Spearman correlation, depending on the nature of the distribution. The differences were considered statistically significant at $p < 0.05$.

RESULTS

The mean age of patients in the treatment group was 62.3 ± 7.4 years, in the control group — 60.8 ± 6.9 years; the differences were not statistically significant. Female participants were the dominant cohort in both groups. The average number of concomitant medications was 4.8 ± 1.6 in the treatment group and 0.9 ± 0.4 in the control group, indicating a significantly higher drug load in patients with xerostomia.

All patients in the treatment group complained of dry mouth of varying severity. The Xerostomia Inventory mean score was 37.8 ± 6.1, which corresponded to severe xerostomia. The

Table. Key analytical modes, reagents, and equipment used in the study

Indicator/stage	Method, reagents, and equipment
Preanalytical stage	The samples were collected in graduated tubes and centrifuged at 3000 rpm for 10 minutes in a CM-6M laboratory centrifuge (ELMI Ltd., Latvia). The resulting supernatant was analyzed in the next stage
Oral fluid pH	The pH was determined immediately after centrifugation using a SevenCompact S220 desktop pH meter (Mettler Toledo, Switzerland) equipped with an InLab Expert Pro-ISM glass electrode. Three-point calibration was performed with standard buffer solutions (pH 4.01, 6.86, and 9.18)
Buffer capacity	To 1.0 mL of oral fluid, we sequentially added 0.1 mL of 0.01 mol/L HCl and 0.01 mol/L NaOH using single-channel pipettes (Research plus, Eppendorf AG, Germany) until the pH shifted by 1.0 unit. The volumes of titrant used were recorded
Total protein content	Biuret method: 1.0 mL of biuret reagent was added to 20 µL of oral fluid, and the mixture was incubated for 10 minutes at 37 °C. Optical density was measured at 540 nm using a Stat Fax 1904 Plus semi-automatic biochemical analyzer (Awareness Technology, USA)
Alpha-amylase activity	Kinetic colorimetric assay using a chromogenic substrate: mixed 20 µL of sample with 1.0 mL of reagent, and measured absorbance at 405 nm on a semi-automatic biochemical analyzer (Stat Fax 1904 Plus, Awareness Technology, USA)
Glucose	Glucose oxidase peroxidase method (GOD-PAP): mixed 10 µL of sample with 1.0 mL of reagent, then incubated for 10 minutes at 37 °C, and performed photometry at 505 nm using a semi-automatic biochemical analyzer (Stat Fax 1904 Plus, Awareness Technology, USA)
Lactate	Enzymatic colorimetric method: 20 µL of sample was mixed with 1.0 mL of reagent, incubated for 10 minutes at 37 °C, and absorbance was measured at 540 nm using a semi-automatic biochemical analyzer (Stat Fax 1904 Plus, Awareness Technology, USA)
Microscopy of sediment	Native oral fluid sediment preparations were studied at magnification ×100 and ×400 on a Primo Star light microscope (Carl Zeiss Microscope GmbH, Germany); the number of epithelial cells, leukocytes, and the presence of yeast-like fungi were evaluated

most typical complaints were a constant feeling of dryness, the need to keep water nearby, difficulty swallowing dry food, and sleep disturbances due to needing to drink water at night. In the control group, the total score of XI was 16.3 ± 3.2; the complaints were episodic and did not affect the quality of life.

In the treatment group, the mucous membrane was often pale or moderately hyperemic, thinned, with a matte surface and pronounced stickiness Papillary atrophy, flattening of the surface, and individual fissures were often observed on the tongue. The DMFT index in xerostomia patients was significantly higher and amounted to 21.4 ± 5.2, while in the control group it was 15.8 ± 4.1 ($p < 0.01$). Moreover, in the treatment group, we registered significantly more cases of multiple carious lesions, including root caries, and non-carious lesions.

Candidal stomatitis (mainly erythematous and pseudomembranous forms) was diagnosed in 32.5% of treatment group participants. These patients reported burning and soreness of the oral mucous membrane, which worsened when consuming spicy or hot food. In the control group, only one patient (5%) showed signs of candidal lesions. Atrophic glossitis was found in about a quarter of patients in the treatment group, while in the control group this condition was very rare.

Sialometry revealed severe hyposalivation in the treatment group. The rate of unstimulated salivation averaged at 0.08 ± 0.03 mL/min and was significantly lower than that in the control group (0.32 ± 0.09 mL/min) ($p < 0.001$). The stimulated salivation rate in xerostomia patients equaled 0.32 ± 0.11 mL/min, whereas in the control group it was 0.86 ± 0.21 mL/min ($p < 0.001$). Both unstimulated and stimulated saliva flow rates indicated pronounced hyposalivation in most treatment group patients.

Laboratory examination of the oral fluid revealed significant qualitative changes. The average pH in the treatment group was 6.47 ± 0.21, significantly lower than in the controls (6.86 ± 0.18) ($p < 0.01$). Xerostomia patients had reduced buffering capacity, which made titrant-induced pH changes occur more rapidly. The oral fluid total protein content in the treatment group was higher than in the control group, potentially indicating compensatory restructuring of the salivary glands' secretory function.

Alpha-amylase activity in the treatment group was also significantly higher than in the control group. At the same time, we registered a moderate growth of the levels of glucose and lactate. Microscopic examination revealed increased numbers of exfoliated epithelial cells and leukocytes, along with more frequent yeast-like Candida fungi. These findings aligned with the clinical signs of candidal stomatitis.

The analysis of drug therapy confirmed the significant role of xerogenic drugs in the development of hyposalivation. Most treatment group patients took antidepressants and antihypertensive drugs in various combinations. The mean integrated xerogenic load index was 7.1±2.4 (arbitrary units). Correlation analysis revealed a statistically significant negative relationship between the total xerogenic score and the rate of unstimulated as well as stimulated salivation, whereas a positive correlation was observed with the Xerostomia Inventory total score.

Thus, patients who take xerogenic medications for a long time develop persistent hyposalivation with pronounced clinical manifestations of xerostomia and a complex of quantitative and qualitative changes in oral fluid that adversely affect dental health.

DISCUSSION

The results of our study confirm previously reported findings that drug-induced xerostomia and hyposalivation are especially common in senior patients receiving combination therapy for chronic somatic diseases [5–7, 11–13, 18]. The registered unstimulated and stimulated salivation rates indicate pronounced hypofunction of the salivary glands, consistent with values reported in clinical recommendations and review papers [5, 7, 16].

High Xerostomia Inventory scores in the treatment group confirm dry mouth's significant impact on the daily activities and quality of life of the patients. The revealed relationship between the total xerogenic load and the severity of subjective complaints corresponds to data on the role of polypragmasia in the pathogenesis of xerostomia [6, 13–15, 18].

Clinical manifestations, including multiple caries, non-carious lesions, candidal stomatitis, and atrophic glossitis are consistent with prolonged saliva deficiency and changes in its composition. A decrease in salivary pH and buffering capacity

favors cariogenic bacteria growth and enamel demineralization, explaining the higher DMFT index in the treatment group [1, 2, 7, 12, 17].

An increase in total protein content and alpha-amylase activity reflects compensatory adaptation in salivary gland secretion as overall secretion volume declines. The more frequent detection of Candida yeasts and the increased incidence of clinically evident candidal stomatitis suggest impaired local immunity and disruption of the oral microbiota [2, 7, 12].

The findings emphasize the need for an interdisciplinary approach to the management of patients with xerostomia. Correcting drug therapy — taking into account the xerogenic properties of the drugs — by a general practitioner, cardiologist, psychiatrist, or other specialists can help reduce symptoms and partially restore normal salivation [5, 11–13]. When therapy cannot be adjusted, local symptomatic measures become more important, including salivation stimulation, use of salivary substitutes, optimization of oral hygiene, prevention of caries and candidiasis [5, 13].

It is clinically important to include not only sialometry but also an extended oral fluid analysis (assessing pH, buffer capacity, protein profile, and enzymatic activity) in protocols for examining patients with dry mouth complaints. This approach enables more accurate quantification of the severity of drug-induced xerostomia, allowing use of the resulting indicators to monitor the effectiveness of preventive and therapeutic measures.

The limitations of this study include a relatively small sample size, the simultaneous nature of the observations, and a lack of stratified analysis for individual classes of xerogenic drugs. In the future, it is advisable to conduct prospective studies involving a larger number of patients and comparing different schemes for the prevention and treatment of drug-induced xerostomia.

CONCLUSIONS

Patients with medication-induced xerostomia develop hyposalivation, characterized by a significant reduction in unstimulated and stimulated saliva flow rates, decreased pH and buffering capacity of oral fluid, and increased total protein content and alpha-amylase activity. Medication-induced xerostomia is accompanied by a high incidence of multiple caries, non-carious lesions, candidal stomatitis, and atrophic changes in the oral mucosa, leading to deteriorated dental status and reduced quality of life. A comprehensive assessment of the clinical and laboratory characteristics of oral fluid enables objective evaluation of drug-induced xerostomia severity, links xerogenic drug load to the degree of hyposalivation, and provides a basis for individualized prevention and treatment programs.

References

1. Afanas'ev VV, Mirzakulova GF. Rotovaya zhidkost' i ee diagnosticheskoe znachenie: uchebnoe posobie. M.: Medicina, 2022; 120 s. Russian.
2. Dawes C, Pedersen AML, Villa A, Ekstrom J, Proctor GB, Vissink A, et al. The functions of human saliva: A review sponsored by the World Workshop on Oral Medicine VI. Arch Oral Biol. 2015; 60 (6): 863–74.
3. Volosova MA, Petrova EN, Zaharov AV. Kserostomiya: klinicheskoe znachenie i podhody k diagnostike v terapevticheskoj stomatologii. Rossijskij stomatologicheskij zhurnal. 2020; 23 (4): 45–52. Russian.
4. Sreebny LM, Valdini A. Xerostomia. Part I: Relationship to other oral symptoms and salivary gland hypofunction. Oral Surg Oral Med Oral Pathol. 1988; 66 (4): 451–8.
5. Plemons JM, Al-Hashimi I, Marek CL. Managing xerostomia and salivary gland hypofunction: executive summary of a report from the American Dental Association Council on Scientific Affairs. J Am Dent Assoc. 2014; 145 (8): 867–73.
6. Villa A, Abati S. Risk factors and symptoms associated with xerostomia: a cross-sectional study. Aust Dent J. 2011; 56 (3): 290–5.
7. Turner MD, Ship JA. Dry Mouth and Its Effects on the Oral Health of Elderly People. J Am Dent Assoc. 2007; 138 (Suppl 1): 15–20.
8. Arakelyan MG, Kostina IA, Vorobeva OV. Medikamentoznaya kserostomiya: patogenez, klinika, principy terapii. Stomatologiya. 2020; 99 (2): 62–68. Russian.
9. Antonova EA, Lebedeva NN. Vliyanie lekarstvennyh preparatov na slyunootdelenie i sostoyanie polosti rta u pacientov s hronicheskimi zabolevaniyami. Klinicheskaya stomatologiya. 2021; 1: 23–29. Russian.
10. Polyakov IV, Reshetov IV. Sostoyanie slizistoj obolochki polosti rta u pacientov posle luchevoj terapii zlokachestvennyh opuholej golovy i shei. Onkostomatologiya. 2022; 2 (1): 15–22. Russian.
11. Villa A, Wolff A, Aframian D, Vissink A, Ekstrom J, Proctor G, et al. World Workshop on Oral Medicine VI: a systematic review of medication-induced salivary gland dysfunction: prevalence, diagnosis, and treatment. Clin Oral Investig. 2015; 19 (7): 1563–80.
12. Aliko A, Wolff A, Dawes C, Aframian D, Proctor G, Ekstrom J, et al. World Workshop on Oral Medicine VI: clinical implications of medication-induced salivary gland dysfunction. Oral Surg Oral Med Oral Pathol Oral Radiol. 2015; 120 (2): 185–206.
13. Wolff A, Joshi RK, Ekstrom J, Aframian D, Pedersen AML, Proctor G, et al. A Guide to Medications Inducing Salivary Gland Dysfunction, Xerostomia, and Subjective Sialorrhea: a systematic review sponsored by the World Workshop on Oral Medicine VI. Drugs R D. 2017; 17 (1): 1–28.
14. Thomson WM, Chalmers JM, Spencer AJ, Williams SM. The Xerostomia Inventory: a multi-item approach to measuring dry mouth. Community Dent Health. 1999; 16 (1): 12–17.
15. Thomson WM, Williams SM. Further testing of the Xerostomia Inventory. Oral Surg Oral Med Oral Pathol Oral Radiol Endod. 2000; 89 (1): 46–50.
16. Navazesh M. Methods for collecting saliva. Ann N Y Acad Sci. 1993; 694: 72–77.
17. Gileva OS, Kuznecova LV, Smirnova NYu. Diagnostika i lechenie kserostomii v stomatologicheskoj praktike: rukovodstvo dlya vrachej. SPb.: SpecLit; 2023. 164 s. Russian.
18. Thomson WM, Chalmers JM, Spencer AJ, Slade GD. Medication and dry mouth: findings from a cohort study of older people. J Public Health Dent. 2000; 60 (1): 12–20.

Литература

1. Афанасьев В. В., Мирзакулова Г. Ф. Ротовая жидкость и ее диагностическое значение: учебное пособие. М.: Медицина, 2022; 120 с.
2. Dawes C, Pedersen AML, Villa A, Ekstrom J, Proctor GB, Vissink A, et al. The functions of human saliva: A review sponsored by the World Workshop on Oral Medicine VI. Arch Oral Biol. 2015; 60 (6): 863–74.
3. Волосова М. А., Петрова Е. Н., Захаров А. В. Ксеростомия:

клиническое значение и подходы к диагностике в терапевтической стоматологии. Российский стоматологический журнал. 2020; 23 (4): 45–52.
4. Sreebny LM, Valdini A. Xerostomia. Part I: Relationship to other oral symptoms and salivary gland hypofunction. Oral Surg Oral Med Oral Pathol. 1988; 66 (4): 451–8.
5. Plemons JM, Al-Hashimi I, Marek CL. Managing xerostomia and salivary gland hypofunction: executive summary of a report from the American Dental Association Council on Scientific Affairs. J Am Dent Assoc. 2014; 145 (8): 867–73.
6. Villa A, Abati S. Risk factors and symptoms associated with xerostomia: a cross-sectional study. Aust Dent J. 2011; 56 (3): 290–5.
7. Turner MD, Ship JA. Dry Mouth and Its Effects on the Oral Health of Elderly People. J Am Dent Assoc. 2007; 138 (Suppl 1): 15–20.
8. Аракелян М. Г., Костина И. А., Воробьева О. В. Медикаментозная ксеростомия: патогенез, клиника, принципы терапии. Стоматология. 2020; 99 (2): 62–68.
9. Антонова Е. А., Лебедева Н. Н. Влияние лекарственных препаратов на слюноотделение и состояние полости рта у пациентов с хроническими заболеваниями. Клиническая стоматология. 2021; 1: 23–29.
10. Поляков И. В., Решетов И. В. Состояние слизистой оболочки полости рта у пациентов после лучевой терапии злокачественных опухолей головы и шеи. Онкостоматология. 2022; 2 (1): 15–22.
11. Villa A, Wolff A, Aframian D, Vissink A, Ekstrom J, Proctor G, et al. World Workshop on Oral Medicine VI: a systematic review of medication-induced salivary gland dysfunction: prevalence, diagnosis, and treatment. Clin Oral Investig. 2015; 19 (7): 1563–80.
12. Aliko A, Wolff A, Dawes C, Aframian D, Proctor G, Ekstrom J, et al. World Workshop on Oral Medicine VI: clinical implications of medication-induced salivary gland dysfunction. Oral Surg Oral Med Oral Pathol Oral Radiol. 2015; 120 (2): 185–206.
13. Wolff A, Joshi RK, Ekstrom J, Aframian D, Pedersen AML, Proctor G, et al. A Guide to Medications Inducing Salivary Gland Dysfunction, Xerostomia, and Subjective Sialorrhea: a systematic review sponsored by the World Workshop on Oral Medicine VI. Drugs R D. 2017; 17 (1): 1–28.
14. Thomson WM, Chalmers JM, Spencer AJ, Williams SM. The Xerostomia Inventory: a multi-item approach to measuring dry mouth. Community Dent Health. 1999; 16 (1): 12–17.
15. Thomson WM, Williams SM. Further testing of the Xerostomia Inventory. Oral Surg Oral Med Oral Pathol Oral Radiol Endod. 2000; 89 (1): 46–50.
16. Navazesh M. Methods for collecting saliva. Ann N Y Acad Sci. 1993; 694: 72–77.
17. Гилева О. С., Кузнецова Л. В., Смирнова Н. Ю. Диагностика и лечение ксеростомии в стоматологической практике: руководство для врачей. СПб.: СпецЛит; 2023. 164 с.
18. Thomson WM, Chalmers JM, Spencer AJ, Slade GD. Medication and dry mouth: findings from a cohort study of older people. J Public Health Dent. 2000; 60 (1): 12–20.

CLINICAL COURSE OF CHRONIC GENERALIZED PERIODONTITIS IN OBESE PATIENTS WITH TYPE 2 DIABETES MELLITUS

Dzaraeva ZR✉, Dulaeva AA, Dudaeva LR, Makieva KA, Tsakhilova ZS, Alakhverdieva SS, Sagilaeva KhM, Kurmagomedov MA, Dzhafarov UL

North Ossetian State Medical Academy, Vladikavkaz, Russia

Type 2 diabetes mellitus (T2D) and obesity enhance systemic inflammation, microcirculation and immune disorders, which can make the course of chronic generalized periodontitis more severe. Comparative assessment of clinical and radiological manifestations of the disease in individuals with these conditions is important for interdisciplinary management of patients. The study aimed to conduct comparative assessment of clinical and radiological manifestations of chronic generalized periodontitis (CGP) in patients with T2D, obesity and having no somatic disorders. A total of 90 patients with moderate CGP aged 35–60 were assessed, who were stratified into three groups (30 individuals per group) matched for gender and age: without any somatic disorders, with T2D and obesity. OHI-S, SBI, periodontal pocket depth (PPD), clinical attachment loss (CAL), and radiological signs of bone resorption were assessed; the analysis of correlations with HbA1c, BMI, and lipid profile was conducted. OHI-S was 1.8 ± 0.3 in group I, 2.3 ± 0.4 in group II, and 2.2 ± 0.5 in group III; SBI was 42 ± 9%, 61 ± 11%, and 56 ± 10%, respectively ($p < 0.05$ for groups II and III compared to group I). PPD and CAL were higher in obese patients with T2D, than in patients having no somatic disorders ($p < 0.05$), while the differences between groups II and III were non-significant (for PPD $p = 0.09$). HbA1c levels were correlated to PPD ($r = 0.42$), CAL ($r = 0.39$), and SBI ($r = 0.36$); BMI was correlated to PPD ($r = 0.33$) and SBI ($r = 0.35$) ($p < 0.05$). Thus, T2D and obesity are associated with the more adverse clinical and radiological manifestations of CGP; it is necessary to consider poorer oral hygiene in patients with comorbidities when interpreting intergroup differences.

Keywords: chronic generalized periodontitis, type 2 diabetes mellitus, obesity, comorbidity, systemic inflammation, metabolic syndrome, HbA1c, alveolar bone loss

Author contribution: Dzaraeva ZR — study concept and design, scientific advising, manuscript editing; Dulaeva AA — clinical material collection, literature review, manuscript writing; Dudaeva LR, Tsakhilova ZS, Alakhverdieva SS — clinical assessment of patients, database creation, statistical processing; Makieva KA, Sagilaeva KhM, Kurmagomedov MA, Dzhafarov UL — interpretation of results, formatting the list of references, manuscript editing.

Compliance with ethical standards: the study was approved by the Ethics Committee of the North Ossetian State Medical Academy (protocol No. 6 dated 18 March 2025). All subjects submitted the informed consent for participation in the study and personal data processing.

✉ **Correspondence should be addressed:** Zarina R. Dzaraeva
Pushkinskaya, 40, Vladikavkaz, 362019, Republic of North Ossetia–Alania, Russia; sogma@minzdrav.alania.gov.ru

Received: 19.03.2026 **Accepted:** 16.04.2026 **Published online:** 28.04.2026

DOI: 10.24075/brsmu.2026.019

КЛИНИЧЕСКОЕ ТЕЧЕНИЕ ХРОНИЧЕСКОГО ГЕНЕРАЛИЗОВАННОГО ПАРОДОНТИТА У ПАЦИЕНТОВ С САХАРНЫМ ДИАБЕТОМ 2-ГО ТИПА И ОЖИРЕНИЕМ

З. Р. Дзараева✉, А. А. Дулаева, Л. Р. Дудаева, К. А. Макиева, З. С. Цахилова, С. С. Алахвердиева, Х. М. Сагилаева, М. А. Курмагомедов, У. Л. Джафаров

Северо-Осетинская государственная медицинская академия, Владикавказ, Россия

Сахарный диабет 2-го типа (СД2) и ожирение усиливают системное воспаление, нарушения микроциркуляции и иммунного ответа, что может утяжелять течение хронического генерализованного пародонтита. Сравнительная оценка клинико-рентгенологических проявлений заболевания при этих состояниях важна для междисциплинарного ведения пациентов. Целью исследования было провести сравнительную оценку клинико-рентгенологических проявлений хронического генерализованного пародонтита (ХГП) у пациентов с СД2, ожирением и без соматической патологии. Обследовали 90 пациентов 35–60 лет с ХГП средней степени тяжести, разделенных на три сопоставимые по полу и возрасту группы по 30 человек: без соматической патологии, с СД2 и с ожирением. Оценивали OHI-S, SBI, глубину пародонтальных карманов (ГПК), потерю клинического прикрепления (КУП) и рентгенологические признаки резорбции кости; выполняли корреляционный анализ с HbA1c, ИМТ и липидным профилем. Индекс OHI-S составил 1,8 ± 0,3 в I группе, 2,3 ± 0,4 во II и 2,2 ± 0,5 в III; SBI — 42 ± 9%, 61 ± 11% и 56 ± 10% соответственно ($p < 0,05$ для II и III групп по сравнению с I). ГПК и КУП были выше у пациентов с СД2 и ожирением, чем у пациентов без соматической патологии ($p < 0,05$), тогда как различия между II и III группами не достигали статистической значимости (для ГПК $p = 0,09$). Уровень HbA1c коррелировал с ГПК ($r = 0,42$), КУП ($r = 0,39$) и SBI ($r = 0,36$), а ИМТ — с ГПК ($r = 0,33$) и SBI ($r = 0,35$) ($p < 0,05$). Таким образом, СД2 и ожирение ассоциированы с более неблагоприятными клинико-рентгенологическими проявлениями ХГП; интерпретация межгрупповых различий должна учитывать худшее гигиеническое состояние полости рта у коморбидных пациентов.

Ключевые слова: хронический генерализованный пародонтит, сахарный диабет 2-го типа, ожирение, коморбидность, системное воспаление, метаболический синдром, HbA1c, резорбция альвеолярной кости

Вклад авторов: З. Р. Дзараева — концепция и дизайн исследования, научное руководство, редактирование текста; А. А. Дулаева — сбор клинического материала, анализ литературы, подготовка рукописи; Л. Р. Дудаева, З. С. Цахилова, С. С. Алахвердиева — клиническое обследование пациентов, формирование базы данных, статистическая обработка; К. А. Макиева, Х. М. Сагилаева, М. А. Курмагомедов, У. Л. Джафаров — интерпретация результатов, оформление списков литературы, редактирование текста.

Соблюдение этических стандартов: исследование одобрено этическим комитетом ФГБОУ ВО «Северо-Осетинская государственная медицинская академия» Минздрава России (протокол № 6 от 18 марта 2025 г.). Все участники подписали добровольное информированное согласие на участие в исследовании и обработку персональных данных.

✉ **Для корреспонденции:** Зарина Руслановна Дзараева
ул. Пушкинская, 40, Владикавказ, 362019, Республика Северная Осетия — Алания, Россия; sogma@minzdrav.alania.gov.ru

Статья получена: 19.03.2026 **Статья принята к печати:** 16.04.2026 **Опубликована онлайн:** 28.04.2026

DOI: 10.24075/vrgmu.2026.019

Chronic generalized periodontitis (CGP) remains one of the most common inflammatory disorders of the oral cavity. In is more and more often considered as a component of the systemic inflammatory continuum. According to the GBD 2021 analysis, the number of cases of severe periodontitis in the world increased by 91.54% in 1990–2021, which emphasizes stable medical and social significance of the disorder [1]. In this context, the growing prevalence of metabolic disorders, primarily type 2 diabetes mellitus (T2D) and obesity, reinforces the urgency of multidisciplinary analysis of periodontal tissue damage [2, 3].

T2D is associated with chronic hyperglycemia, accumulation of advanced glycation end products, impaired microcirculation, and immune dysfunction. These mechanisms make periodontal tissues more susceptible to inflammation, accelerate the clinical attachment loss, and enhance the alveolar bone resorption [4–6]. According to the data of the systematic review and meta-regression analysis of prospective studies, diabetes is associated with higher risk of periodontitis [7], and a modern review reports the increase in the risk of the disease occurrence or progression by 86% (RR 1.86; 95% CI 1.3–2.8) [5].

Obesity is considered as an independent risk factor of inflammatory periodontal disorders. Adipokines and pro-inflammatory cytokines of the adipose tissue support chronic subclinical inflammation, alter tissue reactivity; these also can make the course of periodontitis more severe [8–13]. In one of the studies, among 314 obese young adult patients, gingivitis was found in 63.7% of cases, and stage III periodontitis in 22.6% of cases; the increase in body mass index was positively correlated to the increase in PD, CAL, RD, and PI ($p < 0.05$) [11]. In the published systematic review and meta-analysis, obesity was associated with the increased risk of periodontitis (OR 1.31; 95% CI 1.22–1.41) [14].

Systemic inflammation, endothelial dysfunction, and metabolic disorders provide the common pathogenetic background for periodontitis, T2D, obesity, and cardiovascular disorders [15]. At the same time, direct comparisons of the CGP clinical and radiological phenotype in patient with T2D and obese patients within the same diagnostic protocol are limited. Such comparative assessment is important for the clinical routing of patients and clarification of the factors associated with the more severe disease course. The study aimed to conduct comparative assessment of clinical and radiological manifestations of CGP in patients with T2D, obesity and those having no somatic disorders.

METHODS

A total of 90 patients (42 males and 48 females) aged 35–60 (average age 47.3 ± 6.1 years) with the diagnosis of moderate chronic generalized periodontitis, exacerbation or unstable remission, were included in the comparative cross-sectional clinical trial. All patients were divided into three groups, 30 individuals per group: group I — patients with CGP without any defined somatic disorder; group II — patients with CGP against the background of T2D; group III — patients with CGP against the background of obesity. The groups formed were matched for gender and age.

Inclusion criteria: age 35–60 years, at least 20 teeth, and the confirmed diagnosis of moderate CGP. Patients with acute inflammatory disorders of the oral cavity, severe decompensation of concomitant conditions, and the combination of T2D and obesity were not included in the study. The groups were allocated based on the somatic status and the data on the presence of T2D or obesity from medical records. The smoking status and other behavioral factors were not used as the criteria for stratification of the groups, which was taken into account as a potential limitation of the study when interpreting the results.

Clinical assessment included estimation of the simplified oral hygiene index (OHI-S), sulcus bleeding index (SBI), periodontal pocket depth (PPD), clinical attachment loss (CAL). Measurement was performed using a standard periodontal probe at six points near each tooth. CAL was calculated as the sum of the periodontal pocket depth and the value of the gingival recession/displacement of the gingival margin relative to the cement-enamel junction. Radiological assessment of the alveolar bone condition was performed based on the digital orthopantomography data and targeted intraoral radiographs obtained using the standard protocol in the clinic X-ray room. In patients of group II, the T2D duration, glucose-lowering therapy pattern, and HbA1c levels were also assessed; in patients of group III, body mass index (BMI) and the lipid profile indicators were evaluated.

Statistical data processing was conducted using the standard software package. The data are presented as M ± SD. The distribution was tested for normality using the Shapiro–Wilk test. One-way analysis of variance (ANOVA) with subsequent post-hoc Tukey's test was used to compare quantitative indicators between three groups. Student's *t*-test was used for pairwise comparison, and Pearson's correlation coefficient was used to assess the relationship between traits. The 95% confidence intervals (CI) of the differences of mean values were also calculated for some key intergroup differences. The differences were considered significant at $p < 0.05$.

RESULTS

There were no significant differences in the average age of patients in the groups (I: 46.8 ± 6.0; II: 47.5 ± 5.9; III: 47.7 ± 6.5 years; $p > 0.05$). The share of males was 43.3% in group I, 46.7% in group II, and 46.7% in group III ($p > 0.05$), which suggested that the groups were comparable based on major demographic characteristics.

In group II, the average T2D duration was 9.2 ± 3.8 years; the combination glucose-lowering therapy was reported in 63.3% of cases, and insulin therapy was reported in 36.7% of cases. The average HbA1c level was 8.1 ± 1.0%, which corresponded to insufficient glycemic control in a large number of patients. In group III, BMI was 33.8 ± 3.4 kg/m^2; class II obesity was diagnosed in 46.7% of patients, and class III obesity was reported in 23.3%. Hypercholesterolemia and atherogenic dyslipidemia (increased levels of triglycerides and LDL cholesterol, decreased HDL cholesterol levels) were typical for this group.

The gum hygiene and inflammation indicators were worse in patients with somatic comorbidities. OHI-S was higher in groups II and III (2.3 ± 0.4 and 2.2 ± 0.5 points, respectively) compared to group I (1.8 ± 0.3; $p < 0.05$). The difference between the mean OHI-S values was 0.50 points (95% CI 0.32–0.68) for II–I and 0.40 points (95% CI 0.19–0.61) for III–I. SBI was 42 ± 9% in group I, 61 ± 11% in group II, and 56 ± 10% in group III; the differences II–I and III–I were significant ($p < 0.05$). The difference between the mean SBI values was 19 percentage points (95% CI 13.8–24.2) between groups II and I and 14 percentage points (95% CI 9.1–18.9) between groups III and I. Diffuse gingival bleeding and episodes of spontaneous bleeding with minimal trauma were more often found in patients with T2D, while in obese patients the localized areas of hyperemia and hypertrophy of the interdental papillae with the pronounced bleeding upon probing prevailed.

The periodontal pocket depth and clinical attachment loss values were higher in groups II and III compared to group I. The differences between groups II and I, as well as between groups III and I were significant ($p < 0.05$). There were no significant differences in PPD between groups II and III ($p = 0.09$), and the differences in CAL were also non-significant ($p > 0.05$).

The X-ray examination more often revealed infrabony pockets and uneven resorption of the interalveolar septa, while the combination of the horizontal and focal vertical resorption, especially in the area of multi-rooted teeth, prevailed in obese patients. In group II, a moderate positive correlation between HbA1c levels and the periodontal pocket depth ($r = 0.42$; $p < 0.05$), clinical attachment loss ($r = 0.39$; $p < 0.05$), and SBI ($r = 0.36$; $p < 0.05$) was revealed. In group III, there was a moderate correlation of BMI with PPD ($r = 0.33$; $p < 0.05$) and SBI ($r = 0.35$; $p < 0.05$), and triglyceride levels were correlated to the bone resorption severity ($r = 0.31$; $p < 0.05$).

Thus, in this cross-sectional study T2D and obesity were associated with the less favorable clinical and radiological characteristics of CGP; some intergroup differences could be due to poorer oral hygiene in patients with comorbidities.

DISCUSSION

The data obtained confirm that metabolic disorders considerably modify the CGP course. The less favorable indicators in patients with T2D are consistent with the modern reviews and meta-analyses emphasizing the role of chronic hyperglycemia, advanced glycation end products, oxidative stress, and microcirculation disorders in the progression of periodontitis; in particular, the risk of periodontitis development or progression in patients with diabetes was estimated to be 86% higher (RR 1.86; 95% CI 1.3–2.8) [5].

The identified correlation of HbA1c with the pocket depth, attachment loss, and bleeding suggests the clinical significance of carbohydrate metabolism compensation. This is in line with the concept of bidirectional relation between diabetes and periodontitis, with which inflammation in periodontal tissues maintaining the systemic pro-inflammatory background can make it difficult to achieve glycemic targets [2–6].

In obese patients, a significant worsening of the CGP course compared to the group without somatic disorders was also observed. This is consistent with both distinct case reports and modern reviews. Thus, among obese young adult patients gingivitis was reported in 63.7% of cases, and stage III periodontitis in 22.6% of cases; the increase in BMI was accompanied by the increase in PD, CAL, RD, and PI ($p < 0.05$) [11]. According to the results of the published systematic review and meta-analysis [14], obesity is associated with the increased risk of periodontitis (OR 1.31; 95% CI 1.22–1.41). The association of BMI and triglycerides with periodontal indicators revealed in our study further confirms the involvement of the adipose tissue hormonal and metabolic disorders in the periodontal destruction progression.

When directly comparing the groups with T2D and obesity, the differences in PPD and CAL were non-significant. That is why we cannot declare a definitely more severe overall CGP course in individuals with T2D compared to obese ones based on our data. At the same time, a diffuse bleeding pattern, episodes of spontaneous hemorrhage with minimal trauma, more frequent vertical bone defects, and a correlation of periodontal indicators with HbA1c were more typical for patients with T2D, which suggests differences in the periodontal tissue lesion clinical phenotype. This is likely to reflect differences in predominant pathogenetic mechanisms. However, systemic inflammation linking periodontitis to metabolic syndrome and cardiovascular risk remains a common link for both disorders [15].

The relatively small sample size, cross-sectional design, and the lack of a separate group of patients with the combination of T2D and obesity should be considered the study limitations, which make it impossible to assess a possible synergistic effect of these conditions. The number of patients with a combination of disorders not included in the sample was not separately recorded within the protocol. Furthermore, the groups were not stratified based on the smoking status, and higher OHI-S values in groups II and III indicate a possible confounding influence of behavioral factors and the quality of personal hygiene. This limits the interpretation of the identified intergroup differences as an independent effect of metabolic disorder alone. Prospective studies with the inclusion of local and systemic inflammation biomarkers, a separate group of patients with a combination of T2D and obesity, and a multifactorial adjustment for behavioral risk factors are promising.

CONCLUSIONS

The cross-sectional comparative study revealed poorer oral hygiene and more severe gum inflammation in patients with T2D and obesity, than in patients without any somatic disorder: OHI-S was 2.3 ± 0.4 and 2.2 ± 0.5 vs. 1.8 ± 0.3 points, SBI was 61 ± 11% and 56 ± 10% vs.42 ± 9%, respectively ($p < 0.05$). PPD and CAL were higher in the groups with T2D and obesity, than in the group without somatic disorders ($p < 0.05$), but there were no significant differences in PPD between T2D and obesity ($p = 0.09$), and the differences in CAL were also non-significant. Correlations of HbA1c with PPD ($r = 0.42$), CAL ($r = 0.39$), and SBI ($r = 0.36$) were typical for the T2D group, which suggests the relationship between the degree of carbohydrate metabolism compensation and severity of periodontal changes. The findings should be interpreted considering higher levels of dental plaque in the groups with comorbidities and the lack of stratification by smoking; at the same time, patients with CGP and metabolic disorders need multidisciplinary management involving dentist, endocrinologist, and general practitioner.

References

1. GBD 2021 Oral Disorders Collaborators. Trends in the global, regional, and national burden of oral conditions from 1990 to 2021: a systematic analysis for the Global Burden of Disease Study 2021. Lancet. 2025; 405(10482): 897–910. DOI: 10.1016/S0140-6736(24)02811-3.
2. Senina VO, Usmanova IN, Lakman IA, et al. Vzaimosvyaz' metabolicheskogo sindroma i sakharnogo diabeta 2 tipa s patologiei parodonta (sistematicheskii obzor). Parodontologiya. 2024; 29 (2): 135–149. Russian.
3. Trukhan DI, Sulimov AF, Trukhan LYu. Sakharnyi diabet i zabolevaniya parodonta: vmeste ili parallel'no? Farmateka. 2024; 30 (8): 16-22. DOI: 10.18565/pharmateca.2024.8.16-22. Russian.
4. Zhao M, Xie Y, Gao W, et al. Diabetes Mellitus Promotes Susceptibility to Periodontitis — Novel Insight into the Molecular Mechanisms. Frontiers in Endocrinology. 2023; 14: 1192625. DOI: 10.3389/fendo.2023.1192625.
5. Enteghad S, Shirban F, Nikbakht MH, et al. Relationship Between Diabetes Mellitus and Periodontal/Peri-Implant Disease:

A Contemporaneous Review. International Dental Journal. 2024; S0020-6539(24)00096-0.
6. Tica O, Romanul I, Ciavoi G, et al. A Clinical Review of the Connections Between Diabetes Mellitus, Periodontal Disease, and Cardiovascular Pathologies. Biomedicines. 2025; 13 (9): 2309. DOI: 10.3390/biomedicines13092309.
7. Nascimento GG, Leite FRM, Vestergaard P, Scheutz F, López R. Does diabetes increase the risk of periodontitis? A systematic review and meta-regression analysis of longitudinal prospective studies. Acta Diabetol. 2018; 55(7): 653–667. DOI: 10.1007/s00592-018-1120-4.
8. Ermolaeva LA, Sevbitov AV, Penkovoi EA, et al. Etiopatogeneticheskie mekhanizmy razvitiya vospalitel'nykh zabolevanii parodonta u bol'nykh s ozhireniem. Vestnik Sankt-Peterburgskogo gosudarstvennogo universiteta. Seriya 11: Meditsina. 2022; 12 (4): 385–395. DOI: 10.21638/11701/spbu11.2022.407. Russian.
9. Khabibova NN, Khamroeva DSh, Samadova ShI. Optimizatsiya effektivnosti lecheniya generalizovannogo parodontita u bol'nykh ozhireniem. Mezhdunarodnyi zhurnal prikladnykh i fundamental'nykh issledovanii. 2021; (12-9): 1628–1632. Russian.
10. Zherdeva GV. Vospalitel'nye zabolevaniya parodonta u podrostkov s ekzogenno-konstitutsionnym ozhireniem. Nauchnyi vestnik Kryma. 2020; Spets. vypusk po stomatologii. Russian.
11. Abbas Y, Elsaadany B, Ghallab N. Prevalence of Different Stages of Periodontal Diseases Among a Sample of Young Adult Obese Egyptian Patients: A Hospital-Based Cross-Sectional Study Over 1 Year. BMC Oral Health. 2023; 23.
12. Di Spirito F, Sbordone L, Pilone V, D'Ambrosio F. Obesity and Periodontal Disease: A Narrative Review on Current Evidence and Putative Molecular Links. The Open Dentistry Journal. 2021; 13: 526–536. DOI: 10.2174/1874210601913010526.
13. Araujo EL, Fernandes LA, Miranda TS, Sanabani SS. The Obesity-Periodontitis Axis: Microbial Mechanisms and Clinical Implications. Oral. 2025; 5 (3): 61. DOI: 10.3390/oral5030061.
14. Esperouz F, Ciavarella D, Di Gioia C, Serviddio G, Lorusso M, Lo Russo L. Is Obesity a Risk Factor for Periodontitis? A Systematic Review and Meta-Analysis. Obes Rev. 2025; e70020. DOI: 10.1111/obr.70020.
15. Trukhan DI, Trukhan LYu. Parodontit i serdechno-sosudistye zabolevaniya: parallel'no ili v odnoi svyazke? Consilium Medicum. 2021; (5): 73–79. Russian.

Литература

1. GBD 2021 Oral Disorders Collaborators. Trends in the global, regional, and national burden of oral conditions from 1990 to 2021: a systematic analysis for the Global Burden of Disease Study 2021. Lancet. 2025; 405(10482): 897–910. DOI: 10.1016/S0140-6736(24)02811-3.
2. Сенина В. О., Усманова И. Н., Лакман И. А. и др. Взаимосвязь метаболического синдрома и сахарного диабета 2 типа с патологией пародонта (систематический обзор). Пародонтология. 2024; 29 (2): 135–149.
3. Трухан Д. И., Сулимов А. Ф., Трухан Л. Ю. Сахарный диабет и заболевания пародонта: вместе или параллельно? Фарматека. 2024; 30 (8): 16–22. DOI: 10.18565/pharmateca.2024.8.16-22.
4. Zhao M, Xie Y, Gao W, et al. Diabetes Mellitus Promotes Susceptibility to Periodontitis — Novel Insight into the Molecular Mechanisms. Frontiers in Endocrinology. 2023; 14: 1192625. DOI: 10.3389/fendo.2023.1192625.
5. Enteghad S, Shirban F, Nikbakht MH, et al. Relationship Between Diabetes Mellitus and Periodontal/Peri-Implant Disease: A Contemporaneous Review. International Dental Journal. 2024; S0020-6539(24)00096-0.
6. Tica O, Romanul I, Ciavoi G, et al. A Clinical Review of the Connections Between Diabetes Mellitus, Periodontal Disease, and Cardiovascular Pathologies. Biomedicines. 2025; 13 (9): 2309. DOI: 10.3390/biomedicines13092309.
7. Nascimento GG, Leite FRM, Vestergaard P, Scheutz F, López R. Does diabetes increase the risk of periodontitis? A systematic review and meta-regression analysis of longitudinal prospective studies. Acta Diabetol. 2018; 55(7): 653–667. DOI: 10.1007/s00592-018-1120-4.
8. Ермолаева Л. А., Севбитов А. В., Пеньковой Е. А. и др. Этиопатогенетические механизмы развития воспалительных заболеваний пародонта у больных с ожирением. Вестник Санкт-Петербургского государственного университета. Серия 11: Медицина. 2022; 12 (4): 385-395. DOI: 10.21638/11701/spbu11.2022.407.
9. Хабибова Н. Н., Хамроева Д. Ш., Самадова Ш. И. Оптимизация эффективности лечения генерализованного пародонтита у больных ожирением. Международный журнал прикладных и фундаментальных исследований. 2021; (12-9): 1628–1632.
10. Жердева Г. В. Воспалительные заболевания пародонта у подростков с экзогенно-конституционным ожирением. Научный вестник Крыма. 2020; Спец. выпуск по стоматологии.
11. Abbas Y, Elsaadany B, Ghallab N. Prevalence of Different Stages of Periodontal Diseases Among a Sample of Young Adult Obese Egyptian Patients: A Hospital-Based Cross-Sectional Study Over 1 Year. BMC Oral Health. 2023; 23.
12. Di Spirito F, Sbordone L, Pilone V, D'Ambrosio F. Obesity and Periodontal Disease: A Narrative Review on Current Evidence and Putative Molecular Links. The Open Dentistry Journal. 2021; 13: 526–536. DOI: 10.2174/1874210601913010526.
13. Araujo EL, Fernandes LA, Miranda TS, Sanabani SS. The Obesity-Periodontitis Axis: Microbial Mechanisms and Clinical Implications. Oral. 2025; 5 (3): 61. DOI: 10.3390/oral5030061.
14. Esperouz F, Ciavarella D, Di Gioia C, Serviddio G, Lorusso M, Lo Russo L. Is Obesity a Risk Factor for Periodontitis? A Systematic Review and Meta-Analysis. Obes Rev. 2025; e70020. DOI: 10.1111/obr.70020.
15. Трухан Д. И., Трухан Л. Ю. Пародонтит и сердечно-сосудистые заболевания: параллельно или в одной связке? Consilium Medicum. 2021; (5): 73-79.